

**An optimisation tool for minimising fuel consumption,
emissions and costs from biofuel powered diesel generator-PV-
battery hybrid mini-grids in developing countries**

Nina Victoria Rangel Ortiz

Submitted in accordance with the requirements for the degree of
Doctor of Philosophy

The University of Leeds
School of Chemical and Process Engineering

January 2023

The candidate confirms that the work submitted is his/her own, except where work which has formed part of jointly authored publications has been included. The contribution of the candidate and the other authors to this work has been explicitly indicated below. The candidate confirms that appropriate credit has been given within the thesis where reference has been made to the work of others.

The work in Chapters is based on the following publication:

Rangel, N., H. Li, and P. Aristidou, *An optimisation tool for minimising fuel consumption, costs and emissions from Diesel-PV-Battery hybrid microgrids*. Applied Energy, 2023. **335**: p. 120748.

The candidate is the lead author of this publication, the conceptualization, methodology, software, validation, investigation, data curation, writing, reviewing, and editing were conducted by the candidate. The other authors contributed by supervision, reviewing, and editing of this publication.

This copy has been supplied on the understanding that it is copyright material and that no quotation from the thesis may be published without proper acknowledgement.

The right of Nina Victoria Rangel Ortiz to be identified as Author of this work has been asserted by her in accordance with the Copyright, Designs, and Patents Act 1988.

Acknowledgements

I thank my supervisors Dr Hu Li, Dr Petros Aristidou and Dr Andrew Ross for their guidance.

Special thanks to Dr Hu Li for his continuous and invaluable support throughout the research stages, and for motivating me to finish the tough writing period. Also special thanks to Dr Petros Aristidou for his advice, support and patience during the development of this project.

I thank Scott Prichard, James Hammerton, Francis Olanrewaju and Scott Wiseman for their assistance, training and support to complete the experimental work in the engine lab.

Thank you to Agnes Nakiganda and Shahab Dehghan for their advice on programming and optimisation.

I also thank Karine Alves Thorne, Adrian Cunliffe, Ben Douglas and Stuart Micklethwaite for their assistance and lab training, without their hard work, this project may not have been possible.

I am grateful for the funding received from CONACYT (2018-000009-01EXTF-00174), the University of Leeds and the Engineering and Physical Sciences Research Council (EP/R030243/1) to complete the research project.

Special thanks to Zahida Aslam for her patience, support and motivation that made this PhD a happy journey.

Finally, thank you to my daughter Tamara for her love, motivation and support throughout this journey. And thank you to my father and brother for their endless support and caring words that helped me overcome difficult times.

This thesis is dedicated to my father, brother and daughter because they showed me everything is possible.

Abstract

The purpose of this research was to develop a cost optimisation tool to improve the performance of diesel generators within hybrid microgrids for increasing electrification rates in rural areas of developing countries, especially in sub-Saharan Africa. This study considered the use of widely available vegetable oils, such as castor oil, to widen the fuel options to power diesel generators and reduce their environmental impact and operating costs.

Castor oil-diesel blends were used to assess the performance of a diesel generator and find new fuel estimation equations, which were used to develop a cost optimisation tool for diesel/PV/battery microgrids. The best performance occurred above 60% engine load for all the blends and higher fuel consumption was found for the blends with higher castor oil content.

The developed cost optimisation tool was used to compare the Levelized Cost of Energy (LCOE) and the pollutant emissions (CO_2e , $\text{PM}_{2.5}$, and NO_x) of 8 microgrid system configurations for three estimated electricity demand profiles (high, medium, and low) in the Lindi Region in Tanzania. Installing diesel/PV/battery hybrid systems gives lower LCOE than diesel/battery or conventional systems (only diesel generators). Hybrid systems reduce CO_2e emissions between 20% and 24%, whereas $\text{PM}_{2.5}$ and NO_x can be reduced between 32% and 47%, relative to conventional systems.

Table of Contents

Acknowledgements	ii
Abstract	iii
Table of Contents	iv
Table of Figures	ix
Table of Tables	xvi
Table of Equations	xix
List of Abbreviations	xxiii
Nomenclature	xxvi
Chapter 1 Introduction	1
1.1 Background and Motivation	1
1.2 Aims and Objectives	4
1.3 Thesis Outline	4
Chapter 2 Literature Review	7
2.1 Electrification Status in Africa and Developing Countries	7
2.2 Electricity Systems Diversity: Definitions and SSA Solutions.....	9
2.3 Mini-grid Status Around the World	11
2.3.1 Mini-grids in Africa	12
2.3.2 Cost of Electricity of Mini-grids.....	13
2.3.3 Mini-grid Sizing and Design	15
2.4 The Role of Diesel Generators in Off-grid Systems	18
2.4.1 Genset Configuration and Working Principle	19
2.4.2 Key Parameters for Diesel Generators Performance.....	22
2.4.3 Fuel Consumption Estimation Equations for Diesel Generators	23
2.4.4 Evidence of Genset’s Performance Failure.....	24
2.4.5 Genset Poor Performance Consequences	25
2.5 Performance Improvement Attempts for Diesel Generators	27
2.5.1 Improvements in Diesel Generators Sizing and Selection with Multiple Gensets and Optimisation.....	27
2.5.2 Diesel Generators Performance Improvement through Control and Speed-oriented Models	28
2.5.3 Low Load Diesel Operation.....	28
2.6 Diesel Generators and the Combustion Process	28
2.6.1 Compression-Ignition Engine.....	29

2.6.2 Combustion Process in Compression Ignition Engines.....	30
2.6.3 Emissions from Compression Ignition Engines.....	31
2.6.4 Biofuel and Diesel Engines.....	32
2.6.5 Biofuel Effect on Diesel Engines' Performance.....	36
2.6.6 Fuel Specifications and Standards.....	39
2.7 Theoretical Background of the Proposed Solution for Improving Diesel Generators Performance in Microgrids.....	41
2.8 Literature Review Summary.....	45
Chapter 3 Experimental Work Methodology.....	48
3.1 Fuel Selection and Analytical Lab Work.....	48
3.1.1 Fuel Selection.....	48
3.1.2 Fuel Characterisation.....	49
3.1.2.1 Thermo-gravimetric Analysis (TGA).....	51
3.1.2.2 Bomb Calorimetry.....	52
3.1.2.3 Elemental Analysis.....	52
3.1.2.4 Density and Viscosity.....	54
3.2 Engine Lab work.....	55
3.2.1 Experiment Setup.....	55
3.2.1.1 Motor Exhaust Gas Analyser — MEXA 7100.....	59
3.2.1.2 Gasmet FTIR Emissions Monitoring System.....	62
3.2.1.3 DMS 500.....	64
3.2.1.4 PM _{2.5} Collection System.....	65
3.2.2 Engine Test Procedure.....	67
3.2.2.1 Baseline (diesel) Test.....	70
3.2.2.2 Castor Oil- Diesel (COD) Blend Test.....	71
3.3 Biofuel Impact on Engine's Fuel Injector.....	73
Chapter 4 Biofuel Blends Impact on Diesel Generator's Performance .76	
4.1 Characterisation of Castor Oil-Diesel Blends.....	76
4.1.1 Thermogravimetric Analysis (TGA).....	77
4.1.2 Net Calorific Value Determination by Bomb Calorimetry.....	78
4.1.3 Elemental Analysis for H/C and O/C Determination.....	78
4.1.4 Density and Viscosity Determination at Different Temperatures	81
4.2 Diesel Generator Performance at Different Operating Conditions with COD Blends.....	84
4.2.1 Power Output of Genset.....	84
4.2.2 Fuel Consumption.....	87

4.2.3 Brake Thermal Efficiency	91
4.2.4 Engine Combustion Performance	92
4.2.4.1 In-cylinder Pressure	92
4.2.4.2 Ignition Delay	95
4.2.4.3 Heat Release Rate.....	98
4.2.4.4 Engine Out Exhaust Gas Temperature	102
4.2.4.5 Air Fuel Ratio	103
4.2.5 Engine Exhaust Emissions	104
4.2.5.1 Regulated Pollutant Emissions (CO, HC, and NOx) Measured by the MEXA Analyser.....	104
4.2.5.2 Particulate Matter Emissions PM _{2.5}	109
4.2.5.3 Engine Exhaust Emissions vs European Emission Standards for Nonroad Engines.	111
4.2.5.4 Particle Size Distribution and Total Particle Number Determined by DMS 500 Fast Analyser	113
4.2.5.5 Unregulated Volatile Organic Compounds (VOCs) Measured by the FTIR Analyser.....	117
4.3 Deposits on Fuel Injector Analysis.....	123
4.4 Summary	129
Chapter 5 Cost Optimisation Model Development.....	134
5.1 Cost Optimisation Mathematical Model.....	135
5.1.1 Objective Function	136
5.1.2 Model Constraints	141
5.1.3 Model Inputs	144
5.1.3.1 An Extended Explanation of Emission Factor Adjustment Coefficient Calculation.....	147
5.1.4 Economic Assessment.....	150
5.2 Scenarios for Cost Optimisation.....	153
5.2.1 Electricity Demand Profiles	154
5.2.2 PV System Installed Capacity	156
5.2.3 PV System Performance.....	156
5.2.4 Battery System Type and Installed Capacity	157
5.2.5 Greenhouse Gas Emission Source.....	158
5.2.6 Scenario Summary	162
5.3 Optimisation Model Graphical User Interface	163
Chapter 6 Cost Optimisation Model Implementation: Baseline Optimisation Scenario	168
6.1 Baseline Optimisation Scenario Specifications and Assumptions...	168

6.2 Baseline Optimisation Scenario Findings for 8 System Configurations.	169
6.2.1 Diesel Generators Selection and Performance	171
6.2.1.1 Non-Battery Systems	173
6.2.1.2 Battery Systems	177
6.2.1.3 Diesel/PV/BESS Hybrid Systems	183
6.2.2 Fuel Consumption and Pollutant Emissions	189
6.3 Economic Assessment for 8 System Configurations	192
6.3.1 Life Cycle Cost and Levelized Cost of Energy	192
6.3.2 LCOE vs Emissions Analysis	194
6.4 Summary	197
Chapter 7 Scenario and Sensitivity Analyses for Selected Microgrid Systems.....	201
7.1 Baseline Optimisation Scenario Review	201
7.2 Scenario Analysis	203
7.2.1 High Electricity Demand Profile with SC7-Genset, PV, and Battery (Li-ion).....	203
7.2.2 Medium Electricity Demand Profile with SC7-Genset, PV, and Battery (Li-ion).....	208
7.2.3 Low Electricity Demand Profile with SC8-Genset, PV, and Battery (repurposed)	212
7.3 Sensitivity Analysis	221
7.3.1 High Electricity Demand Profile	223
7.3.2 Medium Electricity Demand Profile	226
7.3.3 Low Electricity Demand Profile	228
7.4 Summary	229
Chapter 8 Conclusions and Future Work.....	232
8.1 Contribution to knowledge	232
8.2 Stage 1: Fuel Selection and Characterisation.....	232
8.3 Stage 2: Engine Tests and Pollutant Emissions.....	233
8.4 Stage 3: Cost Optimisation Model Development and Implementation	235
8.4.1 Baseline Optimisation Scenario Findings.....	236
8.4.1.1 Microgrid without Battery System: SC1-Genset and SC2-Genset and PV	237
8.4.1.2 Microgrid with Battery Energy Storage System: SC3-Genset and Battery (Lead-acid), SC4-Genset and Battery (Li-ion), and SC5-Genset and Battery (repurposed)	237

8.4.1.3 Hybrid Microgrid (genset, PV, and BESS): SC6-Genset, PV and Battery (Lead-acid), SC7-Genset, PV and Battery (Li-ion), and SC8-Genset, PV and Battery (repurposed) ..	238
8.4.1.4 Microgrid Fuel Consumption and Pollutant Emissions	239
8.4.1.5 Economic Assessment of 8 Optimised Microgrid Configurations	239
8.4.1.6 LCOE vs Emissions Analysis of 8 Optimised Microgrid Configurations.	240
8.4.2 Scenario and Sensitivity Analyses Findings for Selected Microgrid Configurations	240
8.4.2.1 Scenario Analysis for Selected Microgrid Configurations	241
8.4.2.2 Sensitivity Analysis for Selected Microgrid Configurations	243
8.5 Concluding Remarks.....	243
8.6 Limitations and Future Work	250
List of References.....	252
Appendix A.....	270

Table of Figures

Figure 1-1 Diagram of the factors affecting the performance of a diesel generator that operates in a microgrid.	3
Figure 2-1 Qualitative representation of mini-grid as the most suitable solution for rural electrification [13].....	11
Figure 2-2 Block diagram of a diesel generator [56].....	19
Figure 2-3 Schematic diagram of the soot formation process [81].	26
Figure 2-4 Illustration of a four-stroke Diesel cycle [99].	29
Figure 2-5 A General classification of biofuels.	32
Figure 2-6 Methodologies for unit sizing and cost optimisation commonly used for IRES systems [136].....	42
Figure 2-7 Optimisation models diagram [137].	43
Figure 2-8 Illustration of the Branch and Bound algorithm [139].	44
Figure 2-9 Branch and Cut representation [141].	45
Figure 3-1. Fuel blend samples for fuel characterisation analyses.....	51
Figure 3-2. Shimadzu TGA50 analyser used for mass loss determination of fuel blend samples.	52
Figure 3-3 Parr 6200 calorimeter used for gross and net calorific values of fuel blend samples.	52
Figure 3-4 Analyser and capsules used for elemental analysis of fuel blend samples.....	53
Figure 3-5 CHNS analysis schematic diagram [148].....	54
Figure 3-6 Experiment setup for density and kinematic determination of fuel blend samples using an SVM 3000 Stabinger viscometer.....	55
Figure 3-7 Schematic diagram of the engine test experiment setup.	56
Figure 3-8 Diesel generator and load bank experiment setup.	58
Figure 3-9 Schematic diagram of a Flame Ionisation Detector [155]....	61
Figure 3-10 Gasmest emission monitoring system components [156].	62
Figure 3-11 Example of FTIR multi-component analysis spectra representation [157].	64
Figure 3-12 DMS500 Fast Particulate Analyser and DMS user interface [158].	64
Figure 3-13 DMS 500 Classifier column [160].....	65
Figure 3-14 PM_{2.5} collection system and glass microfibre filter paper. .	66
Figure 3-15 Illustration of the operation principle of the PM_{2.5} collection system [161].	67

Figure 3-16 FTIR background spectrum.	68
Figure 3-17 FTIR Zero sample check graph.....	69
Figure 3-18 Filter paper conditioning units and test filter used during the PM _{2.5} collection system warmup.	69
Figure 3-19 Load bank controller and engine operating conditions for starting a test.	70
Figure 3-20 Filter papers with particulates collected during engine tests at different loads. Filter paper a) shows a lighter colour compared to filter paper b) due to the lower number of particulates produced at lower loads.....	71
Figure 3-21 Fuel blend preparation for the COD40 (40% castor oil) engine test.....	72
Figure 3-22 LEMAS scanning electron microscope.....	73
Figure 3-23 Sample preparation for SEM analysis.....	74
Figure 3-24 New fuel injector nozzle inside the SEM chamber.	75
Figure 4-1 Thermograms from TGA analysis of 7 castor oil-diesel (COD) fuel blends.....	77
Figure 4-2 Molecular structure of diesel, biodiesel and vegetable oil [169].	79
Figure 4-3 Chemical structure of castor oil fatty acids [170].	80
Figure 4-4 Fatty acid composition of castor oil from eight regions [170].	80
Figure 4-5 Density for 7castor oil-diesel blends at different temperatures.....	82
Figure 4-6 Kinematic viscosity for 7castor oil-diesel blends at different temperatures.	83
Figure 4-7 Genset output power for 5 castor oil-diesel blends at 5 engine test conditions.....	85
Figure 4-8 Alternator efficiency for 5 castor oil-diesel blends.....	86
Figure 4-9 Engine output power for 5 castor oil-diesel blends at 5 engine test conditions.....	87
Figure 4-10 Fuel mass flow for 5 castor oil-diesel blends at 5 engine loads.	88
Figure 4-11 Fuel volumetric flow for 5 castor oil-diesel blends at 5 engine loads.....	89
Figure 4-12 Specific fuel consumption for 5 castor oil-diesel blends at 5 engine loads.....	90
Figure 4-13 Brake specific energy consumption for 5 castor oil-diesel blends at 5 engine loads.	91
Figure 4-14 Brake thermal efficiency for 5 castor oil-diesel blends at 5 engine loads.....	92

Figure 4-15 In-cylinder pressure curves for 5 castor oil-diesel blends at different engine load conditions: (a) 92% engine load, (b) 77% engine load, (c) 50% engine load, (d) 29% engine load and (e) 4% engine load.....	93
Figure 4-16 In-cylinder peak pressure for 5 castor oil-diesel blends at 5 engine loads.....	95
Figure 4-17 In-cylinder pressure and heat release rate curves with combustion characterisation parameters and combustion phases (I: premixed combustion, II: mixing-controlled combustion, III: late combustion phase).....	96
Figure 4-18 In-cylinder pressure curves for diesel (COD0) at five engine loads.	97
Figure 4-19 5 Heat release rate curves at different engine load conditions: (a) 92% engine load, (b) 77% engine load, (c) 50% engine load, (d) 29% engine load, and (e) 4% engine load.....	100
Figure 4-20 Engine out exhaust gas temperature for 5 castor oil-diesel blends at 5 engine loads.	103
Figure 4-21 Air fuel ratio for 5 castor oil-diesel blends at 5 engine loads.	104
Figure 4-22 Carbon monoxide emissions for 5 castor oil-diesel blends at 5 engine loads.....	105
Figure 4-23 Total hydrocarbon emissions for 5 castor oil-diesel blends at 5 engine loads.....	106
Figure 4-24 NOx emissions for 5 castor oil-diesel blends at 5 engine loads.	107
Figure 4-25 Particulate concentration for 5 castor oil-diesel blends at 5 engine loads.....	110
Figure 4-26 CO Specific Emissions for 5 castor oil-diesel blends at 5 engine loads.....	111
Figure 4-27 THC and NOx Specific Emissions for 5 castor oil-diesel blends at 5 engine loads.	112
Figure 4-28 PM_{2.5} Specific Emissions for 5 castor oil-diesel blends at 5 engine loads.....	113
Figure 4-29 Particle size distribution for 5 castor oil-diesel blends at 92% engine load.....	114
Figure 4-30 Particle size distribution for 5 castor oil-diesel blends at 77% engine load.....	114
Figure 4-31 Particle size distribution for 5 castor oil-diesel blends at 50% engine load.....	115
Figure 4-32 Particle size distribution for 5 castor oil-diesel blends at 29% engine load.....	116
Figure 4-33 Particle size distribution for 5 castor oil-diesel blends at 4% engine load.....	116

Figure 4-34 Ethylene and Methane emissions for 5 castor oil-diesel blends from 4% to 92% engine load.....	118
Figure 4-35 Acetylene and Benzene emissions for 5 castor oil-diesel blends from 4% to 92% engine load.....	119
Figure 4-36 Ethane and Hexane emissions for 5 castor oil-diesel blends at from 4% to 92% engine load.	120
Figure 4-37 Ethanol and Formaldehyde emissions for 5 castor oil-diesel blends from 4% to 92% engine load.....	121
Figure 4-38 NO_x emissions correlation between FTIR and MEXA measurements from 4% to 92% engine load for 5 castor oil-diesel blends.	123
Figure 4-39 FB fuel injector dismantled (left) and FB fuel injector nozzle (right).	123
Figure 4-40 SEM image at 50x magnification of a new FB fuel injector nozzle's tip with five holes(left) and SEM image at 500x magnification of one hole (right).	124
Figure 4-41 SEM image at 46x magnification of used FB fuel injector nozzle's tip with deposits after running a diesel engine with five castor oil-diesel blends.	125
Figure 4-42 SEM images at 50x magnification (a,b,d, and d) and 500x magnification (A, B, C, and D) from a used FB fuel injector after running a diesel engine with five castor oil-diesel blends.....	126
Figure 4-43 EDX analysis of the used FB fuel injector's deposits at four different locations (L1, L2, L3, and L4).	128
Figure 4-44 Thermograms from TGA analysis of fresh lube oil (blue line) and used lube oil after running a diesel engine with 5 castor oil-diesel blends.	129
Figure 5-1 Diagram of the hybrid microgrid configuration considered in the cost optimisation model.	134
Figure 5-2 Mass-based fuel consumption for selected diesel generators.	138
Figure 5-3 BTE and SFC curves from a diesel generator running with castor oil-diesel (COD) blends.....	142
Figure 5-4 NO_x specific emissions against engine torque for 5 COD blends.	149
Figure 5-5 PM_{2.5} specific emissions against engine torque for 5 COD blends.	149
Figure 5-6 Electricity flow diagram for a genset/PV/battery hybrid system.	153
Figure 5-7 PDF version of the energy access interactive map showing the Lindi Region and the mini-grid locations in Tanzania [224]. .	154
Figure 5-8 Electricity demand scenarios created for Mpigamiti, Tanzania.	155

Figure 5-9 Output power and representative operating day clusters for a 2kW PV system over five years.	157
Figure 5-10 N₂O emission index against engine torque for 5 COD blends.	159
Figure 5-11 CH₄ emission index against engine torque for 5 COD blends.	160
Figure 5-12 CH₄ total weighted emission index against castor oil content in the fuel blend	161
Figure 5-13 Possible optimisation scenario selection.....	163
Figure 5-14 GUI's main screen for running the cost optimisation model.	164
Figure 5-15 Process block diagram representation of the scenario selection algorithm implemented in the graphical user interface for initialising the cost optimisation model.....	165
Figure 5-16 GUI's window for optimisation results visualisation and sensitivity analysis selection.....	166
Figure 5-17 GUI's windows for sensitivity analysis results selection and original optimised results comparison.....	167
Figure 6-1 Load and power generation curves and the identified low genset performance (below 60%) operating periods in the SC1-Genset for three electricity demand profiles.....	174
Figure 6-2 Load and power generation curves and the identified low genset performance (below 60%) operating periods in the SC2-Genset and PV for three electricity demand profiles.....	176
Figure 6-3 Load and power generation curves and the identified low genset performance operating periods in the SC3, SC4, and SC5 for the high electricity demand profile.....	178
Figure 6-4 Load and power generation curves and the identified low genset performance operating periods in the SC3, SC4, and SC5 for the medium electricity demand profile.....	180
Figure 6-5 Load and power generation curves and the identified low genset performance operating periods in the SC3, SC4, and SC5 for the low electricity demand profile.	182
Figure 6-6 Load and power generation curves and the identified low genset performance operating periods in the SC6, SC7, and SC8 for the high electricity demand profile.....	184
Figure 6-7 Load and power generation curves and the identified low genset performance operating periods in the SC6, SC7, and SC8 for the medium electricity demand profile.....	186
Figure 6-8 Load and power generation curves and the identified low genset performance operating periods in the SC6, SC7, and SC8 for the low electricity demand profile.	188

Figure 6-9 Fuel consumption and CO_{2e} emissions per year for different microgrid configurations with different electricity demand profiles.	190
Figure 6-10 PM_{2.5} and NO_x emissions per year for different microgrid configurations with different load profiles.	191
Figure 6-11 Life Cycle Cost over 25 years for different microgrid configurations with different load profiles.	193
Figure 6-12 Levelized Cost of Energy over 25 years for different microgrid configurations with different electricity demand profiles.	193
Figure 6-13 Pollutant emissions and LCOE comparison for selected HED scenario hybrid system configurations.	195
Figure 6-14 Pollutant emissions and LCOE comparison for selected MED scenario hybrid system configurations.	196
Figure 6-15 Pollutant emissions and LCOE comparison for selected LED scenario hybrid system configurations.	197
Figure 7-1 Load demand and power generation by source diagrams of selected scenarios (a) Baseline, b) Moderate PV Share, c) Low PV Share, d) Optimistic PV performance, e) Pessimistic PV Performance, f) Moderate BESS Capacity, and g) Low BESS Capacity) from the scenario analysis of the high electricity demand profile with SC7-GensetPV, and Battery (Li-ion).	205
Figure 7-2 Load demand and power generation by source diagrams of selected scenarios (a) Baseline, b) Moderate PV Share, c) Low PV Share, d) Optimistic PV performance, e) Pessimistic PV Performance, and f) Low BESS Capacity) from the scenario analysis of the medium electricity demand profile with SC7-GensetPV, and Battery (Li-ion).	209
Figure 7-3 Load demand and power generation by source diagrams of selected scenarios (a) Baseline, b) Moderate PV Share, c) Low PV Share, d) Optimistic PV performance, e) Pessimistic PV Performance, and f) Low BESS Capacity) from the scenario analysis of the low electricity demand profile with SC8-Genset, PV, and Battery (repurposed).	213
Figure 7-4 Scenario ranking for the high electricity demand profile considering six optimisation variables.	217
Figure 7-5 Scenario ranking for the medium electricity demand profile considering six optimisation variables.	219
Figure 7-6 Scenario ranking for the low electricity demand profile considering six optimisation variables.	220
Figure 7-7 Sensitivity analysis for the HED profile with SC1-Genset.	224
Figure 7-8 Sensitivity analysis for the HED profile with SC7-Genset, PV, and Battery (Li-ion).	225
Figure 7-9 Sensitivity analysis for the MED profile with SC1-Genset.	226

Figure 7-10 Sensitivity analysis for the MED profile with SC7-Genset, PV, and Battery (Li-ion).	227
Figure 7-11 Sensitivity analysis for the LED profile with SC1-Genset.	228
Figure 7-12 Sensitivity analysis for the LED profile with SC8-Genset, PV, and Battery (repurposed).	229

Table of Tables

Table 2-1 Sub-Saharan African countries as defined by the United Nations Development Program [12].	8
Table 2-2 Off-grid systems categorisation by size according to IRENA.	10
Table 2-3 Public diesel-PV hybrid mini-grids owned by Kenya Power & Lighting Company [27, 28].	13
Table 2-4 PV-diesel systems included in the mini-grid sizing guidebook.	16
Table 2-5 Hybrid Systems Optimisation Software and Tools.	18
Table 2-6 Key physicochemical properties for characterizing SVO and biodiesel.	34
Table 2-7 Physicochemical properties of selected vegetable oils, biodiesel, and diesel.	35
Table 2-8 Vegetable oil-diesel blends studied by several authors.	38
Table 2-9 Fuel specifications from selected standard limits.	40
Table 2-10 Stage V emission standards for nonroad engines [135].	41
Table 3-1 Development initiatives for biofuel in African countries.	49
Table 3-2 Vegetable Oil availability in Africa.	49
Table 3-3 Physicochemical properties of selected vegetable oils and red diesel.	50
Table 3-4 SVM 3000 Measuring Ranges.	54
Table 3-5 Engine test parameters.	57
Table 3-6 Diesel Generator and Load Bank Technical Specifications	59
Table 3-7 MEXA 7100 detection principles for gas measurement	60
Table 3-8 FTIR species with measuring ranges.	63
Table 3-9 Measuring ranges and calibration gas concentrations for MEXA 7100	67
Table 3-10 Castor oil and diesel content in fuel blends for the engine tests.	72
Table 4-1 TGA parameters for 7 castor oil-diesel blends.	78
Table 4-2 Net calorific values for 7 castor oil-diesel blends.	78
Table 4-3 Elemental analysis results for 7 castor oil-diesel blends.	81
Table 4-4 Density and kinematic viscosity at 30°C and 60°C the 5 castor oil-diesel blends used during engine lab work.	84

Table 4-5 Genset and engine load operating conditions as a percentage of the maximum genset and engine powers.	87
Table 4-6 Start of combustion in crank angle degrees for 5 castor oil-diesel blends at 5 engine loads.	97
Table 4-7 Ignition delay in crank angle degrees for 5 castor oil-diesel blends at 5 engine loads.	98
Table 4-8 Parameters for calculating HRR of COD blends.	99
Table 4-9 Peak heat release rate parameters for 5 castor oil-diesel blends at 5 engine loads.	101
Table 4-10 Diffusion phase peak heat release rate for 5 castor oil-diesel blends at 5 engine loads.	101
Table 4-11 Peak in-cylinder temperature and combustion duration for 5 castor oil-diesel blends at 5 engine loads.	102
Table 4-12 CO emission index and specific emissions for 5 castor oil-diesel blends at 5 engine loads.	108
Table 4-13 THC emission index and specific emissions for 5 castor oil-diesel blends at 5 engine loads.	108
Table 4-14 NO_x emission index and specific emissions for 5 castor oil-diesel blends at 5 engine loads.	109
Table 4-15 PM_{2.5} emission index and specific emissions for 5 castor oil-diesel blends at 5 engine loads.	111
Table 4-16 Total particle number and particle peak diameter for 5 castor oil-diesel blends at 5 engine loads.	117
Table 4-17 Nitrogen monoxide and nitrogen dioxide emissions for 5 castor oil-diesel blends at 5 engine loads.	122
Table 4-18 FB fuel injector hole size from SEM analysis.	124
Table 5-1 Diesel and Castor oil-diesel blends density values at different temperatures.	139
Table 5-2 Input parameters for the optimisation model.	145
Table 5-3 Test Points and weighting factors from ISO 8178 Test Cycles for type D2 engines.	147
Table 5-4 Torque and load factor by torque for COD blends at five engine conditions from lab work engine tests.	148
Table 5-5 NO_x and PM_{2.5} total weighted specific emissions and emission factor adjustment coefficients for 5 COD blends.	150
Table 5-6 Specifications for the high, medium, and low electricity demand scenarios (HED, MED, and LED).	155
Table 5-7 Relevant data for PV array selection (low, medium, and high installed capacity).	156
Table 5-8 Round-trip efficiency and DOD for Lead-acid, Li-ion, and repurposed batteries.	158
Table 5-9 CH₄ total weighted emission index for 5 COD blends.	160

Table 5-10 CO ₂ e emissions calculated from the CO ₂ and CH ₄ emissions generated by the combustion of castor oil.....	161
Table 5-11 CO ₂ e emission factors for tank-to-wheel and well-to-wheel GHG emission scenarios.	162
Table 6-1 Baseline optimisation scenario input conditions.....	169
Table 6-2 Optimised genset selection for high, medium, and low electricity demand profiles.	170
Table 6-3 Legend description for the total power and power generation by source curves.	172
Table 6-4 Power generation of G1 and G2 per operating period for the HED profile with SC8-Genset, PV, and Battery (repurposed).	183
Table 6-5 Baseline values for the LCOE vs emissions analysis.....	195
Table 7-1 Summary of the baseline optimisation scenario findings for three electricity demand profiles.....	202
Table 7-2 Cost optimisation model inputs required for the scenario analysis.....	203
Table 7-3. Summary of the high electricity demand profile scenario analysis reported as percentage variation from the baseline scenario.....	206
Table 7-4 Summary of the high electricity demand profile scenario analysis findings.....	207
Table 7-5 Summary of the medium electricity demand profile scenario analysis, reported as percentage variation from the baseline scenario.....	210
Table 7-6 Summary of the medium electricity demand profile scenario analysis findings.....	211
Table 7-7 Summary of the low electricity demand profile scenario analysis, reported as percentage variation from the baseline scenario.....	214
Table 7-8 Summary of the low electricity demand profile scenario analysis findings.....	215
Table 7-9 Sensitivity analysis input values with a brief description. ..	222
Table 8-1 Microgrid configurations considered in the cost optimisation model.	236
Table 8-2 Cost optimisation model inputs required for the scenario analysis.....	241

Table of Equations

Equation 2-1	14
Equation 2-2	14
Equation 2-3	14
Equation 2-4	14
Equation 2-5	14
Equation 2-6	20
Equation 2-7	20
Equation 2-8	20
Equation 2-9	20
Equation 2-10	20
Equation 2-11	20
Equation 2-12	20
Equation 2-13	21
Equation 2-14	21
Equation 2-15	22
Equation 2-16	22
Equation 2-17	22
Equation 2-18	23
Equation 2-19	30
Equation 2-20	30
Equation 3-1	61
Equation 3-2	61
Equation 3-3	68
Equation 3-4	68
Equation 4-1	84
Equation 4-2	85
Equation 4-3	89
Equation 4-4	91
Equation 4-5	95
Equation 4-6	99
Equation 4-7	107
Equation 4-8	107
Equation 4-9	110

Equation 4-10	110
Equation 5-1	136
Equation 5-2	136
Equation 5-3	136
Equation 5-4	136
Equation 5-5	136
Equation 5-6	136
Equation 5-7	137
Equation 5-8	137
Equation 5-9	137
Equation 5-10	137
Equation 5-11	137
Equation 5-12	139
Equation 5-13	139
Equation 5-14	139
Equation 5-15	139
Equation 5-16	140
Equation 5-17	140
Equation 5-18	140
Equation 5-19	140
Equation 5-20	140
Equation 5-21	141
Equation 5-22	141
Equation 5-23	141
Equation 5-24	141
Equation 5-25	141
Equation 5-26	142
Equation 5-27	142
Equation 5-28	142
Equation 5-29	142
Equation 5-30	143
Equation 5-31	143
Equation 5-32	143
Equation 5-33	143
Equation 5-34	143
Equation 5-35	143

Equation 5-36	143
Equation 5-37	143
Equation 5-38	143
Equation 5-39	143
Equation 5-40	143
Equation 5-41	143
Equation 5-42	143
Equation 5-43	143
Equation 5-44	143
Equation 5-45	144
Equation 5-46	144
Equation 5-47	144
Equation 5-48	144
Equation 5-49	144
Equation 5-50	144
Equation 5-51	147
Equation 5-52	147
Equation 5-53	148
Equation 5-54	150
Equation 5-55	151
Equation 5-56	151
Equation 5-57	151
Equation 5-58	151
Equation 5-59	151
Equation 5-60	151
Equation 5-61	151
Equation 5-62	152
Equation 5-63	152
Equation 5-64	152
Equation 5-65	152
Equation 5-66	152
Equation 5-67	152
Equation 5-68	152
Equation 5-69	152
Equation 5-70	152
Equation 5-71	152

Equation 5-72	153
Equation 5-73	153
Equation 5-74	159

List of Abbreviations

ACF	Annual Cash Flow
AFR	Air Fuel Ratio
ANP	Brazilian National Agency for Petroleum, Natural Gas and Biofuels
ARE	Alliance for Rural Electrification
ASTM	American Society for Testing and Materials
AVR	Automatic Voltage Regulator
BB	Branch and Bound
BC	Branch and Cut
BESS	Battery Energy Storage System
BMEP	Brake Mean Effective Pressure
BOS	Baseline Optimisation Scenario
BSD	Backscattered Electrons Detector
BSEC	Brake Specific Energy Consumption
BSFC	Brake Specific Fuel Consumption
bTDC	Before the Top Dead Centre
BTE	Brake Thermal Efficiency
CAD	Crank Angle Degrees
CEMGs	Clean Energy Mini-grids
CEN	European Committee for Standardization
CI	Compression Ignition
CLA	Chemiluminescence Analysis
CO	Carbon Monoxide
CO ₂	Carbon Dioxide
COD	Castor oil-diesel
cRIO	Compact Reconfigurable Input/Output
DIN	German Institute for Standardization
ECOWAS	Economic Community of West African States
EDX	Energy Dispersive X-ray
EENS	Expected Energy Not Supplied
EEP	Energy and Environment Partnership
EFA	Emission Factor Adjustment
EI	Emission Index
EIR	Energy Index Ratio
EOT	Engine Out Exhaust Gas Temperature
ESMAP	Energy Sector Management Assistance Program
ESS	Energy Storage System
FIA	Flame Ionization Analysis
FID	Flame Ionisation Detector
FIT	Fuel Injection Timing
FTIR	Fourier Transform Infrared

GA	Genetic Algorithm
GCV	Gross Calorific Value
GHG	Greenhouse Gas
GUI	Graphical User Interface
GWP	Global Warming Potential
HC	Hydrocarbons
HED	High Electricity Demand
HEPA	High Efficiency Particulate Absorbing
HOMER	Hybrid Optimization Model for Electric Renewables
HRR	Heat Release Rate
ID	Ignition Delay
IEA	International Energy Agency
ILAS	Integrated Laboratory Automation System
IRENA	International Renewable Energy Agency
IRES	Integrated Renewable Energy Systems
ISO	International Organization for Standardization
KPLC	Kenya Power & Lighting Company
LA	Level of Autonomy
LCC	Life Cycle Cost
LCOE	Levelized Cost of Energy
LED	Low Electricity Demand
LEMAS	Leeds Electron Microscopy and Spectroscopy Centre
LLD	Low Load Diesel
LMIP	Linear Mixed Integer Problem
LPSP	Loss of Power Supply Probability
MED	Medium Electricity Demand
MG	Microgrid
MILP	Mixed Integer Linear Programming
MPD	Magneto-Pneumatic Detection
NCV	Net Calorific Value
NDIR	Non Dispersive Infrared
NO	Nitrogen Oxide
NO ₂	Nitrogen Dioxide
NO _x	Nitrogen Oxides
NPC	Net Present Cost
NRE	Nonroad Engines
NREL	National Renewable Energy Laboratory
NZE	Net Zero Emissions
PHRR	Peak Heat Release Rate
PM	Particulate Matter
PSO	Particle Swarm Optimisation
PV	Photovoltaic
PVGIS	Photovoltaic Geographical Information System
RES	Renewable Energy Systems
SA	Simulated Annealing
SAS	Sustainable Africa Scenario

SC	System Configuration
SDG	Sustainable Development Goal
SE	Specific Emissions
SEM	Scanning Electron Microscope
SFC	Specific Fuel Consumption
SLCP	Start of Late Combustion Phase
SMCC	Start of Mixing-Controlled Combustion
SOC	Start of Combustion
SONABHY	National Oil Products Company of Burkina Faso
SPC	Start of Premixed Combustion
SSA	Sub-Saharan Africa
STEPS	Stated Policies Scenario
SVO	Straight Vegetable Oil
TDC	Top Dead Centre
TGA	Thermo-gravimetric analysis
THC	Total Hydrocarbon
TTW	Tank-To-Wheels
TWEI	Total Weighted Emission Index
TWSE	Total Weighted Specific Emissions
VO	Vegetable Oil
VOCs	Volatile Organic Compounds
WSE	Weighted Specific Emissions
WTT	Well-To-Tank
WTW	Well -To- Wheels

Nomenclature

Functions

C^{cap} :	Capital cost [£].
C^{mnt} :	Maintenance cost [£].
C^{op} :	Operating cost [£].
C^r :	Replacement cost [£].

Sets

B :	Set of candidate fuel blends (4 blend ratios blends).
G :	Set of candidate diesel generators considered in the model (7 gensets of different sizes).
M :	Set of months within each analysis period (12 months).
P :	Set of project analysis periods (25 years).
T :	Set of operating periods (24 hours).

Indices

bld :	Index of fuel blend number, $bld \in \{100,80,60,50\}$
g :	Index of diesel generators
m :	Index of months within each project analysis period.
p :	Index of analysis project periods.
t :	Index of operating periods.

Parameters

a_{bld} :	Curve slope from the fuel consumption equation.
b_{bld} :	“Y” intercept from the fuel consumption equation.
bp_{bld} :	Blend purchase price [£/l].
bEf_{bld} :	Fuel blend emission factor [kgCO ₂ e/l].
BEF_g^{NOx} :	NO _x base emission factor [g/kWh].
$BEF_g^{PM_{2.5}}$:	PM _{2.5} base emission factor [g/kWh].
C^{batt} :	Battery system investment cost [£].

C^{inver} :	Inverter initial investment cost [£].
C^{PV} :	PV system initial investment cost [£].
Cap^{batt} :	Battery capacity [kWh].
$cost^{batt}$:	Cost of the battery [£/kWh].
$cost^{inver}$:	Cost of the inverter [£/kW].
$cost^{PV}$:	Cost of the PV system [£/kWp].
$C_{bld,g}^{CO_2}$:	Carbon dioxide (CO ₂) emissions cost [£].
$C_{bld,g}^{fuel}$:	Fuel consumption cost [£].
$C_{bld,g}^{NO_x}$:	Nitrogen Oxides (NO _x) emissions cost [£].
$C_{bld,g}^{PM_{2.5}}$:	Particulate Matter (PM _{2.5}) emissions cost [£].
C_g^{gen} :	Diesel generator initial investment cost [£].
$C_p^{battrpl}$:	Battery replacement cost [£].
$C_p^{inverpl}$:	Inverter replacement cost [£].
C_p^{PVrpl} :	PV replacement cost [£].
$C_{g,p=estglf}^r$:	Genset replacement cost [£] at the estimated replacement period <i>estglf</i> .
df :	Discount factor.
dr :	Degradation rate.
$EFA_{bld}^{NO_x}$:	NO _x emission factor adjustment.
$EFA_{bld}^{PM_{2.5}}$:	PM _{2.5} emission factor adjustment.
E_{day_g} :	Genset electricity generation per day [kWh].
E_p^{batt} :	Electricity delivered by the battery to the load [kWh/year].
E_p^{gen} :	Total electricity delivered by the genset [kWh/year].
$E_p^{gen_{batt}}$:	Electricity delivered by the genset to the battery [kWh/year].
$E_p^{gen_{load}}$:	Electricity delivered by the genset to the load [kWh/year].
E_p^{load} :	Electricity delivered by the genset and the PV to the load [kWh/year].
E_p^{system} :	Total electricity delivered by the system [kWh/year].
E_p^{PV} :	Total electricity delivered by the PV system [kWh/year].
$E_p^{PV_{batt}}$:	Electricity delivered by the PV to the battery [kWh/year].

E_p^{PVload} :	Electricity delivered by the PV to the load [kWh/year].
E_t^{batt} :	Battery available energy [kWh].
$Fu_{bid,g,t}$:	Amount of fuel consumption of each genset [l/h].
g_g^{upc} :	Genset upfront cost [£/kW].
glf_g :	Genset lifetime [h].
$glfa_g$:	Genset load factor adjustment.
gp_g :	Genset cost [£].
Hga_g :	Genset annual operating hours [h].
$Hgcm_{g,m}$:	Genset cumulative monthly operating hours [h].
Hgd_g :	Genset daily operating hours [h].
Hgm_g :	Genset monthly operating hours [h].
$inst^{PV}$:	Installed PV system [kW].
LCC^{batt} :	Battery Life Cycle Cost or Net Present Cost (NPC) [£].
LCC^{gen} :	Genset Life Cycle Cost or Net Present Cost (NPC) [£].
LCC^{gen_batt} :	Associated costs of the energy generated by the gensets to charge the battery [£].
LCC^{gen_load} :	Associated costs of the energy generated by the gensets to supply the load [£].
LCC^{PV} :	PV Life Cycle Cost or Net Present Cost (NPC) [£].
LCC^{PV_batt} :	Associated costs of the energy generated by the PV to charge the battery [£].
LCC^{PV_load} :	Associated costs of the energy generated by the PV to supply the load [£].
LCC^{system} :	System Life Cycle Cost or Net Present Cost (NPC) [£].
$LCOE^{system}$:	System Levelized Cost of Electricity [£/kWh].
$mntdays$:	Estimated genset maintenance days [days].
$pdays$:	Days considered for the analysis period [days].
P_g^{genmax} :	Max genset output power (genset prime power) [kW].
P_g^{genmin} :	Min acceptable genset output power (60% of the genset prime power) [kW].
$P_g^{selectedmax}$:	Prime power of the selected gensets [kW].

$P_t^{battmaxdischar}$:	Maximum battery discharging power [kW].
P_t^{RE} :	PV system output power [kW].
r :	Real discount rate [%].
$servc$:	Annual service cost [£/kW].
$size_g^{eng}$:	Genset prime power [kW].
SoC^{max} :	Battery maximum state of charge [%].
SoC^{min} :	Battery minimum state of charge [%].
tax^{carbon} :	Cost related to CO ₂ emissions [£/kgCO _{2e}].
U :	Maximum number of operating gensets.
YCF_p^{batt} :	Battery system yearly cash flow [£].
YCF_p^{gen} :	Genset yearly cash flow [£].
YCF_p^{PV} :	PV system yearly cash flow [£].
η :	Battery roundtrip efficiency [%]
η^{batt} :	Battery efficiency [%].
ρ_{bld} :	Blend density [kg/l].

Variables

$char_t \in \{0,1\}$:	Battery charging periods.
$dischar_t \in \{0,1\}$:	Binary discharging periods.
$genslack_{g,t}$:	Slack variable for operating a genset below the determined limits.
$k_{g,t,bld} \in \{0,1\}$:	Fuel blend selection in each operating period.
$K_{p=1,bld} \in \{0,1\}$:	Fuel blend selection in the analysis period.
$P_{g,t}^{gen}$:	Genset output power [kW].
$P_t^{battchar}$:	Battery charging power [kW].
$P_t^{battdischar}$:	Battery discharging power [kW].
$replace_{g,m}^{engine} \in \{0,1\}$:	Replace engine.
$replace_{g,m}^{alternator} \in \{0,1\}$:	Replace alternator.
$s_{g,t} \in \{0,1\}$:	Genset selection.
$w_{g,t} \in \{0,1\}$:	Genset operating periods.

Chapter 1

Introduction

Increasing electricity access in rural areas from developing countries and reducing the environmental impact of the energy sector are two of the challenges addressed by the United Nations 2030 Agenda for Sustainable Development, set in 2015 [1]. The agenda includes 17 Sustainable Development Goals (SDGs) and 169 targets covering the three pillars of sustainable development (economic, social and environmental). Although significant progress was made to increase electrification rates between 2010-2020 for achieving SDG7¹[2], Sub-Saharan Africa remains to be the least electrified region, where 568 million people have no access to electricity [3].

For expanding electricity access in places where national grid extension is unfeasible or where the grid provides an intermittent supply of electricity, mini-grid deployment is being considered. Mini-grids are small-scale electricity generation systems (10 kW to 10MW) that operate independently from the national grid and can serve a limited number of customers [4]. When mini-grids incorporate renewable energy generation sources, they are known as hybrid systems. Solar hybrid systems have become the most common type of system installed today as they can be easily installed in remote areas [5]. It has been estimated by the World Bank that about 140,000 mini-grids are needed in Africa for meeting the universal energy access goal by 2030 [6].

1.1 Background and Motivation

The electrification and environmental challenges mentioned above lead this project to contribute to achieving SDG7. The contribution is projected to be according to efficiency improvements for better energy mix integration within hybrid microgrids. Finding the optimum solution to enhance the coexistence between conventional and renewable energy technologies is most for having a brighter future for electricity generation. This research highlights that there is not always a “one size fits all” solution for common challenges; it untangles a very significant flaw detected within the planning stage of hybrid micro and mini-grid systems for rural electrification.

The flaw is caused by the common sizing techniques for selecting an important element of the system, the diesel generator or genset, which is hardly substituted by renewable energy systems (RES). A rough sizing technique tends to cause excessive fuel consumption that translates into high operating

¹ SDG7: ensure access to affordable, reliable, sustainable and modern energy for all.

costs and high environmental impacts. Typically, microgrids are designed to serve a total level of peak or sustained load with a certain schedule. Diesel-based microgrids are widely used around the world because they present a relatively low upfront capital cost [7] but relying on diesel generators for rural electrification is becoming unsustainable due to high fuel dependency, price volatility, and availability of fossil fuels [8]. Even in countries with subsidised fuels, the final cost of generation is increased when oil products should be delivered to remote communities [9]. Especially since 2021 with the soaring oil prices, as they increment the already high operating cost of gasoline and diesel generators, which are common solutions for stand-alone systems in African countries [10]. Hence, the use of diesel generators brings an interesting situation when speaking of microgrids, and distributed generation systems implementation.

The high operating costs and environmental impacts caused by the excessive fuel consumption of diesel generators that can supply electricity in rural areas is a problem that should be addressed to generate electricity reliably and cost-effectively. Efforts to solve this problem have been made with the inclusion of RES into diesel microgrids that operate in standalone mode (which is a proper operation in most rural areas). As those microgrids highly depend on gensets, the problem continues. The inadequate fuel consumption results from merging different factors such as the so-called oversized configuration and common system design techniques for selecting gensets, the unpredictable electricity demand, the share of RES included, the inertia from rural communities to integrate RES, and the slow biofuel utilisation. These factors affect the generators' performance, directly or indirectly, and increase the operating cost of the system.

In literature, it can be found plenty of work dedicated to improving the performance of mini-grids as a whole, where reducing the use of gensets has become a synonym for reducing fuel consumption by installing bigger battery storage systems. Few studies have been found addressing the performance of diesel generators from the engine-alternator configuration but none of them considers biofuel blend utilisation. Even though some evidence was found revealing that using more than one diesel generator results in fuel savings, to the knowledge of the author, no study considers the effects of castor oil-diesel blends or the impact of RES inclusion for generator selection based on the engine's performance. Therefore, this work is dedicated to finding a solution to improve the performance of diesel generators within hybrid microgrids, considering the effect of biofuel blends and RES share, to reduce their fuel

consumption and environmental impact, which highly depends on the operating characteristics of the whole system.

This background motivates the development of a cost optimisation model capable of including the variety of factors affecting the fuel consumption of a diesel generator through a closer study of the interactions occurring among the fuel, the genset, the renewable energy share and the battery type installed in a microgrid. Developing the cost optimisation model was the major task of this research and was done by integrating the factors shown in the diagram from Figure 1-1. The branches linked to the power label in the diagram can be classified as the chemical-mechanical group (left) and the mechanical-electrical group (right), all of which influence the performance of the diesel generator. On the other hand, the branches that appear below the power label, represent the variables by which the optimisation model determines the convenient genset selection for minimising the fuel consumption, the operating costs and the pollutant emissions of the system.

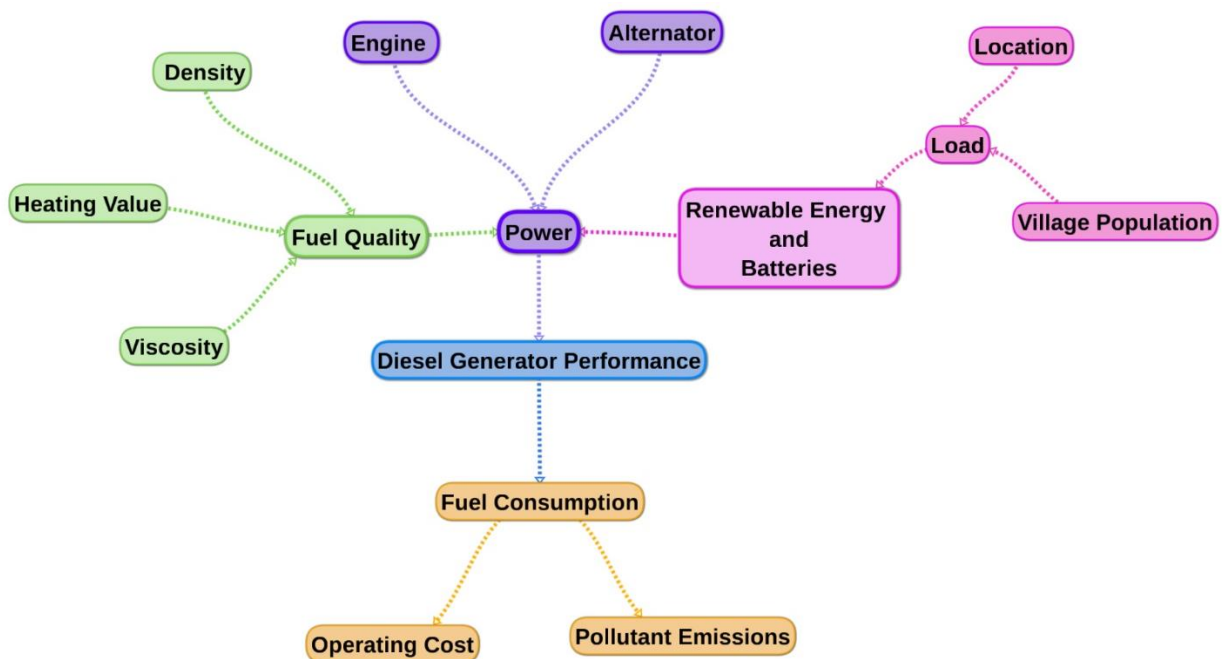


Figure 1-1 Diagram of the factors affecting the performance of a diesel generator that operates in a microgrid.

By optimising the interaction among the factors presented in Figure 1-1, the model determines a cleaner and cost-effective solution for satisfying a given electricity demand profile, after evaluating the impact of biofuel blends, renewable energy share, and battery systems on the generators' performance.

1.2 Aims and Objectives

The overall aim of this research is to optimise diesel generators' performance within hybrid microgrids, considering the effect of biofuel blends to contribute to SDG7. Specifically, the research aims to reduce the cost and environmental impact related to diesel utilisation for electricity generation in African rural areas and assess a locally available vegetable oil (castor oil) blended with diesel for widening the fuel options to power the generators of different microgrid configurations.

Objectives:

1. To assess the performance of a diesel generator with castor oil-diesel blends to evaluate the variation in fuel consumption and pollutant emissions for specific power outputs.
2. To find an equation or set of equations for better fuel consumption estimation that can be adapted for biofuel blends.
3. To develop a cost optimisation model for hybrid microgrids, able to consider the effects that biofuel blends, renewable energy share (PV), and battery systems have on the generator's performance.
4. To optimise the selection of diesel generators to improve their performance within microgrids (hybrid or conventional), to satisfy a required demand (either at load low demand or total peak demand), with the minimum cost and the least environmental impact, for any village size in rural areas.
5. To compare the selection of diesel generators and the LCOE of different microgrid configurations for different electricity load profiles.

1.3 Thesis Outline

This thesis is divided into eight chapters, a brief outline is listed below.

Chapter 1. Introduction

The background and motivation of this work are included in Chapter 1. The chapter addresses the aims and objectives of this research and outlines the thesis structure.

Chapter 2. Literature Review

This chapter presents the literature survey relevant to this project. It starts with an overview of the electrification status in developing countries, followed by a summary of the mini-grid projects implemented around the world, including their

common economic parameters and sizing techniques. Then, diesel generators are presented as a key element of mini-grids with a brief description of their working principle and performance parameters. Evidence from the poor performance of diesel generators in mini-grids is included as well as an overview of the performance improvement attempts reported by several authors. For further understanding of the performance of diesel generators, the combustion process of diesel engines is included, considering the effect of biofuels. Finally, a theoretical background of the method and algorithms for building the proposed cost optimisation model is presented at the end of the chapter.

Chapter 3. Experimental Work Methodology

This chapter has three sections. The first one explains the fuel selection process and the analytical lab techniques required to characterise the fuel blends that were used during the engine lab work. The second one describes the engine lab work and provides a brief explanation of the operating principles of each instrument, as well as the procedure followed during the engine tests to assess the parameters related to the performance of a diesel generator. Finally, the third section describes the analysis done on the engine's fuel injector once the engine tests were completed, for evaluating the impact of using biofuel blends.

Chapter 4. Biofuel Blends Impact on Diesel Generator's Performance

Chapter 4 presents the findings on the fuel blend characterisation, the engine's combustion performance, and the pollutant emissions from the combustion process. This chapter also includes a discussion regarding the impact produced by the biofuel blends on the engine's fuel injector.

Chapter 5. Cost Optimisation Model Development

This chapter presents the mathematical formulation of the cost optimisation model developed for a hybrid microgrid (diesel/PV/battery) that considers biofuel options to assess the genset's performance. The chapter also presents the graphical user interface (GUI) that was created for the optimisation scenarios selection and the optimisation results visualisation.

Chapter 6. Cost Optimisation Model Implementation: Baseline Optimisation Scenario

Chapter 6 is divided into four sections. The first section introduces the assumptions and specifications considered for a baseline optimisation scenario. The second part of the chapter presents the findings of the baseline optimisation scenario for 8 microgrid system configurations, using three electricity demand profiles. The third section includes an economic assessment of the eight systems and an LCOE vs. emissions analysis to determine the configuration with the major environmental and financial benefits. Finally, the last part of the chapter gives a review of the main findings presented.

Chapter 7. Scenario and Sensitivity Analysis for Selected Microgrid Systems

This chapter presents the findings of the scenario and sensitivity analysis done on the system configurations selected from the LCOE vs. emissions analysis presented in Chapter 6. The results show the impacts on the gensets' performance, the fuel selection, and the LCOE after varying some of the baseline optimisation input conditions and certain economic parameters.

Chapter 8: Conclusions

The final chapter summarises the findings of this work, emphasizing the importance of keeping diesel generators within the recommended operating limits to improve their performance within hybrid microgrids. Some future work is recommended regarding vegetable oil-diesel blends for further development of the presented cost optimisation model.

Chapter 2

Literature Review

This chapter presents relevant data and concepts that support the aims and objectives of this research. It starts with an overview of the electrification status in developing countries, followed by a summary of the mini-grid projects implemented around the world, including their common economic parameters and sizing techniques. Then, diesel generators are presented as a key element of mini-grids with a brief description of their working principle and performance parameters. Evidence from the poor performance of diesel generators in mini-grids is included as well as an overview of the performance improvement attempts reported by several authors. For further understanding of the performance of diesel generators, the combustion process of diesel engines is included, considering the effect of biofuels. Finally, a theoretical background of the method and algorithms that were used to develop the proposed solution for improving the performance of diesel generators within hybrid microgrids (a cost optimisation model) is presented at the end of the chapter.

2.1 Electrification Status in Africa and Developing Countries

The electricity access status reported by the International Energy Agency (IEA) in the World Energy Outlook 2021 report [11], mentions that 770 million people have no access to electricity, with the majority located in Africa and developing countries in Asia. The report highlights that the COVID-19 crisis slowed the electrification process in different regions and that, for the first time since 2013, the number of people without access in sub-Saharan Africa (SSA) increased in 2020 [11]. Similarly, the Africa Energy Outlook 2022 [10] mentions that 600 million people in Africa have no access to electricity (43% of the African population), and 590 million are located in SSA. Sub-Saharan Africa is formed by the 46 countries that appear in Table 2-1, according to the United Nations Development Program [12].

Table 2-1 Sub-Saharan African countries as defined by the United Nations Development Program [12].

Angola	Congo	Guinea	Mozambique	South Sudan
Benin	Côte d'Ivoire	Guinea-Bissau	Namibia	Togo
Botswana	The Democratic Republic of the Congo	Kenya	Niger	Uganda
Burkina Faso	Equatorial Guinea	Lesotho	Nigeria	United Republic of Tanzania
Burundi	Eritrea	Liberia	Rwanda	Zambia
Cabo Verde	Eswatini (Kingdom of)	Madagascar	Sao Tomé and Príncipe	Zimbabwe
Cameroon	Ethiopia	Malawi	Senegal	
The central African Republic	Gabon	Mali	Seychelles	
Chad	Gambia	Mauritania	Sierra Leone	
Comoros	Ghana	Mauritius	South Africa	

About 50% of the SSA population without electricity access live in the Democratic Republic of Congo, Ethiopia, Nigeria, Tanzania, and Uganda [10]. Increasing electricity access in SSA will require the Sustainable Africa Scenario (SAS), which aims for implementing all the African climate pledges, including universal access to modern energy by 2030. Under the SAS, achieving affordable electricity requires connecting around 90 million people each year, three times the current connection rates [10]. The progress should be even faster in rural areas where more than 80% of the African population live without electricity access. Within this scenario, reaching universal access to electricity by 2030 relies on mini-grids and stand-alone systems deployment. Mini-grids are the most appropriate type of system for rural electrification as national electricity grid extension is too expensive and mini-grids provide benefits such as speed of deployment and flexibility of technical and operational models, especially when renewable energy sources are included [13]. However, although 70% of the stand-alone systems are renewable-based, the rest is comprised of diesel or gasoline generators [10]. Generators are common solutions in some African countries despite their high operating costs as they have a low upfront cost.

The IEA projections reveal that most developed countries in Asia will achieve universal access by 2030, however, in SSA countries only 60% of the access will be achieved by the end of the decade if not all governments reach their goals as assumed in the

Stated Policies Scenario (STEPS) [11]. In contrast, with the Net Zero Emissions by 2050 Scenario (NZE), which addresses the SAS, key energy-related goals from the United Nations could be met, particularly gaining universal access by 2030 with major air quality improvements. For the NZE scenario to happen, the new connections should be implemented through mini-grids and stand-alone systems [11]. Although meeting any of the scenarios is a challenging task, Africa's situation ought to be solved because it is the poorest continent in the world and its poverty is related to the lack of access to energy [14]. Longe et al. [15] mention that sub-Saharan countries roughly generate the same amount of power as that generated in Spain; power consumption per capita is about 124 kWh per year (a tenth of that found elsewhere among developing countries).

2.2 Electricity Systems Diversity: Definitions and SSA Solutions

To clarify the concepts of the various systems that can be used to provide electricity access, the definitions expressed by the IEA [16] are included below.

On-grid: provides electricity access through a connection to a local network or grid extension linked to a transmission network. The power is produced by a centralised power plant such as coal, natural gas, hydro, etc.

Decentralised systems: this term generally refers to off-grid systems and mini-grids.

Mini-grid: is a localised power network, without transmission infrastructure beyond its service area. It relies on modular generation technologies (solar PV, wind turbines, small-scale hydropower, and diesel generators). It needs a stable flow of power, often supplied by backup diesel generators or battery energy storage systems (BESS).

Off-grid: refers to a stand-alone system that is not connected to a grid. Diesel generators and PV systems are commonly used to provide electricity access.

Another important definition is the one for microgrids, as cited by Ainah and Folly [17]:

“A single electrical power subsystem associated with a small number of distributed energy resources, both renewable and/or conventional sources, including photovoltaic, wind power, hydro, internal combustion engine, and gas turbine together with a cluster of loads and it mainly relies on the robust performance of diesel generators.”

The microgrid definition stated above goes in hand with the definition mentioned by Raymond Kimera et al. [8] which describes a hybrid microgrid as a system designed to incorporate renewable energy generation technologies with a conventional diesel generator.

In this work, the term off-grid system refers to either mini-grids or stand-alone systems, where both operate independently of a national electricity grid, as defined by the Alliance for Rural Electrification (ARE) [4]. The reader should be aware that mini-grid and microgrid terms are sometimes interchangeable terms, however, the main difference between those systems is their size and electricity generation capacity. According to the Mini-grid Policy Toolkit [13], mini-grids can generate from 10 kW to 10 MW, while microgrid capacity is in the range of 1 to 10 kW. Mini and microgrids connect a limited number of consumers to meet their electrical needs within proximity. On the other hand, stand-alone systems mainly consisting of small diesel generators and PV solar can generate up to 150 Wp¹. Those values agree with the off-grid system categorisation by size (installed capacity) suggested by IRENA [18], as shown in Table 2-2.

Table 2-2 Off-grid systems categorisation by size according to IRENA.

System	Size (kW)
Standalone	0 – 0.1
Picogrid	0 – 1
Nano grid	0 – 5
Microgrid	5 – 100
Mini-grid	0 – 100 000

The definitions above clarify why Ainah and Folly [17] suggest that one solution to improve electric power conditions in sub-Saharan Africa is the use of distributed generation in microgrid systems, even though there are technical challenges to integrating them in a cost-effective, reliable and efficient way. This idea is supported by the Mini-grids Market Report [5], which considers mini-grid technology as the most suitable option for many areas with low or medium density.

Moreover, microgrids might represent energy systems with economic benefits and environmental friendliness if renewable energy is included. Fortunately, in sub-Saharan Africa, there are abundant renewable energy sources and among the 35 top countries leading in solar, wind, hydro and geothermal resources, 17 are located in Africa [15]; these sources could be used especially to electrify rural areas.

There is evidence that for increasing electrification rates some microgrid projects had been implemented in sub-Saharan countries such as Nigeria, Uganda, Zambia, Kenya, Ghana, Tanzania, and some others; the descriptive discussion of individual projects is contained in [17]. Similarly, Hirsh et al. [19] explain that microgrids have been deployed in different countries and that

¹ Watt Peak (Wp) is the unit to specify the achievable output power of a solar module under full solar radiation.

hybrid microgrids have the potential to lower microgrid operating costs in island communities and remote areas.

Although Africa is the continent with the most challenging electrification situation, limited research about the practical experience of renewable energy mini-grids has been carried out [20]. The latter can be attributed to the common national electrification plans in sub-Saharan Africa, which generally focus on electricity grid expansion, with fossil-fuel-based or hydroelectric generation facilities, and also because the existing off-grid electricity supply is mainly constituted by diesel-power generators [21]. However, it has been projected by IRENA [22] that nearly 60% of the additional electricity generation should be supplied by off-grid systems for meeting universal access to electricity in Africa. Figure 2-1 presents a qualitative representation of the wide opportunity for mini-grid development, considered the best option for rural electrification.

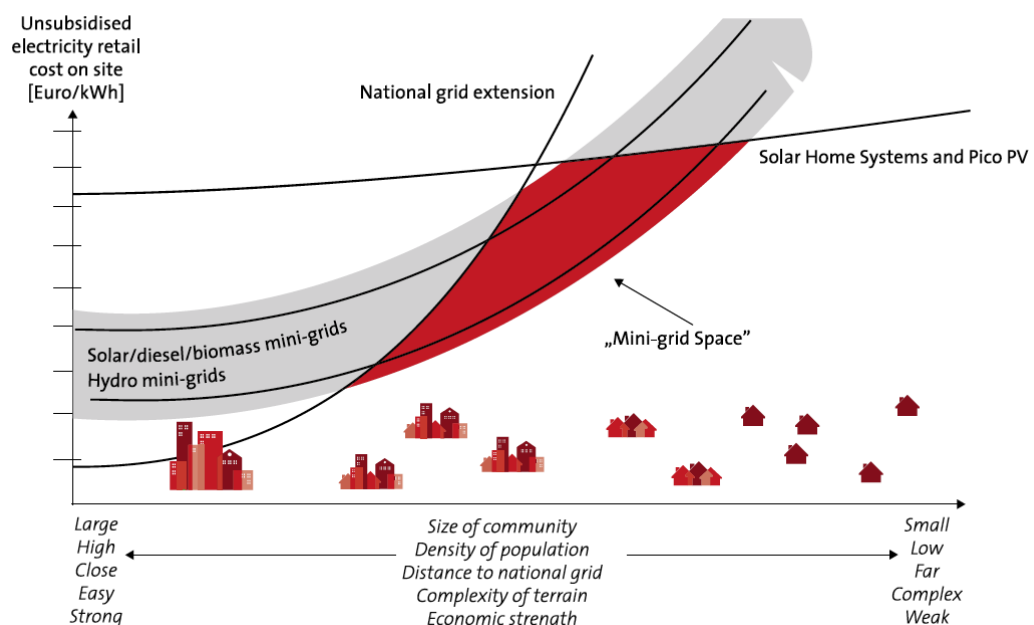


Figure 2-1 Qualitative representation of mini-grid as the most suitable solution for rural electrification [13].

2.3 Mini-grid Status Around the World

A survey conducted by the Energy Sector Management Assistance Program (ESMAP), the first attempt for counting and characterising mini-grids on a global scale, suggests that there are about 19,163 mini-grids globally, and around 1,465 are in sub-Saharan Africa. Most of the projects are between 10 and 100 kW in size but hundreds are 500 kW or larger. In developing countries, the mini-grids are mostly small diesel and hydro-powered systems serving 200 to 2000 people. There are 7,507 mini-grids planned for global development, mostly solar or solar hybrid. More than 4,000 are planned for Africa, from which 1,217 will be

in Senegal and 879 in Nigeria, the rest in diverse locations. Data suggest that more than 80 percent of planned mini-grids will use solar PV, while about half of the existing mini-grids run only on diesel generators [23]. Also, according to [5] there is a strong mandate for hybridising diesel mini-grids with solar energy, therefore, many modern systems incorporate PV and BESS combined with diesel generators for providing cleaner and more reliable electricity. Regarding BESS, lead-acid batteries are commonly used for rural electrification, but lithium-ion batteries have become of interest in recent years.

2.3.1 Mini-grids in Africa

According to the ECREE report [24], in West Africa, within the Economic Community of West African States (ECOWAS)² region, the total installed capacity related to clean energy mini-grids (CEMGs)³ is around 21 MW of which diesel generators represent 49%. The average size of PV-diesel systems is 28 kWp solar PV and 60 kVA diesel generators, giving a diesel–PV ratio of 2.14. The smallest and largest PV-diesel hybrid systems are located in Mali, the 6.9 kWp/ 8 kVA is in Kandia village and there are two systems of 384 kWp/ 675 kVA each one in Bankas and one in Koro village respectively [24].

The Opportunities and Challenges in the Mini-Grid Sector in Africa report [25], mentions that in the Southern and East African countries, covered by the Energy and Environment Partnership (EEP) mini-grid portfolio⁴, Tanzania is the dominant country with 17 projects of mini-grid systems. In the East solar and hydropower systems are common, whereas, in the southern region, projects include biomass and waste-to-energy components [25].

On the other hand, according to a case study report for Kenya mini-grids [26], in Kenya there are private, public, and community-own mini-grids, but the sector is dominated by public mini-grids owned by Kenya Power & Lighting Company (KPLC) [26]. Table 2-3 shows the details of the hybridised (diesel-solar) systems reported for Kenya.

² ECOWAS region: Cape Verde, Senegal, The Gambia, Guinea Bissau, Guinea, Sierra Leone, Liberia, Cote D'Ivoire, Burkina Faso, Ghana, Togo, Benin, Nigeria, Mali, Niger.

³ Defined by the Sustainable Energy for All Initiative (SE4All) as mini grids powered by renewable energy or hybrid systems that include renewable energy and fossil fuel generation.

⁴ EPP mini-grid portfolio: Botswana, Burundi, Kenya, Mozambique, Namibia, Rwanda, South Africa, Tanzania, Uganda, and Zambia.

Table 2-3 Public diesel-PV hybrid mini-grids owned by Kenya Power & Lighting Company [27, 28].

County	Locality	Diesel Installed Capacity (kW)	Solar Installed Capacity (kW)	Number of Customers
Homa Bay	Mfangano	650	10	3000
Isiolo	Merti	250	10	1485
Mandera	Elwak	740	50	1700
Mandera	Mandera	3,130	330	8000
Mandera	Rhamu	520	50	400
Mandera	Takaba	320	50	500
Marsabit	Laisamis	264	80	160
Tana River	Hola	800	60	1300
Turkana	Lodwar	3425	60	9598
Wajir	Eldas	184	30	342

In Tanzania, according to the Accelerating Mini-grid Deployment in sub-Saharan Africa report [29], there are about 109 mini-grids with a total installed capacity of 158 MW of which 46% is fossil fuel-based. In terms of the number of mini-grids, hydro represents 45%, biomass 22%, fossil fuel systems 17.4%, solar 11.9 %, and hybrid only 2.8 % of the total number of systems. Still, often the preferred option across the country for off-grid systems is diesel mini-grids as they are inexpensive to procure and many technicians are familiar with their operation and maintenance, nevertheless, they are expensive to operate and maintain. Their operation factors range from 20 to 50 percent, depending on if the system serves a village/district township, a regional township, or if it is a small unlicensed mini-grid that supplies small clusters of households. There are sixteen plants operated with internal combustion engines that can run on diesel or straight vegetable oil from *Jatropha* plant seeds, they are known as flex-fuel systems. Of the 3 hybrid systems that have been implemented in Tanzania one of them is a 24 kW/60 kWp diesel-PV solar that connects 250 customers [29].

2.3.2 Cost of Electricity of Mini-grids

In terms of electric power generation, a desirable project is one capable of supplying the electricity demand but having minimum capital and operating costs [30]. In recent years, the reduction in PV and BESS costs has made hybrid systems highly compelling compared to conventional (diesel) mini-grids [5]. The economic comparison for different projects could be done by calculating

the annual cash flow (ACF), the life cycle cost (LCC), the levelized cost of energy (LCOE), or the annualized maintenance, operating and replacement costs using Equation 2-1 to Equation 2-5 [30], but LCOE is often used.

The annual cash flow given by Equation 2-1 calculates the expected expenses for a certain year of the project.

$$C(j) = C_c(j) + C_o(j) + C_m(j) + C_r(j) \quad \text{Equation 2-1}$$

where, $C(j)$ is the energy system cost in the year j while C_c , C_o , C_m , and C_r are the capital, operational, maintenance, and replacement cost of the energy system in the year j , respectively.

The LCC shown in Equation 2-2 determines the cost of the project over its lifetime.

$$LCC = \sum_{j=1}^N \frac{C(j)}{(1+d)^j} \quad \text{Equation 2-2}$$

where, N is the number of years in the project and d represents the annual discount rate.

The levelized cost of energy given by Equation 2-3 is a useful method to compare the total cost of energy of different electrification options.

$$LCOE = \frac{LCC}{\sum_{j=1}^N \left(\frac{E_{GEN}(j)}{(1+d)^j} \right)} \quad \text{Equation 2-3}$$

where, E_{GEN} is the energy output of the system in the given year j .

The annualized maintenance, operating and replacement cost computes the expected cost of power production after the equipment capital cost has been provided. The operational system expense is given by Equation 2-4, and Equation 2-5 is the annualized expense that calculates the average yearly expenses needed to keep the system operating [31].

$$C_{op}(j) = C_o(j) + C_m(j) + C_r(j) \quad \text{Equation 2-4}$$

$$AV_{op} = \left(\frac{d(1+d)^j}{(1+d)^j - 1} \right) \cdot \left(\sum_{j=1}^N \frac{C_{op}(j)}{(1+d)^j} \right) \quad \text{Equation 2-5}$$

Using the equations above, Akinyele [30] compared different nano-grids able to supply a 12.51 kWh demand of 5 rural houses in Nigeria. He concluded that the initial cost of the diesel nano-grid was around 6-22% lower than the other systems (hybrid systems), but the author observed a higher LCC due to fuel costs. Similarly, Szabó et al. [32] reported from their spatial electricity cost model that fuel consumption represents the major portion of the levelized cost. They noted that further analysis of biomass, hybrid microgrids, and adequate fuel use is required over a vast African region, to determine a viable solution for rural energy services, due to their high sensitivity to diesel prices.

2.3.3 Mini-grid Sizing and Design

Off-grid systems have different sizes, components, and operating conditions. Every country follows its guidelines for mini-grid implementation. In Africa, for example, the Tanzanian operating guidelines state that microgrids are typically for less than 250 customers, but the number could be higher [33]. In Senegal, a mini-grid could be placed in areas with a household density greater than 50 households per km² [34] and there are some hybrid mini-grids (solar-diesel or solar-wind-diesel) that can provide electricity in villages with approximately 700 inhabitants [35]. These differences, especially if several countries are compared at the same time, might bring complications and confusion during an off-grid system sizing and design. Considering this, in the year 2000 the Energy Sector Management Assistance Program (ESMAP) published a mini-grid design manual to have a specific guideline that homogenises microgrid design and implementation [36]. The manual encourages and supports the design of better electrification schemes in rural villages. Also, there are some useful recommendations such as those included in the mini-grid sizing guidebook [37]. The guidebook mentions that combining PV with diesel generators or storage systems is usually the least-cost option for electrifying rural communities, which makes those systems a viable set-up for sub-Saharan projects. The guidebook also emphasises that every village and community has different needs and conditions, hence no standard for sizing a mini-grid could be dictated but the recommendations can be adapted accordingly. The guidebook includes the three different PV- diesel configurations shown in Table 2-4.

Table 2-4 PV-diesel systems included in the mini-grid sizing guidebook.

System Configuration	Description
PV-battery with diesel generator back-up	The battery leads the cost of the system, the diesel generator is only used when the solar power or the battery state of charge are low. The design for this configuration usually allows three days of autonomy for the system.
PV-diesel	This design has the lowest initial investment cost. Diesel generators operate during demand periods as required and ensure the quality of the system.
PV-diesel-battery	This configuration allows the battery to cover the demand during low load periods, it is charged with the excess energy from the PV and diesel generator. The design does not consider the battery for several days of autonomy.

Despite the existence of the manual and guidebook, it is not possible to find a unique methodology able to dictate a “fit all” criteria for microgrids. The evidence reported by Schnitzer et al. [7] explains that any microgrid developer has found the perfect strategy for microgrid success in rural areas. The reason is that for getting a successful microgrid system besides the technical aspects, it is necessary to consider the social and economic characteristics of the site it would be implemented. It ought to be remembered that microgrids can be operated in off-grid or on-grid mode depending on the load demand and the energy sources available in specific regions. Therefore, for the best microgrid implementation, the Microgrids for Rural Electrification report [7] suggests considering demand projections and site assessments as well as following the ESMAP manual recommendations.

It should be noted, however, that during the system design stage, it is common to size the gensets to meet the total load demand considering line losses without renewable energy sources [38] for obtaining a proper electricity supply. If renewable energy technologies are considered, then the different configurations of renewable-diesel combinations should allow each energy source to supply loads separately or to meet a high demand by combining them at the same time [39]. According to Diaz et al. [40], diesel generator power is calculated to cover a peak demand plus an extra of around 10%.

Optimum design (sizing) of microgrids has been conducted and reported by [40-44]. Other authors use artificial intelligence with a multi-objective optimisation approach to minimise the total capital cost for sizing PV systems, but they rely on conventional sizing techniques for the genset selection [45].

The review made by Mellit et al. [45] presents the application of artificial intelligence techniques such as Neural Networks and Genetic Algorithms among others for sizing PV systems. Their work includes a section with studies for sizing hybrid PV systems for the optimum selection of solar array panels, wind turbines, and battery configurations. It also includes more than one study for finding the optimal total capital cost depending on the loss of power supply probability.

According to Bernal-Agustin et al. [46], the optimum design is usually carried out by minimising the Net Present Cost (NPC) or the Levelized Cost of Energy (LCOE) of a project, using simulation and optimisation software tools available for hybrid systems. Their study mentions that the most-used optimisation software is the Hybrid Optimization Model for Electric Renewables (HOMER) [47]. The review made by Connolly et al. [48] of 37 computer tools, commonly used to analyse the integration of renewable energy in different systems, revealed that no energy tool addresses all aspects of the integration. However, in their review, HOMER appeared as one of the most used tools for stand-alone applications. Similarly, in the review made by Sinha [49], where 19 optimisation software tools were analysed, it was indicated that HOMER has been used extensively for hybrid renewable energy system optimisation, regardless of the limitations noted by the authors. In Suman's et al. work [50] for hybrid system optimisation in rural areas, HOMER was shown as one of the software tools efficiently used for sizing hybrid renewable energy systems, but the authors appeal to a modern technique in optimal sizing of renewable energy sources that implements evolutionary algorithms such as Particle Swarm Optimisation (PSO), Differential Evolution, Genetic Algorithm (GA), Simulated Annealing (SA), and others. Their work presented a swarm-based optimisation method for allowing the users to employ customised constraints and avoid the existing limitations of available optimisation tools.

A list of existing optimisation software taken from Bernal-Agustin [46] and Fathima et al. [51] is included in Table 2-5.

Table 2-5 Hybrid Systems Optimisation Software and Tools.

Software Name	Software Full Name	Developer
HOMER	Hybrid Optimization of Multiple Energy Resources	National Renewable Energy Laboratory (NREL).
HYBRID 2	Probabilistic computer model for hybrid systems	Renewable Energy Research Laboratory (RERL) of the University of Massachusetts.
HOGA	Hybrid Optimization by Genetic Algorithms	Electric Engineering Department of the University of Zaragoza, Spain.
TRNSYS	Transient System Simulation Tool	The University of Wisconsin and the University of Colorado, USA.
HYDROGEMS	Hydrogen Energy Models	Institute for Energy Technology (IFE), Norway.
HYBRIDS	Renewable Energy System Assessment Application and Design Tool	Solaris Homes
INSEL	Integrated Simulation Environment Language	The University of Oldenburg.
ARES	Autonomous Renewable Energy Systems	The University of Cardiff.
RAPSIM	Renewable Alternative Power Systems Simulation	The University of Murdoch in Perth, Australia.
SOMES	Simulation and Optimization Model for Renewable Energy Systems	Utrecht University, The Netherlands.
SOLSIM	Solar-thermal Conversion Systems Simulation	Fachhochschule Konstanz, Germany.

2.4 The Role of Diesel Generators in Off-grid Systems

Different authors suggest that diesel generators are commonly used to electrify off-grid areas [32, 43, 44, 52]. Due to the wide use of diesel generators and their environmental impact, there is a keen interest to reduce fuel consumption without forgetting the goal of supplying reliable electricity. In Diaz et al. study [40] the hybridisation of diesel systems appears as an interesting solution because the genset is aimed to work only when the renewable system is not able to supply the power. Of the variety of existing renewable energy sources, the most promising power-generating ones are solar and wind energy due to their availability and advantages in remote areas as cited by Haghghat et al. [53]. Both technologies have been broadly studied and hybrid systems

consisting of PV or wind combined with a diesel generator may guarantee a minimum fuel consumption, assuring a good overall operating cost, as well as a low environmental impact [53]. Complementary information from Alzola et al. [54] shows that diesel generators are suitable for hybrid systems, as a backup when combined with solar photovoltaic, during low insolation or high demand periods. According to Fu et al. [38], the genset is the main source to control the voltage and frequency of a microgrid operating in islanded mode. The authors pointed out that when a load is applied to or removed from the microgrid, the voltage and frequency go from transient to steady-state values. The magnitude of those values depends on the generator exciter and engine governor controls. So, the genset must be able to keep within a certain limit the right voltage and frequency values as part of good system performance. Therefore, regardless of the share of renewable energy included in the system, special attention should be given to the sizing of diesel generators to ensure the best performance.

2.4.1 Genset Configuration and Working Principle

As explained above, gensets are key elements for operating microgrids, therefore understanding what they are and how their performance can be affected is important for finding the optimum and cost-effective system configuration, especially if renewable energy is included.

A genset, also known as a diesel generator or generator set, is a device that produces electrical power. Gensets consist of a diesel engine attached to an electrical generator, generally a synchronous alternator. The engine is controlled by an engine governor and the alternator is controlled by an automatic voltage regulator (AVR) [55], Figure 2-2 shows a simplified block diagram of a genset configuration.

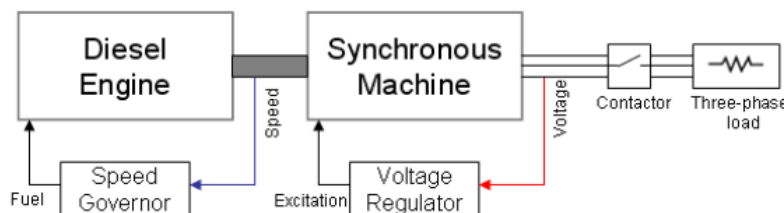


Figure 2-2 Block diagram of a diesel generator [56].

The prime mover in a genset, in this case, the diesel engine, produces mechanical work to rotate the synchronous alternator. It comprises an engine block, cylinder head, cylinders, running gear, pistons, fuel system, valve and injection systems, air charge system, and cooling and exhaust systems. The engine's speed is maintained constant typically at 1500 or 1800 rpm [56]

depending on the desired frequency as presented in Equation 2-6 and Equation 2-7 [55].

$$n = f \frac{60}{P} \quad \text{Equation 2-6}$$

$$P = p/2 \quad \text{Equation 2-7}$$

where, n is the engine speed in rpm, f is the frequency in Hz, P is the number of pole pairs in the alternator, and p is the number of poles in the alternator.

The synchronous machine is usually a salient-pole generator, a very popular is the four-pole alternator. A similar relationship as that shown in Equation 2-6 appears in Equation 2-8, where ω_e is the electrical speed, ω_m is the mechanical speed (both in rads/s).

$$\omega_e = \frac{p}{2} \omega_m \quad \text{Equation 2-8}$$

From Equation 2-8 it is possible to relate the electrical and mechanical characteristics of a genset according to the equations shown from Equation 2-9 to Equation 2-12.

$$T_e = \frac{P_e}{\omega_m} \quad \text{Equation 2-9}$$

$$T_a = T_m - T_e \quad \text{Equation 2-10}$$

$$P_e = \frac{3V_\phi E_A \sin\delta}{X_s} \quad \text{Equation 2-11}$$

$$T_e = \frac{3V_\phi E_A \sin\delta}{\omega_m X_s} \quad \text{Equation 2-12}$$

where, T_e is the electromagnetic torque from the generator in Nm, P_e is the real power supplied at the generator terminals in kW, T_m is the mechanical or shaft torque in Nm, T_a represents the accelerating torque in Nm, for a machine in synchronism $T_a = 0$. The phase or output voltage of the generator in volts is represented by V_ϕ . The induced voltage, also in volts, is E_A . The angle between V_ϕ and E_A is known as the torque angle in degrees. And the synchronous reactance of the generator, in ohms, is given by X_s .

According to Knudsen et al. [57], the motion behaviour of a synchronous machine is described by the swing equation, which can be represented in terms of torque or power, as shown in Equation 2-13 and Equation 2-14.

$$J\dot{\omega}_m = T_m - T_e \quad \text{Equation 2-13}$$

$$\dot{\omega}_m = \frac{1}{M} (P_m - P_e) \quad \text{Equation 2-14}$$

where, J is the moment of inertia of the rotor in kgm^2 , $\dot{\omega}_m$ is the angular acceleration in rad/s^2 , M is the inertia constant in MJ/s/rad , and P_m is mechanical or brake power in kW.

These equations help to visualize the relationship existing in the coupled system of any genset and bring out the important role played by the speed and torque⁵ [58] produced at the engine's crankshaft. It is important to notice that, as the frequency of the generated voltage is directly proportional to the engine's speed, it is possible to say that the engine will be responsible for the frequency output and that the load demand will affect both elements. A large increase in load causes a reduction in the synchronous machine's terminal voltage and the engine's speed. It is common to oversize gensets to prevent excessive voltage and frequency deviations. If excessive voltage is present it is convenient to temporarily reduce the terminal voltage with the AVR and recover the desired engine speed. The speed will be adjusted with the supplied fuel to the system, controlled by the governor. For assessing the genset's performance ISO 8528-5 is often used. It classifies the gensets into two categories: by voltage error (below 20%) or by speed error (below 10%) performance [56].

As said before the prime mover is responsible for providing the required speed, for this reason, the engine's parameters should be strictly considered, specifically the torque produced by the combustion of the fuel and the resulting crankshaft speed. Equation 2-15 to Equation 2-17 [55] relate the engine's parameters such as brake power⁶ [58], mechanical torque and cylinder pressure. Equation 2-16 is the characteristic equation to calculate the brake mean effective pressure⁷ (BMEP) [58].

⁵ The engine torque is a measure of the work done per unit rotation of the crankshaft.

⁶ The brake power is defined as the rate at which work is done.

⁷ The mean effective pressure is defined as the external shaft work per unit volume done by the engine.

$$P_m = \omega_m T_m \quad \text{Equation 2-15}$$

$$BMEP = \frac{2\pi n_{csr} T_m}{n_c V_d} \quad \text{Equation 2-16}$$

$$V_d = n_c S C_A \quad \text{Equation 2-17}$$

where, P_m is the brake power in kW, $BMEP$ is the brake mean effective pressure [58] in Pa, n_{csr} is the number of crankshaft rotations per complete cycle ($n_{csr}=2$ for a 4-stroke engine and $n_{csr}=1$ for a 2-stroke engine) in number of working strokes per unit of time. The displacement volume of the cylinder in m^3 is V_d , n_c is the number of active cylinders in the engine, and S represents the piston stroke in metres. The area of the piston in m^2 is given by C_A .

2.4.2 Key Parameters for Diesel Generators Performance

The performance of the genset relies on both parts of its configuration: the diesel engine and the alternator. With that existing interdependency, a disturbance in either element of the configuration will jeopardize the overall efficiency of the system. A combined efficiency from a genset range between 30-55%. It is usually reported based on the specific fuel consumption (SFC) in litre/hour or g/kWh. This value helps to calculate the operating cost of the set. For different systems, the SFC could vary depending on the operating and maintenance practices, the loading, and the ambient conditions. Loading refers to the electrical load applied to the genset compared with its rated capacity [59]. The load factor is the ratio of the average load to the maximum possible load in a certain period [60]. The minimum load ratio is the instantaneous load divided by the rated capacity of the generator as defined in Schnitzer's work [61]. A very important characteristic of the genset's performance is how the SFC may be affected by the size of the set and the applied load parameters. Regarding the set size, better performance can be achieved in large systems (over 500 kVA) if they operate at 100% load. From the load parameter, it is convenient to operate the genset around 75-80% of its rated capacity, it is worth bearing in mind that below a 25% load, the SFC presents the worst values [59]. However, Kusakana and Vermaark [62] explain that when supplying electricity in rural areas, the genset might run between 30 to 60 % load. That operating range is not exactly recommended by some manufacturers, especially if the genset operates below

30% load for long periods, as that would negatively impact the diesel generator. The negative impact results from the reduced heat in the engine's cylinder leading to unburnt fuel and oil deposits leakage through the exhaust slip joints. Therefore, long low load operating periods would lead to deposit formation behind the piston rings and may develop deposits inside the cylinder as well. As a consequence, the performance of the diesel generator will be reduced, leading to power losses and accelerated wear of the engine's components [63].

2.4.3 Fuel Consumption Estimation Equations for Diesel Generators

In literature, it is possible to identify equations to estimate the fuel consumption of a diesel generator. The most common equation is the linear expression (see Equation 2-18) presented by Reiniger [64] in 1986, where $q(t)$ is hourly fuel consumption in l/kWh; $P(t)$ is the power generated by the generator in kW; P_r is the rated/nominal power of the generator in kW; a and b are the model coefficients in l/kWh.

$$q(t) = a \cdot P(t) + b \cdot P_r$$

Equation 2-18

Equation 2-18 has been used ever since by several authors [42, 44, 65, 66] for the "black box" modelling technique of diesel generators in microgrids [67]. Rohani et al. [68] presented a similar equation, which is the linear equation implemented by HOMER [69]. This equation allows for adjusting the coefficients presented by Reiniger ("a" and "b" coefficients) as "a" can be estimated when at least two fuel consumption parameters at different loads are known, and "b" can be computed from the no-load consumption divided by the rated power of the generator [70, 71]. There is another fuel equation that uses a quadratic function found by Ashok [72], who emphasized that during low working conditions, a linear equation is a good approximation but near rated power conditions a second-order polynomial is required for the appropriate fuel consumption estimation. Agarwal et al. [73] also used a quadratic expression, in which coefficients were determined from the manufacturer's specifications, the same way as reported by [72]. Pelland et al. [74] also selected a quadratic equation but they emphasized that the fuel analysis is very sensitive to the type of fit applied, especially for loads below 25% rated power, producing large uncertainties in the final fuel estimation. The work presented by Gan et al. [75] estimated the fuel consumption through a third-order polynomial function, using empirical data instead of manufacturer's data, but they revealed that more work

should be done to have better generator sizing. Those equations are good approximations for fuel consumption according to the data presented by each author, however, all of them assume diesel as the fuel that powers the diesel generator.

2.4.4 Evidence of Genset's Performance Failure

When designing microgrids it is commonly assumed that diesel generators operate at the recommended conditions by the manufacturer. Nevertheless, case studies at different locations around the world demonstrate that real-time operating conditions are quite different from the assumed ones. In some cases, the system operates below the 25% regime which gives a poor performance [40], and there are situations where the fuel consumption might be five times greater than the manufacturer's specifications [76]. There is evidence in literature revealing a common failure in gensets' performance leading to higher operating costs. The findings presented by Schnitzer [61] reveal that the microgrids installed in 36 municipalities in Haiti rarely operate if they do at all. He mentions that the size of the generators, relative to the load demand, represents a high fuel cost. The results from his analysis of the Coteaux and Port-a-Piment sites showed that microgrids operate less than the scheduled plan and that, while operating, the total load was significantly less than the gensets' rated capacity. He pointed out that it would be beneficial to replace those oversized generators with smaller-scale systems.

The study of three microgrids in the Lake Sentani region of Papua, Indonesia made by Soto [76] revealed that the highest operation performance was 33% while the lowest was 6% of the rated load capacity of the generator. None of the studied systems reached half of their operational design and both of them never operated beyond 20% of their load capacity. He concluded that generator sizes with better load matching could reduce fuel consumption while improving reliability and lowering maintenance needs.

Besides the operating load, it is important to consider the interaction between the genset and the renewable energy implemented within the system. For example, the situation presented by Diaz et al. [77] concerning seven villages located in the province of Jujuy, Argentina, electrified by PV-diesel systems illustrates that as PV arrays were undersized; the increased energy demand has been met by the diesel generators. It caused fuel consumption to almost double over 8 years period and a higher operating cost.

Although some diesel/solar hybrid microgrids include battery storage units, as reported by several authors and cited by Yamegueu et al. [42]; it has become of

interest to implement hybrid systems without battery storage. The latter brings a major concern regarding the hybrid system performance because the share of PV (or other renewable energy) within the system affects the optimal functioning of the diesel engine. It has been reported by Yamegueu et al. [42] that a high share of PV in a low load system does decrease the optimal functioning of a genset (below 62% of its rated power); they recommend a design that allows the genset to operate near its nominal power. A similar situation is present in African countries where a poor demand prediction results in having oversized microgrids that leads to a low load performance. This is why Booth et al. [78] suggest that an ideal solution would consist of the appropriate sizing of the systems during the design phase. What these cases have in common is the high operating cost due to the high fuel consumption derived from a low load demand and the wrong sizing of the power sources. As mentioned by Sinn [60], for meeting a low load factor a high-power diesel engine, able to meet the required power during peak demand, operates with low capacity giving high operation and maintenance costs in return.

As seen so far different locations present similar conditions regarding the genset's performance, and it became clearer how the load profile could be the main factor. The existing evidence supports the idea that better sizing is required to reduce fuel consumption. The task is not as easy as it may sound due to the uncertainty of electricity demand in rural areas. Schnitzer [61] emphasizes that electricity demand is extremely hard to predict and it is even harder for villages which have not had access to electricity before. Sinn [60] complements that idea by concluding that electricity demand in isolated microgrids is driven by an unfavourable evening peak from households. In the same way, it is also worthy to recall Edwards et al. work [79] showing that residential electrical consumption is highly dependent on human behaviour, which may cause an unpredictable fluctuation.

2.4.5 Genset Poor Performance Consequences

It has been mentioned in the previous sections that the performance of a diesel generator depends on several factors and that operating it below the manufacturer's specifications may increase fuel consumption, thus the operating costs. Besides the excessive fuel consumption derived from the poor performance, if a genset operates below the recommended parameters, the engine might present some of the adverse situations cited and described by Hamilton et al. [55]. The adverse situations are caused due to the thermal imbalance during fuel combustion, which may further decrease the performance of the generator. These adverse situations are defined below.

- Wet stacking: a condition resulting from low cylinder temperatures, it is appreciated from unburnt fuel condensing within diesel engine exhaust. It is considered a positive feedback process because the initial incomplete combustion reduces the subsequent combustion efficiency cycles.
- Oil dilution: results from low cylinder temperature and pressure, these conditions allow an excessive oil film to be present against the cylinder walls. The oil will be subsequently mixed with fuel and will present modified properties; requiring a more frequent replacement.
- White smoke: is present at low-temperature combustion with fuel vapour produced from the unburnt fuel.
- Blow-by: condition referring to the exhaust gas blowing past the piston ring and into the crankcase. Excessive blow-by increases the crankcase pressure, leading to oil leakages.
- Black smoke: is present at low-temperature combustion with black carbon particulate from the carbonized oil and fuel residue. It usually occurs after a low load operation period. Black smoke is made up of soot particles, which are caused by the incomplete combustion of the fuel [80]. The soot formation process diagram is included in Figure 2-3, which shows that the fuel undergoes pyrolysis and produces soot precursors such as polycyclic aromatic hydrocarbons (PAH) before nucleation, surface growth and agglomeration occur [81].

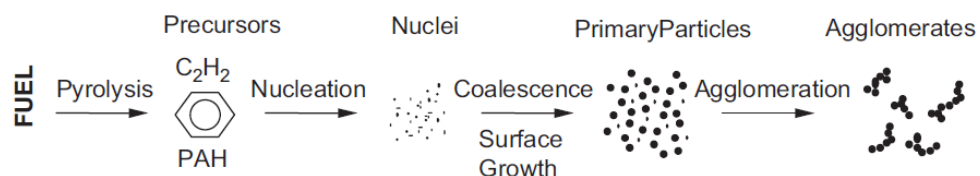


Figure 2-3 Schematic diagram of the soot formation process [81].

- Con rod bearing wear: caused by the varying cylinder pressure with a non-uniform load profile across the connecting rod bearings. Excessive loads tend to reduce bearing life.
- Cylinder liner wear: it results from the contaminated oil affecting the optimum surface roughness of the liner. It might be caused by bore glazing or bore polishing and it will reduce the liner's capacity to hold the required oil film for the right lubrication. Bore glazing refers to fuel and oil derivatives coating the liner. Bore polishing refers to the mirror finish within the cylinder bore caused by local mechanical wear. Both cases might lead to the cylinder and oil replacement.

- Piston ring carbonization: this is the accumulation of carbon on the piston ring that can cause polishing with a high risk of a piston seizure.

Having any of these problems is undesirable because they might impact the operating costs and, in the worst-case scenario, the electricity supply might not be met due to the complete failure of the engine. Therefore, finding the optimum genset configuration for matching, as accurately as possible, the load demand at all times and avoiding the poor performance of diesel generators is of the utmost interest in this work.

2.5 Performance Improvement Attempts for Diesel Generators

Literature shows that even when using novel optimisation algorithms such as the Particle Swarm Optimisation-Grey Wolf Optimiser used by Kumar et al. [50], the performance of diesel generators receives little attention and their fuel consumption estimation still relies, in many cases, on the linear equation presented in 1986 by Reiniger [64]. The performance improvements found in the literature mostly refer to studies addressing the optimum design of microgrids. Those studies reduce overall project costs by reducing fuel consumption through renewable energy technologies implementation.

Despite the awareness of the importance of re-sizing diesel generators, only a few authors have studied the benefits of using more than one diesel generator for optimum matching in genset size, power output and load demand for reducing their fuel consumption.

2.5.1 Improvements in Diesel Generators Sizing and Selection with Multiple Gensets and Optimisation

Alramlawi et al. [82] observed that installing three diesel generators instead of only one, in combination with a PV array without a battery was more efficient in the system of their study. In the study by Pelland et al. [74], fuel savings were reported by adding PV arrays, reducing dump loads and using smaller diesel generators. The authors suggested that further optimisation for genset sizing and system would contribute to more fuel savings that would be translated into less greenhouse gas (GHG) emissions. Another study that explored the benefits of operating two smaller engines for diesel-based standalone applications was presented by Kusakana [83]. The author reported fuel savings of around 30% if two diesel generators are used in parallel instead of a single unit, as one of them operates at a high load factor and the second one has reduced operating

time. Also, with the optimisation techniques used by Jesper Knudsen et al. [84], gradient search approach and genetic algorithm approach, potential fuel savings from 0.1 to 3% could be achieved in a multiple diesel generator independent power producer power plant.

2.5.2 Diesel Generators Performance Improvement through Control and Speed-oriented Models

On the other hand, some authors have developed control-oriented models to understand and simulate the dynamic characteristics of gensets for improving the automatic generation control for better response under variable loads [57, 85-92], and achieving variable speed operation [93-96], to avoid the existing synchronous speed limitations on diesel generators.

2.5.3 Low Load Diesel Operation

A very contrasting approach for reducing fuel consumption, known as the Low Load Diesel (LLD) operation criteria, brings a debatable perspective toward improving electrification strategies in hybrid systems. According to Hamilton et al. [97], LLD refers to a modified engine application that allows the engine's full capacity utilisation. Their research presents an alternative solution to the Energy Storage System (ESS) integration. The convention for the LLD is to set load limits between 30% and 40% of the engine's rated capacity. The aim is to achieve the lowest diesel load limit to have a greater share of renewable generation for hybrid systems. The LLD differs from the conventional diesel operation as it has modified parameters such as lower cylinder temperature and pressure. The authors concluded that LLD offers commercial and environmental benefits because fuel savings between 8% and 18% could be obtained in systems with medium renewable energy penetration. A supporting survey work from Hamilton et al. [98] shows that the LLD application became of interest due to the inability of diesel generators to operate at low loads, which represents an obstacle to including a high share of renewable energy in remote areas. Their results showed that by presenting the LLD performance, with its suggested benefits to the gensets' operators, the inefficient diesel operation would not represent a barrier anymore for adopting the LLD.

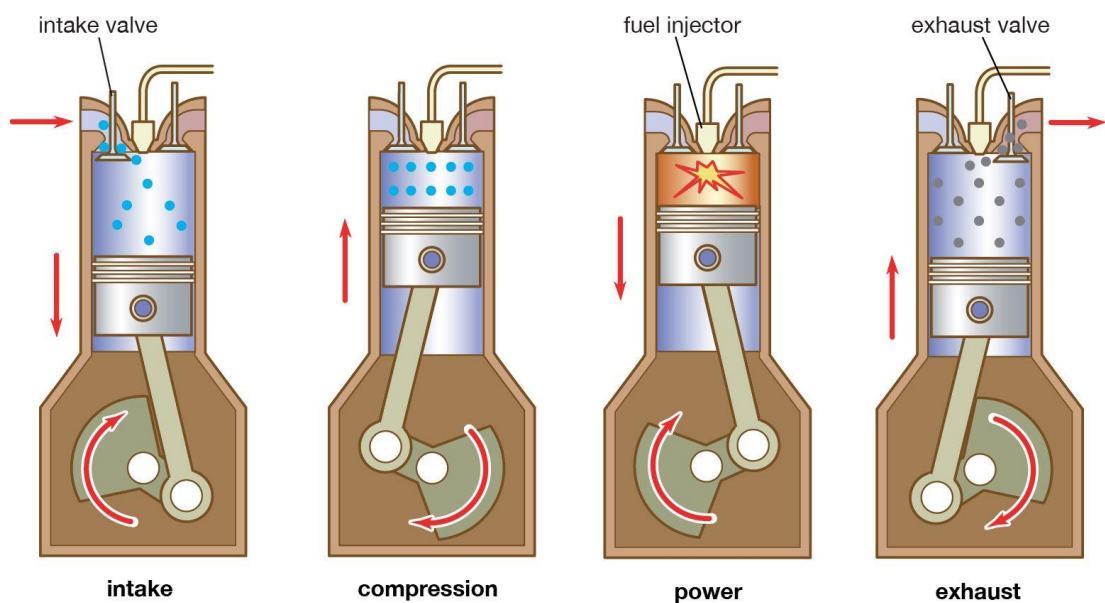
2.6 Diesel Generators and the Combustion Process

As mentioned before, there is a keen interest in reducing the fuel consumption of diesel generators. The fuel consumption depends on the combustion process

that occurs in the engine, which in turn is highly dependent on the physicochemical properties of fuel burned inside the combustion chamber. Therefore, reducing fuel consumption requires an understanding of the main combustion characteristics of diesel engines.

2.6.1 Compression-Ignition Engine

A compression ignition (CI) engine is a type of internal combustion engine, which by definition uses the released chemical energy of a fuel to produce mechanical work and operates with a Diesel Cycle. The Diesel Cycle was named after Rudolph Diesel who developed a direct injection engine in 1897, an illustration of a four-stroke Diesel Cycle sequence is shown in Figure 2-4.



© Encyclopædia Britannica, Inc.

Figure 2-4 Illustration of a four-stroke Diesel cycle [99].

In the intake stroke, the air is drawn into the engine's cylinder that enters through the opened intake valve while the piston moves downward. During the compression stroke, the piston moves upwards and the air temperature rises above the auto-ignition temperature of the fuel. Near the end of the compression stroke fuel is sprayed into the cylinder. The power stroke begins in the later stages of the compression stroke where evaporation, mixing and ignition occur followed by the combustion of the fuel that pushes the piston downwards. Finally, in the exhaust stroke, the piston moves upwards pushing out the combustion gases that exit the cylinder via the opened exhaust valves. An important characteristic of diesel engines is that the output power is controlled by the amount of fuel injected into the cylinder and they operate with high compression ratios that allow the ignition of the fuel-air mixture [58].

Hence, the performance of a diesel engine depends on the adequate mixing of fuel and air during the compression stroke, which will start the combustion process as the fuel reacts with the oxygen from the surrounding air. It should be noted that three types of the air-fuel mixture can be identified according to the air-fuel ratio (AFR) used by the engine compared to the ideal (stoichiometric) AFR as defined by the equivalence factor (λ) in Equation 2-19, where AFR_{ideal} for diesel combustion is 14.5:1 and AFR_{engine} can be found with Equation 2-20.

$$\lambda = \frac{AFR_{engine}}{AFR_{ideal}} \quad \text{Equation 2-19}$$

$$AFR_{engine} = \frac{m_{air}^{engine}}{m_{fuel}^{engine}} \quad \text{Equation 2-20}$$

If $\lambda < 1$ an incomplete combustion occurs as there is not enough oxygen to burn all the fuel and it is known as a rich air-fuel mixture. When $\lambda = 1$ the air-fuel mixture is stoichiometric or ideal as there is an exact amount of air to burn all the fuel. If $\lambda > 1$ then, there is excess oxygen in the air-fuel mixture and it's known as lean, this is the type of air-fuel mixture for diesel engines.

2.6.2 Combustion Process in Compression Ignition Engines

The main factors controlling the combustion and emissions of CI are spray and air-fuel mixture formation. The latter is controlled by fuel injection parameters, in-cylinder air motions and fuel properties such as density, viscosity, surface tension, and volatility (fuel's ability to vaporise) [100]. The combustion process in CI engines can be divided into three phases: premixed combustion, mixing-controlled combustion, and late combustion phase, all of which occur after the ignition delay (ID). The ID refers to the time interval between the start of fuel injection and the start of combustion (SOC), during this time the atomisation and vapourisation of the fuel occur and its temperature is raised for autoignition. Premixed combustion is defined by the spontaneous ignition of vapour-air mixture regions that form around the fuel jet as it is injected into the cylinder. The controlled combustion phase happens when the rest of the fuel jet burns as it mixes with the surrounding air, this combustion is limited by the rate at which the remaining fuel mixes with the air. The amount of fuel that burns in the combustion phases is dependent on the design characteristics of the engine and fuel injector but it is influenced by the fuel type and the operating load. At idle conditions, most of the fuel burns during premixed combustion [58]. The late combustion phase occurs during the expansion stroke, where the combustion continues as a result of the reassociation of dissociated gasses and unburnt fuel [101].

2.6.3 Emissions from Compression Ignition Engines

When hydrocarbons are burnt, some pollutants can be produced such as VOCs, CO, NO_x, SO₂, and PM. Diesel fuel is made from petroleum after a refining process; it is a very complex mixture of compounds, mostly belonging to the paraffinic, naphthenic or aromatic class of hydrocarbons, with carbon numbers between 10 and 22. The main pollutants emitted by diesel engines are Carbon monoxide (CO), hydrocarbons (HC), particulate matter (PM) and Nitrogen oxides (NO_x) which have adverse health and environmental effects. CO is produced as a result of incomplete combustion where there is not sufficient oxygen in the air-fuel mixture to convert all the carbon in the fuel to carbon dioxide (CO₂). As CI run on lean mixtures, their CO emission is very low but as the combustion is not a homogeneous process, some regions of incomplete combustion generate the CO. Hydrocarbons are formed when trapped fuel in the injector or along the cylinder walls is not burned due to insufficient temperature. Their emission is low in diesel engines but at low loads the emission increases. Particulate matter has two main components: solid carbon or soot and organic fraction mainly generated by incomplete combustion of the hydrocarbons of the fuel and lube oil. High concentrations of PM are visible as black smoke. When the engine operates at low loads, more PM is generated due to the lower in-cylinder temperature that contributes to soot particle formation within the rich-fuel regions of the non-homogenous combustion process [102]. Nitrogen oxides refer to nitrogen oxide (NO) and nitrogen dioxide (NO₂) emissions. NO_x is generated when nitrogen reacts with oxygen at high temperatures (above 1600°C). Most of the NO_x is generated in the early stages of the combustion when the piston is still near the top dead centre (TDC) and the flame is at its highest temperature. As the NO_x formation is temperature-dependent, at higher loads, more NO_x is emitted. NO_x emissions are mainly NO (85-95%) which is then converted to NO₂ in the atmosphere [58, 103]. In this work, NO_x and fine particulate matter (PM_{2.5}) are of utmost interest because it has been estimated that in SSA backup fossil-fuel-based generators account for the majority of these two pollutant emissions within the power sector and both impact human health and the environment [104]. The Air Quality Expert Group define PM_{2.5} as the mass of particulate matter per unit volume of air passing a size-selective inlet with a 50% cut point efficiency at 2.5-micrometre particle aerodynamic diameter [105], and it is considered the most dangerous pollution to human health due to its ability to penetrate bloodstream [106].

Other types of hydrocarbons that can be used to power diesel engines are biofuels. These fuels are produced from organic matter in a relatively short

period like days, weeks, or months; which differ from fossil fuels that take millions of years to form [107]. Biofuels have different properties because they can be produced from diverse feedstock, and are classified according to the type of process or feedstock required to obtain them as shown in Figure 2-5.

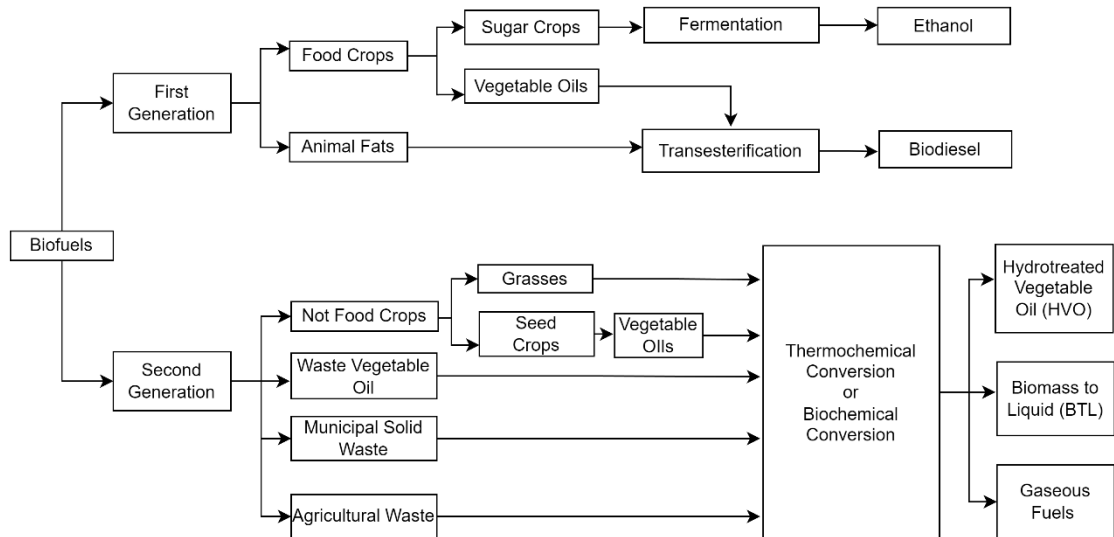


Figure 2-5 A General classification of biofuels.

2.6.4 Biofuel and Diesel Engines

According to Sajjadi et al. [108], there are more than 350 recognized oil crops around the world as potential sources for biodiesel production. More than 95% of biodiesel is produced from food crops such as rapeseed, sunflower, palm oil, and soybean. This production has derived into a food security debate and some other negative discussions regarding sustainability and environmental problems. A plausible way to overcome this situation is by producing biodiesel from non-edible crops. For that purpose, crops such as jatropha, karanja, rubber seed, rice bran, mahua seed, tobacco seed, Chinese tallow, jojoba seed, and babassu tree, among others have become a major source of biodiesel production. In the same way, using non-edible crops for straight vegetable oil (SVO) production and increasing its usage would be beneficial to reduce diesel consumption. For using biofuels in diesel engines it is necessary to assess some of the key physicochemical properties shown in Table 2-6, as they allow for a comparison of the quality of different fuels [108-112]. The reference values considered for density, viscosity, flash point, cetane number, heating value, and cloud point mentioned in Table 2-6 refer to the SVO (edible and non-edible) and their respective biodiesel as reported in [108]. The edible SVO included are canola, cottonseed, coconut, corn, groundnut, jojoba, hazelnut, bay laurel

leaves, bay laurel fruit, moringa, mustard, olive kernel, olive pomace, palm, peanut, pequi, poppyseed, pumpkin, rapeseed, rice bran, safflower, sal seed, sesame, soybean, sunflower, wheat germ, wheat grain, and walnut kernel. The non-edible SVO included are *Argemone mexicana*, babassu, bitter almond, carapa, castor, camelina, crambe, *Croton megalocarpus*, Ethiopian mustard, *Euphorbia lathyris*, *Forsythia suspensa*, *Idesia polycarpa* var. *vestita* fruit oil, *Jatropha curcas* L., karanja, kusum, *Lesquerella fendleri*, linseed, mahua, merrill, Meliaceae, *Michelia champaca*, milkweed, nahar, neem, niger, patchouli, polanga, poon, *Putranjiva roxburghii*, rubber, rice bran, *Stillingia*, sour plum, *Syringa*, tobacco, tung, *Terminalia catappa*, *Terminalia bellirica* roxb.

Table 2-6 Key physicochemical properties for characterizing SVO and biodiesel.

Property	Definition	Effect on the engine	Comparison
Density	Mass per unit volume is useful to estimate the injected amount of fuel for proper combustion.	It influences fuel atomization and thermal efficiency.	Diesel~ 0.85 g/cm ³ , SVO ~0.91-0.93 g/cm ³ biodiesel ~0.85-0.90.
Viscosity	The measure of resistance to flow from any liquid.	Affects fuel injection, higher viscosity leads to poor fuel atomization. High viscosity reduces thermal efficiency. Its effect is critical at low speed or light load conditions.	Diesel is around 9 to 17 times less viscous than SVO and ~1.6 less viscous than biofuel.
Flash Point	The temperature at which fuel ignites when exposed to a flame or spark.	A higher flash point makes the fuel safer for storage and handling.	SVO and biodiesel have a higher flash point compared to diesel.
Cetane Number	Measures the fuel's auto-ignition quality.	A Higher cetane number reduces ignition delay, which allows the engine to start faster and run smoothly. It influences the peak cylinder pressure, which characterizes the fuel's ability to mix with air and burn.	The diesel cetane number is higher than that of SVO or biodiesel.
Heating Value	Amount of energy released per unit of fuel after complete combustion.	Higher calorific values release higher heat and improve engine performance during combustion.	The diesel heating value is higher than that of SVO or biodiesel.
Cloud Point	The temperature at which a fuel presents a solid wax. Assess fuel's performance at low temperatures.	Block filters and injectors	Diesel ~ -17°C to -18 °C, generally resists lower temperatures than biodiesel or SVO.
Oxidative stability	An indicator of the degree of oxidation and reactivity with air.	Unstable fuel can lead to increased viscosity.	It depends on storing conditions.

Table 2-7 includes the physicochemical properties of selected vegetable oils, biodiesel, and diesel reported in the literature [108, 113-115] for comparison purposes.

Table 2-7 Physicochemical properties of selected vegetable oils, biodiesel, and diesel.

Type of crop	Vegetable Oil							Biodiesel					
	Crop	Density at 15°C (kg/m ³)	Viscosity at 40 °C (mm ² /s)	Flash Point (°C)	Cloud Point (°C)	Cetane number	Heating value (MJ/kg)	Density at 15°C (kg/m ³)	Viscosity at 40 °C (mm ² /s)	Flash Point (°C)	Cloud Point (°C)	Cetane number	Heating value (MJ/kg)
Edible	Palm oil	897	40.65	258	19.8	41	39.867	870	4.53	176.7	14.25	60.21	34.4 L
	Rapeseed	912.5	38.15	263	-3.9	37.6	39.7 H	879	4.4	169.5	-3.5	48.25	35.8 L
	Soybean	916	31.83	255	-5.5	38	39.6 H	882	4.15	140.1	0	44.7	35.74 L, 39.84H
	Sunflower	918	34.01	256	12.75	38.1	39.56 H	869	4.26	180.33	1.33	45.7	34.71 L, 40.6 H
Non-edible	Jatropha	916.5	37.28	211.7	-	21	38.96	865.5	4.52	175.5	5.66	55.43	40.79
	Karanja	933	39.9	222	-	32	35.992	889	4.79	157.4	13.3	56.55	36.56
	Mahua	942	32.01	231	-	45	36.85	895	4.77	129.5	4.33	55	36.9L, 39.4H
	Rubber	917	42.54	257	-	49.73	38.64	875	5.6	173.4	3.1	53	39.174
	Rice bran	918	40.86	304	4	0	38.945	889	5.15	161	0.55	64.95	38.17
	Tobacco	918	27.7	220	-7.8	38.7	39.4	865	3.56	165	-	51.5	42.22
Fossil Fuel													
Fuel	Density at 15°C (kg/m ³)	Viscosity at 40 °C (mm ² /s)	Flash Point (°C)	Cloud Point (°C)	Cetane number	Heating value (MJ/kg)							
Diesel	834 to 855	1.3–4.1	60 to 80	-15 to -5	47	42–43.8							

2.6.5 Biofuel Effect on Diesel Engines' Performance

Different authors have studied the effect of vegetable oils and biodiesel blends since the performance of a diesel engine and its emissions strongly depend on the physicochemical properties of the selected fuel. Common parameters to evaluate the engine's performance, are the Brake Thermal Efficiency (BTE), the brake specific fuel Consumption (BSFC), and the generated emissions. BTE is also known as fuel conversion efficiency because it indicates the quality of the conversion from the chemical energy of the fuel to work, it usually increases with higher loads [112]. The BSFC is the parameter that measures the efficiency of the combustion of an engine, it is defined as the ratio of the total fuel consumed to the brake power generated by an engine. The emission generation parameters mainly reported are hydrocarbon (HC), carbon monoxide (CO), carbon dioxide (CO₂), nitrogen oxides (NO_x), smoke, and particulate matter (PM). HC results from the incomplete combustion of the fuel inside the combustion chamber. CO appears as the product of intermediate combustion due to ineffective mixing between fuel and air. CO₂ indicates the completeness of combustion and it is one of the main greenhouse gases. NO_x is formed by factors like high flame temperature, oxygen content in fuel and duration of the reaction. Smoke and PM are present when inefficient combustion takes place [110].

A major drawback of using Vegetable Oils (VO) is their high viscosity, which leads to incomplete combustion and carbon deposits. Still, there are options for using them; according to No [116] VO can be applied in internal combustion engines through engine or fuel modifications. Engine modifications may include a dual fuelling engine or modifying the injection system. On the other hand, fuel modifications refer to complex processes like pyrolysis, micro-emulsion, transesterification, hydrodeoxygenation or to a simplified process of blending VO with petrodiesel, known as dilution, to reduce fuel's viscosity. The latter requires an appropriate blend to achieve optimum performance; most authors found that a 20% share of VO in the blend gives acceptable results as cited by Atabani et al. [115]. There are some cases where a 50% share of VO (jatropha oil) in the blend reported acceptable thermal efficiency. A very interesting review made by Che Mat et al. [114] highlights that unheated or preheated SVO can be used as a direct fuel in diesel engines but gives lower BTE and higher BSFC compared to diesel. In the same way, de Almeida et al. [117] reported that the lower heating values from vegetable oils slightly increased SFC. The review also mentions that for SVO-diesel blends the BSFC is higher, for higher SVO percentage present in the blend, therefore BTE decreases. The NO_x

emissions from SVO and its blends were lower than those of diesel. At high loads, CO emissions from SVO are reduced but HC and smoke emissions are greater compared to diesel emissions. The author's overall conclusion was that vegetable oil-diesel blends can replace diesel and give better results than neat SVO. Similarly, Almeida et al. [117] proved that a diesel generator could be adapted to run with palm oil. A relevant fact reported by Altin et al. [113] on the study of nine VO is that a minimum BSFC is achievable within the vicinity of the maximum torque area. Hossain et al. [118] concluded in their 17 raw plant oil review that the significant physicochemical properties of the fuel are mostly within 12% of their corresponding values for standard diesel, except viscosity. They remarked that plant oils are about 6 to 14 times more viscous than diesel and that the BSFC is increased by 2 to 15 %. As a reference, Table 2-8 presents the variety of VO-diesel blends, studied by several authors [114-116, 119-123] aiming to reduce SVO viscosity.

Table 2-8 Vegetable oil-diesel blends studied by several authors.

Crop	Amount of VO (%) in the fuel blend
Rubber seed ^a	20, 40, 60, 80
Cotton seed ^a	10, 20
Corn ^a	10, 20
Coconut oil ^b	10, 20, 30, 40, 50, 60, 80
Sunflower ^a	10, 20
Soybean ^a	10, 20
Olive kernel ^a	10, 20
Rapeseed oil ^a	20,25, 50, 75
Crude Palm oil ^a	25, 50, 75
Canola oil ^a	5, 10, 20
Karanja oil ^a	10,20,50, 75
Linseed oil ^a	10, 20, 30, 50
Mahua oil ^a	10, 20, 30
Rice bran oil ^a	10, 20, 30
Palm oil ^a	5, 10, 15, 20
Putranjiva roxburghii oi ^c	10, 20, 30, 40
Turpentine oil ^d	60-65
Jatropha ^e	2.6, 5, 10, 20, 30, 40, 50,70, 75, 80
Castor oil ^f	10,20,30,40,25,50,75
Mustard oil ^g	20,30, 40, 50

^aData taken from [114], ^bdata taken from [111], ^cdata taken from [123], ^ddata taken from [124], ^edata taken from [125-129], ^fdata taken from [130, 131], ^gdata taken from [132].

2.6.6 Fuel Specifications and Standards

Biofuels present variations in their properties depending on the feedstock used for their production, so for using them as fuels, they should comply with specific standards dictated by the existing organizations. There are three main biodiesel¹ [133] standards [134] issued by the American Society for Testing and Materials (ASTM), the European Committee for Standardization (CEN), and the Brazilian National Agency for Petroleum, Natural Gas and Biofuels (ANP) standards. The fuel specifications are established within the ASTM D6751 and the EN290 for standard diesel, the EN 14214 for biodiesel, and the ANP No. 7/2008 standards respectively. For SVO the DIN 51605 standard from the German Institute for Standardization (DIN) should comply. It is also of interest to mention the standards commonly used for petroleum fuels (fuel oils) that run diesel engines. According to Blin J. et al. [134], the ASTM D-396 and ISO 3104 are the worldwide references while certain specifications recommended by the National Oil Products Company of Burkina Faso (SONABHY) are the widely applied standards within West African countries.

Table 2-9 summarises the fuel specifications according to standard limits, gathered from several sources [108, 115, 133, 134], to have an easier comparison among them.

¹ Biodiesel is defined by the ASTM as “a fuel comprised of mono-alkyl esters of long chain fatty acids derived from vegetable oils or animal fats, designated B100”.

Table 2-9 Fuel specifications from selected standard limits.

Fuel Type	Fuel Property	Standard Limits		
Diesel		ASTM [115]	EUROPE [133]	SONABHY [134]
	Density at 15°C (kg/m ³)	820–860	820-845	820 to 890
	Viscosity at 40°C (mm ² /s)	2.0 to 4.5	2.0-4.5	1.6 to 5.9 (at 37.8°C)
	Flash point (°C)	60 to 80	>55	61 (minimum)
	Cetane number (minimum)	46	51	50
	Oxidation stability (g/m ³)	-	25	-
	*Heating value (MJ/kg)	-	-	42.3 (minimum)
Distillate Diesel Oil (DDO)		SONABHY [134]		
	Density at 15°C (kg/m ³)	835 to 950		
	Viscosity at 40°C (mm ² /s)	5.9 to 15 (at 37.8°C)		
	Flash point (°C)	66		
	Cetane number	40		
	Heating value (MJ/kg)	42.3 (minimum)		
Biodiesel		ASTM [108, 115]	Europe [108, 115]	Brazilian [134]
	Density at 15 °C (kg/m ³)	880	860-900	850–900
	Viscosity at 40°C (mm ² /s)	1.9–6.0	3.5-5.0	3.0–6.0
	Flash point (°C)	93	101	100
	Cetane number (minimum)	47	51	report
	Oxidation stability (h, 110°C)	3	6	6
	*Heating value (MJ/kg)	-	-	-
Vegetable Oil		DINV51605 [134]		
	Density at 15°C (kg/m ³)	900–930		
	Viscosity at 40°C (mm ² /s)	<36		
	Flash point (°C)	220		
	Cetane number	>39		
	Oxidation stability (h, 110°C)	6		
*Heating value (MJ/kg)	36 (minimum)			

*Most common values reported for heating values in MJ/kg are 42 to 45.9 for diesel and 34.4 to 45.2 for biodiesel.

Considering the different properties, characteristics and environmental concerns of diesel consumption, it is useful to include the emission limits from the European Emission Standards for nonroad engines (NRE). The Stage V standards are summarised in Table 2-10, taken from the DieselNet portal [135].

Table 2-10 Stage V emission standards for nonroad engines [135].

Category	Ign.	Net Power	Date	CO	HC	NOx	PM	PN
		kW						
NRE-v/c-1	CI	$P < 8$	2019	8.00	7.50 ^{a,c}		0.40 ^b	-
NRE-v/c-2	CI	$8 \leq P < 19$	2019	6.60	7.50 ^{a,c}		0.40	-
NRE-v/c-3	CI	$19 \leq P < 37$	2019	5.00	4.70 ^{a,c}		0.015	1×10^{12}
NRE-v/c-4	CI	$37 \leq P < 56$	2019	5.00	4.70 ^{a,c}		0.015	1×10^{12}
NRE-v/c-5	All	$56 \leq P < 130$	2020	5.00	0.19 ^c	0.40	0.015	1×10^{12}
NRE-v/c-6	All	$130 \leq P \leq 560$	2019	3.50	0.19 ^c	0.40	0.015	1×10^{12}
NRE-v/c-7	All	$P > 560$	2019	3.50	0.19 ^d	3.50	0.045	-

^a HC+NOx
^b 0.60 for hand-startable, air-cooled direct injection engines
^c A = 1.10 for gas engines
^d A = 6.00 for gas engines

2.7 Theoretical Background of the Proposed Solution for Improving Diesel Generators Performance in Microgrids

In section 2.3.3 the different techniques reported in the literature for sizing microgrids were presented, with being HOMER one of the preferred solutions. Although the full approach for sizing and designing a whole off-grid system is out of the scope of this research, a brief overview of the criteria for unit sizing and cost optimisation of integrated renewable energy systems (IRES) is included in this section for further explanation of the proposed solution of this project.

The review made by Chauhan and Saini [136] summarises the existing criteria for unit sizing and cost optimisation of IRES. The authors highlighted that optimum unit sizing is crucial for the economic and efficient utilisation of the energy sources included in the system. For that matter, the economics and power reliability of the system should be evaluated. For evaluating the economic criteria parameters such as NPC, LCOE, annualised cost of the system, payback period, and internal rate of return are commonly used. For evaluating the reliability of the intermittent sources, authors usually consider parameters such as loss of power supply probability (LPSP), expected energy not supplied (EENS), energy index ratio (EIR), level of autonomy (LA), etc. The

sizing methodologies mentioned in the same review, often reported by authors for IRES-based power generation are presented in Figure 2-6.

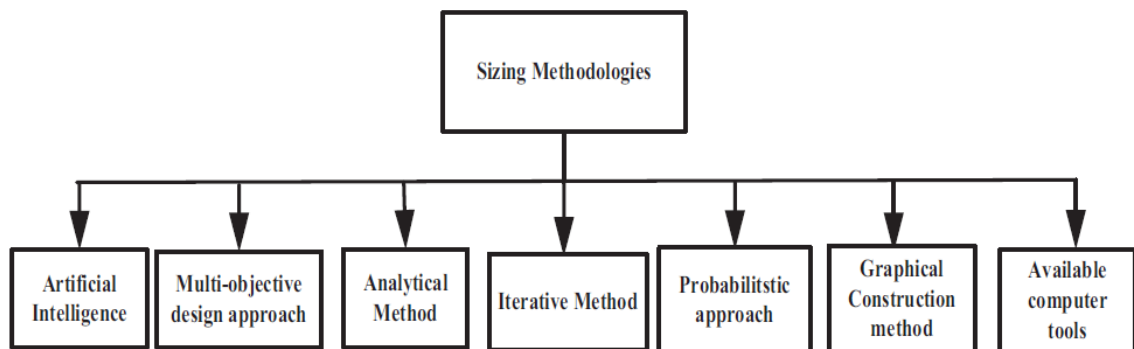


Figure 2-6 Methodologies for unit sizing and cost optimisation commonly used for IRES systems [136].

From the sizing methodologies shown above, the Iterative Method is the one of interest in this work. The iterative method is a deterministic method that evaluates the performance of an integrated system using a recursive program, which stops when the optimum system design is found. With this method, the cost of the system can be minimised by linear programming techniques, through mathematical programming optimisation models. According to [137], mathematical programming is one of the most successful models for formulating and solving decision-making problems. A classification of optimisation models is included in Figure 2-7, where the three types of mathematical programming are shown.

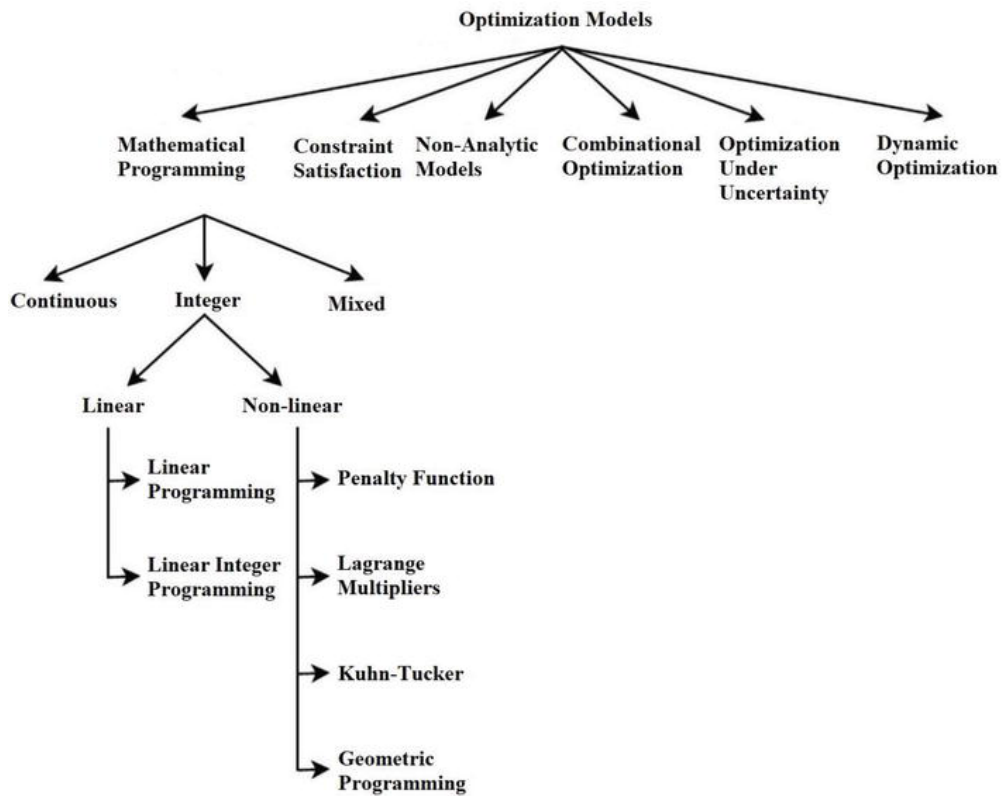


Figure 2-7 Optimisation models diagram [137].

Considering the optimisation models and the sizing methodologies, the proposed solution of this work for improving the performance of diesel generators in hybrid microgrids was developed as a mixed integer linear programming (MILP) model. MILP is a useful model that has been used to evaluate the techno-economic performance of rural hybrid energy systems [138]. For solving MILP it is common to use the Branch-and-Bound (BB) algorithm, which enumerates all the solutions to the problem until it finds the optimal solution, Figure 2-8 shows a representation of the BB algorithm.

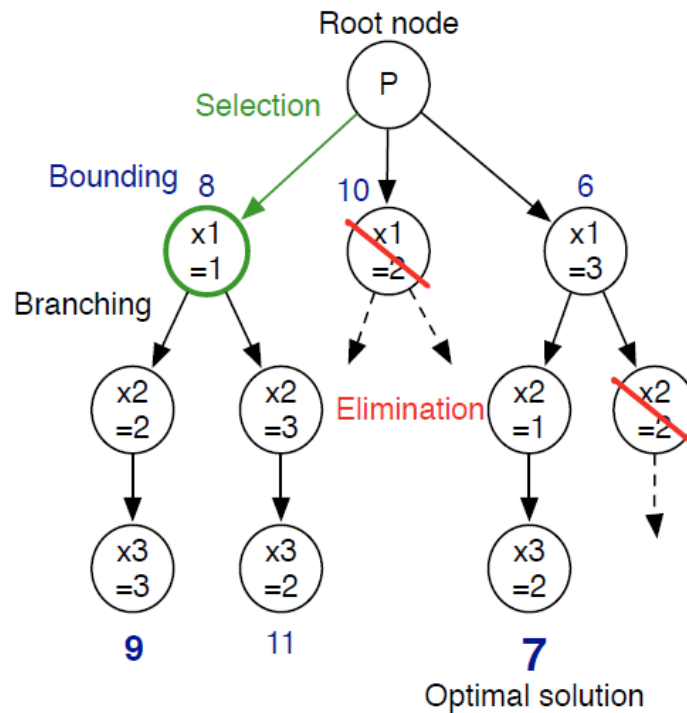


Figure 2-8 Illustration of the Branch and Bound algorithm [139].

The BB algorithm can be combined with the cutting planes method to form a complex algorithm known as Branch and Cut (BC). The BC algorithm is widely used by modern commercial optimisation solvers, such as Gurobi [140], for finding optimal solutions to MILP. Figure 2-9 shows the representation of the BC algorithm, where the green curve limits the solution space, whereas the red and the blue lines are the cuts that tighten the tree bounds for finding the optimal integer solution. A detailed explanation of the proposed solution is included in Chapter 5, which presents the developed cost optimisation model and the specifications of the graphical user interface created for testing the model.

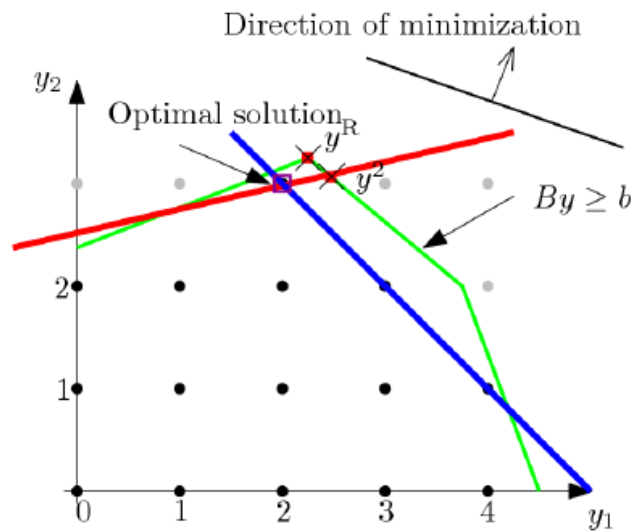


Figure 2-9 Branch and Cut representation [141].

2.8 Literature Review Summary

This section pointed out that 770 million people have no access to electricity [11] of which 590 million are located in sub-Saharan Africa, with 50% of that population concentrated in the Democratic Republic of Congo, Ethiopia, Nigeria, Tanzania, and Uganda [10]. Although diesel generators are a common solution for electrification purposes in some African countries (despite their high operating costs and environmental impact), achieving universal access to electricity by 2030 would need the implementation of mini-grids and stand-alone systems [10]. These systems operate independently of a national electricity grid and may be comprised of diesel generators or diesel generators operating in combination with renewable energy technologies (i.e., hybrid systems) [8, 16].

In recent years, the reduction in PV and BESS costs has made hybrid systems highly compelling compared to diesel mini-grids, and there is a strong mandate for hybridising diesel mini-grids with solar energy systems [5]. However, in countries such as Tanzania, the preferred option for off-grid systems implementation is diesel mini-grids as they are inexpensive to procure and technicians are familiar with their operation and maintenance but they are expensive to operate and maintain [29]. Literature showed that the economic comparison of different systems can be done by calculating the annual cash flow (ACF), the life cycle cost (LCC), the levelized cost of energy (LCOE), or the annualized maintenance, operating and replacement cost as presented by Equation 2-1 to Equation 2-4. In studies that use these economic tools, it has been reported that diesel systems have higher LCC than hybrid systems due to fuel costs [30] and that fuel consumption accounts for the major portion of the LCOE [32]. The latter brought the authors to the conclusion that further analysis

of biomass, hybrid microgrids and adequate fuel use is required over a vast African region for finding feasible solutions for rural energy services, which are highly dependent on diesel prices. Literature also showed that, usually, combining PV with diesel generators or storage systems is the least-cost option for electrifying rural communities [37]. Nevertheless, as each village and community has different needs and conditions, it is difficult to dictate a standard for sizing mini-grids [37], but usually diesel generators are sized to cover a peak demand plus a security margin of 10% [40]. It was found that sizing mini-grids relies on the use of simulation and optimisation software tools, available for hybrid systems, by minimising the Net Present Cost or the LCOE [46]. According to several authors [46, 48-50], the most-used optimisation software is the Hybrid Optimization Model for Electric Renewables (HOMER).

Literature confirmed that diesel generators are key elements for operating microgrids as they are the main source to control the voltage and frequency of the system when operating in islanded mode [38]. Understanding how the performance of a diesel generator can be affected is relevant for finding the optimum and cost-effective system configuration. Specific fuel consumption (SFC) is an important parameter for determining the performance of diesel generators. The SFC is mainly affected by the electrical load applied to the diesel generator, compared to its rated capacity. When diesel generators operate below 25% load, the SFC gives the worst values [59]. Literature showed that some systems operate below 25% engine load [40], and some others operate as low as 6% load, where the fuel consumption might be five times greater than the fuel consumption specified by manufacturers [76]. Some evidence was found that in hybrid systems, without battery storage, the share of PV or other renewable energy may affect the performance of diesel generators. For example, installing a high share of PV in low load systems decreases the performance of diesel generators below 62% of their rated capacity [42], whereas when the PV system is undersized, the fuel consumption increases as reported by Diaz et al. [77]. From the studies presented, it was concluded that these systems have high operating costs due to high fuel consumption, derived from a low load demand and the wrong sizing of the power sources. Therefore, better generator sizing is needed for operating the generators near their nominal power [42], to achieve their best performance. Better generator sizing is also needed for better load matching which would lead to reducing fuel consumption [76]. It was also found that improving the performance of diesel generators would reduce the negative impact on the engine such as wet stacking and black smoke [55].

Although the evidence showed the need to improve the performance of diesel generators, through better sizing to reduce fuel consumption and operating costs, only a few authors had reported the benefits of using more than one diesel generator for optimum matching in genset size, power output and load demand [74, 82-84]. Moreover, this literature review showed that even when using novel optimisation techniques for microgrid design, the performance of diesel generators receives little attention and the fuel consumption relies, in many cases, on the fuel consumption equation presented by Reiniger [64] in 1986. Another common equation for estimating the fuel consumption of diesel generators is the one used in HOMER [69]. These equations are good approximations for the fuel consumption according to the specific data presented by each author, however, they assume diesel as the fuel powering the generator. The latter limits the assessment of the effects that locally produced biofuel blends may have on the combustion process and the pollutant emissions of the generator, as both are highly dependent on the physicochemical properties of the fuel.

Assessing the effect that biofuel blends may have on the performance of a diesel generator, during the microgrid design phase (optimisation) would lead to finding the optimum fuel blend that could reduce the use of diesel in different regions. However, the existing optimisation tools do not include biofuel blends for mini-grid optimisation. Hence, this work was focused on developing an optimisation tool for improving the performance of diesel generators in hybrid microgrids, able to consider the effect of biofuel blends. The proposed tool uses an iterative method, which is one of the sizing methodologies often reported by authors for Integrated renewable energy systems (IRES) [136]. The iterative method is a deterministic method that evaluates the performance of an integrated system using a recursive program, which stops when the optimum system design is found. This method allows for minimising the cost of the system using linear programming techniques, such as mathematical programming. This work uses mathematical programming for the proposed solution, as it is one of the most successful models for formulating and solving decision-making problems [137]. Specifically, the proposed solution was developed as a mixed integer linear programming (MILP) model because this type of model has been used to evaluate the techno-economic performance of rural hybrid energy systems [138]. The optimal solution of the model was found using Gurobi [140], which implements the Branch and Cut (BC) algorithm.

Chapter 3

Experimental Work Methodology

This chapter presents the methodology followed for finding a suitable vegetable oil to reduce the use of red diesel and assess relevant parameters related to the performance of a diesel generator. The chapter is divided into three sub-sections, the first one addresses the fuel selection process and the analytical lab techniques required for fuel characterisation. The second sub-section describes the engine lab experiment setup providing a brief explanation of the instruments' operating principles and the procedure followed during the engine tests. Finally, the third sub-section mentions the analysis done on the engine's fuel injector after the engine tests were concluded for evaluating the impact of using biofuel blends.

3.1 Fuel Selection and Analytical Lab Work

As discussed in the previous chapter, one of the factors that can affect the performance of a genset is the type of fuel that powers the engine as its physicochemical properties may alter the engine's combustion process and its pollutant emissions. For that reason, this research started by selecting a fuel to assess the performance of a diesel generator that can also be a feasible fuel option for diesel substitution within the sub-Saharan African (SSA) region.

3.1.1 Fuel Selection

The fuel selection process reflects the interest to reduce diesel consumption and the intention of using local resources to reduce operating costs for remote electricity generation. Recalling from the literature review chapter, biofuels are an alternative option to diesel, therefore this work considered a second-generation biofuel that can be obtained from the seeds of any non-food crop available in the study area of this research.

The study area was determined by locating an SSA region that could benefit from the output of this research, as the SSA faces the greatest lack of access to electricity according to the Electrification Status section. For details on the electrification rates, the table created using the electricity access data from the World Bank 2016 indicators [142] for all the African countries can be consulted in Appendix A.

Once the biofuel type and the area of study were delimited, the programs and initiatives for biofuel production and the main crops for vegetable oil production

in Africa were investigated. Table 3-1 and Table 3-2 show the summary of the findings according to the data presented by Sekoai et al. [143].

Table 3-1 Development initiatives for biofuel in African countries.

Country	Program or Initiative	Crop
Burkina Faso	biofuel	jatropha oil
Ghana	biofuel	cassava, sugarcane, maize, and jatropha oil seeds
Mali	biofuel	jatropha oil
Malawi	biodiesel-based production plant	jatropha oil
	bioethanol production plant	sugarcane molasses
Mozambique	bioethanol production plant	cassava
	biodiesel production	jatropha oil
Nigeria	bioethanol production	N/A
	biodiesel production	N/A
Senegal	biofuel	jatropha oil, castor oil, and sunflower oil
South Africa	bioethanol production	sorghum
	biodiesel production	soya beans
Tanzania	biofuel	jatropha oil
	biodiesel production	jatropha oil

Table 3-2 Vegetable Oil availability in Africa.

Feedstock	Litres of Oil per Hectare	Countries that Grow Feedstock
Palm oil	5950	Angola, DRC, Ghana, Nigeria, Tanzania
Coconut	2689	Ghana, Mozambique, Nigeria, Senegal, Tanzania
Jatropha	2638	Benin, Tanzania, Malawi, Mozambique, Nigeria, Ghana
Avocado	1892	DRC, Ghana, Nigeria, Senegal, South Africa
Castor oil	1413	Angola, Congo Dem. Rep., Mozambique, South Africa

From the data included in Table 3-1 and Table 3-2, it was determined that jatropha and castor oil were viable vegetable oil (VO) options for the engine tests as both are non-edible feedstock and are produced in several African countries. However, jatropha oil has been widely studied and useful information is available in the literature, therefore castor oil was selected as the substitute fuel to carry out the experimental work.

3.1.2 Fuel Characterisation

As discussed in the Literature review chapter VO have different properties compared to diesel but VO can be used in diesel engines if diluted. The recommended dilution is around 20% VO and 80% diesel, except for jatropha

oil, which reported successful cases with up to 50% VO blends. Table 3-3 summarises the commonly reported physicochemical properties of the viable VO options and red diesel. Red diesel, also known as gas oil, is the fuel used in off-road vehicles, such as diesel generators, and it has a lower tax compared to white diesel [144].

Table 3-3 Physicochemical properties of selected vegetable oils and red diesel.

Crop	Density at 15°C (kg/m ³)	Viscosity at 40 °C (mm ² /s)	Flash Point (°C)	Cloud Point (°C)	Cetane number	Heating value (MJ/kg)
Jatropha ^a	916.5	37.28	211.7	-	21	38.96
Castor oil ^a	950	259.4	288.5	- 5.5	42.3	36.74
Red diesel ^b	860	3.5-4.5	>62	2	48	45.4

^a values taken from [108], ^b values taken from [144].

According to Sayyed et al. [145] two temperature-dependent physical properties of fuel, viscosity and density, strongly affect the fuel consumption of an engine. Agarwal and Agarwal [129] explained that the low volatility of VO is another relevant factor affecting fuel consumption, as it worsens the vaporisation of the fuel altering the combustion process. Also, the results presented by Agarwal and Agarwal [129] revealed that the viscosity of jatropha oil decreases remarkably with an increase in temperature. In their work, the authors measured the viscosity of jatropha oil with a temperature ranging from 40°C to 100°C. They also evaluated the viscosity of the blends at 40°C and reported that the viscosity of two of the blends (20% and 30% VO) was slightly higher than that of diesel but within the ASTM limits. Similarly, Pramanik [128] measured the viscosity of jatropha oil-diesel blends varying the temperature in the range from 25°C to 75°C. The author found that the viscosity of the blends is higher than that of diesel at all temperatures, nevertheless, a 30% and 40% jatropha oil blend could be used even without heating, as those blends have similar values to that of diesel if the temperature range is around 35 to 45 °C. On the other hand, castor oil has not been studied that much but according to Prasad et al. [130], dilution of castor oil with diesel reduces the viscosity considerably. Aware of this situation, the viscosity variation of the castor oil and castor oil-diesel (COD) blends, their density, and their volatility characteristics needed to be investigated.

To investigate the physicochemical characteristics of COD blends, 60 ml bottle fuel samples were prepared with different castor oil content by volume from 0% to 100% as shown in Figure 3-1.



Figure 3-1. Fuel blend samples for fuel characterisation analyses.

For each blend, a Thermo-gravimetric analysis (TGA) and an Elemental (CHNS-O) analysis were carried out. The gross calorific value (GCV) and net calorific value (NCV) were determined with the Bomb calorimetry technique. Also, the densities and viscosities of each blend were determined at different temperatures as explained in the following subsections.

3.1.2.1 Thermo-gravimetric Analysis (TGA)

A TGA is a helpful technique to characterise thermal stability, it measures the physical or chemical properties of substances as a function of temperature and time [145]. TGA has been used by other authors to measure onset volatilisation temperatures for various oils as the different volatility can influence the ignition quality of the fuel [146]. In this work, TGA was done to compare the volatility characteristics of the fuel blends by looking at their onset volatilisation temperatures and the mass loss stages found in their thermograms.

The TGA for the blends was done using the Shimadzu TGA50 analyser shown in Figure 3-2. With a disposable Pasteur pipette, a drop of each blend (about 30 mg) was dispensed into the alumina crucible to measure the sample mass loss against time and temperature with a heating rate of 10°C/min from room temperature up to 610°C in a Nitrogen atmosphere. At 610°C the Nitrogen atmosphere was switched to air, holding that temperature for 10 minutes.

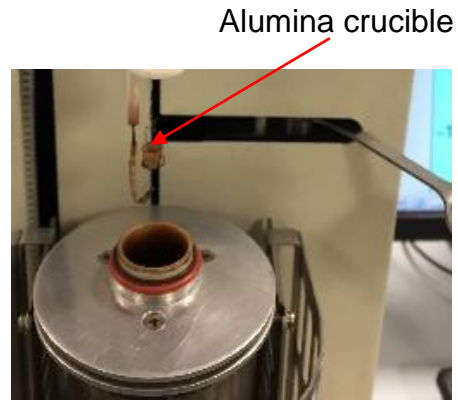


Figure 3-2. Schimadzu TGA50 analyser used for mass loss determination of fuel blend samples.

3.1.2.2 Bomb Calorimetry

About 0.2 g of each fuel blend were placed in a combustion cup and burnt in pure oxygen within a sealed bomb surrounded by a water bath using a Parr 6200 calorimeter shown in Figure 3-3. The calorimeter uses the heat released from the combustion and divides the result of the energy released by the weight of each sample to determine the GCV and the NCV.

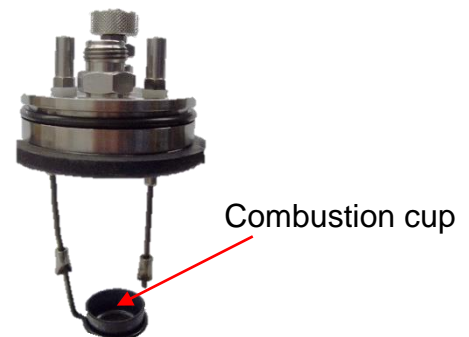


Figure 3-3 Parr 6200 calorimeter used for gross and net calorific values of fuel blend samples.

3.1.2.3 Elemental Analysis

To determine the Carbon, Hydrogen, Nitrogen and Sulphur (CHNS) content of the samples, a Thermo Scientific Flash EA2000 elemental analyser shown in Figure 3-4 was used.



Figure 3-4 Analyser and capsules used for elemental analysis of fuel blend samples.

The analyser determines the composition of the samples by the combustion of fuel capsules (2-4mg) fed into the furnace at 900°C where pure oxygen is added to ensure the complete combustion of the products. When the oxygen is added, it reacts with the tin capsule and the temperature increases to 1800°C. After the combustion, the fuel components are separated in a gas chromatographic column to be detected by a thermal conductivity detector. The thermal conductivity detector consists of a stainless-steel block with two pairs of filaments that have the same electrical resistance. The filaments are electrically connected following a Wheatstone bridge circuit and are powered at a constant voltage. One pair of filaments is fed with pure carrier gas, whereas the second one is fed with the gas flowing from the furnace (sample and carrier gas). Once the bridge is powered, the filaments heat at a certain temperature that depends on the thermal conductivity of the gas that feeds the filaments. The eluted components of the sample gas produce a change in heat transfer, which in turn varies the filaments' temperature. The temperature variation allows the detector to generate a signal proportional to the difference in thermal conductivity between each eluted component and the carrier gas. Finally, the signal is processed by the data acquisition software [147]. Figure 3-5 shows the schematic diagram of a CHNS analysis.

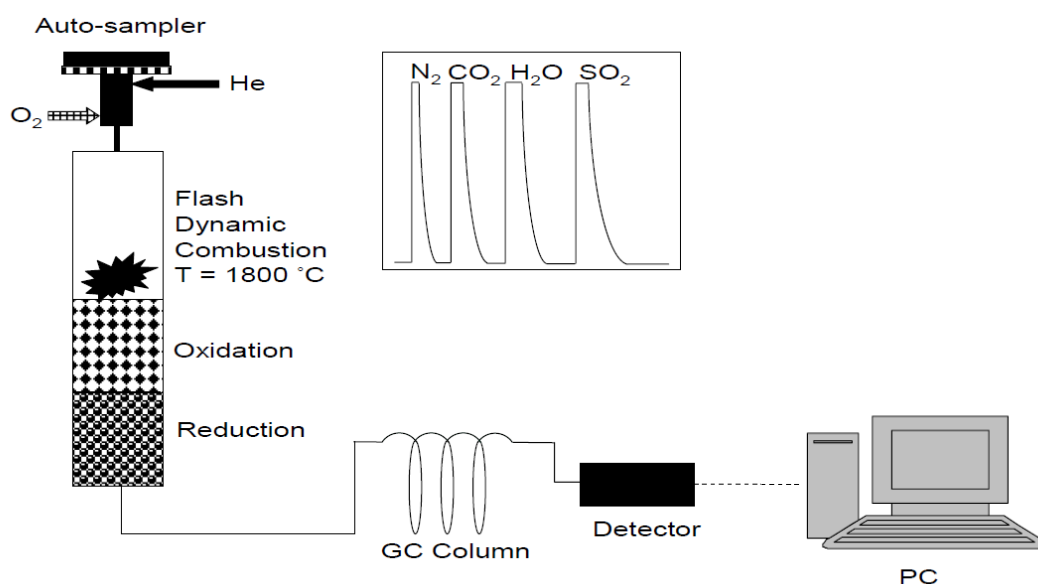


Figure 3-5 CHNS analysis schematic diagram [148].

3.1.2.4 Density and Viscosity

The density and kinematic viscosity of each blend were determined using an Anton Paar Stabinger viscometer (SVM 3000), its measuring ranges are listed in Table 3-4.

Table 3-4 SVM 3000 Measuring Ranges.

Property	Measuring Range
Dynamic viscosity (mPa·s)	0.2 – 20.000
Kinematic viscosity (mm ² /s)	0.2 – 20.000
Density (g/cm ³)	0.65 – 3
Temperature (°C)	-56 – 100

Both properties were measured by injecting 5 ml of each sample into the sample injection port as indicated in Figure 3-6. The first measurement was done at 15°C and further measurements were done from 20°C to 100°C with a 10°C step increment between measurements.

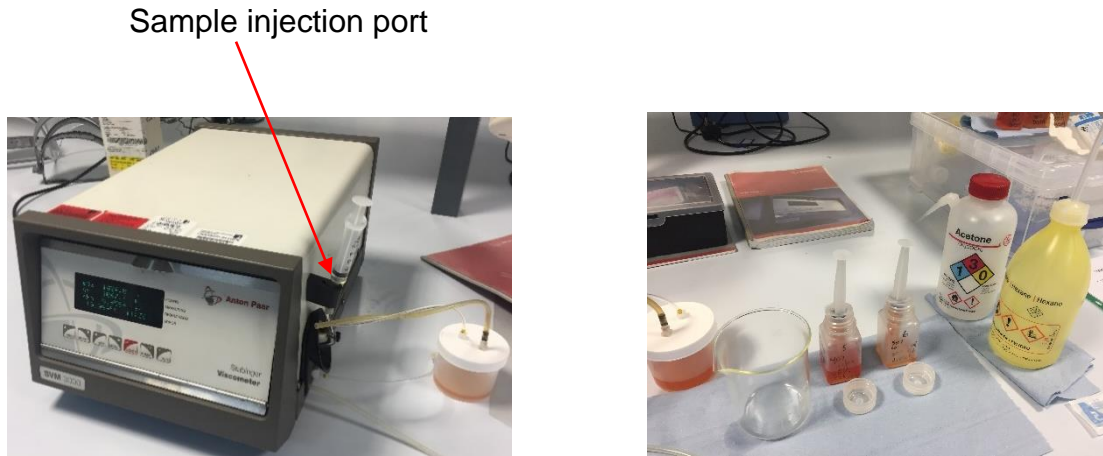


Figure 3-6 Experiment setup for density and kinematic determination of fuel blend samples using an SVM 3000 Stabinger viscometer.

3.2 Engine Lab work

In chapter 2 it was mentioned that a diesel generator relies on the interaction between a diesel engine and an alternator. This interaction dictates the performance of any genset as a function of the engine's output power and the alternator's efficiency. Both parameters depend on the engine's and alternator's design characteristics, their operating conditions (working load), and the type of fuel running the engine. Two key indicators for evaluating the performance of an engine are the Brake Specific Fuel Consumption (BSFC) and Brake Thermal Efficiency (BTE). To determine those indicators and the genset's pollutant emissions the experimental work described in the coming sections was carried out in the Engine laboratory from the Combustion and Future Fuels laboratories testing the genset at 5 operating conditions, using 5 castor oil-diesel blends. The experimental work was repeated three times at every engine operating condition with its corresponding fuel blend for data reliability. The standard deviation of the data sets was calculated and it was used to display the error bars (\pm one standard deviation) of the results presented in Chapter 4.

3.2.1 Experiment Setup

The engine lab work was done using the experiment setup shown in the schematic diagram of Figure 3-7.

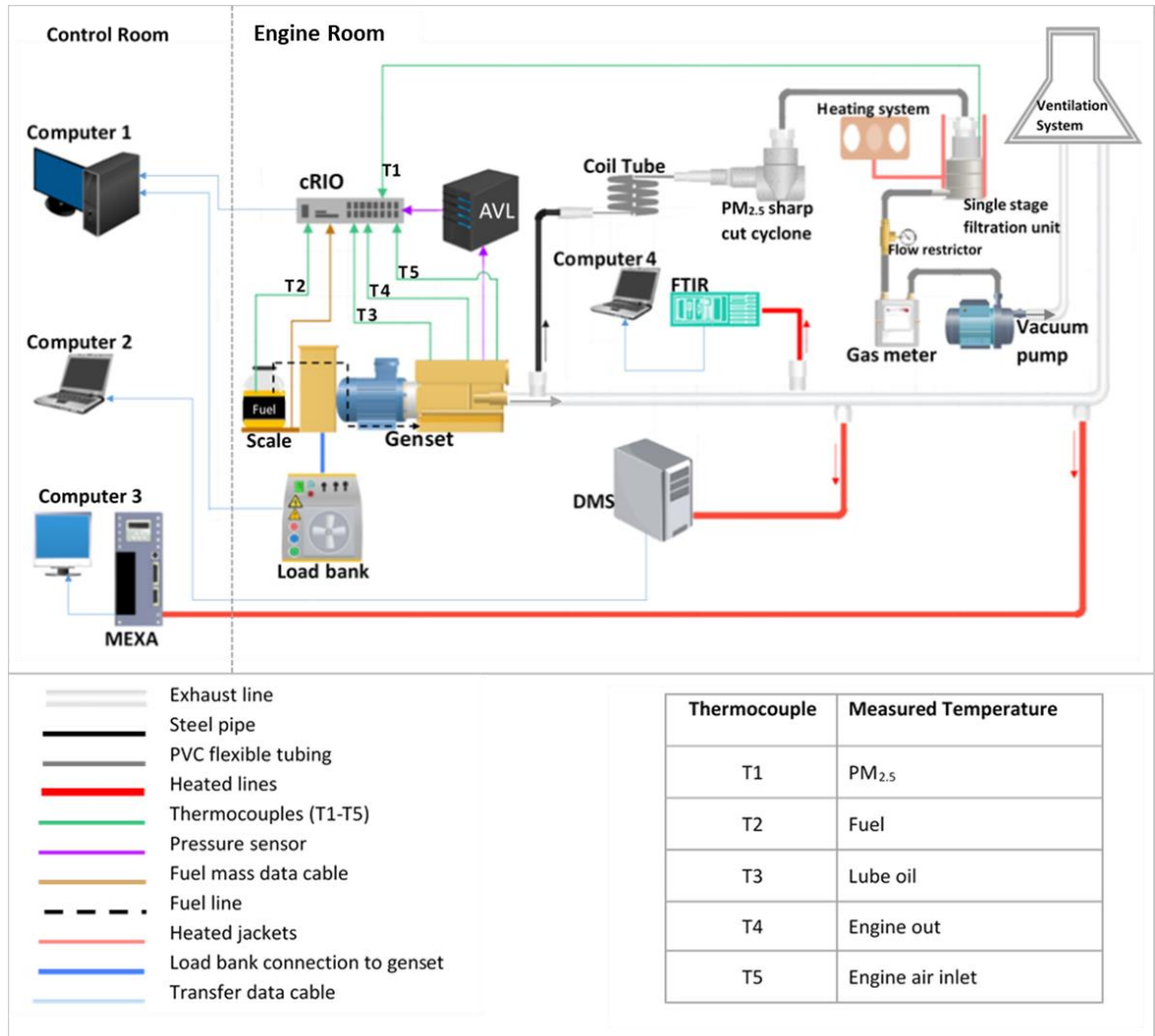


Figure 3-7 Schematic diagram of the engine test experiment setup.

A 10 kW Hillstone load bank [149] was connected to the 230V- single-phase socket of a 6 kVA diesel generator to vary the working load from the genset's maximum power to zero-load conditions. The zero-load in this work refers to the generator's no-load operating conditions, where the prime mover is set to 0 kW at its constant speed (3000 rpm). This condition defers from the idling definition used for vehicles where the engine is decoupled from the gearbox at idle. In the genset situation, the engine is permanently connected to the alternator, therefore some voltage and current will be generated as long as the engine is kept at its constant speed. A diesel generator is a constant-speed machine that regulates the amount of fuel injected to compensate for the tendency to slow down when a load is applied or speed up at lower loads. Table 3-5 shows the engine and load bank parameters that were monitored during the engine tests.

Table 3-5 Engine test parameters.

	In-cylinder pressure (bar)
	Engine exhaust temperature (°C)
	Engine air inlet temperature (°C)
	Lube oil temperature (°C)
Engine Parameters	Fuel temperature (°C)
	Single-stage filtration unit temperature (°C).
	Fuel Mass (kg)
	Engine Speed (rpm)
	Crank Angle (deg)
	Voltage (V)
Load Bank Parameters	Current (A)
	Frequency (Hz)
	Power (kW)

The in-cylinder pressure was monitored with a piezoelectric pressure sensor (GH14D) from AVL manufacturer. The pressure sensor has a measuring range from 0 to 250 bar and it was installed in the cylinder head of the engine. The temperatures listed in Table 3-5 were monitored using k-type thermocouples (T1-T5), as previously indicated in the schematic diagram from Figure 3-7. The fuel consumption was monitored using a CPWplus 35 scale located beneath the fuel bottles as shown in Figure 3-8. The scale can be used to weigh up to 35 kg with a resolution of 10 grams.

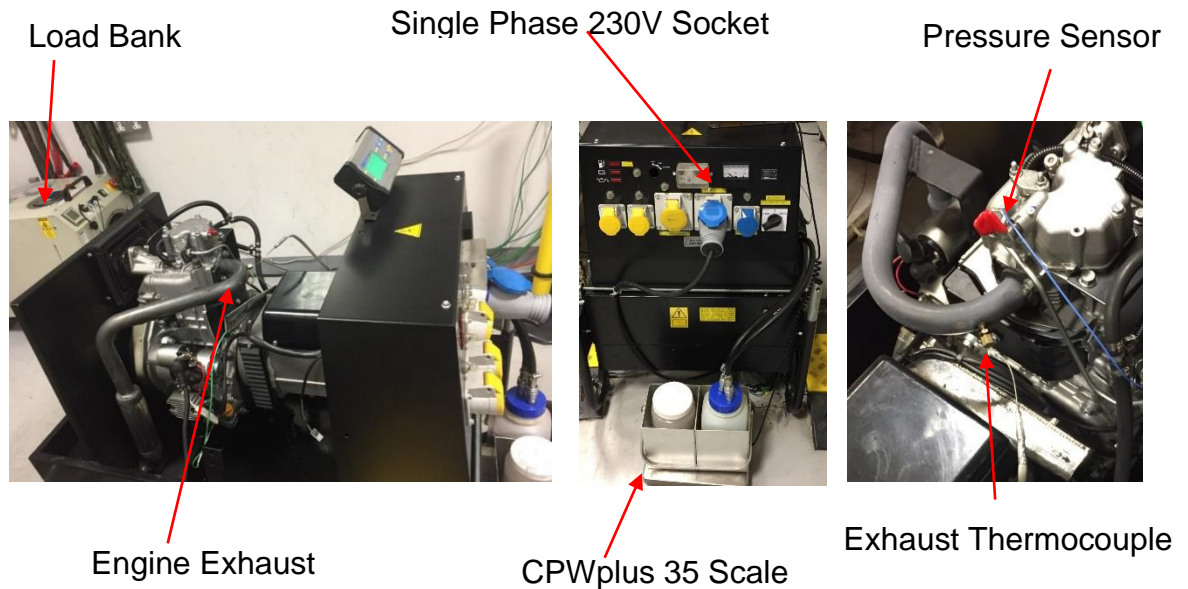


Figure 3-8 Diesel generator and load bank experiment setup.

The pressure sensor data was sent to an AVL Flexifem combustion measuring system for signal amplification and data acquisition. The outputs from the AVL, thermocouples, and scale were connected to a compact reconfigurable input/output (cRIO) controller from National Instruments [150]. The controller was connected via an Ethernet port to computer 1 in the control room where the output from the cRIO was then visualised using Lab View software. From the pressure sensor readings (360 pulses per rotation) the engine speed in rpm was calculated by considering an initial crankshaft point of rotation at the piston's top dead centre (TDC) and assuming a constant angular velocity of the crankshaft. The engine speed was then converted to crank angle degrees (CAD) with a resolution of 0.5 CAD, where the TDC pressure corresponds to zero CAD. The rpm and CAD calculations were automatically done by the algorithm included in Lab View before the final data visualisation was generated. The data from the load bank was logged, stored and visualised with the Hillstone ACLoadView software [151] also using computer 1. The rpm, temperature and load bank readings were logged every second during the engine experiment. Table 3-6 shows the technical specifications of the genset and the load bank.

Table 3-6 Diesel Generator and Load Bank Technical Specifications

Genset	Linz Alternator	E1C10M H
	Generator Power (230 V)	6 kVA / 4.8kW
	Yanmar Engine	L100V
	Fuel	Diesel
	Cylinder	1
	Displacement	0.435 l
	Compression Ratio	21.2
	Engine Speed	3000 rpm
	Max Power	6.3 kW
	Continuous Power	5.7 kW
	Cooling system	Air
	Starting System	Electric
	Load bank	Hillstone Load bank
Power		10 kW at 240V
Max Volts		240 V
Amps at 240 V		42 A

The engine exhaust gases were also monitored to measure the engine's pollutant emissions. The engine exhaust was directed through an exhaust line where the pollutant emissions monitoring units were then connected. For the pollutant measurement, a Horiba gas analyser (MEXA 7100), a Gaset Fourier Transform Infrared spectroscopy (FTIR) emissions monitoring system, a Cambustion Fast Particulate Analyser (DMS 500) and a PM_{2.5} collection system were used. The MEXA 7100, FTIR, and DMS 500 were connected to the exhaust line with the specified sampling probes (heated lines) from each manufacturer and the PM_{2.5} collection system was connected using a 6.25 mm inside diameter stainless steel pipe. The details for each pollutant monitoring instrument are described below.

3.2.1.1 Motor Exhaust Gas Analyser — MEXA 7100

The gas analyser MEXA 7100 manufactured by HORIBA measures the concentration of CO, CO₂, THC, NO_x and O₂. The analyser is configured as a

modular system with an Integrated Laboratory Automation System (ILAS) that enables special functions such as averaging and accumulation of measurement data, calculation of air-fuel ratios and real-time graphic display, among others [152]. The gas components were measured with specific analyser modules that use different detection principles [153] as summarised in Table 3-7. The measured data was logged every 10 seconds and stored for further analysis with the DaTAQ Pro software.

Table 3-7 MEXA 7100 detection principles for gas measurement

Gas component	Detection Principle	Analyser Model
CO and CO₂	Non Dispersive Infrared absorption (NDIR)	AIA-72X
THC	Flame Ionization Analysis (FIA)	FIA-725A
NO_x /NO	Chemiluminescence Analysis (CLA)	CLA-720MA
O₂	Magneto-Pneumatic Detection (MPD)	MPA-720

The NDIR principle is used to identify the components of a sample gas when it is exposed to infrared light. The analyser detects one component at a time as specified in the instrument depending on the wavelength absorbed by the gas molecule, for example, CO₂ is detected at 4.26 μm wavelength.

For the FIA the sample gas is burned using a hydrogen flame inside a flame ionisation detector (FID), the ions resulting from any hydrocarbon present in the sample are detected by a metal collector [154]. In the FID the sample gas is burned in a heated chamber to prevent water vapour condensation, Figure 3-9 shows a schematic diagram of an FID.

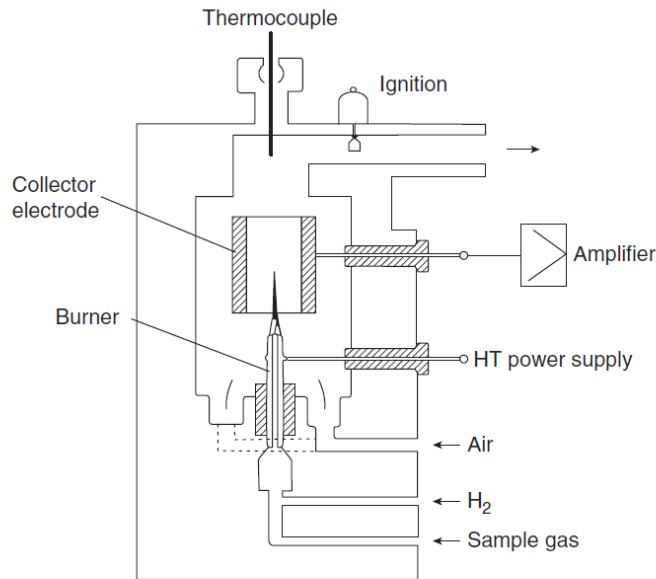
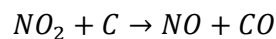


Figure 3-9 Schematic diagram of a Flame Ionisation Detector [155].

The CLA principle relies on the amount of light (photons) emitted by the chemical reaction between Nitrogen monoxide (NO) and Ozone (O₃). For exhaust gases where nitrogen compounds exist as a mixture of NO and NO₂, the chemical reaction happens when the NO reacts with the ozone generated by the electrically discharged Oxygen in a heated vacuum chamber before it enters the reaction chamber. The light generated is proportional to the NO concentration and it is measured by a photomultiplier [155]. To measure the NO₂, it should be first converted to NO by reacting with Carbon (C) [153]. The chemical reactions are shown in Equation 3-1 and Equation 3-2 to clarify the chemiluminescence process.



Equation 3-1



Equation 3-2

The MPD principle relies on the greater response of oxygen to a magnetic field compared to other gases. In the oxygen analyser module, a magnetic field is created by passing AC through an electromagnet, when the sample passes through the magnetic field, the pressure around the magnetic poles rises depending on the amount of oxygen present in the sample gas. The pressure variation is sensed by a capacitor microphone detector as an alternating signal due to the electric capacity changes [153].

3.2.1.2 Gasmet FTIR Emissions Monitoring System

The Gasmet emission monitoring system comprises a DX4000 FTIR analyser and a Portable Sampling System (PSS) shown in Figure 3-10.

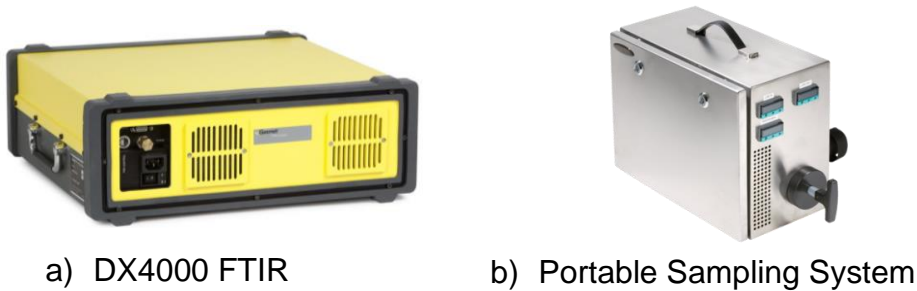


Figure 3-10 Gasmet emission monitoring system components [156].

To measure the gas emissions, a heated line was connected from the exhaust line to the SSP in-sample port at 180°C to avoid water condensation. Then the pump inside the SSP delivered the sample to the analyser at a flow rate between 1 and 5 lpm through a heated line connected between the SSP out-sample port and the analyser.

As in the NDIR, the FTIR uses infrared spectroscopy, the technique for chemical analysis and determination of molecular structure for the liquid, or gas state of the sample of study. The technique is based on the molecular vibrations and characteristic absorption frequencies of chemical compounds that occur in the infrared region of the electromagnetic spectrum, particularly within the 2.5 and 16 μm wavelengths (4000 - 625 cm^{-1}). For each wavelength, the transmittance (T) represents the intensity of IR that passes through the sample gas (I) divided by the intensity of the IR beam (I_0), where 100% transmittance ($T = 1$) means no absorption. The IR absorption for each gas can be graphically represented by plotting the absorbance ($A = \log_{10} \left(\frac{1}{T} \right)$) vs. the wave number in cm^{-1} (the reciprocal of the wavelength) as the absorbance is directly proportional to the concentration of the sample gas [157]. The FTIR can measure up to 50 different gases utilising Fourier Transform Infrared spectroscopy as it measures all the infrared wavelengths simultaneously to produce a full spectrum. Table 3-8 shows the species measured by the FTIR with their corresponding measuring range.

Table 3-8 FTIR species with measuring ranges.

Species		Measuring Range
1	Water Vapor	H ₂ O 0-25 vol%
2	Carbon dioxide	CO ₂ 0-20 vol%
3	Carbon monoxide	CO 0-10,000 ppm
4	Nitrous oxide	N ₂ O 0-500 ppm
5	Nitrogen monoxide	NO 0-500 ppm
6	Nitrogen dioxide	NO ₂ 0-1000 ppm
7	Sulphur dioxide	SO ₂ 0-1000 ppm
8	Ammonia	NH ₃ 0-500 ppm
9	Hydrogen chloride	HCl 0-500 ppm
10	Hydrogen fluoride	HF 0-100 ppm
11	Methane	CH ₄ 0-500 ppm
12	Ethane	C ₂ H ₆ 0-100 ppm
13	Ethylene	C ₂ H ₄ 0-100 ppm
14	Propane	C ₃ H ₈ 0-100 ppm
15	Hexane	C ₆ H ₁₄ 0-100 ppm
16	Formaldehyde	CHOH 0-200 ppm
17	Benzene	C ₆ H ₆ 0-100 ppm
18	Acetylene	C ₂ H ₂ 0-200 ppm
19	Acetic acid	C ₂ H ₄ O ₂ 0-100 ppm
20	Furfural	C ₅ H ₄ O ₂ 0-100 ppm
21	Terpinen-4-ol	C ₁₀ H ₁₈ O 0-100 ppm
22	Hydrogen cyanide	HCN 0-100 ppm
23	Ethanol	C ₂ H ₆ O 0-100 ppm
24	Acetaldehyde	C ₂ H ₄ O 0-100 ppm
25	Butadiene	C ₄ H ₆ 0-100 ppm

The monitoring system operates with Calmec software that collects, stores and visualizes the FTIR spectra of the sample gas [156]. Figure 3-11 shows an example of a multi-component analysis spectra that considers a sample gas and two reference gases.

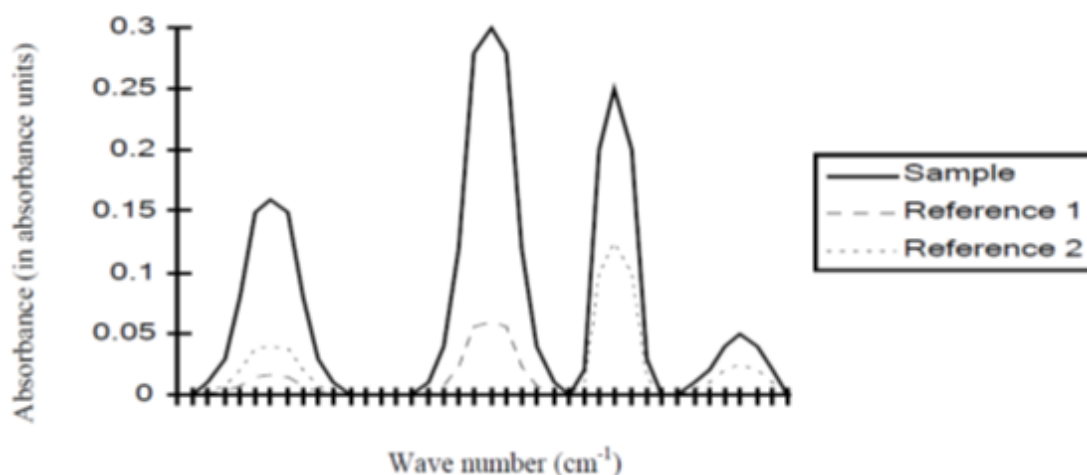


Figure 3-11 Example of FTIR multi-component analysis spectra representation [157].

3.2.1.3 DMS 500

The Combustion DMS500 Fast Particulate Analyser (see Figure 3-12) determines the particle size distribution and number/mass concentrations of engine exhaust for particles between 5 and 1000nm [158]. For diesel engine emissions the size range of most interest goes from 10 to 200 nm. The data is processed, stored, and visualised with the Combustion software that comes with a user interface to operate the analyser. Figure 3-12 shows the DMS analyser (left) and the user's interface main screen (right).

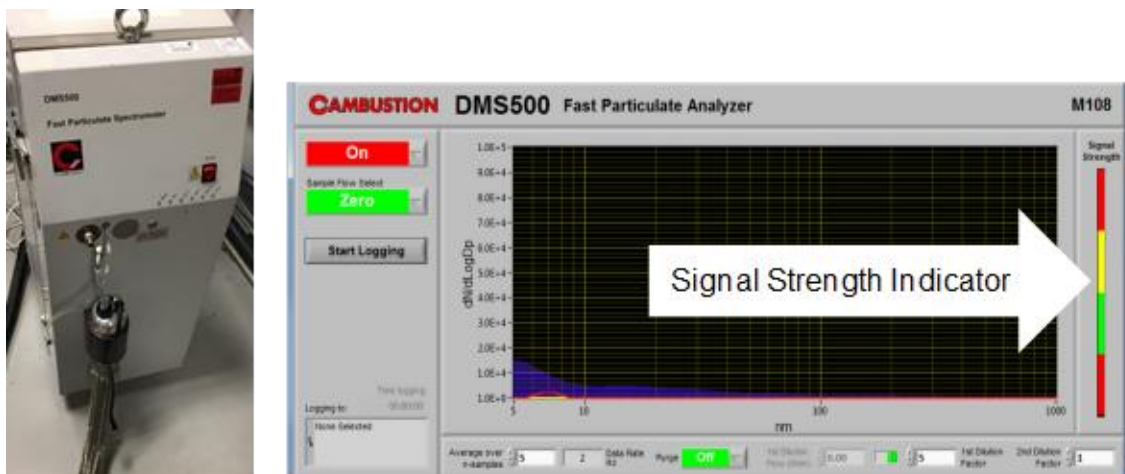


Figure 3-12 DMS500 Fast Particulate Analyser and DMS user interface [158].

The DMS was connected to the exhaust line through a heated line that has a heated sampler directly connected to the exhaust line. In the heated sampler, a first dilution stage occurs as the sample gas is diluted with dry compressed air (coming from a vacuum pump connected to the DMS) using a dilution factor of

5:1 to prevent water vapour condensation. Still inside the heated sampler, after the first dilution, the gas passes through a cyclone separator that removes particles >1000nm to prevent clogging the DMS. The gas that comes out from the cyclone travels along the heated line (towards the DMS) and passes through a rotating disc diluter and a High Efficiency Particulate Absorbing (HEPA) filter for a second dilution stage. The second dilution stage allows diluting high concentration aerosols before they reach the classifier column. The second dilution factor should be adjusted by the user (within a range between 12 and 500) to maintain the signal to noise ratio within the green zone of the signal strength indicator [158, 159] that appears on the user's interface main screen. During the experimental work, the second dilution factor was kept at about 160. After the second dilution stage, the particles from the sample gas (drawn by the DMS 500 at 8 lpm) received a positive charge proportional to its surface area by a corona charger (with a voltage range between 3,200 and 4,250 V) before entering the classification column, like the one shown in Figure 3-13.

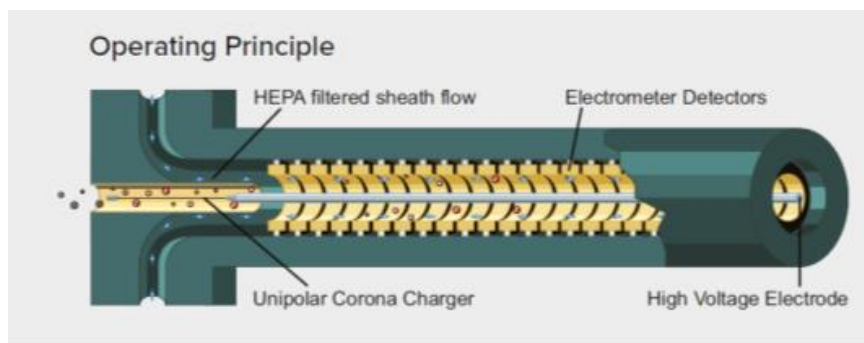


Figure 3-13 DMS 500 Classifier column [160].

In the classification column, the electrical field of a positive high voltage electrode drifts the particles towards electrometer detectors. The particles are detected at different distances within the column because smaller particles are easily deflected towards the detectors whereas the bigger ones land on a further detector along the column. Therefore, the number and size of the particles in the sample gas can be determined.

3.2.1.4 PM_{2.5} Collection System

To monitor the PM_{2.5} particulates during the engine tests, a modified Andersen Impactor particle sampling device was used. A single-stage filtration unit consisting of the last stage of an Andersen's sampler was selected to collect all the PM_{2.5} from the exhaust gas onto a single filter paper. The exhaust gas was

directed from the exhaust line through a stainless steel pipe, wrapped with pipe lagging, towards the bottom inlet of a coiled stainless steel pipe covered with aluminium foil. The upper end of the coiled pipe was connected to the lateral inlet of a PM_{2.5} sharp cut cyclone which was connected with PVC flexible tubing to a single-stage filtration unit. The filtration unit was kept at 50°C by wrapping it with a heating jacket controlled by a heat controller unit and monitored with a thermocouple connected to the cRIO controller. The filtration unit was connected to a gas meter and the gas meter to a vacuum pump that kept the flow rate at 16.7 lpm. For every test, a Whatman glass microfibre filter paper (GF/F) was placed inside the filtration unit using a rubber O-ring to collect the particulates (see Figure 3-14).

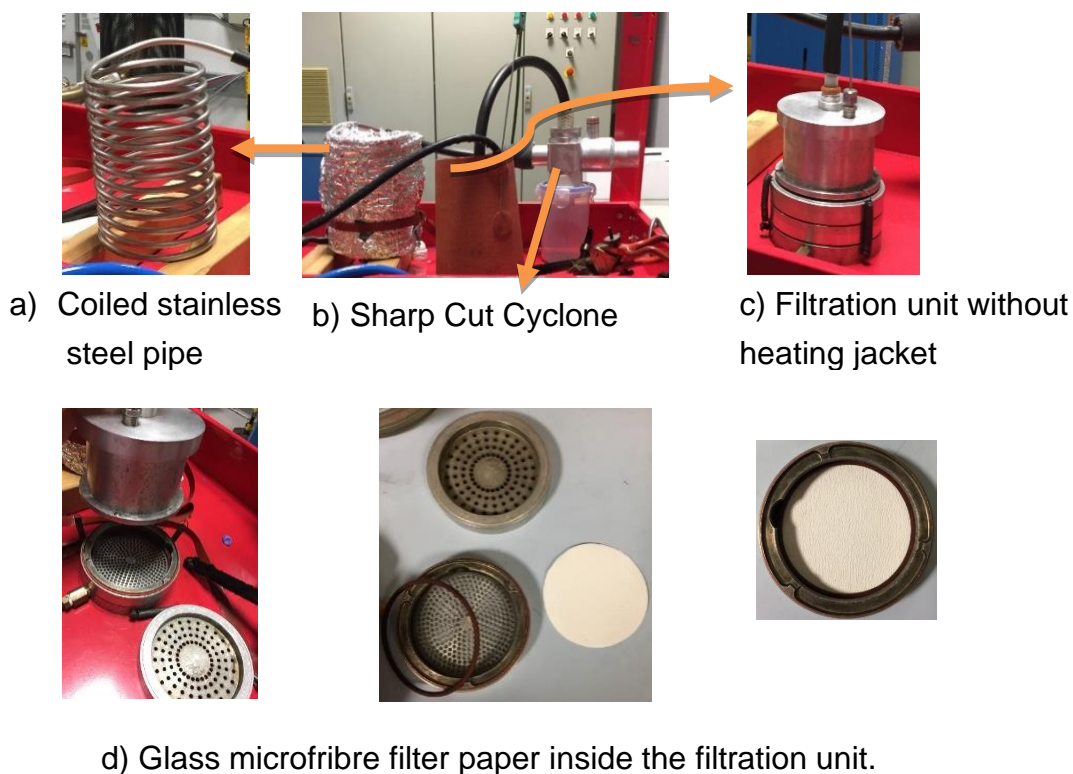
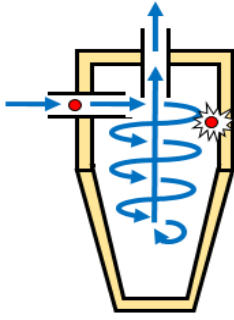


Figure 3-14 PM_{2.5} collection system and glass microfibre filter paper.

The PM_{2.5} collection system relies on the inertia of the particles that flow in the stream drawn by the vacuum pump. If the particles entering the cyclone nozzle are larger than the cut-off diameter, they collide with the wall of the cyclone and accumulate at the bottom. Then, from the stream that leaves the cyclone and enters the separation unit, only the PM_{2.5} particles are collected when the sample gas passes through the filter paper. A representation of the cyclone operation principle is shown in Figure 3-15.



a) Cyclone

Figure 3-15 Illustration of the operation principle of the PM_{2.5} collection system [161].

3.2.2 Engine Test Procedure

Every test started with a warmup protocol to prepare the instruments for the engine test. The first step was turning on every instrument and waiting for their sampling units to reach the right operating temperature at 191°C for MEXA, 55°C for DMS, and 180°C for the FTIR, the temperature of the PM_{2.5} impactor was set to 50°C. Once the warmup was finished, the next step was to open the span gas lines connected to the MEXA and FTIR. At this point, the MEXA analysers were calibrated for the measurement ranges shown in Table 3-9.

Table 3-9 Measuring ranges and calibration gas concentrations for MEXA 7100

Component	Measuring Range	Calibration Gas Concentrations
CO _{high}	0 – 12.0 (Vol %)	2.08 (Vol %)
CO ₂	0 – 20 (Vol %)	6.93 (Vol%)
CO _{low}	0 – 5,000 (ppm)	-
O ₂	0 – 25 (Vol %)	High purity
THC	0 – 50,000 (ppmC)	465 ppmC
NOx/NO	0 – 10,000 (ppm)	459ppm/457ppm

The MEXA Air-fuel Ratio (AFR) settings were adjusted to match the elemental ratios for Hydrogen to Carbon (H/C), and Oxygen to Carbon (O/C), of the fuel to be used during the engine test. The molecular ratios were found using the results from the elemental analysis and Equation 3-3 and Equation 3-4.

$$H/C = \frac{\frac{\text{Hydrogen weight (\% in sample)}}{\text{Hydrogen atomic mass}}}{\frac{\text{Carbon weight (\% in sample)}}{\text{Carbon atomic mass}}} \quad \text{Equation 3-3}$$

$$O/C = \frac{\frac{\text{Oxygen weight (\% in sample)}}{\text{Oxygen atomic mass}}}{\frac{\text{Carbon weight (\% in sample)}}{\text{Carbon atomic mass}}} \quad \text{Equation 3-4}$$

The DMS was calibrated with the calibration file for diesel engines supplied by the manufacturer and the electrometers were zeroed to remove any offset voltages. The FTIR sample cell was flushed with Nitrogen for 5 minutes and then background and Zero checks were done to ensure the analyser was ready to use. The background graph plots the single beam spectrum showing the absolute intensity of the IR transmitted through the sample cell filled with Nitrogen and represents the comparison level (zero level) to which the sample values are compared for calculating the absorbance and transmittance of each component [157]. An example of the background spectrum and Zero sample check graphs are shown in Figure 3-16 and Figure 3-17.

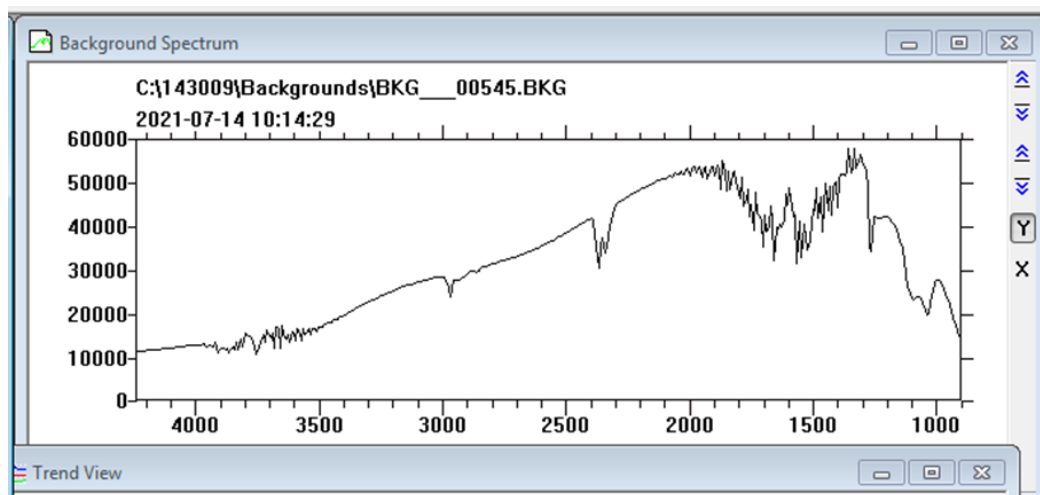


Figure 3-16 FTIR background spectrum.

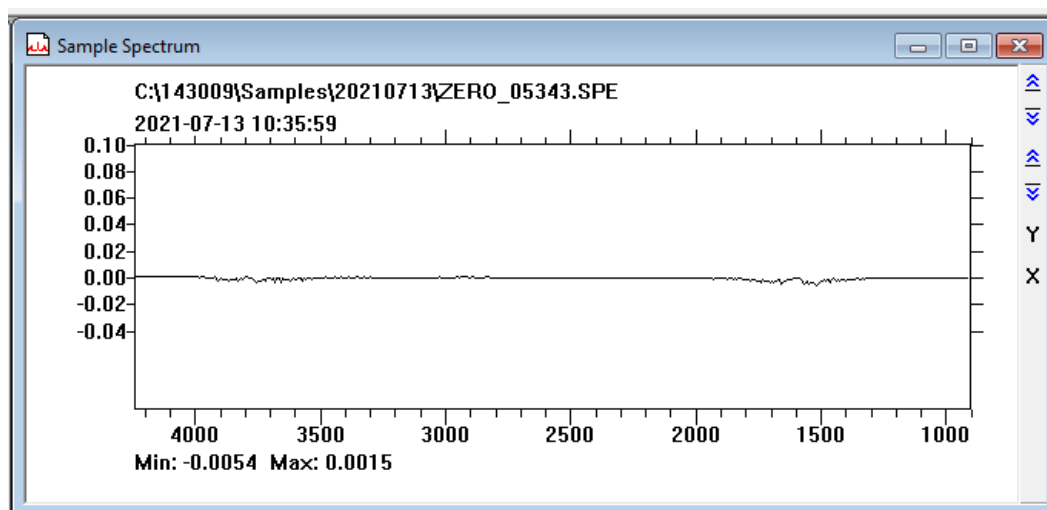


Figure 3-17 FTIR Zero sample check graph.

For operating the PM_{2.5} collection unit the flow rate from the vacuum pump was set to 16.7 lpm always having a test filter paper placed inside the impactor. Once the flow rate was set, a new, clean, and conditioned filter paper was used to replace the test filter paper. For the conditioning of filter papers, each GF/F filter paper was trimmed from its original diameter (90mm) to 81 mm using a stainless-steel cutter to fit the impactor dimensions. After the trimming process, the filter papers were dried inside a desiccator, like the one shown in Figure 3-18, for at least 24 hrs using silica gel as the drying agent. After the adequate drying period, each filter paper was weighed with a Metler Toledo electronic balance before using it for the engine test.



a) Stainless Steel Cutter.



b) Desiccator with clean filter papers.



c) Test filter paper.

Figure 3-18 Filter paper conditioning units and test filter used during the PM_{2.5} collection system warmup.

The next step was checking the engine's lube oil and fuel levels to prevent any damage to the engine during the test. Finally, the engine was started, and it was kept running with red diesel for about 10 to 15 minutes to bring the engine to stable conditions with a lube oil temperature above 48°C. After the warmup

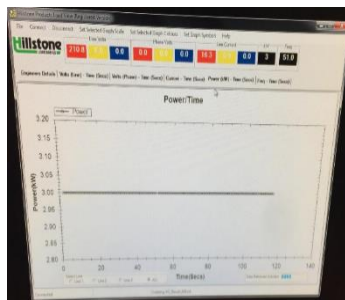
period, a 20 min run was carried out for each working load and every fuel blend selected as explained below. It should be noted that during the 20 min engine run, the ambient temperature was about 30°C as the room temperature increased once the engine warm up and engine stable conditions working periods were done.

3.2.2.1 Baseline (diesel) Test

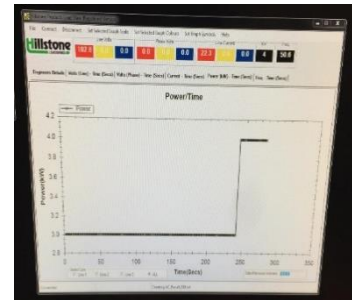
An initial set of engine tests was done running the genset with red diesel to determine the baseline parameters for BSFC, BTE and pollutant emissions at different loads (4kW, 3kW, 2kW, 1 kW and 0.18 kW). For starting a new test, after the warmup protocol was carried out, the engine was brought to the desired load using the load bank controller shown in Figure 3-19. Once the right load was reached, the engine was run at that load for about 3 minutes to ensure steady operating conditions (see Figure 3-19) before starting data logging for DMS, FTIR, MEXA and turning on the vacuum pump for particulate collection.



a) Load bank controller.



b) Engine at steady conditions.



c) Engine load increased.

Figure 3-19 Load bank controller and engine operating conditions for starting a test.

At the end of the 20 minutes engine test, the vacuum pump and the engine were turned off, and the data logging in all instruments was stopped. Once the instruments were stopped, the filter paper with the collected particulates, similar to those appearing in Figure 3-20, was removed from the impactor and placed inside the desiccator for a 24 hrs drying period before weighing it again to check the gained weight.



a) Used filter paper from engine test at 0.18 kW.



b) Used filter paper from engine test at 4 kW.

Figure 3-20 Filter papers with particulates collected during engine tests at different loads. Filter paper a) shows a lighter colour compared to filter paper b) due to the lower number of particulates produced at lower loads.

For starting the next run, at a different load, a clean filter paper was placed in the impactor and the fuel bottle was topped up when necessary.

Finally, at the end of the last run of the day, all the instruments were turned off.

3.2.2.2 Castor Oil- Diesel (COD) Blend Test

To complete the engine lab work, five blends were prepared to assess the effects on the engine's performance by increasing the castor oil content by 20, 40, 50, 60 and 80% in the running fuel. For every test with COD blends, two bottles of fuel blend (2.2 litres each) like the ones from Figure 3-21 were prepared before the warmup period.



Figure 3-21 Fuel blend preparation for the COD40 (40% castor oil) engine test.

Each bottle was prepared by blending the right amount of diesel and castor oil according to the data presented in Table 3-10 as appropriate for the run of the day.

Table 3-10 Castor oil and diesel content in fuel blends for the engine tests.

	Castor Oil (ml)	Red Diesel (ml)	Fuel Blend (ml)
COD0	0	2200	2200
COD20	440	1760	2200
COD40	880	1320	2200
COD50	1100	1100	2200
COD60	1320	880	2200
COD80	1760	440	2200

Once the fuel blends were ready, the same baseline test procedure was followed but a small modification to the procedure was implemented. The first modification was done immediately after the warmup period where an empty bottle was connected to the fuel line to run the engine without further fuel intake. When the engine stopped, as no more fuel was left in the fuel line, the empty bottle was replaced with a bottle of fuel blend and the engine was started again. The engine was running for about 3 to 5 minutes until stable conditions (with the fuel blend) and the engine test continued as described in the diesel baseline section. It should be noted that for the COD60 and COD80 tests, the fuel blend temperature was increased to reduce their viscosity. The COD60 temperature was maintained between 55°C and 60 °C by submerging the fuel bottles in a hot water bath. The COD80 bottle was also submerged in a hot water bath and a heating jacket was placed at the bottom of the fuel bottle to keep its temperature at about 70°C.

The second modification was done when the last run of the day was completed by replacing the fuel blend bottle with a diesel one. The engine was started again to run for about 15 minutes (flushing time) and remove any castor oil remaining in the fuel line. After the flushing time, the engine was shut down and ready for the next day.

3.3 Biofuel Impact on Engine's Fuel Injector

After the engine tests an inspection of the fuel injector was done to verify the impact (deposits formation) of using such a viscous fuel during the experimental work. The inspection of the fuel injector was done using the Carl Zeiss EVO MA15 Scanning Electron Microscope (SEM) shown in Figure 3-22 and Energy Dispersive X-ray spectroscopy (EDX) from the Leeds electron microscopy and spectroscopy centre (LEMAS).



Figure 3-22 LEMAS scanning electron microscope.

An SEM is an instrument commonly used in material analysis as it can generate detailed topographic images of a sample and determine its chemical composition. The SEM uses an electron beam to scan the surface of a sample and detects the signals generated during the scanning process from the interactions between the electrons in the beam and the atoms in the sample. The signals are differentiated by the penetration depth of the beam and are received by different detectors that provide specific information about the sample's structure or composition depending on the type of signal received. The signal generated by secondary electrons comes from a shallow region of the sample, this signal generates a topographic image. The Backscattered Electrons signal comes from a deeper region and has more energy compared to the secondary electrons. The Backscattered electrons detector (BSD) produces

a contrast image based on the atomic number (Z) of the elements found in the sample material. Elements with higher atomic numbers emit more backscattered electrons and are brighter in the image than the low atomic number elements. The characterisation of the sample's composition was done with the Energy Dispersive X-ray (EDX) detector. The X-ray signal is produced by the energy difference of the electrons moving within the energy levels of an atom after the electron beam hits the inner shell of that atom. The X-ray is unique to specific elements, therefore an EDX spectrum can be mapped for the elements found in the sample [162].

For doing the SEM and EDX analysis, the fuel injector was removed from the engine and dismantled to separate the needle and the nozzle from the body of the injector. A sample preparation procedure was done to the needle and the injector's nozzle to remove any oily residues and prevent any damage to the SEM. A new injector nozzle was also prepared for the SEM analysis for comparison purposes. The samples were individually submerged in a toluene bath for 2 hours in glass beakers as shown in Figure 3-23.



a) Dismantled fuel injector.



b) New fuel injector nozzle in toluene bath.



c) Used fuel injector nozzle and needle in toluene bath.

Figure 3-23 Sample preparation for SEM analysis.

Then, the samples were washed with acetone and placed in a vacuum oven to dry overnight at 180°C. Once ready, the samples were mounted on the sample holder, inside the SEM chamber, using a conductive adhesive paste (Leit-C

Plast) to keep them in place during the analysis (see Figure 3-24). The nozzle with the deposits was analysed separately from its needle and the new nozzle due to space constraints.

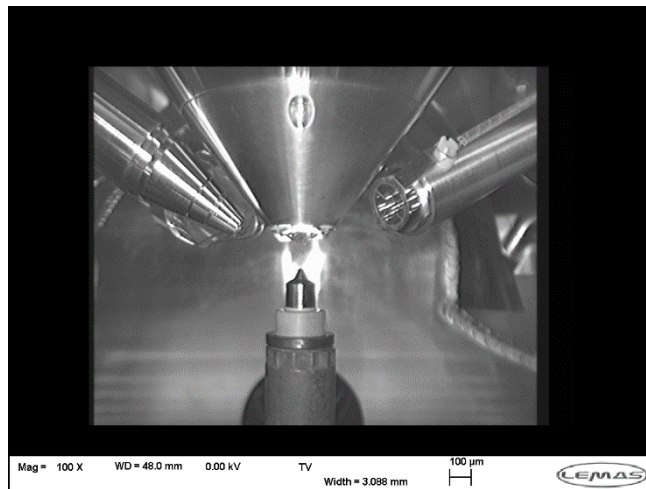


Figure 3-24 New fuel injector nozzle inside the SEM chamber.

Chapter 4

Biofuel Blends Impact on Diesel Generator's Performance

The performance of a diesel generator (genset) is determined by the mechanical-electrical interaction of its components, (i.e. the engine and the alternator). This interaction is mainly limited by the engine's and alternator's design but it is influenced by the type of fuel that powers the engine and the electrical load demand, which alters the engine's operating conditions. Two important parameters for assessing the performance of a diesel generator are Brake Thermal Efficiency (BTE) and Specific Fuel Consumption (SFC). Those parameters are highly dependent on the physicochemical properties of the fuel and the working load of a specific engine.

This chapter presents the findings on the fuel characterisation of castor oil-diesel (COD) blends and their effect on the performance of a 6kVA (4.8kW) diesel generator operating at different engine loads. The COD blends are identified by the number that accompanies the fuel name (e.g. COD#). The number accompanying the fuel name represents the percentage of castor oil included in the blend (0%, 20%, 40%, 50%, 60%, 80% or 100%). For example, COD0 corresponds to 0% castor oil, whereas COD100 corresponds to 100% castor oil. The findings on the engine's combustion performance and its pollutant emissions are also included in this chapter. In the last section, the impact produced by the COD blends on the engine's fuel injector is discussed. The understanding of these findings was a crucial step in developing the optimisation model described in Chapter 5.

4.1 Characterisation of Castor Oil-Diesel Blends

Diesel engines are designed to run with diesel, and using other fuels poses certain complications on the combustion controlling factors (spray and air-fuel mixture formation) that can alter the combustion, hence the overall performance of a diesel generator. Given that the mechanical work of a diesel generator relies on the chemical energy released by a fuel during the combustion process that occurs inside the engine's cylinder, it is imperative to study the properties of the fuel that will run the engine. From the literature review (see Chapter 2) it was identified that physicochemical properties such as volatility, heating value, density, and viscosity are important parameters that can be used to compare different fuels, as they are directly related to the spray, air-fuel mixture formation and the energy content of the fuel. Therefore those properties were investigated for the COD blends characterisation in this work.

4.1.1 Thermogravimetric Analysis (TGA)

The weight loss as a function of temperature diagrams that appear in Figure 4-1, obtained from the TGA data shows that the fuel blends with castor oil started evaporation later than diesel. The curves also show that as the castor oil increases in the blend, a higher temperature is required to finish the thermal degradation (up to 98% mass loss). It was found that COD0 finishes at 276.14 °C whereas COD100 finishes at 469.24 °C.

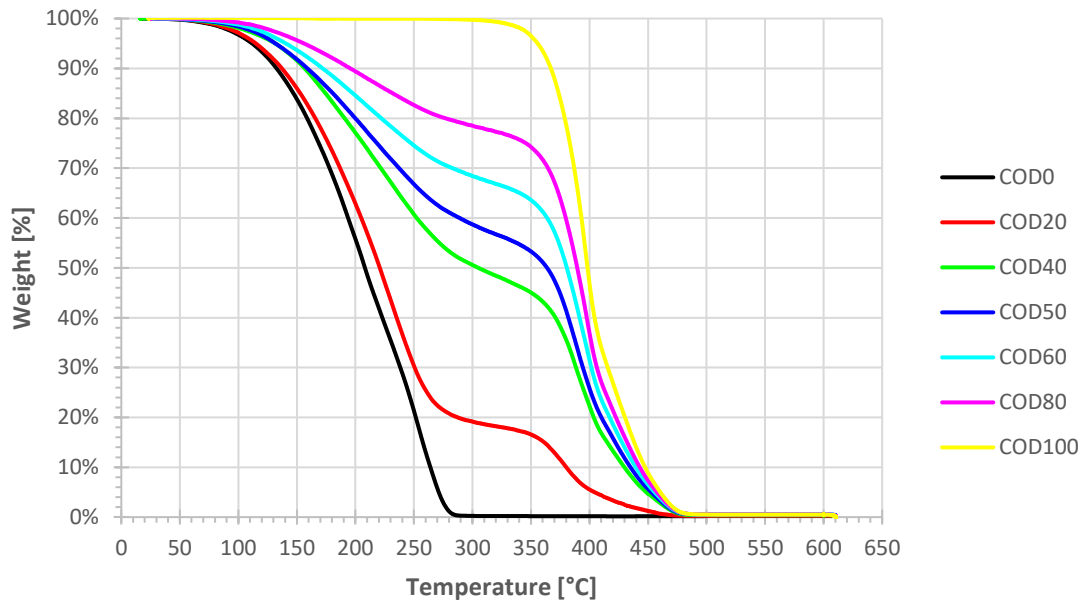


Figure 4-1 Thermograms from TGA analysis of 7 castor oil-diesel (COD) fuel blends.

Table 4-1 summarises the mass loss start temperatures (T_{smi}), the onset volatilisation temperatures (T_{onset}), and the 98% mass loss temperatures (T_{98ml}) found for each fuel blend. The T_{smi} is the temperature at which 1% mass was lost, whereas T_{onset} was determined by locating the intersection point between the starting mass baseline and the tangent line to the TGA curve at the maximum gradient point [163, 164]. It is worth mentioning that the Shimadzu analyser has a precision of 0.001 mg [165], which suggests that the uncertainty of the experimental results could be mainly attributed to human error during the blend preparation. However, only one batch of blends was prepared which minimised the risk of having different castor oil content in each blend during the experimental work repeats. It should be noted that the non-linear behaviour of the curves presented in Figure 4-1 can be attributed to the stronger intermolecular forces of castor oil, as its unique ricinoleic acid composition makes castor oil more polar than most fats [166]. This effect is represented by the change in the curve behaviour as the castor oil increases in the fuel blend.

Table 4-1 TGA parameters for 7 castor oil-diesel blends.

Fuel Blend	T _{smi} [°C]	T _{onset} [°C]	T _{98ml} [°C]
COD0	31.84	131	276.14
COD20	65.23	135	430.03
COD40	68.23	261	462.38
COD50	72.73	269	464.52
COD60	79.9	292	466.15
COD80	88.54	316	467.35
COD100	314.47	362	469.24

The TGA results confirmed that the fuel blends with higher castor oil content are less volatile compared to red diesel (COD0) and may alter the air-fuel mixture formation due to their lower capacity to vaporise. As reported by [167] the volatility of a fuel affects the fuel-air mixing and the spray formation through the effect caused on the droplet size, i.e., low volatility fuel results in larger drops with higher penetration that are likely to impinge on the cylinder walls.

It was found that the T_{smi} and T_{onset} values for COD0 are similar to the values reported by Leonardo et al. [163]. Also, the onset temperature found for COD100 is very similar to the 365°C reported in the literature [168].

4.1.2 Net Calorific Value Determination by Bomb Calorimetry

The net calorific values (NCV) in MJ/kg of each COD blend, determined by a Parr 6200 calorimeter, are summarised in Table 4-2. The highest value was found for COD0 and the lowest for COD100.

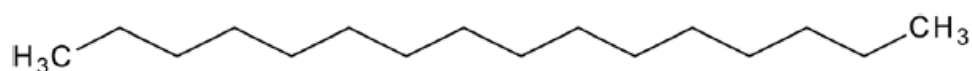
Table 4-2 Net calorific values for 7 castor oil-diesel blends.

Fuel Blend	Bomb Calorimeter Net Calorific Value [MJ/kg] (lower heating value)
COD0	44.19
COD20	42.55
COD40	40.91
COD50	40.09
COD60	39.28
COD80	37.64
COD100	36.00

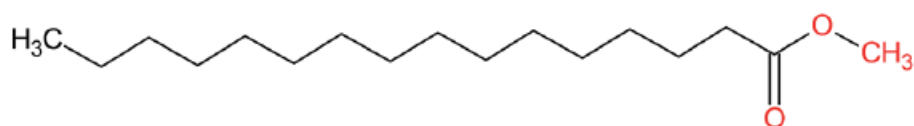
4.1.3 Elemental Analysis for H/C and O/C Determination

As diesel and castor oil have different molecular structures, elemental analysis of the fuel blends was needed to determine the hydrogen-to-carbon (H/C) and

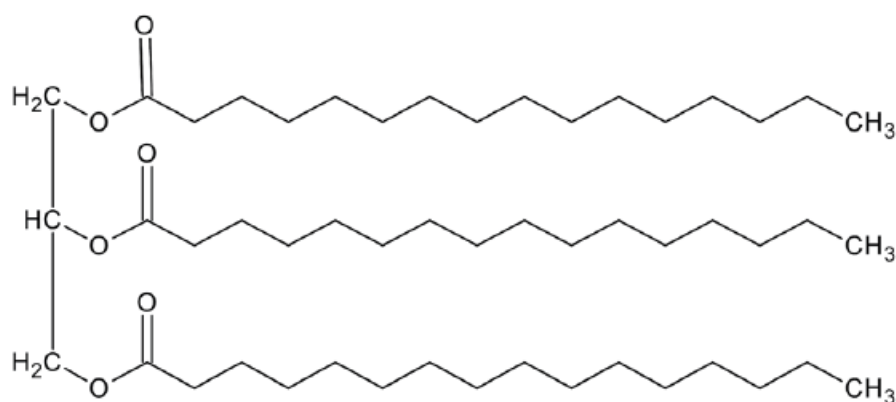
oxygen-to-carbon (O/C) ratios of the blends. Figure 4-2 shows the molecular structure of petroleum diesel, biodiesel and vegetable oil for comparison purposes. It can be appreciated how diesel contains only hydrocarbon chains whereas biodiesel and vegetable oil contain carbon and hydrogen atoms with ester functional groups. It should be noted that vegetable oil molecules have larger structures than diesel molecules, the large-sized structure is known as triglyceride [169].



(a) Petroleum diesel



(b) Biodiesel



(c) Vegetable oil or Triglyceride

Figure 4-2 Molecular structure of diesel, biodiesel and vegetable oil [169].

Castor oil contains several fatty acids but ricinoleic acid is its major component (~90%), the relative proportion of the fatty acids can vary depending on the geographical origin of the crop and other factors as indicated by [170]. Figure 4-3 shows the chemical structures of the fatty acids found in castor oil and Figure 4-4 presents the composition of castor oil from different regions.

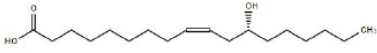
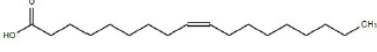
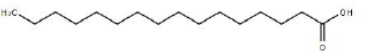
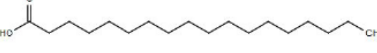
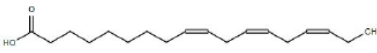
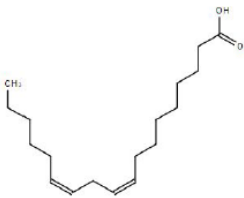
Fatty acid composition	Molecular formula	Type of fatty acid	Number of bonds and position	Chemical structures
Ricinoleic	$C_{18}H_{34}O_3$	Monounsaturated	One, and at the 12 th carbon	
Oleic	$C_{18}H_{34}O_2$	Monounsaturated	One, and at the 12 th Carbon	
Palmitic	$C_{16}H_{32}O_2$	Saturated	-	
Stearic	$C_{18}H_{36}O_2$	Saturated	-	
Linolenic	$C_{18}H_{30}O_2$	Unsaturated	Three, and at the 9 th , 12 th , and 15 th carbon	
Linoleic	$C_{18}H_{32}O_2$	Polyunsaturated	Two, and at the 9 th and 12 th carbon	

Figure 4-3 Chemical structure of castor oil fatty acids [170].

Fatty acid	India (a)	China (b)	Brazil (c)	Ethiopia (d)	Pakistan (e)	Saudi Arabia (f)	Nigeria (g)	Tanzania (h)
Ricinoleic (C18:1-OH)	87.3	90.85	88.2	91.06	94.59	75.77	86.96	87.8
Oleic (C18:1)	4.69	2.82	3.8	2.93	2.05	7.40	5.10	4.1
Linoleic (C18:2)	4.92	3.74	4.9	3.48	1.84	8.94	nd	4.3
Stearic (C18:0)	1.241	0.64	0.9	0.91	0.45	3.05	nd	1.4
Palmitic (C16:1)	1.016	0.72	1.4	1.08	0.31	2.77	0.56	2.4
Linolenic (C18:3)	0.63	-	0.3	0.316	nd	nd	nd	nr

(a) (Ramanjaneyulu et al., 2013) (b) (Guo et al., 2018) (c) (Souza Schneider et al., 2004) (d) (Beruk et al., 2018) (e) (Panhwar et al., 2016) (f) (Sbihi et al., 2018) (g) (Omohu & Omale, 2017) (h) (Omari et al., 2015). Key; nr-not reported, nd-not detected.

Figure 4-4 Fatty acid composition of castor oil from eight regions [170].

The elemental analysis results confirmed that none of the fuels has any sulphur content in their composition and that carbon, hydrogen and nitrogen are higher in diesel compared to castor oil. On the other hand, as expected, the oxygen content is greater for castor oil than for diesel. Table 4-3 summarises the elemental analysis results and also includes the hydrogen to carbon (H/C) and oxygen to carbon (O/C) ratios calculated with Equation 3-3 and Equation 3-4 presented in Chapter 3. The H/C and O/C ratios were the most important

parameters found from the elemental analysis as those values were required for the air-fuel ratio calculation for the engine tests.

Table 4-3 Elemental analysis results for 7 castor oil-diesel blends.

Fuel Blend	N (wt %)	C (Wt%)	H (%)	S (wt %)	O (wt%)	H/C	O/C
COD0	0.53	85.07	14.10	0.00	0.30	1.97	0.00
COD20	0.48	82.84	13.30	0.00	3.38	1.91	0.03
COD40	0.42	80.62	12.50	0.00	6.47	1.85	0.06
COD50	0.40	79.50	12.10	0.00	8.01	1.81	0.08
COD60	0.37	78.39	11.69	0.00	9.55	1.78	0.09
COD80	0.31	76.16	10.89	0.00	12.64	1.70	0.12
COD100	0.26	73.93	10.09	0.00	15.72	1.63	0.16

4.1.4 Density and Viscosity Determination at Different Temperatures

Determining the density and the viscosity of the COD blends was important because fuel injection is carried out in a volume-controlled system and injecting fuels with higher density compared to diesel, will increase the fuel mass injected [171]. Also, as the viscosity indicates the resistance of an oil to flow, a high viscosity fuel will alter the fuel injectors' operation leading to poor atomisation. The results from the density analysis are shown in Figure 4-5, it was found that the density of all the blends was higher when compared to diesel at corresponding temperatures. However, it was observed that by heating some of the blends, the diesel reference density at 15°C (0.84 g/cm³) can be achieved. COD20 matches the reference density when heated at 30°C (0.8489 g/cm³) or 40°C (0.8419 g/cm³). COD40 and COD50 need to be heated to 90 °C and 100°C respectively for having a density close to the reference value (0.8449g/cm³ and 0.8466 g/cm³). In contrast, the densities of COD80 (0.8790 g/cm³) and COD100 (0.9054 g/cm³) do not match the reference value even if the blends reach 100°C. The precision of the Stabinger viscometer SVM3000 for density measurements is 0.0005g/cm³ [172], therefore, as mentioned in the TGA results, the uncertainty of the experiment results can be mainly attributed to human error during the blend preparation stage. However, the same samples were used consistently throughout the experimental work to minimise the error. On the other hand, the non-linear behaviour of the curves shown in Figure 4-5, could be attributed to the same effect discussed in the TGA section, derived from the strong intermolecular forces of castor oil. The effect of the intermolecular forces becomes more evident as the castor oil content increases in the fuel blend.

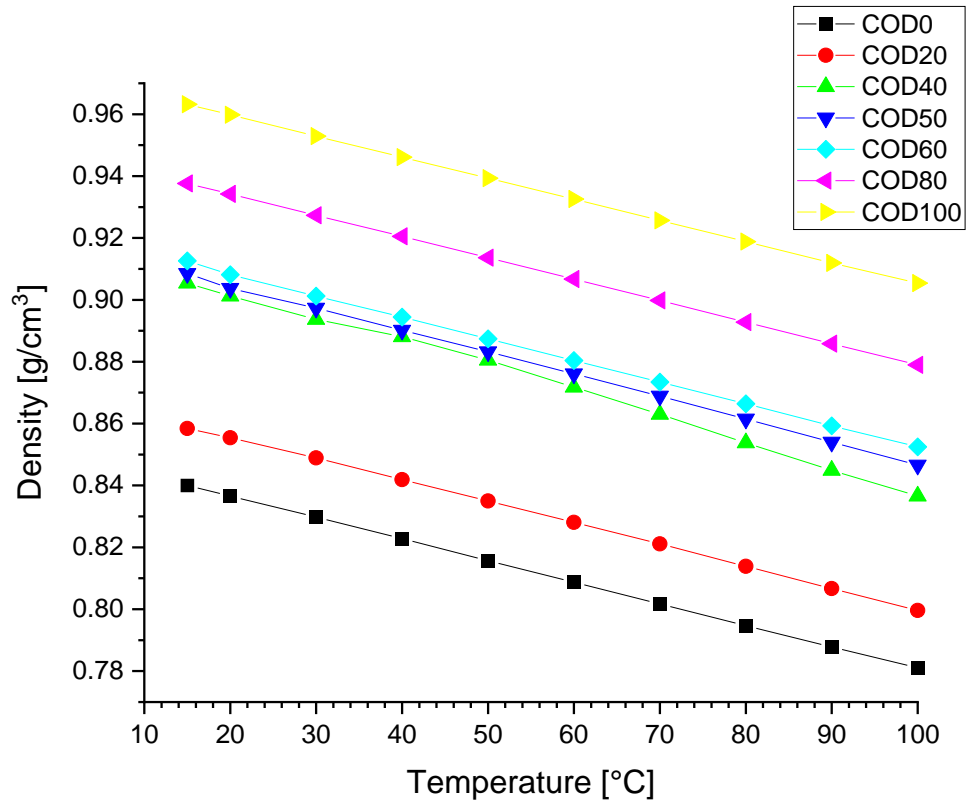


Figure 4-5 Density for 7castor oil-diesel blends at different temperatures.

The viscosity results are shown in Figure 4-6, it can be observed that all the blends have higher viscosity compared to diesel at the corresponding temperatures. It was found that by heating some of the blends, the diesel reference viscosity at 15°C (5.7886 mm²/s) can be achieved. For example, at 40°C COD20 has a viscosity of 5.4850 mm²/s and COD40 has a viscosity of 5.8592 mm²/s when heated to 70°C. Similarly, COD50 at 90°C has a viscosity of 5.7721 mm²/s and COD60 at 100°C has a viscosity of 5.5570 mm²/s. On the other hand, at 100°C the viscosities of COD80 (10.3507 mm²/s) and COD100 (19.1103 mm²/s) were 1.78 and 3.30 times higher than the reference value, respectively.

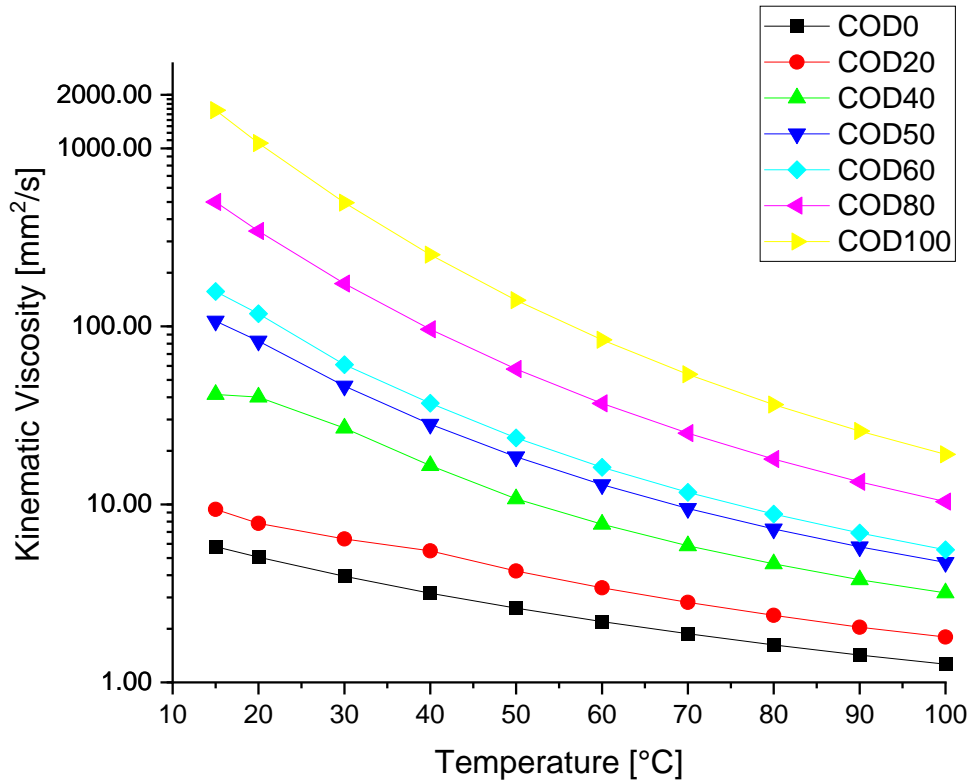


Figure 4-6 Kinematic viscosity for 7 castor oil-diesel blends at different temperatures.

Table 4-4 summarises the density and viscosity values of the blends used during the engine tests (COD0 to COD60), no runs were done with COD80 or COD100 due to heating system limitations. COD80 and COD100 might need temperatures higher than 80°C to run the engine but the maximum temperature achievable during the experiments was 70°C. The density values for each blend at 30°C presented in the table comply with the existing standard for SVO the DIN 51605 (see Table 2.9), which density limit is .900g/cm³. On the other hand, the viscosity values of COD50 and COD60 at 30°C exceed the 39 mm²/s limit from the standard (see Table 2.9). Therefore, for running the engine with COD60, the blend was heated to 60°C, whereas the rest of the blends were used at room temperature (30°C). It should be noted that no preheating was done for COD50 as its viscosity at 30°C is not that far from the standard limit.

Table 4-4 Density and kinematic viscosity at 30°C and 60°C the 5 castor oil-diesel blends used during engine lab work.

Fuel	Density [g/cm ³]		Kinematic Viscosity [mm ² /s]	
	at 30°C	at 60°C	at 30°C	at 60°C
COD0	0.83	0.81	3.94	2.19
COD20	0.85	0.83	6.39	3.40
COD40	0.89	0.87	26.86	7.74
COD50	0.90	0.88	46.25	12.92
COD60	0.90	0.88	60.98	16.17

4.2 Diesel Generator Performance at Different Operating Conditions with COD Blends

The fuel characterisation presented above showed that diesel and castor oil do have different properties that may impact the combustion process and the performance of a diesel generator. Therefore, the performance of a 6 kVA diesel generator running on castor oil-diesel blends was assessed at different engine loads. The load was varied from high load to no-load conditions by connecting a 10 kW Hillstone load bank, the results were compared against the baseline parameters produced by running the engine with red diesel (COD0).

4.2.1 Power Output of Genset

The first parameter for assessing the generator's performance is the electric power generated during the engine tests at different loads. The genset's power (P_{gen}) in kW was calculated using Equation 4-1 [173], where V and A represent the volts and amperes readings from the load bank respectively, and PF is the power factor. PF is equal to 1 as the load bank is purely resistive [174].

$$P_{gen} = \frac{V * A}{1000} * PF$$

Equation 4-1

Figure 4-7 presents the genset's output power generated by each COD blend at every engine test. The baseline power per load was taken from the engine tests using COD0 (test 0: 0.18 kW, test 1: 1.13 kW, test 2: 2.06 kW, test 3: 3.29, test 4: 4.1 kW). It should be noted that as the power output comes from the volts and amperes reading (see Equation 4-1), the power for each engine test had a slight variation, within the 5% voltage regulation as specified by the manufacturer [175]. The results show that the power delivered by the genset

was slightly lower for the blends with higher castor oil content in all tests, compared to the output power produced by COD0, but no reduction was observed with COD20. The output power reduction was ~1% with COD40 whereas, for COD50 and COD60, the reduction was ~2% and 3%, respectively. However, a lower power value of 3.96 kW was found in test 4 for COD50, that power is nearly 4% lower than the power produced with COD0 (4.10 kW) at the same load. This difference should be beard in mind as it might impact the trend in the results of other performance parameters. The average genset power values for each test are also included in Figure 4-7, those values are referred to as Genset Load hereafter and correspond to 4%, 26%, 47%, 76%, and 95% of the genset's prime power. Note that from Figure 4-7 onwards, the error bars shown in each figure, correspond to the standard deviation derived from repeat experimental work, as discussed in Chapter 3.



Figure 4-7 Genset output power for 5 castor oil-diesel blends at 5 engine test conditions.

The genset power (P_{gen}) was converted to the engine's output power (P_{eng}) in kW using Equation 4-2, where η_{alt} represents the alternator's efficiency at a given load.

$$P_{eng} = \frac{P_{gen}}{\eta_{alt}}$$

Equation 4-2

The alternator's efficiency is usually reported by manufacturers at 100% and 75% load and sometimes 50% and 25% load efficiency are also included. The η_{alt} values of Equation 4-2 were found by substituting the x variable of the

equation shown in Figure 4-8 with the genset power of each engine test. The equation from Figure 4-8 was generated by fitting the available Linz alternator manufacturer's data in the polynomial regression that appears as a dotted curve in the same figure.

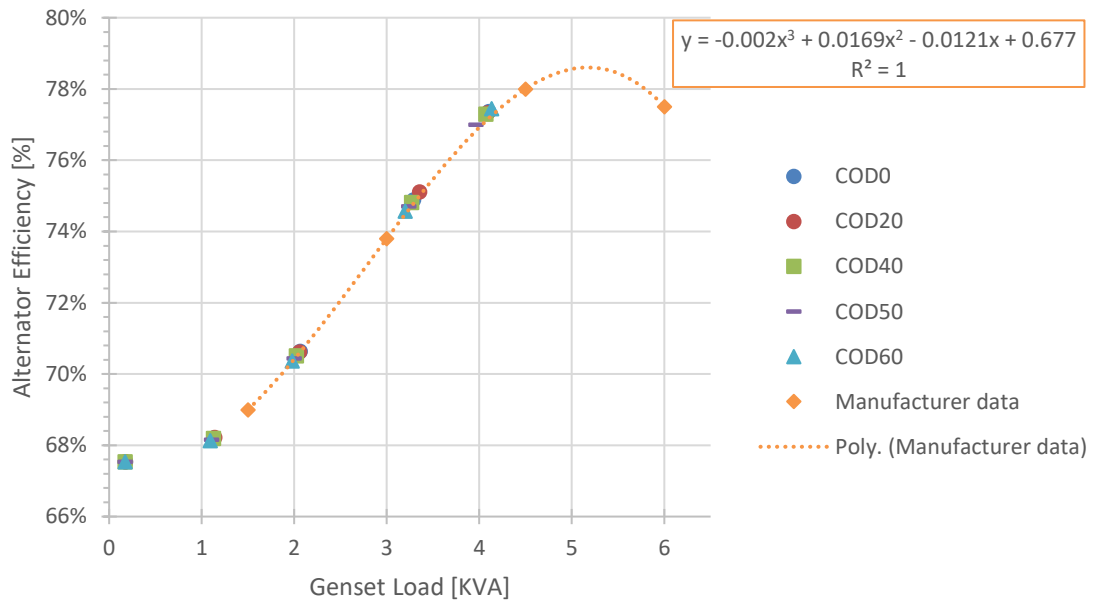


Figure 4-8 Alternator efficiency for 5 castor oil-diesel blends.

Figure 4-9 shows the engine power and the average engine power values found for each test with their corresponding fuel. The engine average power values are referred to as Engine Load hereafter and correspond to 4%, 29%, 50%, 77%, and 92% of the engine's continuous rated output power (5.7 kW).

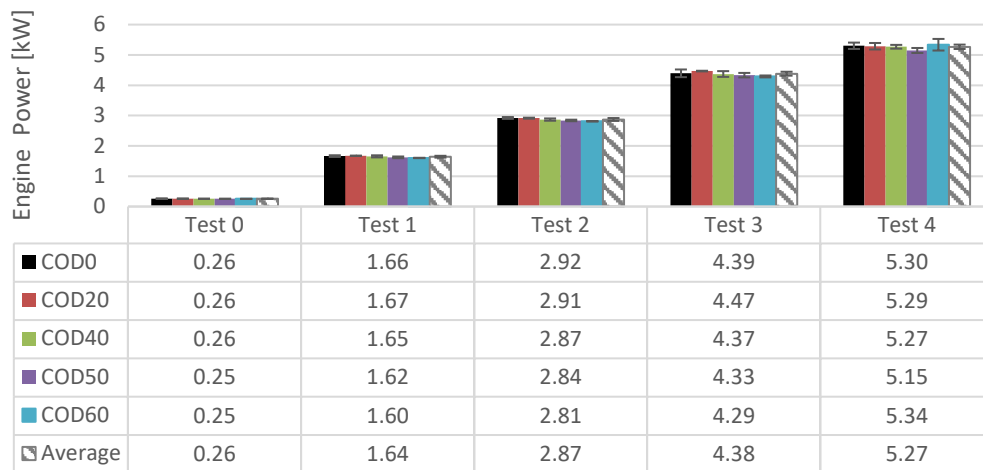


Figure 4-9 Engine output power for 5 castor oil-diesel blends at 5 engine test conditions.

Table 4-5 summarises the average genset and engine output powers (presented in Figure 4-7 and Figure 4-9) with their corresponding genset and engine load percentages. The Engine Load values will be used to present the findings of the coming sections.

Table 4-5 Genset and engine load operating conditions as a percentage of the maximum genset and engine powers.

Engine Test	Genset		Engine	
	Genset Power [kW]	Genset Load [%]	Engine Power [kW]	Engine Load [%]
Test 0	0.17	4	0.26	4
Test 1	1.12	26	1.64	29
Test 2	2.02	47	2.87	50
Test 3	3.28	76	4.38	77
Test 4	4.07	95	5.27	92

4.2.2 Fuel Consumption

The second parameter needed for assessing the performance of the diesel generator is its fuel consumption. The results from the mass-based fuel consumption from Figure 4-10 show that, as expected, more fuel was consumed at higher loads. The fuel consumption also increased for the fuel blends with higher castor oil content, this trend can be attributed to the higher density of castor oil compared to diesel. Since density is mass per unit volume,

if the fuel has higher density, then more mass enters the combustion chamber as the fuel injection is controlled by volume [176]. Having more fuel injected may result in incomplete combustion, which in turn would require more fuel to maintain the same output power as that with the fuel with lower density. It was found that at 4% engine load, the fuel consumption increased up to 20% when the engine was fuelled with COD60. Similarly, the fuel consumption with COD60 increased up to 18%, 16%, and 14% at 29%, 50%, and 92% engine load, respectively. Note that at 77% engine load the minimum variation in the fuel consumption values, relative to COD0 was found. At that load, the highest value of 1.25kg/h (with COD60) was only 7% higher than that of diesel (1.17kg/h). The minimum variation can be attributed to the design of the diesel generator, generally diesel generators are designed for optimum working conditions between 50 and 85 percent engine load for prime power or between 70 and 100 percent engine load for continuous power [63].

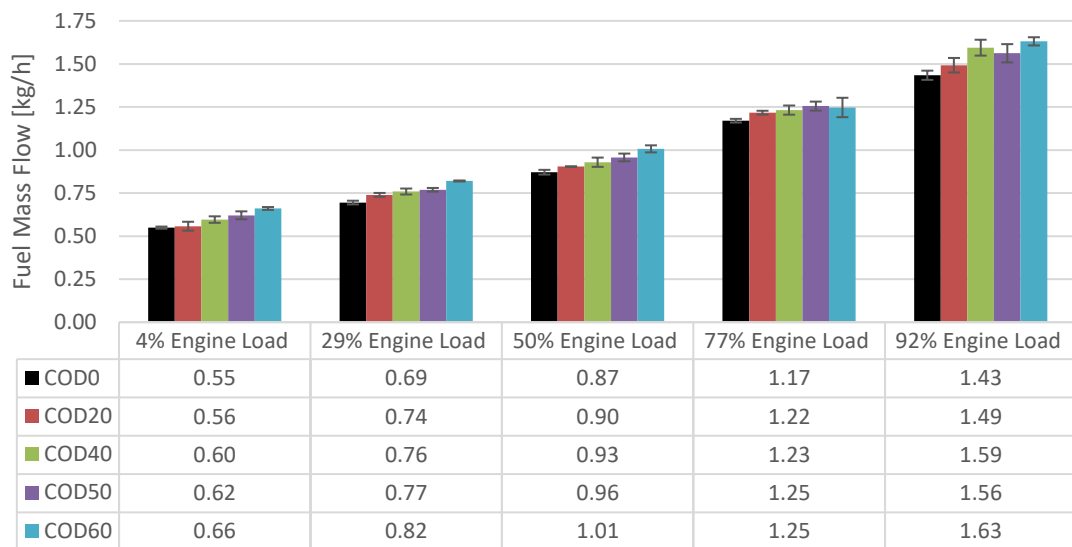


Figure 4-10 Fuel mass flow for 5 castor oil-diesel blends at 5 engine loads.

The fuel mass flow was converted to fuel volumetric flow by dividing each value presented in Figure 4-10 by its corresponding density value given in Table 4-4. The results from Figure 4-11 show a similar trend to that of the fuel mass-based findings, i.e., the fuel consumption increases with higher engine load and higher castor oil content in the blend. However, the percentage increase in fuel consumption, relative to diesel, shows an apparent lower variation across blends. It was found that at 4% engine load, the volumetric fuel consumption increased up to 13% when the engine was fuelled with COD60. Similarly, the volumetric fuel consumption with COD60 increased up to 11%, 9%, and 7% at 29%, 50%, and 92% engine load, respectively. But consistently, the minimum

variation in the fuel consumption values, relative to COD0 was also found at 77% engine load. At this load, no significant increase was found in fuel consumption for COD60. If the wrong density values are used to calculate the volumetric fuel consumption, the real fuel consumption might be jeopardised. Hence, mass-based fuel consumption should be preferred for accurate calculations.

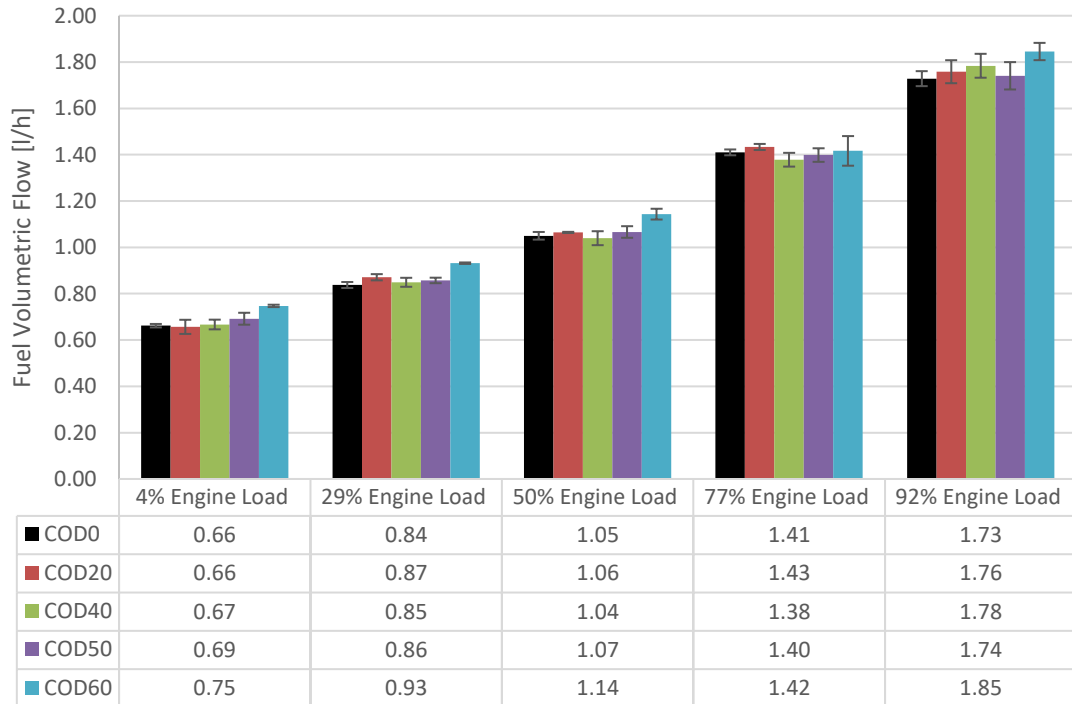


Figure 4-11 Fuel volumetric flow for 5 castor oil-diesel blends at 5 engine loads.

From the fuel mass flow (\dot{m}_{fuel}) and the engine output power (P_{eng}) findings, the specific fuel consumption (SFC) in g/kWh was computed using Equation 4-3.

$$SFC = \frac{\dot{m}_{fuel}}{P_{eng}}$$

Equation 4-3

Figure 4-12 shows the SFC results from all tests, the highest SFC values were found at 4% engine load. The SFC at that engine load is approximately 8 times higher than the SFC at 92% engine load for all the COD blends. Using COD60 increased the SFC by about 20% compared to the COD0 values at 4%, 29%, and 50% engine load. At 77% and 92% engine load, the SFC only increased by 9% and 13% using COD60 compared to the SFC values found for COD0. A similar fuel consumption trend was reported by [131] and [130].

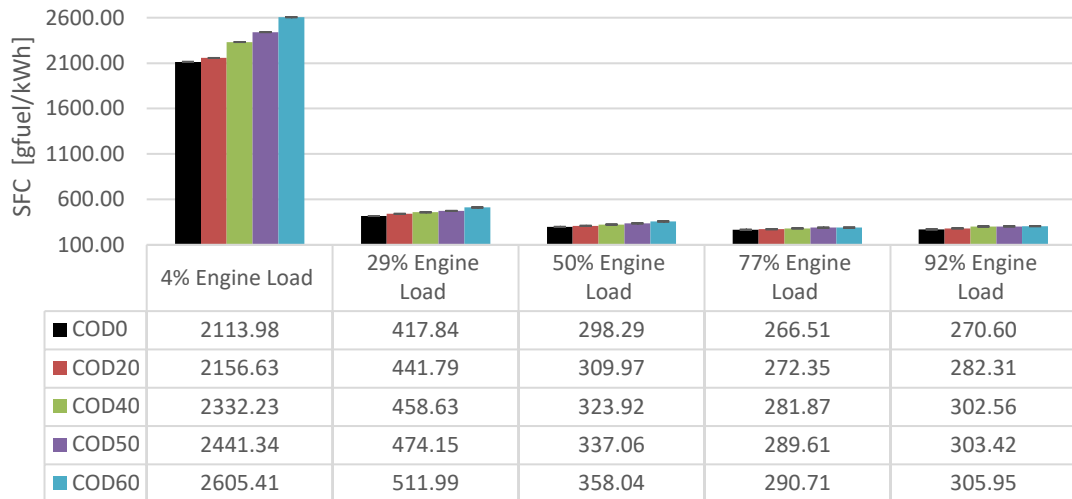


Figure 4-12 Specific fuel consumption for 5 castor oil-diesel blends at 5 engine loads.

These SFC results agree with the data reported by Hossain et al. review [118], which mentions that several authors found higher SFC (~2 to 15%) when using plant oils and their blends to run diesel engines, compared to diesel figures. The higher fuel consumption may be attributed to the vegetable oil's higher viscosity.

A significant factor that also increases fuel consumption is the lower calorific value of vegetable oil compared to diesel. Both, low calorific value and high viscosity alter fuel injection leading to poor atomisation, which in turn leads to less efficient air-fuel mixing, resulting in incomplete combustion. However, it should be noted that although fuel consumption increases, part of the mass of the castor oil-diesel blends is oxygen, which would lead to shortening the combustion duration (premixed combustion) and increasing the combustion temperature [81].

Note that according to Agarwal et al. [119], the brake specific energy consumption (BSEC), which considers the NCV and density of fuel, is a better fuel consumption parameter to compare different fuels than SFC. Figure 4-13 presents the BSEC results found by multiplying the SFC values by the corresponding NCV given in Table 4-2. As expected, the highest BSEC was found for COD60 as it has the lowest NCV (39.28 MJ/kg). The BSEC results show that the gap between COD0 and COD60 gets smaller, compared to the SFC results, especially as the engine load increases.

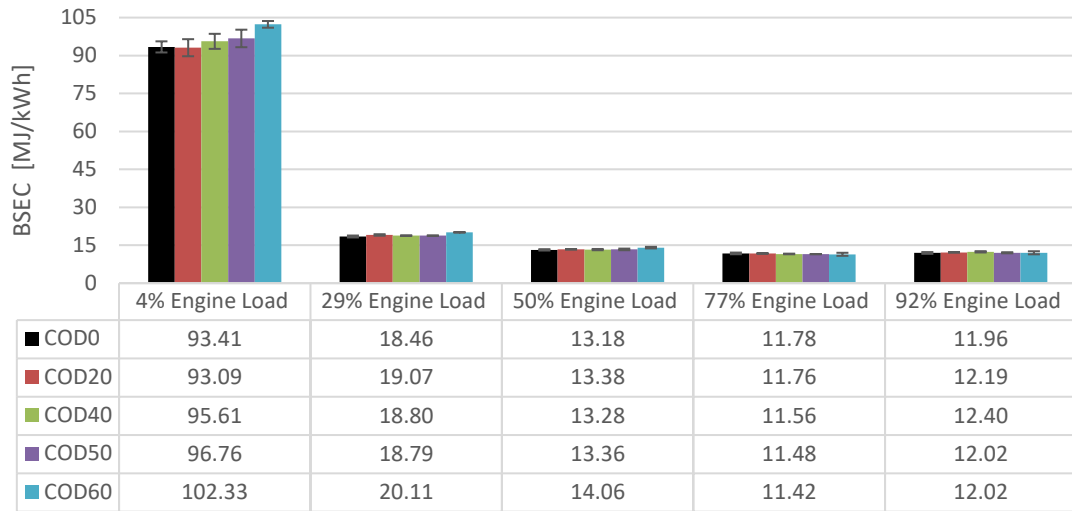


Figure 4-13 Brake specific energy consumption for 5 castor oil-diesel blends at 5 engine loads.

4.2.3 Brake Thermal Efficiency

The BTE was calculated with Equation 4-4 and the NCV (in MJ/kg) from Table 4-2. For the BTE calculations, it was considered that 1MJ= 0.277778 KWh.

$$BTE = \frac{1}{SFC * NCV * 0.277778}$$

Equation 4-4

The best BTE values (31% for COD0 to COD50 and 32% for COD60) were found at 77% engine load as shown in the efficiency curve from Figure 4-14. The BTE curve suggests that it is better to run the diesel generator at higher loads (above 50% engine load) and it would be recommended to operate it above 60% engine load for achieving the best performance. The BTE graph agrees with the curve reported by [131].

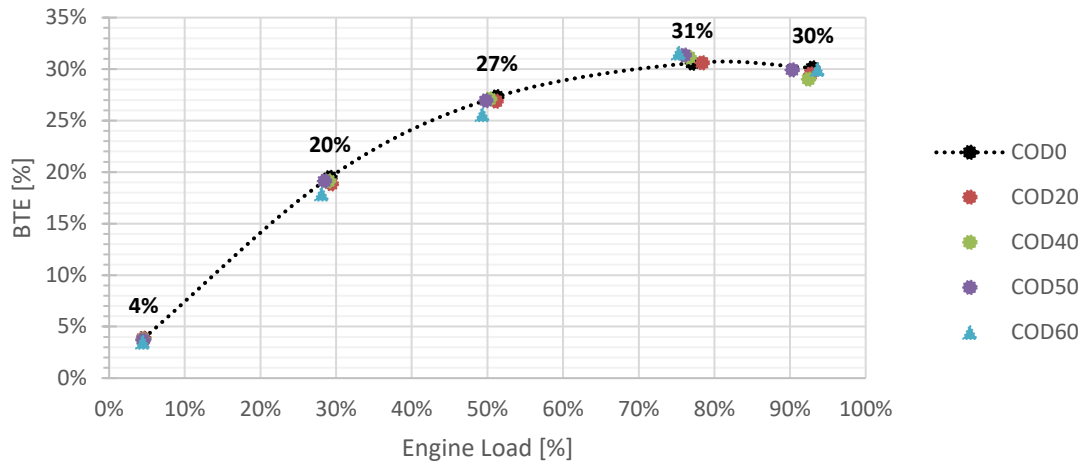


Figure 4-14 Brake thermal efficiency for 5 castor oil-diesel blends at 5 engine loads.

4.2.4 Engine Combustion Performance

Fuel spray, atomisation, vaporisation and air-fuel mixture formation are the controlling factors of the combustion process and the emissions of compression ignition (CI) engines. Those factors are highly dependent on the injection parameters, the turbulence produced inside the engine's cylinder, the density and viscosity of the fuel as well as its ability to vaporise. Useful parameters for characterising the combustion process in CI engines are in-cylinder pressure, ignition delay (ID), heat release rate (HRR), air-fuel ratio (AFR), and the engine out exhaust gas temperature (EOT). Thereof, these parameters were included in this section followed by the pollutant emissions from the emissions monitoring systems.

4.2.4.1 In-cylinder Pressure

As diesel engines rely on the compression of the air to convert the chemical energy of a fuel to mechanical work, it is essential to look into the in-cylinder pressure curves to characterise the engine combustion process. The pressure values near the piston's top dead centre (TDC), which occurs at the end of the compression stroke, can detect how a certain fuel blend affects the pressure profile compared to that of diesel. From an in-cylinder pressure curve, two peaks can be identified, the first one corresponds to the TDC at 0 crank angle degrees (CAD) and the second one is caused by the main combustion process.

Figure 4-15 shows the in-cylinder pressure versus crank angle curves for each engine test, from highest to lowest engine load (92%, 77%, 50%, 29%, and 4%), for the five fuels used during the lab work.

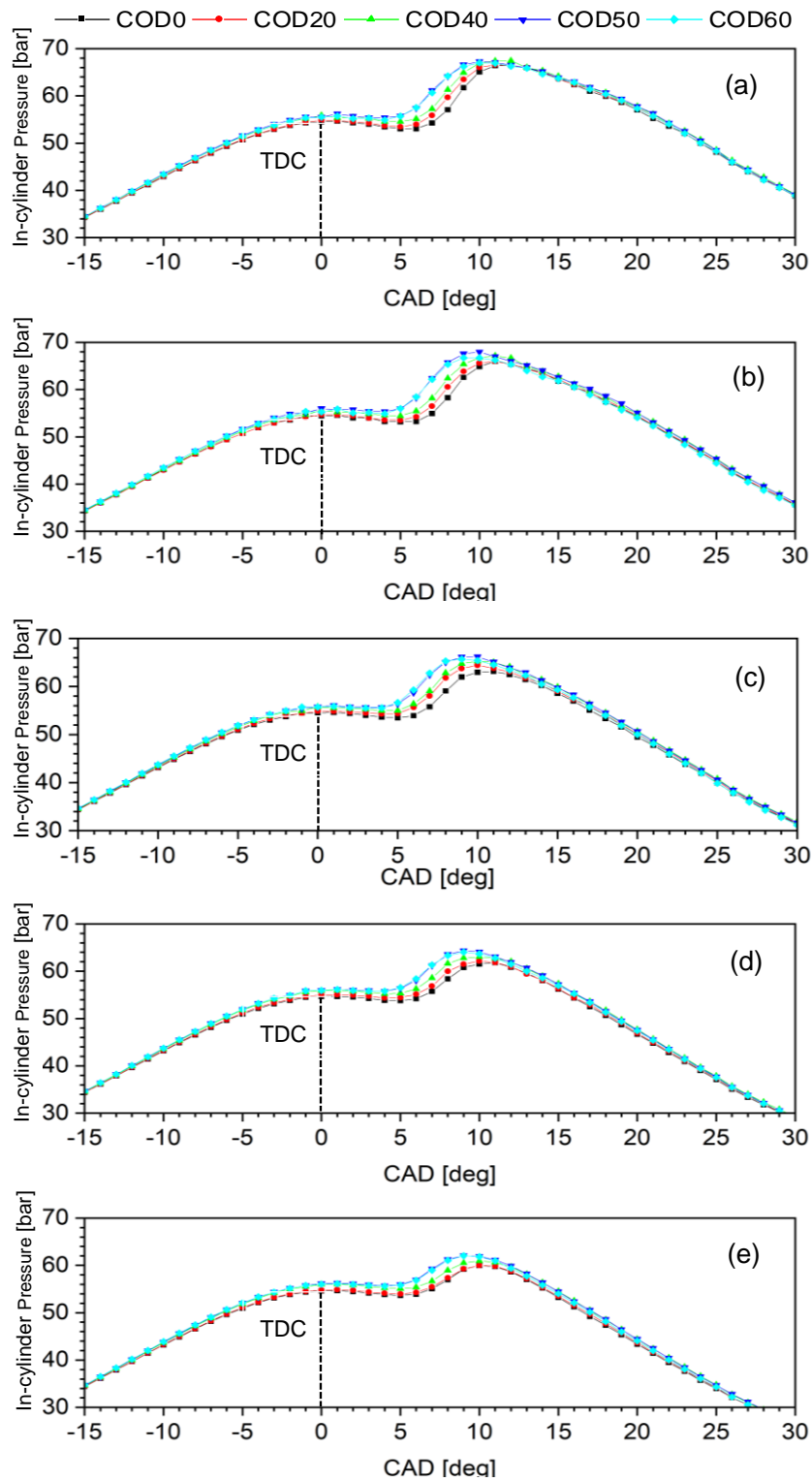


Figure 4-15 In-cylinder pressure curves for 5 castor oil-diesel blends at different engine load conditions: (a) 92% engine load, (b) 77% engine load, (c) 50% engine load, (d) 29% engine load and (e) 4% engine load.

It was found that the pressure values for COD0 were lower compared to the rest of the fuel blends in every engine load condition. The figures show that as the castor oil content increases, the pressure increases and the peak pressure

values are slightly shifted to the left, compared to the COD0 curve. The rise in the pressure curves at TDC might be attributed to the different specific heat capacities (C_p) of the fuels; castor oil has a C_p of 1.8 J/gK [177] and the C_p for diesel is 1.9 kJ/kgK [178]. The fuel blends having a lower C_p will have less heat transfer from the hot air, thus the in-cylinder temperature will be higher, leading to higher pressure values. On the other hand, the rise in the pressure curves at the second peak (at around 9 to 11 CAD) might be attributed to the increase of oxygen content in the fuel blends with higher castor oil. In Table 4-3 it was reported that the oxygen content by volume in diesel was 0.30%, whereas for castor oil it was 15.72%. According to [179] high oxygen content in the fuel could lead to shorter ignition delay. A shorter ignition delay would cause an earlier start of combustion, when the piston is closer to the TDC, producing higher pressures for the blends with higher castor oil content as shown in Figure 4-15. In contrast, lower in-cylinder pressure was produced with diesel as the start of combustion occurred when the piston was already in the expansion stroke phase.

From the pressure curves presented above, it was also observed that the peak pressure increases as the engine load increases. This trend was expected as more fuel is injected at higher loads, and more power is produced. Although it was found that the peak pressure increases with higher castor oil content in the blend, COD50 produced higher peak pressure values than COD60 at four engine operating conditions (29%, 50%, 77%, and 92% engine load) as shown in Figure 4-16. However, as the values fall within the error bars, the trend remains.

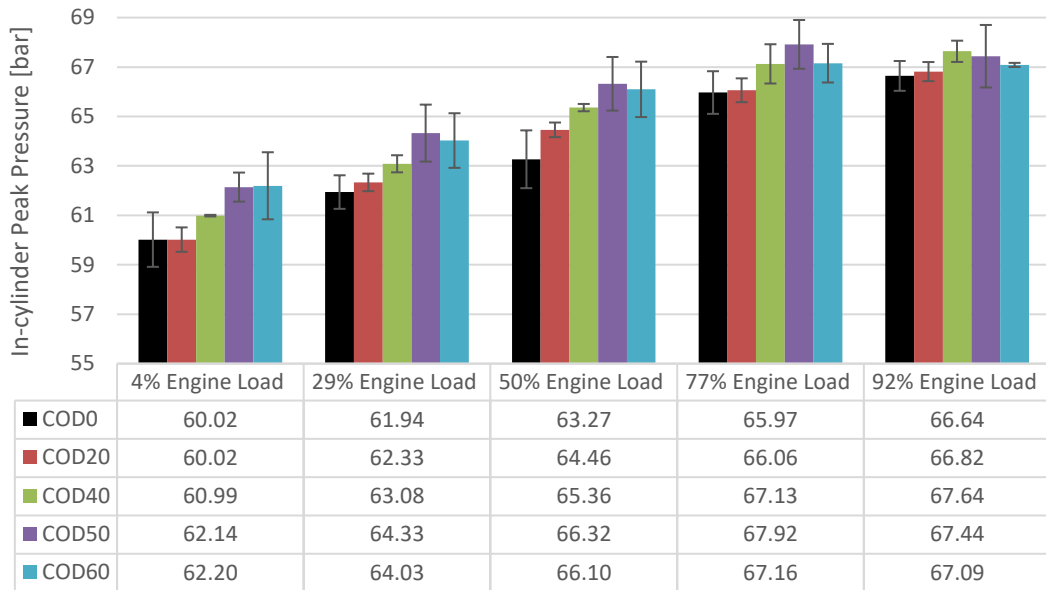


Figure 4-16 In-cylinder peak pressure for 5 castor oil-diesel blends at 5 engine loads.

The higher peak pressure values from COD50 could be attributed to its higher density (0.90 g/cm^3) and kinematic viscosity ($46.25 \text{ mm}^2/\text{s}$) at 30°C compared to the density (0.88 g/cm^3) and kinematic viscosity ($16.17 \text{ mm}^2/\text{s}$) of the preheated COD60 at 60°C .

4.2.4.2 Ignition Delay

Ignition delay (ID) is a combustion parameter defined as the time interval between the fuel injection timing (FIT) and the start of the premixed combustion (SPC). In other words, it is the time that allows the air-fuel mixture formation that leads to the first phase of the combustion process, it is commonly expressed in crank angle degrees. The ID can be determined using Equation 4-5.

$$ID = FIT + SPC$$

Equation 4-5

The FIT occurs at 13.5 CAD before the top dead centre (bTDC) according to the engine's manufacturer specifications. The SPC was determined from the pressure traces at the crank angle where the in-cylinder pressure first derivative zero value was found, as illustrated in Figure 4-17. In the same figure, the heat release rate (HRR) curve and its first derivative are also shown as both are good indicators of combustion behaviour. Note that the SPC, although determined from the pressure first derivative, also corresponds to the HRR first derivative sharp rise preceding the HRR peak. On the other hand, the minimum of the HRR first derivative curve helps to identify the start of the mixing-

controlled combustion (SMCC). Inspecting the HRR curve from the SMCC to the start of the late combustion phase (SLCP) around 26 CAD facilitates the comparison of the combustion processes across different fuel blends.

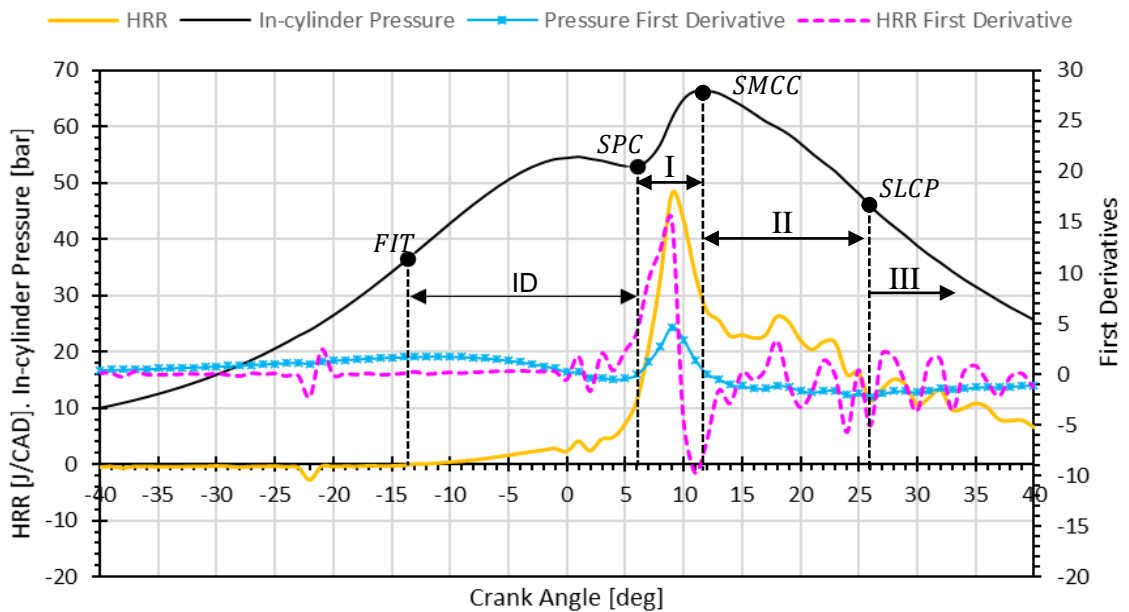


Figure 4-17 In-cylinder pressure and heat release rate curves with combustion characterisation parameters and combustion phases (I: premixed combustion, II: mixing-controlled combustion, III: late combustion phase).

The visual inspection of the red diesel (COD0) baseline pressure curves shown in Figure 4-18, suggests that *SPC* should occur around 5 to 6 CAD for the five engine operating conditions tested in this work.

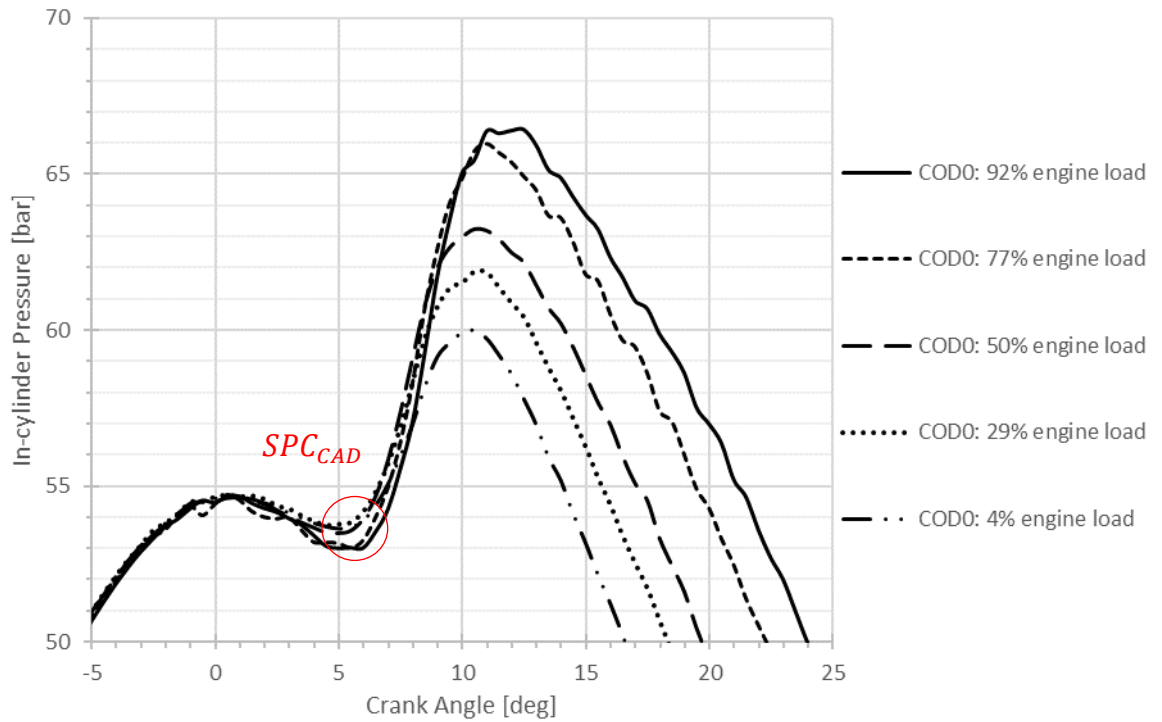


Figure 4-18 In-cylinder pressure curves for diesel (COD0) at five engine loads.

The SPC values found for each fuel blend during the engine tests are included in Table 4-6. The numbers revealed that the combustion started at 5 ± 0.5 CAD for all the fuels with castor oil in the blend, whereas for diesel the combustion occurred at 5.5 ± 0.5 CAD instead. These values confirmed the earlier start of combustion represented by the left-wise shift observed in the pressure curves presented in the previous section (see Figure 4-15).

Table 4-6 Start of combustion in crank angle degrees for 5 castor oil-diesel blends at 5 engine loads.

Engine Load [%]	Start of Premixed Combustion [CAD]				
	COD0	COD20	COD40	COD50	COD60
92%	5.9	5.3	5.1	4.9	5.5
77%	5.5	5.0	5.0	5.0	5.1
50%	5.3	4.9	4.8	4.8	5.0
29%	5.5	5.0	5.0	5.1	4.5
4%	5.5	5.0	5.5	5.2	4.6

The values from Table 4-6 were used to compute the ID for all the fuel blends at different loads using Equation 4-5, the results are summarised in Table 4-7. It was found that the ID for COD0 was about 19 ± 0.5 CAD, whereas for the rest of the COD blends the ID was about 18.5 ± 0.5 CAD.

Table 4-7 Ignition delay in crank angle degrees for 5 castor oil-diesel blends at 5 engine loads.

Engine Load [%]	Ignition Delay [CAD]				
	COD0	COD20	COD40	COD50	COD60
92%	19.4	18.8	18.6	18.4	19.0
77%	19.0	18.5	18.5	18.5	18.6
50%	18.8	18.4	18.3	18.3	18.5
29%	19.0	18.5	18.5	18.6	18.0
4%	19.0	18.5	19.0	18.7	18.1

The ± 0.5 CAD error is within the instrument detection limits, but overall, COD0 presented a slightly longer ID compared to the castor oil blends at every operating load. Although it could have been expected a shorter ID for diesel, due to its higher cetane number (48) [180], compared to the castor oil (42) [134], the shorter ID of the castor oil blends could be attributed to the fatty acid composition of castor oil. Hellier [181] showed that groundnut and palm oils with lower cetane numbers (41.8 and 42, respectively) compared to diesel, presented a shorter ignition delay. The details about how the CN were obtained are not provided in Hellier's work but the study cited by this author for the palm oil cetane number [182] reported the cetane index of the fuels according to the ASTM Method D-163 for cetane number determination. The shorter ID reported by Hellier [181] was correlated to a low number of double bonds and the carbon chain length of the vegetable oils. Of the six vegetable oils compared by the authors, groundnut and palm oil have less than 50% linoleic acid (C18:2) in their composition with oleic (C18:1) and palmitic (C16:0) accounting for the majority of the acids contained in their structure. Similarly, castor oil possesses around 4% of C18:2 and 93% is made up of other acids with one double bond like oleic (3%) and ricinoleic acid (~90%) [183, 184]. Also, the shorter ID of the castor oil blends could be attributed to their higher oxygen content. Song et. al [179] reported shorter ID, compared to diesel ID, in fuels with oxygen content between 3% and 9%.

4.2.4.3 Heat Release Rate

The heat release rate (HRR) curve is useful to compare the combustion process of different fuels as the amount of heat released depends on the ID, air-fuel mixture, and the heating value of the fuel [112]. The HRR was calculated using the Leeds HRR model developed by Olanrewaju et al. [185] presented in Equation 4-6.

$$\frac{dQ}{d\theta} = \frac{\gamma}{\gamma - 1} p \frac{dV}{d\theta} + \frac{1}{\gamma - 1} V \frac{dp}{d\theta} + \frac{dQ_W}{d\theta} + h_{bb} \frac{dm_{bb}}{d\theta} + q_e \frac{dm_f}{d\theta} \quad \text{Equation 4-6}$$

where,

$\frac{dQ}{d\theta}$ = rate of release of heat energy from injected fuel, J/deg.

γ = ratio of specific heats.

p = instantaneous pressure of the cylinder, Pa.

V = instantaneous volume of the cylinder, m³.

$\frac{dQ_W}{d\theta}$ = heat losses through the walls, J/deg.

h_{bb} = enthalpy of blow-by gases, J/kg.

$\frac{dm_{bb}}{d\theta}$ = blow-by mass flow, kg/deg.

q_e = heat of evaporation of fuel, J/kg.

$\frac{dm_f}{d\theta}$ = rate of evaporation of injected fuel, kg/deg.

θ = crank angle degree (CAD).

Each term of Equation 4-6 was calculated following the methodology explained in [185] using their reported coefficients for the gamma functions required to estimate the ratio of specific heats (γ). However, for finding the HRR of the castor oil-diesel blends the parameters shown in Table 4-8 were used. The stoichiometric air-fuel ratios for COD20, COD40, COD50, and COD60 were calculated using the diesel stoichiometric value (14.50) and the determined castor oil stoichiometric value (11.57) based on the molecular formula given by [186]. Also, the heat of vaporisation values for CO20, COD40, COD50, and COD60 were found using the diesel value (232,400J/kg) and the heat of vaporisation of rapeseed oil (209,000 J/kg) [187], as no value was found for castor oil.

Table 4-8 Parameters for calculating HRR of COD blends.

Blend	Density [kg/m ³]	Low Heating Value [MJ/kg]	Heat of vaporisation [J/kg]	Stoichiometric Air-fuel Ratio
COD0	829.77	44.19	232,400	14.50
COD20	848.87	43.17	227,720	13.91
COD40	893.73	41.00	223,040	13.33
COD50	897.30	39.63	220,700	13.03
COD60	880.40	39.28	218,360	12.74

The HRR curves for the five fuel blends at different engine conditions (from 92% to 4% engine load) are shown in Figure 4-19.

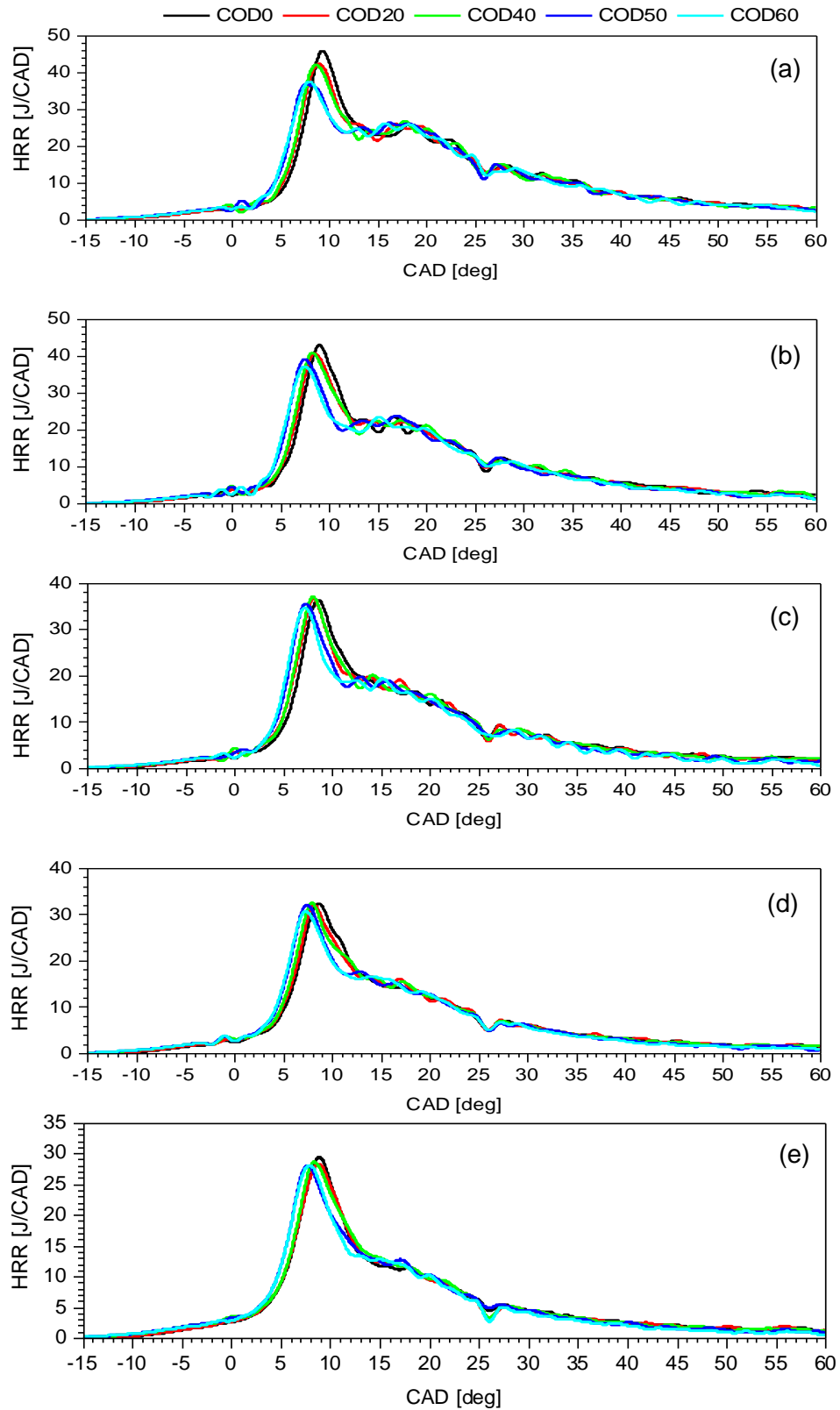


Figure 4-19 5 Heat release rate curves at different engine load conditions: (a) 92% engine load, (b) 77% engine load, (c) 50% engine load, (d) 29% engine load, and (e) 4% engine load.

The highest peak heat release rate (PHRR) value (48.11J/CA) was found for COD0 at 92% engine load (see Figure 4-19 a). It was observed that PHRR decreases for all blends as the engine load decreases. Also, as the castor oil content increases the PHRR decreases, thus the lowest PHRR values were found at 4% engine load for the blends with higher castor oil content (see Figure 4-19 e). Table 4-9 summarises the PHRR findings with the respective crank angle degree at which the PHRR was found for each blend.

Table 4-9 Peak heat release rate parameters for 5 castor oil-diesel blends at 5 engine loads.

Engine Load [%]	Peak HRR [J/CAD]					Location of Peak HRR [CAD]				
	COD0	COD20	COD40	COD50	COD60	COD0	COD20	COD40	COD50	COD60
92%	48.11	43.46	42.6	37.23	39.26	9.1	9	8.5	7.1	8
77%	46.13	41.5	43.02	39.94	37.48	9	8.2	8.1	7.1	7.5
50%	37.11	39.69	39.79	37.05	36.12	8.5	8	8	7.1	7.1
29%	33.26	35.08	35.05	33.06	32.09	8.8	8	8	7.1	7.1
4%	31.12	29.31	29.56	28.85	29.06	9	8.9	8.2	7.8	7.9

The lower peak HRR values from the castor oil blends can be attributed to their shorter ID and to their higher oxygen content, which reduced the amount of fuel burned during the premixed combustion phase. It was observed that the shorter ID led to longer combustion duration and slightly higher PHRR values for the castor oil blends, compared to diesel, during the mixing-controlled combustion (diffusion phase) which occurred from around 11.5 CAD to 26 CAD. This effect on the HRR profile caused by a shorter ID was also reported by [188]. Table 4-10 presents the mixing-controlled combustion PHRR values.

Table 4-10 Diffusion phase peak heat release rate for 5 castor oil-diesel blends at 5 engine loads.

Engine Load [%]	Mixing-controlled Combustion Peak HRR [J/CAD]				
	COD0	COD20	COD40	COD50	COD60
92%	27.30	28.88	28.45	27.29	26.83
77%	24.89	27.00	27.83	24.42	24.61
50%	20.60	20.76	22.73	20.97	20.56
29%	17.95	21.17	21.49	18.11	17.51
4%	15.89	21.13	20.31	17.72	16.90

The higher PHRR values of castor oil blends during the mixing-controlled combustion agree with the high-peak in-cylinder pressure values previously shown in Figure 4-16. The high PHRR values during the mixing-controlled

combustion are responsible for the higher peak in-cylinder temperatures found for the blends with castor oil, compared to the values found for diesel. The summary with the in-cylinder temperature and the combustion duration is included in Table 4-11. The combustion duration was considered from the SPC values (see Table 4-6) to the end of the mixing-controlled combustion (start of the late combustion phase). The start of the late combustion phase is represented by the drop in HRR for all blends that appears in Figure 4-19 at 26 CAD.

Table 4-11 Peak in-cylinder temperature and combustion duration for 5 castor oil-diesel blends at 5 engine loads.

Engine Load [%]	Peak In-cylinder Temperature [K]					Combustion Duration [CAD]				
	COD0	COD20	COD40	COD50	COD60	COD0	COD20	COD40	COD50	COD60
92%	1716.7	1721.0	1731.9	1729.7	1723.8	20.1	20.7	20.9	21.1	20.5
77%	1619.9	1621.1	1634.4	1633.6	1607.9	20.5	21.0	21.0	21.0	20.9
50%	1480.5	1495.3	1504.9	1501.6	1487.9	20.7	21.1	21.2	21.2	21.0
29%	1404.2	1410.0	1426.8	1424.2	1420.2	20.5	21.0	21.0	20.9	21.5
4%	1323.5	1331.2	1348.9	1350.7	1341.0	20.5	21.0	20.5	20.8	21.4

An important remark of this section is that as the PHRR for COD0 (diesel) occurred later than the PHRR of the other fuel blends, there were lower peak pressure values reported for diesel (see Figure 4-16). The lower pressure values can be explained due to the position of the piston when the PHRR occurred, i.e., for diesel the piston was already in the expansion stroke phase, whereas for the other blends the piston was closer to the TDC.

4.2.4.4 Engine Out Exhaust Gas Temperature

The EOT depends on the engine operating load as well as the calorific value of the fuel. The results from Figure 4-20 show that EOT increases as the load increases. The results also showed that despite the lower calorific values of castor oil blends, compared to diesel, the EOT was very similar across blends in each test. The effect of the lower calorific value was minimised or compensated with the slightly higher amount of fuel injected as previously shown in the mass-based results (see Figure 4-10). However, the 13% fuel mass flow increase reported for COD60 may have caused the significant EOT rise at 92% engine load. The larger variability shown for COD60, compared to the other COD blends, can be attributed to the fact that COD60 was the only preheated blend. Therefore, a slight variation in the fuel temperature could have affected the viscosity of the blend, leading to less fuel burned during the premixed

combustion and extended mixing-controlled combustion, resulting in higher EOT during the repeat experimental work. In contrast, the low EOT of COD50 at 92% engine load can be attributed to its lower output power compared to the other blends (~4% lower than COD 0) reported in Figure 4-9.

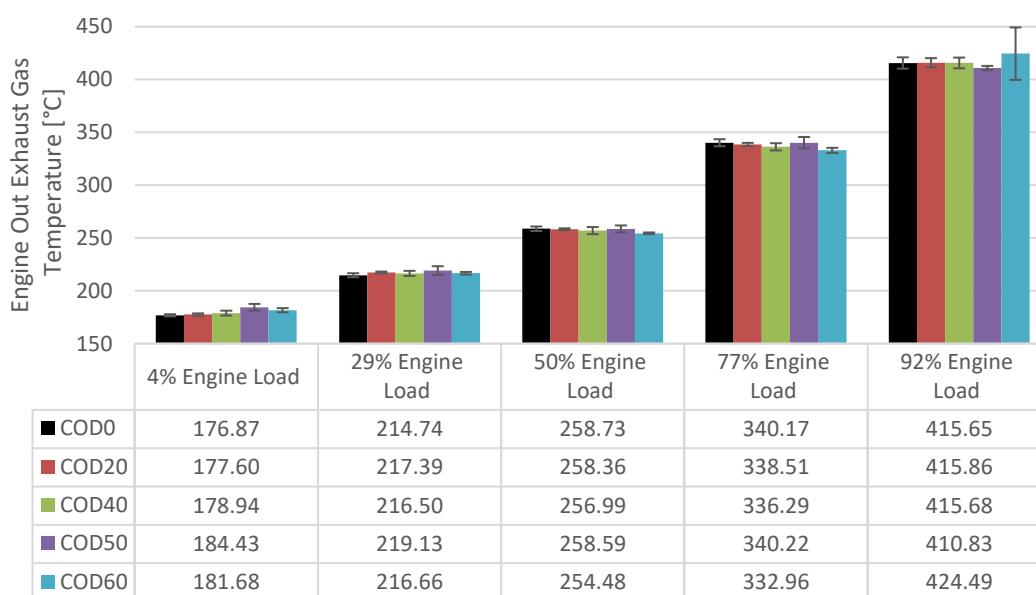


Figure 4-20 Engine out exhaust gas temperature for 5 castor oil-diesel blends at 5 engine loads.

4.2.4.5 Air Fuel Ratio

Air Fuel Ratio (AFR) is an indicator of the available oxygen to burn the fuel during combustion. Diesel engines run with mixtures that have more oxygen than required to burn the fuel (lean mixture) and their AFR varies from 18:1 to 80:1 [189] depending on the operating load. Lower AFR corresponds to higher loads because more fuel is injected compared to lower loads, whereas the air supply is kept constant irrespective of load, hence the AFR gives smaller values when load increases. The AFR of each test was directly calculated by the MEXA analyser based on the Brettschneider/Spindt Method algorithm [190]. The algorithm relies on the calculation of the moles of air used during the combustion based on the molecular ratios of carbon (x), hydrogen (y), and oxygen (z) of the fuel running the engine and the measured gas concentrations of the exhaust sample. To calculate the AFR for each test, the ratios presented in Table 4-3 (H/C and O/C) and C/C=1 were used, the results are shown in Figure 4-21. A good correlation between the AFR and the load was found, the higher AFR values (~70) appeared at 4% engine load and the smaller AFR values (~25) appeared at 92% engine load. Moreover, the results also showed the expected decreasing trend in each test for the blends with higher castor oil

content as more fuel mass was injected at higher loads. Note that COD60 presented the lowest values in all tests despite its lower density (due to higher temperature) compared to COD50. In this case, the trend could be mainly attributed to the lower H/C and higher O/C ratios from COD60 rather than to the sole density effect.

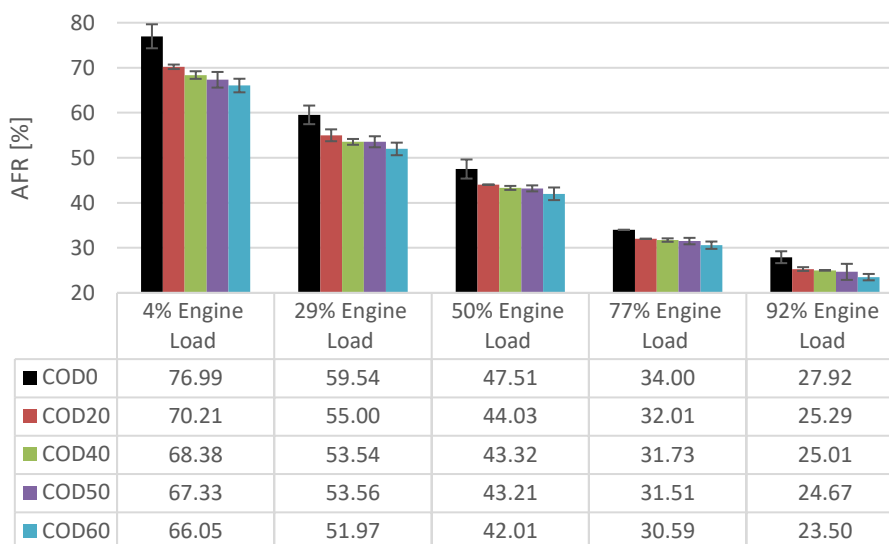


Figure 4-21 Air fuel ratio for 5 castor oil-diesel blends at 5 engine loads.

4.2.5 Engine Exhaust Emissions

This section presents the findings of the exhaust emissions monitored during the engine tests. The regulated pollutant emissions detected by the MEXA analyser (CO, HC, and NO_x) are presented first, followed by the particulate matter (PM_{2.5}) findings. After the PM_{2.5} sub-section, the particle number size distribution and total particle numbers from the particulate analyser (DMS 500) are presented. The last part of this section is dedicated to the unregulated volatile organic compounds (VOCs) found with the FTIR analyser.

4.2.5.1 Regulated Pollutant Emissions (CO, HC, and NO_x) Measured by the MEXA Analyser

Three regulated emissions (CO, HC, and NO_x) were measured with the MEXA analyser, the findings are presented below.

The CO results from Figure 4-22 show that COD0 had the lowest CO emissions at 4 engine loads: 245 ppm (92% engine load), 351 ppm (77% engine load), 483 ppm (50% engine load), and 709 ppm (4% engine load). At 29% engine load the lowest emission was found for COD20 (568 ppm). The figure shows

that CO emissions increase at lower loads, at 4% engine load the emissions were 2.89 and 2 times higher for COD0 and COD60 respectively, compared to their corresponding values at 92% engine load. The emissions increase with higher castor oil content in the fuel blend (~70% higher at 92% engine load with COD60). However, in all tests, COD50 gave lower values than COD40 which seems to be a contradiction. Fortunately, the lower CO emissions with COD50 can be related to the fuel impingement effect explained by Hellier et al. [181]. The authors explained that the high viscosity of vegetable oils causes fuel impingement on the piston bowl and cylinder walls, but as the viscosity increases, the fuel impingement is reduced as a result of the reduced spray penetration. Their results showed that VO with higher viscosities produced lower CO emissions. Therefore, as COD50 has higher viscosity compared to COD 40 and COD60 (at 60°C) it is reasonable to have lower CO emissions when using COD50 as less fuel from the fuel impingement will be left unburnt.

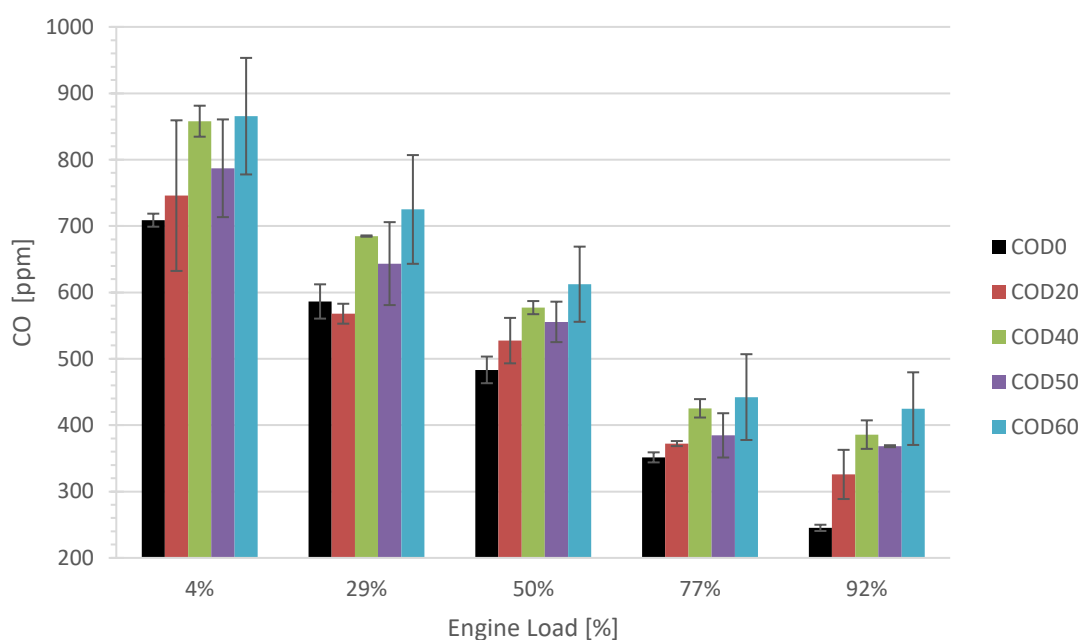


Figure 4-22 Carbon monoxide emissions for 5 castor oil-diesel blends at 5 engine loads.

The findings on THC are shown in Figure 4-23. It was found that the THC emissions increase with higher castor oil content in the blend, however, the effect caused by the high viscosity of COD50 discussed in the CO findings is also observed in the results. The lowest THC values correspond to COD0 in all tests: 138 ppmC, 179 ppmC, 219 ppmC, 227 ppmC, and 294 ppmC at 92%, 77%, 50%, 29%, and 4% engine load, respectively. The THC emissions decreased at higher loads for COD0 whereas, for the rest of the blends, a

significant rise occurred at 92% engine load, preceded by the decreasing trend (similar to that of diesel) at lower loads. The significant rise might be attributed to the incomplete combustion of a greater amount of fuel injected at the highest load and the reduced AFR, compared to diesel, as previously reported in Figure 4-10 and Figure 4-21. This peculiar increase of THC at 92% engine load, specifically the peak of COD40, could be an indicator of the fuel injector fouling, probably due to deposit formations that might have altered the fuel spray. This hypothesis could explain the lower power produced at that load with COD50 and the further complications when COD60 was run for the first time (without preheating the fuel blend). During the first run with COD60, the engine was shut down as it wasn't able to hold any load and the cylinder head was removed for a quick inspection. A "pool of fuel" was found on top of the piston, inside the combustion chamber, it was cleaned up and the cylinder head was put back together. Then the engine was run with diesel and after that, the preheated COD60 was tested successfully.

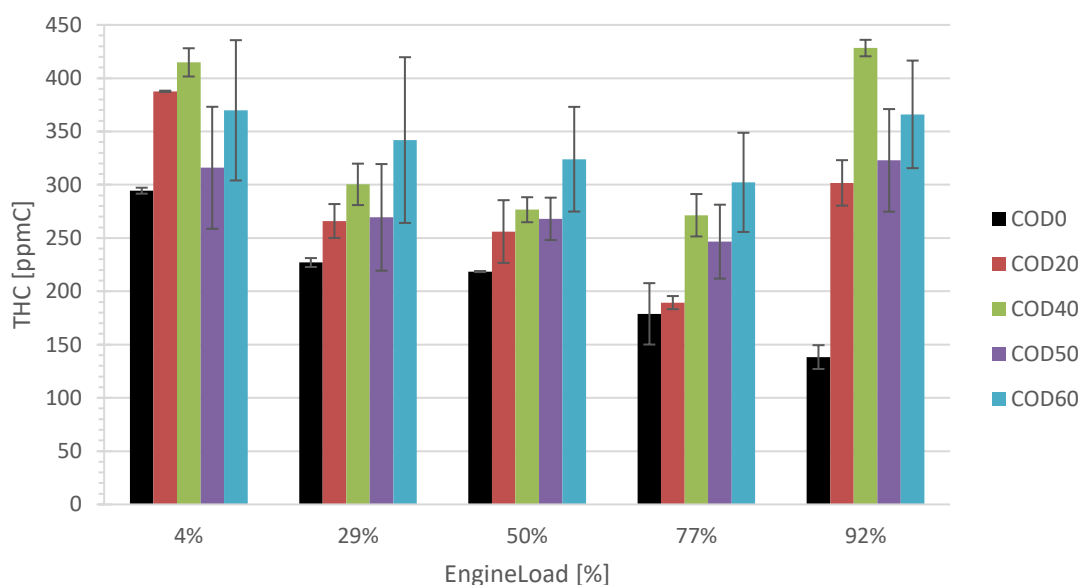


Figure 4-23 Total hydrocarbon emissions for 5 castor oil-diesel blends at 5 engine loads.

The NO_x results are presented in Figure 4-24 which shows that the NO_x emissions increase as the engine load increases. This trend was expected as NO_x is produced by the reaction of oxygen and nitrogen at higher temperatures. In Table 4-11 it was reported that the cylinder temperatures at 92% engine load were higher than the temperature at the other engine loads for all blends. It was found that COD0 had the highest NO_x emissions at all loads: 612 ppm (92% engine load), 492 ppm (77% engine load), 320 ppm (50% engine load), 240

ppm (29% engine load), and 171 ppm (4% engine load). The emissions produced by COD0 at 92% engine load were between 1% and 9% higher than the emissions produced by the other blends at the same load. The results followed a similar trend as that reported by Sisi et al. [191].

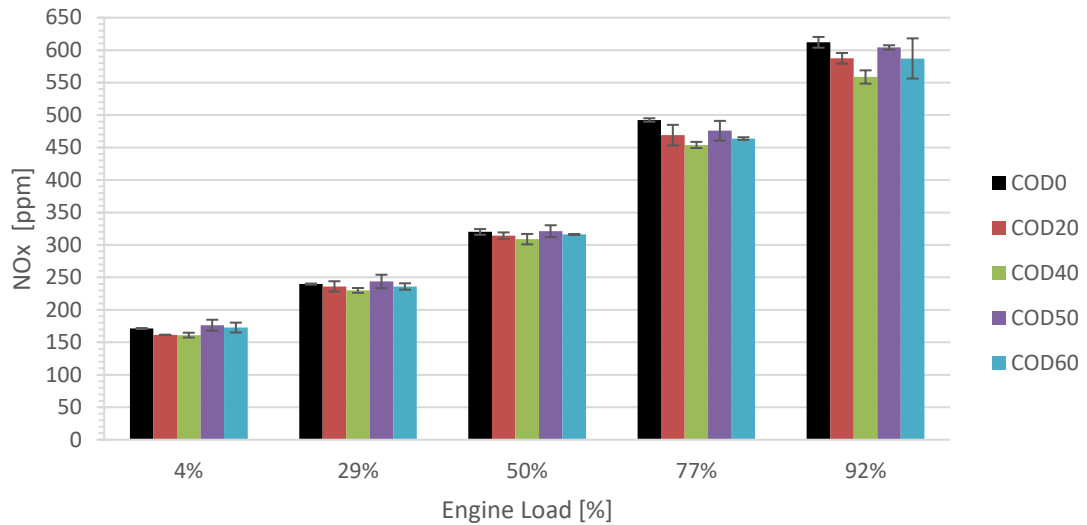


Figure 4-24 NOx emissions for 5 castor oil-diesel blends at 5 engine loads.

For ease of pollutant emissions cross-comparison among fuel blends, the emission index (EI) and the specific emissions (SE) from the CO, HC, and NOx data were computed using Equation 4-7 and Equation 4-8.

$$EI_{gas} = k_{gas} * C_{gas} * CAF * (1 + AFR) * 1000 \quad \text{Equation 4-7}$$

$$SE_i = EI_i * SFC \quad \text{Equation 4-8}$$

where,

EI_{gas} is the emission index in g/kgfuel of each gas and C_{gas} is the gas concentration (in % or ppm). CAF is a concentration adjusting factor equal to 10^{-2} if the gas concentration is given in % or equal to 10^{-6} if the concentration is given in ppm. The conversion coefficient k_{gas} is defined as the ratio of molecular weight for specific emission components to the total sample gas (air). The k_{gas} values for the pollutant emission of interest are: $k_{CO} = 0.971$, $k_{THC} = 0.555$, and $k_{NOx} = 1.595$ [192]. SE_i represents the specific emissions in g/kWh for each gas and SFC is the specific fuel consumption in g/kWh.

Table 4-12 summarises the EI and SE findings for CO emissions, the numbers show that overall, increasing the castor oil content in the blend increases the emissions per kg fuel and per kWh. Using COD60 represents a 70% increase in emissions when running the engine at a high load (92% engine load), whereas, at lower loads, the increase is about 30%. It was also found that at 92% engine load, the rest of the fuel blends produced their highest SE relative to diesel. The relatively higher emissions from castor-diesel blends at 92% engine load can be

attributed to a higher amount of fuel injected that suffers incomplete combustion. However, it should not be overlooked the fact that overall, the CO SE increase as engine load decreases, especially for higher castor oil content in the fuel.

Table 4-12 CO emission index and specific emissions for 5 castor oil-diesel blends at 5 engine loads.

Engine Load [%]	CO EI [g/kgfuel]					CO Specific Emissions [g/kWh]				
	COD0	COD20	COD40	COD50	COD60	COD0	COD20	COD40	COD50	COD60
92%	6.89	8.31	9.74	9.18	10.13	1.84	2.35	2.91	2.79	3.17
77%	11.94	11.93	13.52	12.13	13.54	3.17	3.25	3.79	3.52	4.01
50%	22.74	23.06	24.83	23.84	25.53	6.71	7.15	8.14	7.92	9.15
29%	34.44	30.88	36.27	34.05	37.23	14.17	13.64	16.65	16.09	18.46
4%	53.66	51.54	57.78	52.16	56.28	112.04	113.23	136.10	128.14	146.72

The summary of EI and SE for THC emissions is included in Table 4-13, the results show that higher emissions are produced by the fuels with higher castor oil content. It was found that at 92% engine load, the THC emissions had a sharp rise being COD40 the worst case as its SE tripled while COD20, COD50, and COD60 emissions doubled, all compared to diesel. The sharp rise of COD40 can be attributed to the deposit formations that altered the fuel spray, indicating the fuel injector fouling, as discussed previously for the THC results. On the other hand, the SE showed an increase between 2% and 70% for the rest of the engine loads for all the fuel blends.

Table 4-13 THC emission index and specific emissions for 5 castor oil-diesel blends at 5 engine loads.

Engine Load [%]	THC EI [g/kgfuel]					THC Specific Emissions [g/kWh]				
	COD0	COD20	COD40	COD50	COD60	COD0	COD20	COD40	COD50	COD60
92%	2.22	4.41	6.18	4.58	4.99	0.59	1.25	1.84	1.39	1.56
77%	3.47	3.47	4.93	4.44	5.29	0.92	0.94	1.38	1.29	1.56
50%	5.88	6.40	6.80	6.57	7.71	1.74	1.98	2.23	2.18	2.77
29%	7.62	8.27	9.10	8.14	10.02	3.14	3.65	4.18	3.85	4.96
4%	12.74	15.32	15.98	11.95	13.74	26.60	33.58	37.63	29.43	35.82

Table 4-14 shows the EI and SE values found from the NO_x emissions. For this pollutant, a reduction between 3 % to 5% was observed on the SE for most of the fuel blends at different loads. However, it should be noted that for COD50

and COD60 at 50%, 29%, and 4% engine load, the NOx SE increased from around 3% to 8%.

Table 4-14 NOx emission index and specific emissions for 5 castor oil-diesel blends at 5 engine loads.

Engine Load [%]	NOx EI [g/kgfuel]					NOx Specific Emissions [g/kWh]				
	COD0	COD20	COD40	COD50	COD60	COD0	COD20	COD40	COD50	COD60
92%	28.23	24.64	23.17	24.73	22.93	7.54	6.97	6.91	7.52	7.19
77%	27.49	24.70	23.70	24.68	23.37	7.28	6.73	6.65	7.16	6.93
50%	24.75	22.57	21.83	22.65	21.68	7.31	7.00	7.15	7.53	7.76
29%	23.14	21.09	20.00	21.22	19.94	9.53	9.32	9.18	10.03	9.92
4%	21.30	18.35	17.82	19.23	18.48	44.47	40.21	41.97	47.08	48.13

4.2.5.2 Particulate Matter Emissions PM_{2.5}

The results of the particulate matter concentration, collected with the GF/F filter papers from the PM_{2.5} unit during each engine test are shown in Figure 4-25. It can be observed that COD0 PM_{2.5} emissions increase as the load increases, a similar trend was reported by Raghu B. and & Rajasekhar B. [193] in their study using a 4.5 kW diesel generator. The increase of particulate matter at higher loads can be attributed to the reduced AFR, which generates more fuel-rich areas in the combustion chamber, as indicated in Wang et al. review [194]. The lowest PM_{2.5} values at 4 engine loads were found for COD0 0.015 g/m³ (4% engine load), 0.015g/m³ (29% engine load), 0.024 g/m³ (50% engine load), and 0.035 g/m³ (92% engine load), whereas at 77% engine load the lowest value (0.017 g/m³) was found for COD20. On the other hand, the increase in PM_{2.5} emissions, found for the blends with higher castor oil content, could be attributed to the worsened fuel spray, atomisation and vaporisation as a result of the higher viscosity and lower volatility of castor oil. Therefore, the highest value found for COD40 at 92% load could be attributed to the suspected deterioration of the fuel injector as discussed in the THC results.

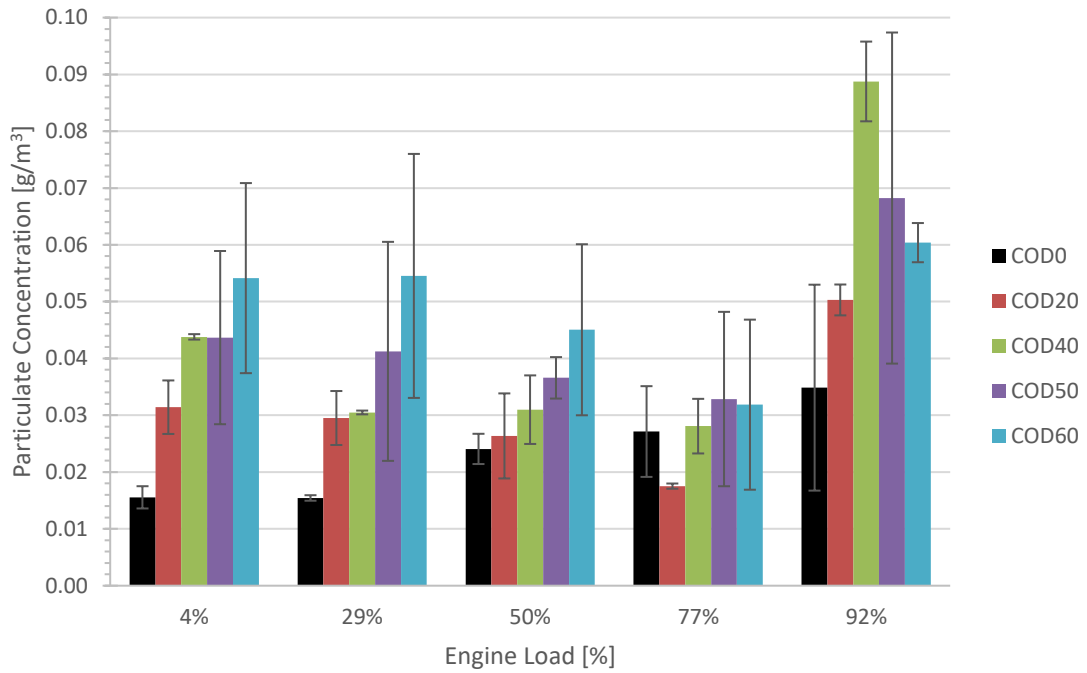


Figure 4-25 Particulate concentration for 5 castor oil-diesel blends at 5 engine loads.

From the particulate matter concentration ($C_{PM_{2.5}}$) data in g/m^3 , the emission index ($EI_{PM_{2.5}}$) in g/kg_{fuel} was calculated using Equation 4-9.

$$EI_{PM_{2.5}} = \frac{C_{PM_{2.5}}}{\rho_s} * (1 + AFR) \quad \text{Equation 4-9}$$

The density of the sample gas (ρ_s) was considered as 1.18 kg/m^3 [195]. AFR corresponds to the air-fuel ratio values obtained from the MEXA analyser. Also, the specific emissions ($SE_{PM_{2.5}}$) in g/kWh were computed from Equation 4-10 using the specific fuel consumption (SFC) values presented in Figure 4-12.

$$SE_{PM_{2.5}} = EI_{PM_{2.5}} * SFC \quad \text{Equation 4-10}$$

Table 4-15 summarises the EI and SE findings for the $PM_{2.5}$ emissions, the results show that, overall, higher emissions are produced by the fuels with higher castor oil content. The highest EI and SE values were found at 4% engine load for all blends. It was observed that at 92% engine load, the emissions produced by COD40 were about 3.6 times higher than the emissions produced by COD0. Also, it was found that using COD60 below 50% engine load would increase the emissions by more than 300%, relative to COD0.

Table 4-15 PM_{2.5} emission index and specific emissions for 5 castor oil-diesel blends at 5 engine loads.

Engine Load [%]	PM _{2.5} EI [g/kg _{fuel}]					PM _{2.5} Specific Emissions [g/kWh]				
	COD0	COD20	COD40	COD50	COD60	COD0	COD20	COD40	COD50	COD60
92%	0.62	1.12	1.96	1.40	1.25	0.16	0.32	0.58	0.43	0.39
77%	0.86	0.49	0.78	0.87	0.85	0.23	0.13	0.22	0.25	0.25
50%	0.94	1.01	1.16	1.34	1.63	0.28	0.31	0.38	0.44	0.59
29%	0.78	1.40	1.41	1.86	2.44	0.32	0.62	0.65	0.88	1.20
4%	1.10	1.90	2.57	2.48	3.07	2.29	4.15	6.06	6.13	8.00

4.2.5.3 Engine Exhaust Emissions vs European Emission Standards for Nonroad Engines.

This section compares the engine exhaust emission findings presented above against the emission limits from the European emission standard for nonroad engines (Stage V) that were mentioned in Chapter 2 (see Table 2-10). According to this standard, the emission limits for engines with net power below 8 kW are 8 g/kWh for CO emissions, 7.50 g/kWh for the combined THC and NO_x emissions and 0.40 g/kWh for PM emissions. The CO emissions are shown in Figure 4-26 where the dashed line represents the standard limit. The figure shows that when operating the engine at or above 50% engine load, the emissions stayed below 8 g/kWh for all blends.

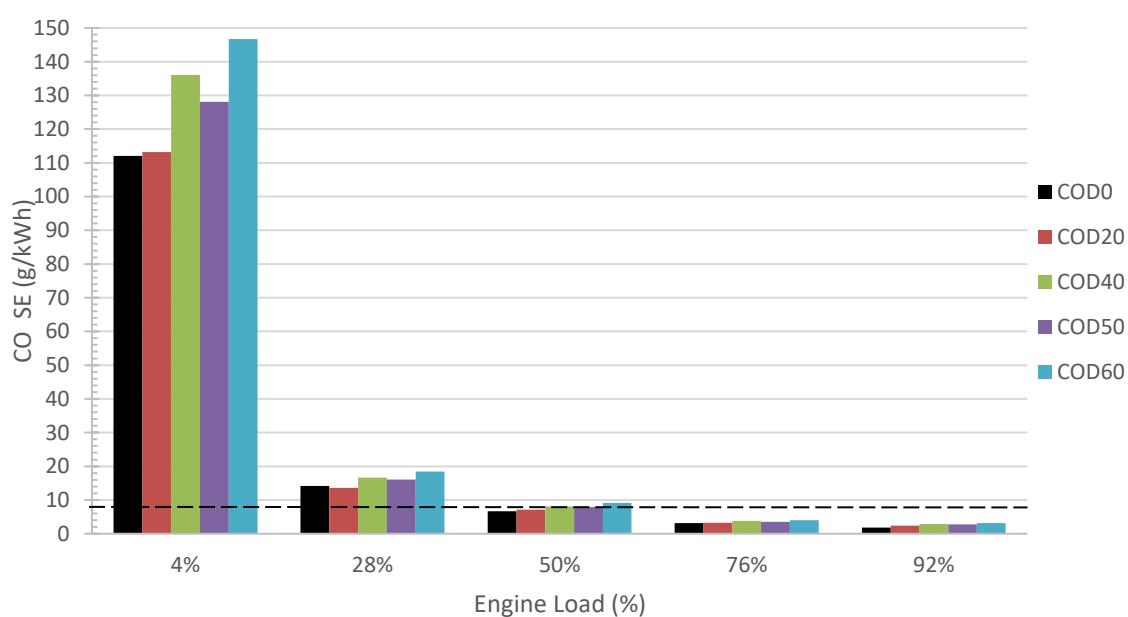


Figure 4-26 CO Specific Emissions for 5 castor oil-diesel blends at 5 engine loads.

Figure 4-27 shows the combined THC and NOx emissions, in this case, only when using COD0 or COD20, the emissions stayed below 7.5 g/kWh (at 76% and 92% engine load).

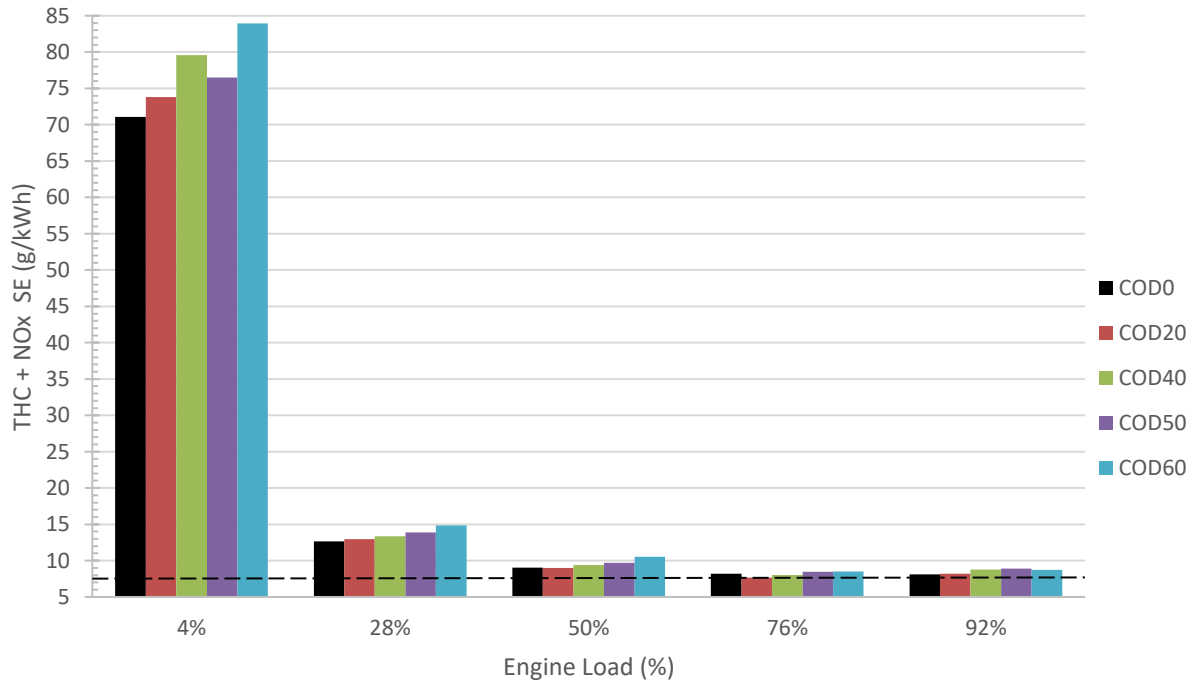


Figure 4-27 THC and NOx Specific Emissions for 5 castor oil-diesel blends at 5 engine loads.

The PM_{2.5} emission findings are shown in Figure 4-28, where the emission limit is again represented by the dashed line. In the figure, it can be appreciated that when operating the engine at or above 50% engine load, the emissions stayed below 0.4 g/kWh for most of the blends.

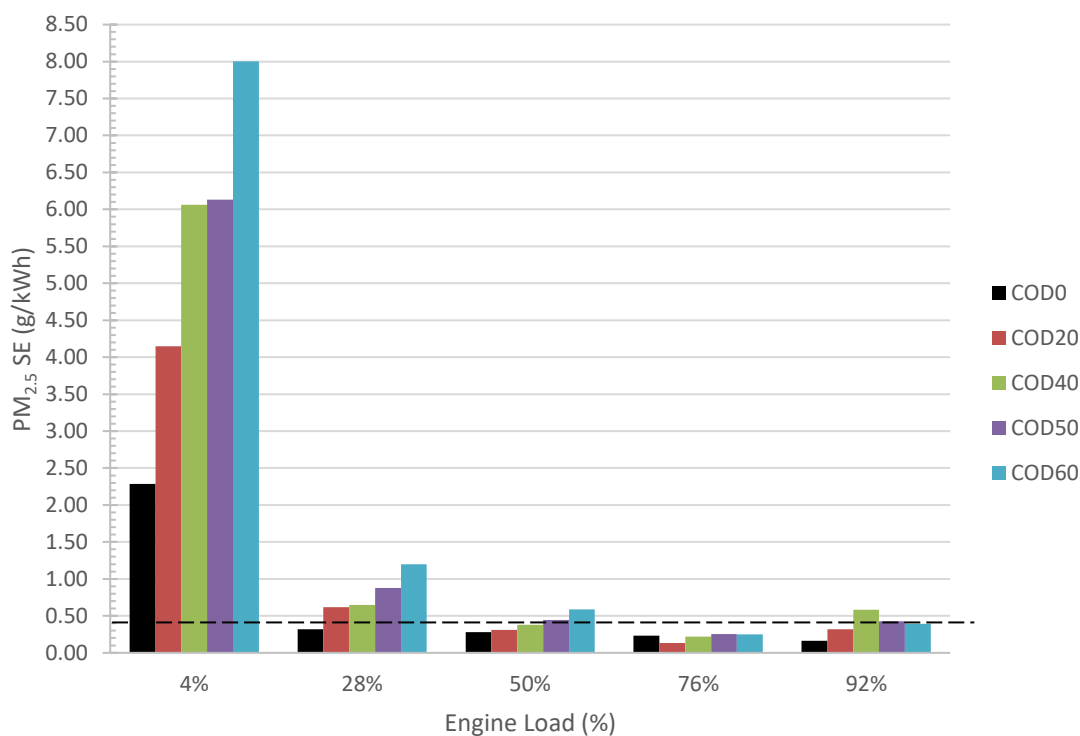


Figure 4-28 PM_{2.5} Specific Emissions for 5 castor oil-diesel blends at 5 engine loads.

Figure 4-26 to Figure 4-28 illustrate the importance of operating diesel generators above 50% engine load for avoiding low load operation, regardless of the fuel used to power the engine. It should be mentioned that using castor oil blends does not seem to reflect an environmental benefit, especially if the engine operates at low loads. However, in Chapter 5, further discussion regarding the potential use of castor oil-diesel blends is included.

4.2.5.4 Particle Size Distribution and Total Particle Number Determined by DMS 500 Fast Analyser

To compare the impact on particle production by using different COD blends, the particle number size distribution and the total particle number data obtained from the DMS 500 analyser are included in this section. The particle size range measured by the DMS was from 4.87nm to 1000nm.

Figure 4-29 shows the particle size distribution for the five fuel blends at 92%, it is clear how COD40, COD50 and COD60 produce more particulates within the nucleation mode (closer to 10nm), whereas COD0 and COD20 particulate production peak within the accumulation mode region (~100nm). This can be attributed to unburnt fuel droplets and condensation of semi-volatile matters to elemental carbon. Therefore, more nucleation occurs for the blends with higher

castor oil content, as more fuel remains unburnt due to their higher viscosity compared to diesel and COD20.

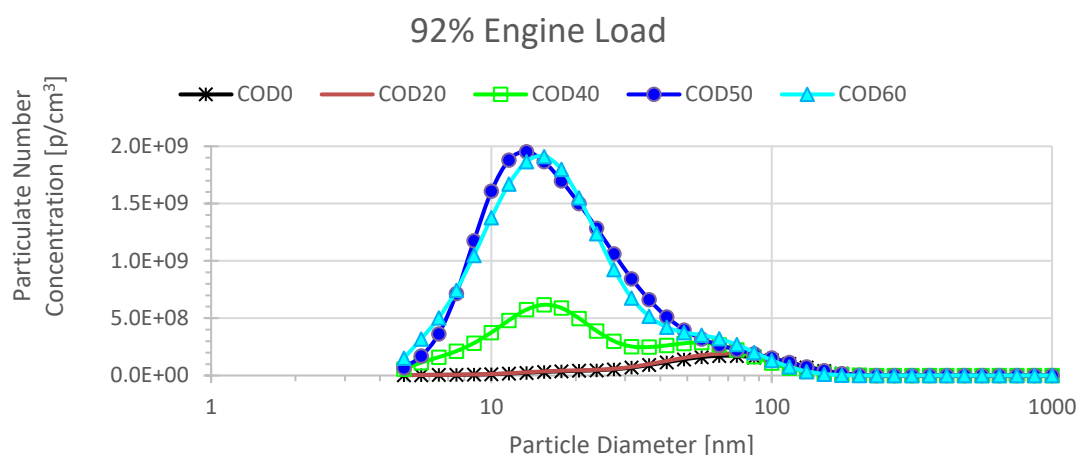


Figure 4-29 Particle size distribution for 5 castor oil-diesel blends at 92% engine load.

In Figure 4-30, at 77% engine load, the peaks of the particulate number concentration for COD40, COD50, and COD60 remained closer to the nucleation mode, while for COD20 and COD0, the peaks remained closer to the accumulation mode. However, for all the blends a bimodal distribution had a better definition. It was observed that the particulate production was reduced compared to the particulate production at 92% but still, COD60 had the highest particulate number concentration.

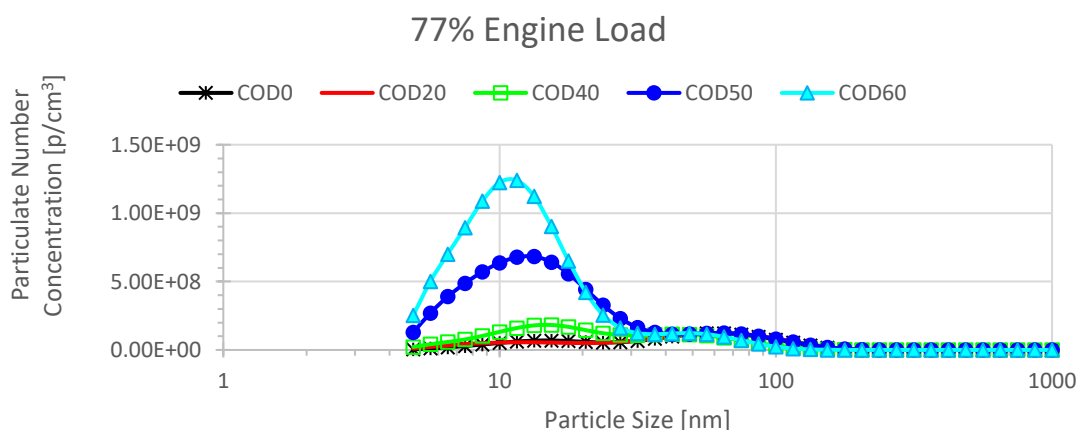


Figure 4-30 Particle size distribution for 5 castor oil-diesel blends at 77% engine load.

At 50% engine load, the curves from Figure 4-31 show that for COD40, COD50, and COD60, their respective peak particulate number shifted in the

opposite direction compared to the previous figure. On the other hand, a well-defined bimodal curve appeared for COD0 with two similar peaks at the nucleation and accumulation mode. The highest particulate number was found for COD20, at its peak near the nucleation mode. For the other three fuel blends (COD40, COD50, and COD60) it was found that their peak is near the accumulation mode and their particulate number concentration decreased, compared to their values at 77% engine load. The peak near the accumulation mode for these blends can be attributed to the lower temperatures produced at lower loads, which lead to more incomplete combustion and thus more unburnt fuel or semi-volatile matters. The latter may lead to particle agglomeration and according to Tree and Svensson [81], the temperature has the greatest effect on the parameters involved in the soot formation process.

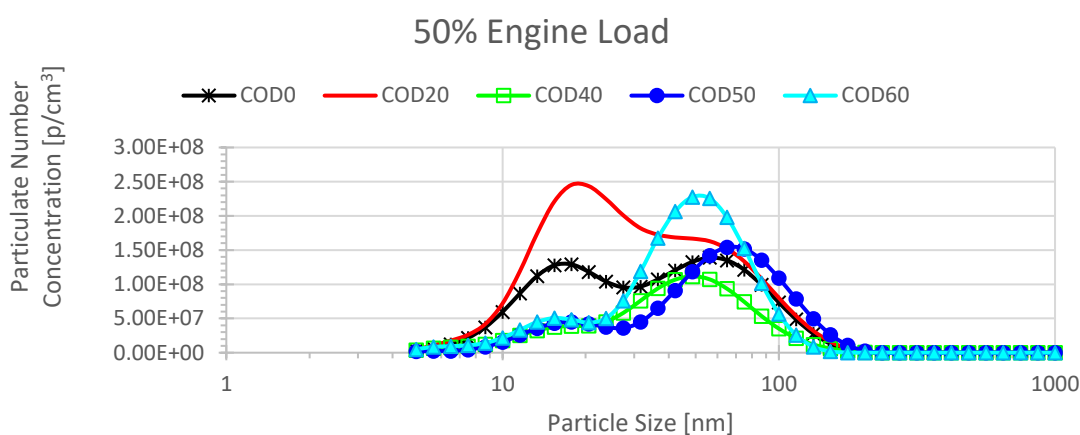


Figure 4-31 Particle size distribution for 5 castor oil-diesel blends at 50% engine load.

Figure 4-32 shows that at 29% engine load all the blends reduced their bimodal curve shape. It was found that the particulate numbers from COD40, COD50, and COD60 increased compared to their values at 50% load, whereas for COD20 and COD0 a reduction was detected.

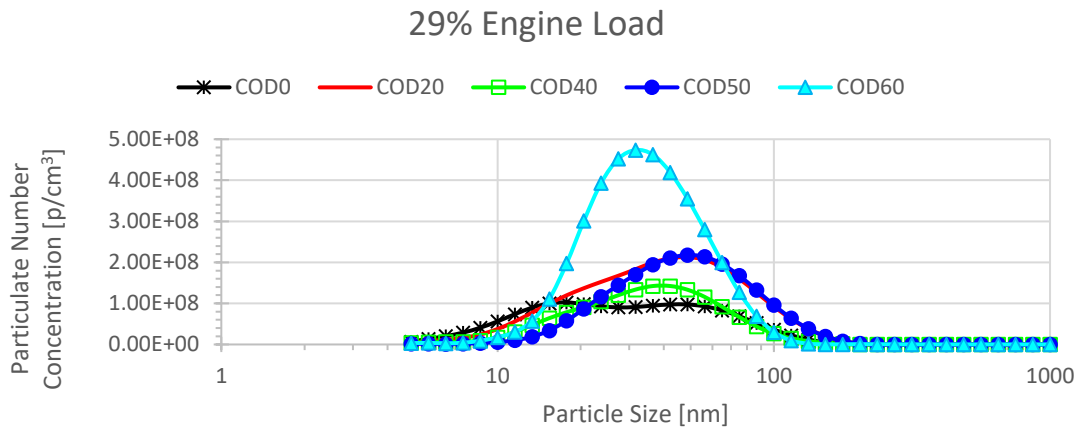


Figure 4-32 Particle size distribution for 5 castor oil-diesel blends at 29% engine load.

In Figure 4-33 it can be observed how at 4% engine load, the particulate concentration for all blends peaked between 20 and 40 nm (in the middle of the nucleation and the accumulation modes) and the bimodal curve shape was lost. At this load, the particulate number was increased for all blends, compared to the previous figure.

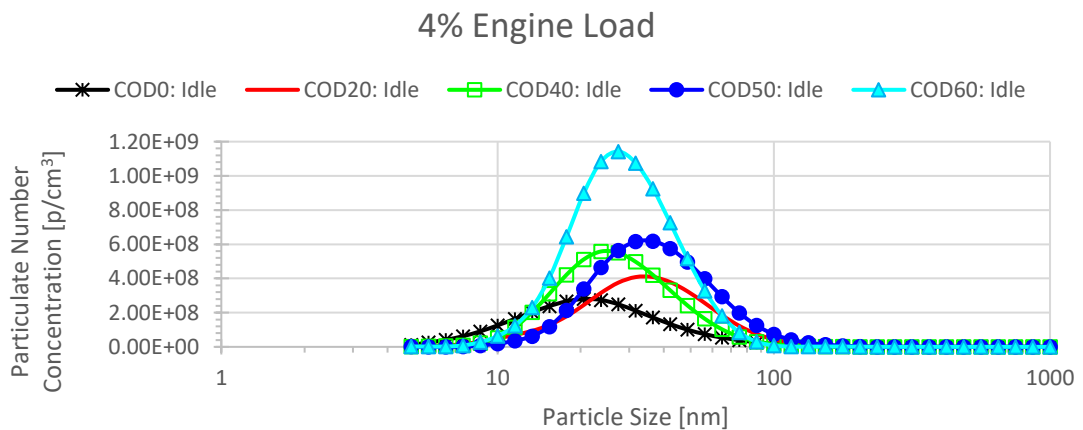


Figure 4-33 Particle size distribution for 5 castor oil-diesel blends at 4% engine load.

From the curves presented above, it is hard to find a unique trend to compare the behaviour of one blend at different loads or to cross-compare the blends at a specific load. However, two main trends can be determined by comparing the total particle number produced by each blend at 92% and 4% engine load (see Table 4-16). The first trend was observed for COD0 and COD20, their particle number increases by 65% and 96%, respectively, at 4% engine load, compared

to their corresponding values at 92% engine load. In contrast, it was found that for COD40, COD50, and COD60 the particle number decreases by 32%, 72%, and 54%, respectively at 4% engine load, compared to their corresponding values at 92% engine load. Although it is generally expected to see an increasing trend in the particle number with higher loads in diesel engines, Betha and Balasubramanian [193] reported a similar decreasing trend at higher loads using a 4.5 kW stationary diesel generator fuel with diesel and biodiesel. Their results also agree with the work presented by Chung et al. [196] after testing a 4.8 kW diesel generator. On the other hand, the increasing particle numbers found for the blends with higher castor oil content can be explained by the particulate formation enhancement due to fuel-rich areas in the combustion chamber [194].

Also, it was found that as the total particle number increases with higher castor oil content in the blend, using COD60 would increase the particulate number up to 10 times at 92% engine load compared to COD0. A summary of the total particle number and the peak diameter size found for each blend is included in Table 4-16.

Table 4-16 Total particle number and particle peak diameter for 5 castor oil-diesel blends at 5 engine loads.

Engine Load [%]	Total Particle Number [#/cm ³]					Peak Diameter [nm]				
	COD0	COD20	COD40	COD50	COD60	COD0	COD20	COD40	COD50	COD60
92%	1.09 x10 ⁸	1.20x10 ⁸	4.30x10 ⁸	1.20x10 ⁹	1.16x10 ⁹	64.94	64.94	15.4	13.34	15.4
77%	9.90x10 ⁷	1.03x10 ⁸	1.46x10 ⁸	4.52x10 ⁸	6.42x10 ⁸	64.94	64.94	15.4	13.34	11.55
50%	1.27x10 ⁸	1.90x10 ⁸	7.07x10 ⁷	9.26x10 ⁷	1.19x10 ⁸	56.23	17.78	48.7	64.94	48.7
29%	9.81x10 ⁷	1.64x10 ⁸	9.44x10 ⁷	1.39x10 ⁸	2.51x10 ⁸	17.78	48.7	36.52	48.7	31.62
4%	1.80x10 ⁸	2.36x10 ⁸	2.90x10 ⁸	3.32x10 ⁸	5.32x10 ⁸	20.54	36.52	23.71	36.52	27.38

4.2.5.5 Unregulated Volatile Organic Compounds (VOCs) Measured by the FTIR Analyser

The FTIR data was useful to determine the unregulated volatile organic compounds (VOCs) emissions generated by the five fuel blends. It was found that the ethylene and methane emissions increase as the engine load decreases, and as the castor oil increases in the blend as shown in Figure 4-34. Therefore, the highest ethylene value was found with COD60 at 4% engine load (28.65 ppm), which represents a 60% increase compared to the 17.92 ppm from COD0 at the same load. It should be noted that even using the fuel with the lowest emissions (COD0), the emissions increased up to 3.6 times if the engine runs at 4% engine load, compared to the 4.86 ppm emissions at 92% engine load. Similarly, the methane emissions with COD0 increased up to 6

times if the engine runs below 29% engine load compared to the emissions at 92% engine load (0ppm). The highest methane emissions were found for COD60 at 4% engine load (7.57 ppm), which represents an increase of 27% relative to COD0 at that load.

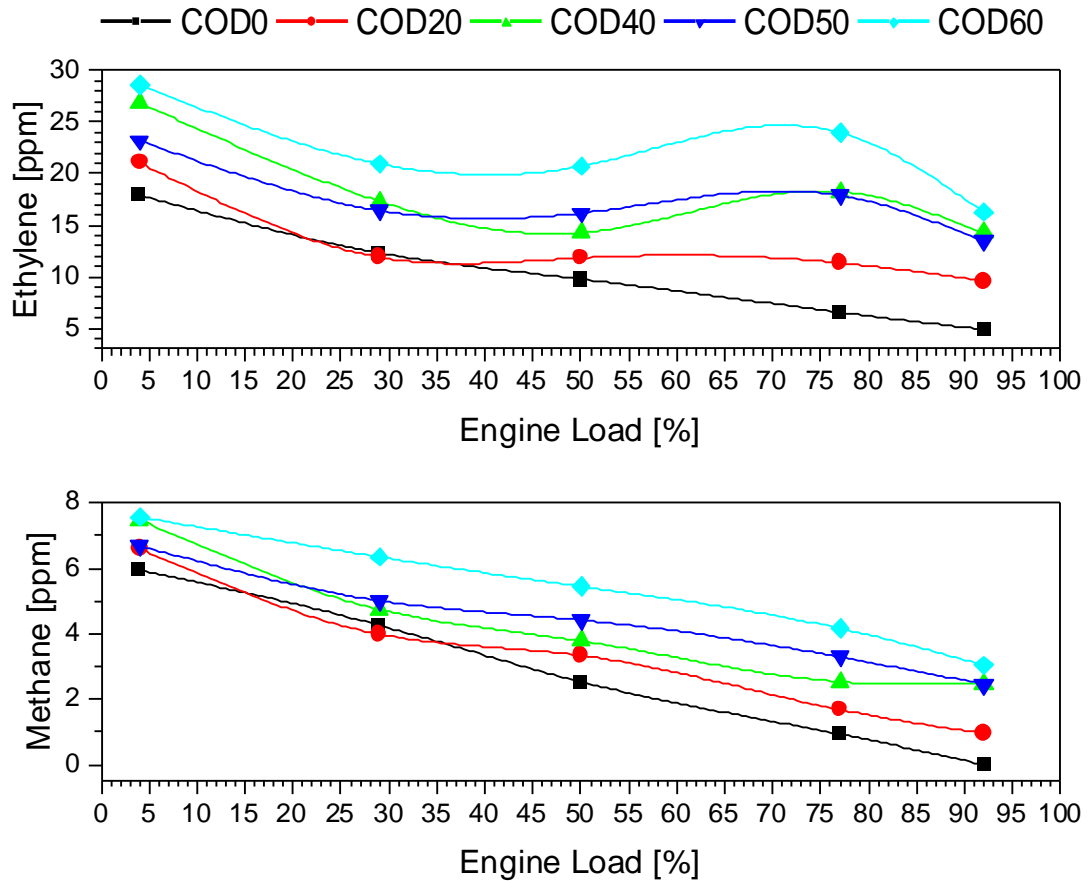


Figure 4-34 Ethylene and Methane emissions for 5 castor oil-diesel blends from 4% to 92% engine load.

The acetylene and benzene emissions were lower at higher loads for all blends according to Figure 4-35. Both emissions tend to increase as the castor oil content increases, however, COD0 had the highest benzene emissions (4.97 ppm and 2.66 ppm) at 4% and 29% engine load.

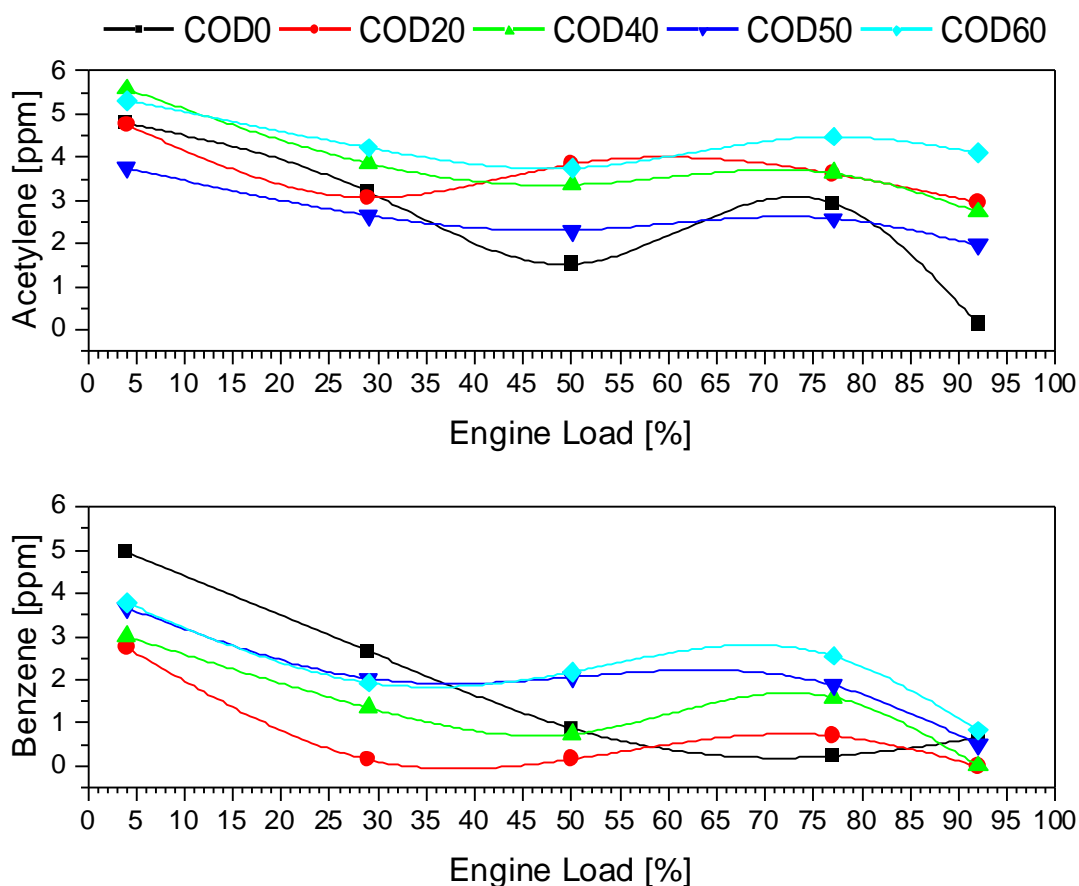


Figure 4-35 Acetylene and Benzene emissions for 5 castor oil-diesel blends from 4% to 92% engine load.

The results for ethane and hexane are shown in Figure 4-36. It was found that COD0 generated the lowest emissions at all loads and its emissions were reduced as the engine load increased. In contrast, ethane and hexane emissions were higher for the rest of the blends with an increasing load. The highest ethane (31.51 ppm) and hexane (51.57 ppm) emissions were found for COD40 at 92% engine load. Those values were 8.25 and 3.69 times higher than the lowest COD0 emissions of 3.82 ppm and 13.98 ppm, respectively. The best ethane values (11.21ppm, 14.56 ppm, 13.50 ppm, and 16.01ppm) for COD20, COD40, COD50, and COD60 were found at 77% engine load. Similarly, the best hexane values (17.84 ppm, 23.47 ppm, 22.77 ppm, and 24.71 ppm) for COD20, COD40, COD50 and COD60 were also found at 77% engine load.

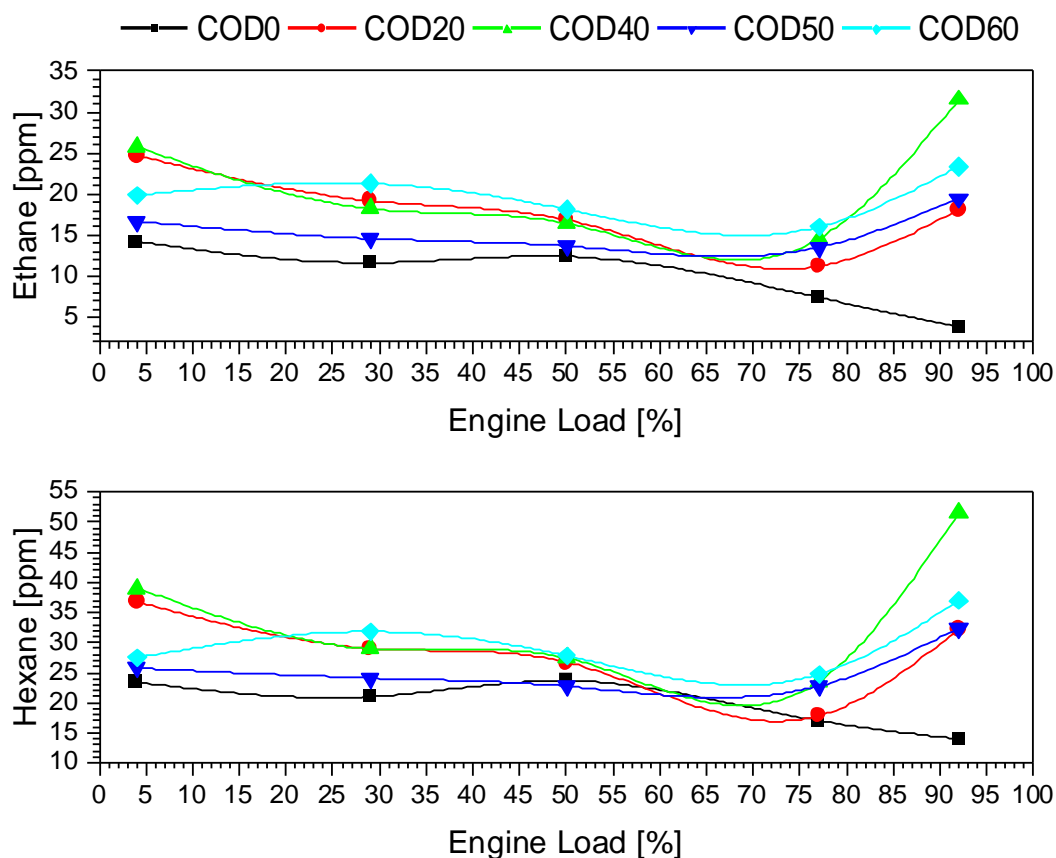


Figure 4-36 Ethane and Hexane emissions for 5 castor oil-diesel blends at from 4% to 92% engine load.

The results from other non-hydrocarbon VOCs, ethanol and formaldehyde, are shown in Figure 4-37. For ethanol, it was found that the emissions decrease at middle loads and increase at 4% and 92% engine load. The highest emissions (18.64 ppm) were produced by COD40 at 92% engine load, that value was 2.18 times higher than the COD0 emissions (8.43 ppm) at the same load. In contrast, the lowest emissions (0 ppm) were found for COD20 at 29% engine load.

On the other hand, for formaldehyde, it was found that the emissions decrease as the engine load increases for all blends. Also, it was observed that the emissions increase as the castor oil content increases in the blend. Hence, the lowest values (2.69 ppm, 9.08 ppm, 12.68 ppm, 16.61 ppm, and 25.59 ppm) were found for COD0 at 92%, 77%, 50%, 29%, and 4% engine load, respectively. Running the engine at 4% engine load increases the emissions by 9.52 times compared to the emissions produced at 92% engine load. The worst value (44.63 ppm) was found for COD60 at 4% engine load, which represents 74% more emissions compared to COD0.

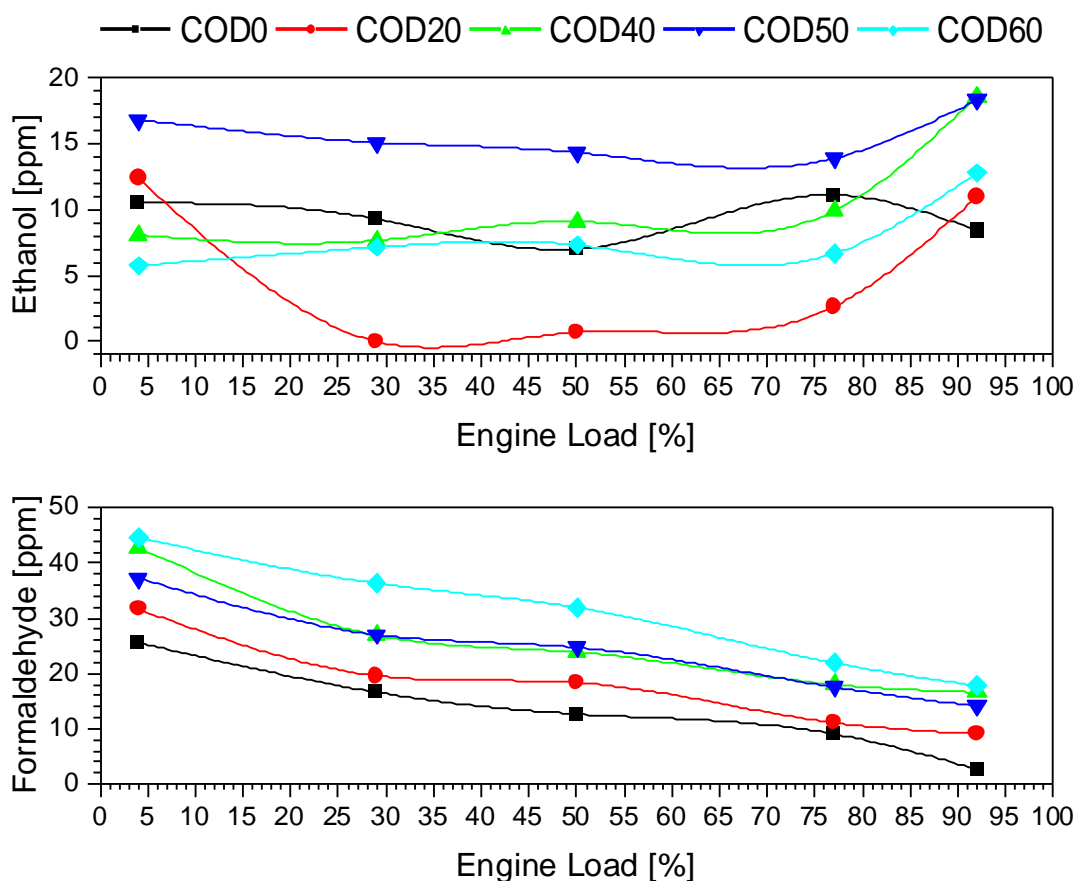


Figure 4-37 Ethanol and Formaldehyde emissions for 5 castor oil-diesel blends from 4% to 92% engine load.

The FTIR findings presented above showed that, overall, VOCs increased as the castor oil increased in the blend. Although no direct comparison can be made for the species presented in Figure 4-34 to Figure 4-37, as no studies were found for VOCs emissions from diesel generators fuelled with vegetable oil-diesel blends, the literature findings suggest that the VOCs emissions generated by COD blends follow the same trend reported for fuels with higher viscosity and higher oxygen content, compared to diesel. For example, the findings presented above agree with the trend reported by Lea-Langton et al. [197] when comparing the formaldehyde emissions of an engine fuel with diesel, waste cooking Methyl Ester (WME) and rapeseed oil (RSO). In [197] it was found that RSO produced higher emissions, compared to diesel and WME, the higher formaldehyde emissions were attributed to the higher viscosity of RSO, which affects the fuel injection and the fuel-air mixing. Therefore, the higher formaldehyde emissions generated by the COD blends (see Figure 4-37) can be also attributed to the higher viscosity of castor oil, compared to diesel. Also, it was found that benzene emissions tend to increase as the content of palm oil biodiesel was increased in the experimental work done by [198].

Finally, the results presented by [199] showed that some VOCs increased as the canola oil blend ratio increased. This trend was attributed to the higher viscosity and higher oxygen content of canola oil compared to diesel.

From the FTIR findings, the amount of NO and NO₂ emitted by each blend was also determined, the results are summarised in Table 4-17. It was observed that the NO emissions decrease as the engine load decreases, the numbers at 4% engine load are only 18% compared to the values at 92%. The highest NO emissions were found for COD0 at 92% and 4% engine loads, whereas the lowest values were found for COD40 at all loads. On the other hand, it was observed that the NO₂ emissions increase at lower loads and the highest emissions (84 ppm) were found for COD60 at 4% engine load.

Table 4-17 Nitrogen monoxide and nitrogen dioxide emissions for 5 castor oil-diesel blends at 5 engine loads.

Engine Load [%]	Nitrogen Monoxide (NO) [ppm]					Nitrogen Dioxide (NO ₂) [ppm]				
	COD0	COD20	COD40	COD50	COD60	COD0	COD20	COD40	COD50	COD60
	92%	581	565	537	573	558	0	0	0	0
77%	438	426	417	440	434	0	4	3	0	0
50%	239	232	227	241	236	6	40	60	61	58
29%	163	164	152	163	158	56	48	72	75	75
4%	104	95	91	102	97	71	57	71	80	84

A good correlation was found between the NO_x emissions measured by the FTIR and the NO_x emissions measured by the MEXA analyser as shown in Figure 4-38. The R² for COD0 was 0.97 and 0.99 for the rest of the blends.

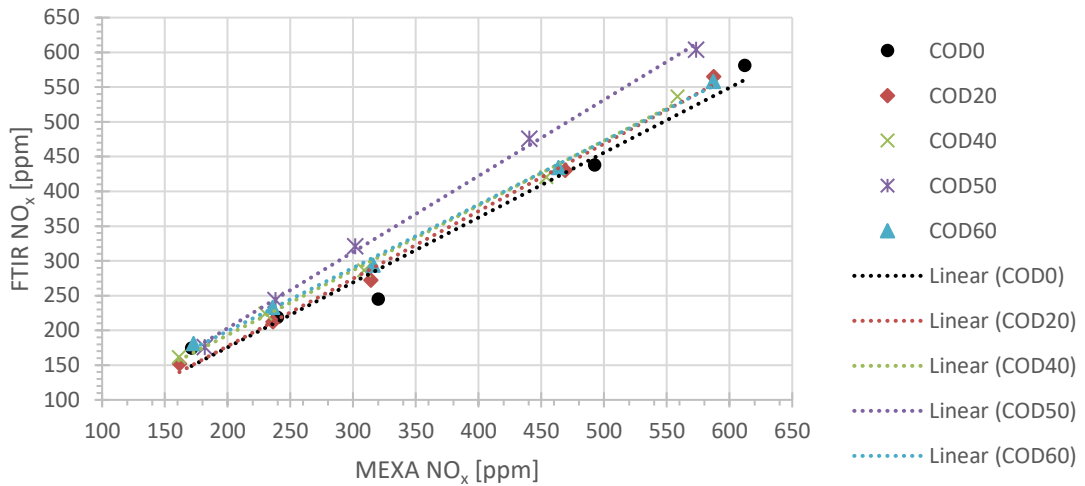


Figure 4-38 NO_x emissions correlation between FTIR and MEXA measurements from 4% to 92% engine load for 5 castor oil-diesel blends.

4.3 Deposits on Fuel Injector Analysis

The final step for assessing the impact of using castor oil-diesel blends to run a diesel generator was carried out when all the engine tests were concluded. This step was dedicated to the analysis of the engine's fuel injector. During the engine tests, an FB injector like the one shown in Figure 4-39 was used.



Figure 4-39 FB fuel injector dismantled (left) and FB fuel injector nozzle (right).

To verify the injector's nozzle diameter hole size, a scanning electron microscope (SEM) analysis was done on a new FB injector. From the SEM images that appear in Figure 4-40, five holes can be identified in the image at 50x magnification (left). Further magnification of 500x (right image) was needed to determine the diameter of each hole.

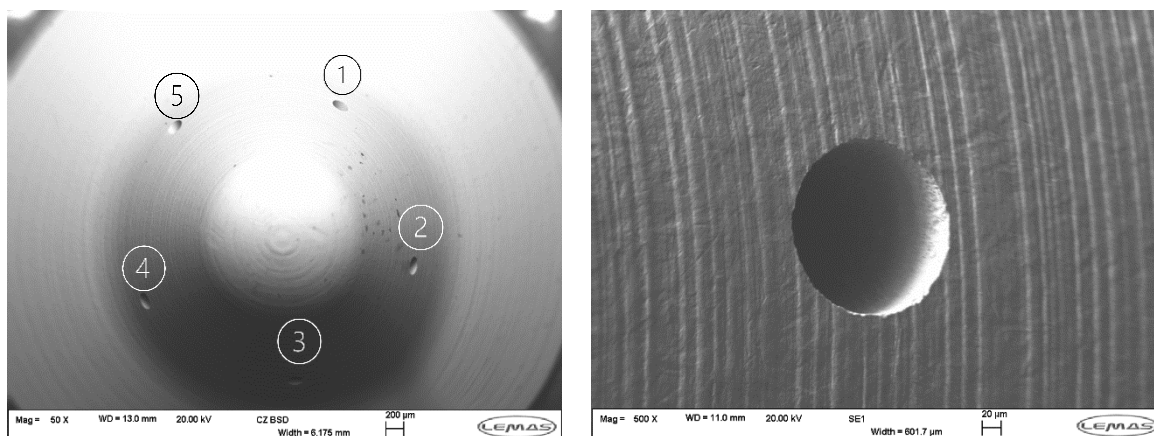


Figure 4-40 SEM image at 50x magnification of a new FB fuel injector nozzle's tip with five holes(left) and SEM image at 500x magnification of one hole (right).

The results from the measured diameters of each nozzle's hole are included in Table 4-18. The numbers from the table are close enough to the expected size of 185 μm as indicated in the nozzle's label. However, the measured diameters are slightly different due to the irregular surface (crevices) only visible with the 500x resolution.

Table 4-18 FB fuel injector hole size from SEM analysis.

Diameter [μm]				
Hole 1	Hole 2	Hole 3	Hole 4	Hole 5
188.6	187.5	188.0	188.6	183.9

After the engine tests were completed, an SEM analysis was done on the used injector's nozzle to investigate the effect caused by the castor oil-diesel blends. The injector's nozzle frontal view that appears in Figure 4-41 shows the nozzle's tip with deposit formations. From that view, it is difficult to visualise the holes, but 4 holes were identified once the injector's nozzle was tilted to the left while rotating counterclockwise. The fifth hole was not found as it was completely covered with deposits.

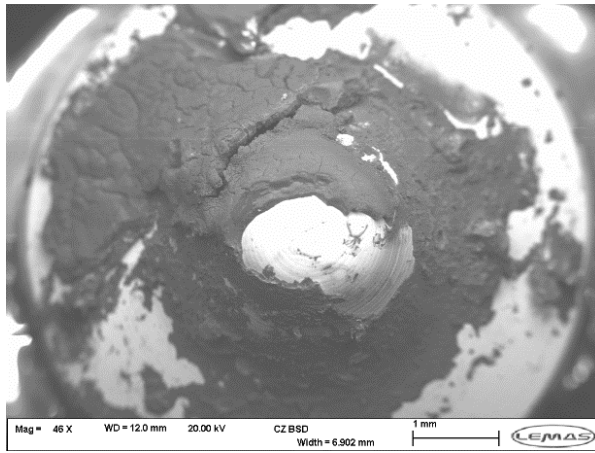


Figure 4-41 SEM image at 46x magnification of used FB fuel injector nozzle's tip with deposits after running a diesel engine with five castor oil-diesel blends.

The diameter of the visible holes at 50x magnification with the tilted view, shown in Figure 4-42 (see images a,b,c, and d), was measured using their corresponding 500x magnification as shown in images A, B, C, and D.

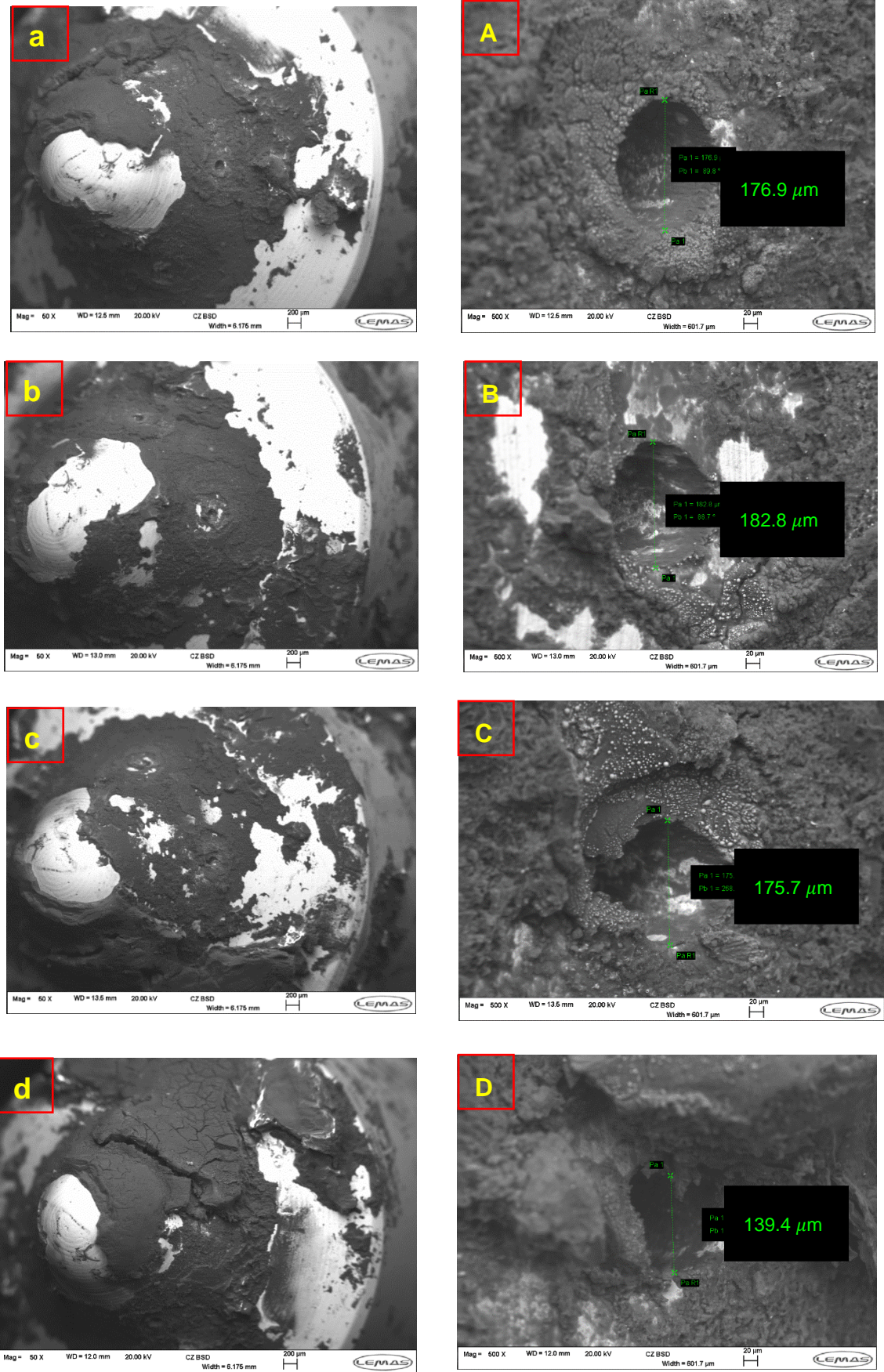


Figure 4-42 SEM images at 50x magnification (a,b,d, and d) and 500x magnification (A, B, C, and D) from a used FB fuel injector after running a diesel engine with five castor oil-diesel blends.

From the SEM images, it is clear the negative impact that castor oil had on the fuel injector regardless of the relatively short period of the engine running on castor oil- diesel blends (~20 hours). The deposits might be mostly attributed to the higher castor oil content blends (COD50 and COD60) according to the findings reported by Barsik and Humke [200] on deposit formation rates using peanut and sunflower oils and their 50% diesel blends. The authors found that the rate of formation is not significantly different for the pure oils compared to their 50% blends after running a diesel engine for about 20 hours. However, the formation of the deposits was suspected to start during the COD40 runs, where a THC increase was noted. The THC increase could be attributed to the deposits as deposits are formed due to fuel incomplete combustion [201]. The deposits could also help to explain the power loss reported for COD50 during test 4. The power loss could have been generated due to a disturbance in the spray pattern. The disturbance results from the reduced fuel flow through the holes, which also reduces the atomisation and fuel-air mixing when deposits are built up in the injector's tip [202].

To determine the elemental composition of the deposits, an energy dispersive X-ray (EDX) analysis was done at different locations of the nozzle's tip, as shown in Figure 4-43 (see images L 1, L2, and L3). Also, the EDX was done to the deposit flakes attached to the nozzle's base (see image L4).

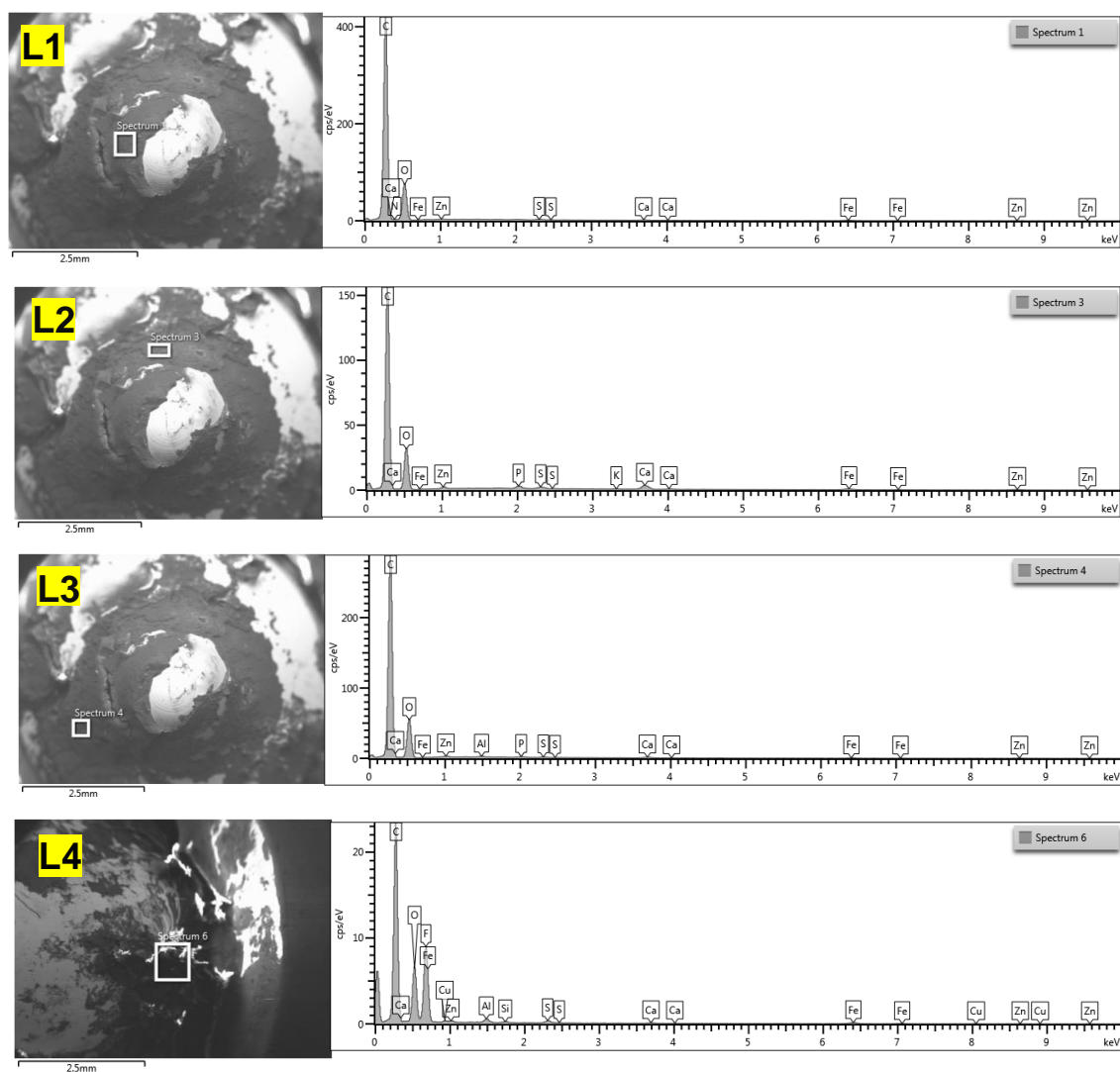


Figure 4-43 EDX analysis of the used FB fuel injector's deposits at four different locations (L1, L2, L3, and L4).

For L1, L2, and L3 it was found that the composition of the deposits was about 69% carbon (C), 30% oxygen (O) and the remaining 1% was mainly composed of iron (Fe), zinc (Zn) and calcium (Ca) in different proportions. For L4 the composition was about 56% C, 18% O, 24% fluorine (F), and the remaining 2% was composed of Fe (.94%), .48% aluminium (Al), .36% sulphur (S), and some traces of copper (Cu), silicon (Si), Ca, and Zn. The F content was attributed to the nozzle's base material and not to the deposits. The high carbon and oxygen concentrations are similar to the results reported by Hoang et al. [201] after running an engine with preheated vegetable oil (jatropha oil). Also, the authors reported the presence of Ca derived from lube oil degradation, which can be the case in this work as well. Figure 4-44 shows the TGA curves of the engine's lube oil. The curves suggest that some degradation occurred during the engine tests as the used lube oil (ULO) has a slightly different pattern compared to the initial conditions of the fresh lube oil (FLO) curve. It was found that the onset volatilisation temperature of the ULO was 280 °C, whereas for the FLO it was

300°C. Similar characteristics of the TGA curves from fresh and used lube oil were reported by [203].

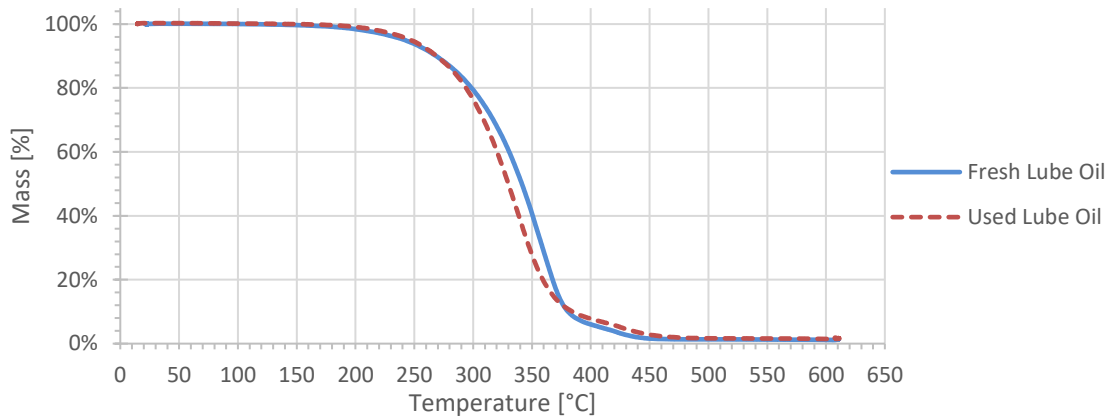


Figure 4-44 Thermograms from TGA analysis of fresh lube oil (blue line) and used lube oil after running a diesel engine with 5 castor oil-diesel blends.

4.4 Summary

The physical and chemical properties of castor oil-diesel (COD) blends with 0%, 20%, 40%, 50%, 60%, 80% and 100% castor oil were investigated for assessing their impact on the performance of a 6 kVA diesel generator. Engine tests with 20%, 40%, and 50% castor oil were done without preheating the blends. The 60% COD blend was tested with the fuel being preheated to 60°C and no engine tests were done with 80% or 100% castor oil due to fuel heating system limitations. The following remarks summarise the findings presented in the chapter:

1. The volatility and the net calorific value (NCV) decrease as the castor oil increases in the blend. The lower volatility leads to higher onset volatilisation temperatures (T_{onset}). The T_{onset} for COD20 is only 3°C higher than the COD0 T_{onset} (131°C), whereas for COD60 a difference of 161°C was found. Higher T_{onset} impacts the combustion process as the air-fuel mixture formation is altered due to the lower volatility of castor oil. The NCV of the COD60 blend (39.28 MJ/kg) is 12% lower than the NCV of COD0 (44.19 MJ/kg).
2. Density and kinematic viscosity increase as castor oil content increases in the blend. Both properties are temperature-dependent and decrease as temperature increases. The highest values for density and kinematic viscosity of the unheated blends (COD50) are 8% and 11.75 times higher than the COD0 values at 30°C. The density and viscosity values for

COD60 (at 60°C) are only 6% and 4.10 times higher than the COD0 values at 30°C. Despite the higher viscosity and density of castor oil compared to diesel, COD20, COD40, and COD50 can be used in the engine without preheating. However, preheating these blends could prevent the early fouling of the fuel injector. On the other hand, a 60% castor oil blend can be used if the fuel temperature is kept at 60°C. The use of 80% castor oil blends could be considered if the fuel is kept above 80°C as it was found that heating the COD80 at 70°C was not enough to power the engine. Due to temperature limitations, it was not possible to run more tests with COD80 or COD100, but future work could be considered using the waste heat from the exhaust gas.

3. The genset output power was slightly lower for the blends with higher castor oil content compared to the output power produced by COD0. The output power reduction was ~1% with COD40 whereas, for COD50 and COD60, the reduction was ~2% and 3%, respectively. No reduction was observed with COD20. The reduction percentages remained unchanged once the genset output power was converted to engine output power.
4. The mass-based fuel consumption increases as the engine load increases and it also increases with higher castor oil content in the blend. The highest fuel consumption of 1.63 kg/h (with COD60) at 92% engine load was ~14% higher than the fuel consumption with COD0 (1.43 kg/h) at the same load. Running the engine at 77% load only increases the fuel consumption up to 7% for the blend with the highest castor oil content (COD60). In contrast, if the engine runs at 4% load, the fuel consumption increases up to 20% using COD60.
5. The volumetric fuel consumption showed a similar trend to that of the mass-based fuel consumption results. However, it showed an apparent lower percentage fuel consumption increase compared to COD0 at all loads. Although the minimum variation in volumetric fuel consumption was also found at 77% for some blends, at this load no variation was found for COD60. Using the volumetric fuel consumption may mislead the interpretation of the real fuel consumption if the wrong density values are used. Therefore, mass-based fuel consumption was preferred in this work for developing the cost optimisation model presented in Chapter 5. The model considers the fact that volumetric fuel consumption is commonly reported by engine manufacturers and that end users purchase fuel by volume, which is why the model converts the volumetric fuel consumption to its mass-based equivalent for each fuel blend
6. The specific fuel consumption (SFC) and brake specific energy consumption (BSEC) increase as the engine load increases and as

castor oil content increases in the blend. Therefore, the worst SFC (2.61 kgfuel/kWh) and BSEC (102.33 MJ/kWh) values were found for COD60 at 4% engine load. Those values are 23% and 10% higher than the values found for COD0, respectively. The best SFC and BSEC values for all blends were found at 77% engine load.

7. The maximum brake thermal efficiency (BTE) was found at 77% for all blends. The maximum BTE for COD0 to COD50 was 31% whereas for COD60 it was 32%, these numbers showed that no deterioration in BTE occurred.
8. The oxygen content increases as the castor oil increases in the blend. COD60 has 9.55% oxygen whereas COD0 has 0.3%. Higher oxygen content produced higher peak in-cylinder pressure and higher in-cylinder temperatures for COD blends. Also, as the higher oxygen content of the castor oil blends reduced the amount of fuel burned during the premixed combustion, a lower peak heat release rate was observed for those blends.
9. The ignition delay (ID) reduces as castor oil increases. The shorter ID was attributed to the castor oil fatty acid composition. The combustion duration was only varied by the ID as the mixing-controlled combustion ended at 26 crank angle degrees for all the blends.
10. The THC emissions decrease at higher loads for COD0. In contrast, for the rest of the blends, the emissions increased at 92% engine load. The high emissions at 92% engine load were attributed to the fuel injector's deposits that altered the fuel flow.
11. The NO_x emissions increase as the engine load increases, COD0 produced higher emissions than the rest of the blends at all loads. The emissions produced by COD0 were up to 6% and 9% higher, relative to the other COD blends emissions at 4% and 92% engine load, respectively.
12. The PM_{2.5} emissions increase with higher castor oil content in the blend. The high emissions reported at 92% engine load were attributed to the reduced air-fuel ratio, as more fuel is injected but the air intake remains constant. As the air-fuel ratio was further reduced for the blends with higher castor oil content, their emissions were between 1.4 and 2.5 times higher than the COD0 emissions at that engine load. It was noted that if the engine runs below 50% load, the emissions produced by the blends with higher castor oil can be up to 3.5 times higher than the COD0 emissions.
13. The total particle number detected by the fast particulate analyser (DMS500) increases with higher castor oil content in the blend (up to 10

times at 92% engine load using COD60). On the other hand, the effect of the engine load on particle production showed two different trends, one for COD0 and COD20 and the other one for the blends with higher castor oil content (COD40, COD50, and COD60). The particle number produced by COD0 and COD20 at 4% engine load was increased by 65% and 96% respectively, compared to their corresponding particle production at 92% engine load. In contrast, the particle production at 4% engine load from COD40, COD50, and COD60 was reduced by 32%, 72%, and 54% respectively, compared to their corresponding emissions at 92% engine load.

14. The FTIR analyser results revealed the presence of the following unregulated volatile organic compounds: ethylene, methane, acetylene, benzene, ethane, hexane, ethanol, and formaldehyde. From the FTIR results, it was also determined that the NO emissions increase as the engine load increases. The highest NO emissions were produced by COD0 at 92% and 4% engine loads, compared to the rest of the blends at the same engine loads. In contrast, NO₂ emissions increase as the engine load decreases. COD60 produced the highest NO₂ emissions (84 ppm) at 4% engine load.
15. Deposits were found on the fuel injector after running a diesel generator with castor oil-diesel blends. The deposits covered one of the five nozzle holes, which may have altered the combustion process. It was suspected that the formation of the deposits started after using the COD40, which impacted the results of COD50. Therefore, it could be beneficial to preheat all the blends if more than 20% castor oil is included for further viscosity reduction of the blends. The latter may prevent deposit formation, but more tests would be needed to confirm this assumption.

The findings presented in this chapter showed that castor oil-diesel blends could be used to power diesel generators, obtaining similar brake thermal efficiency and similar specific fuel consumption, regardless of the different viscosity and net calorific value of castor oil, compared to diesel fuel. However, it was found that the higher oxygen content of the castor oil blends produced a shorter ignition delay, which in turn reduced the fuel burned during the premixed combustion leading to higher PM_{2.5} emissions, especially at low loads (below 50% engine load). It was also found that using castor oil-diesel blends causes deposits in the fuel injector after running the engine for about 20 hours. The deposit formation reduces the expectations of using castor oil-diesel blends as a promising alternative to diesel fuel. However, as the deposit formation was

suspected to start when using a 40% castor oil blend, using 20% blends would still be considered an alternative to diesel. It was also noted that further tests using the high castor oil diesel blend (COD80) at temperatures above 80°C are needed to determine if at higher temperatures, by reducing the viscosity of the blend, COD80 could power the engine. It would also be beneficial to run more tests with all the blends at higher temperatures to assess how the reduced viscosity would impact the deposit formation, the pollutant emissions, and the performance of the diesel generator.

Chapter 5

Cost Optimisation Model Development

From the literature survey, it was identified that little attention is given to the performance of diesel generators during the optimisation process carried out in the planning stage of hybrid microgrids (MG). It was also identified that the poor performance of oversized diesel generators leads to higher pollutant emissions and operating costs. Moreover, it was noticed that optimisation models generally assume diesel as the fuel for powering diesel generators. This assumption limits the possibility of assessing other fuels that might be of interest for hybrid systems deployment for rural electrification (i.e., vegetable oils and vegetable oil-diesel blends). This chapter presents the cost optimisation model developed to assess the selection of diesel generators for a hybrid microgrid system. The diagram of Figure 5-1 shows the hybrid microgrid configuration used for the cost optimisation model development. The hybrid system configuration considers solar energy (PV), battery energy storage systems (BESS), and diesel generators (gensets) fuelled with castor oil-diesel (COD) blends. The selection of diesel generators depends on the performance of each generator, the pollutant emissions generated, and the available fuel blends. The mathematical formulation as well as the graphical user interface (GUI), created for the visualisation of the optimisation results, are included in the following sections.

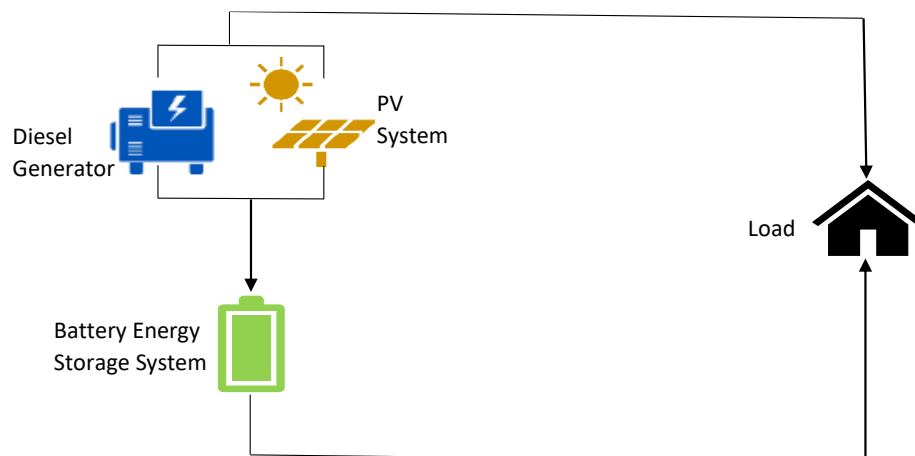


Figure 5-1 Diagram of the hybrid microgrid configuration considered in the cost optimisation model.

5.1 Cost Optimisation Mathematical Model

The cost optimisation mathematical model was developed to minimise the yearly cash flow expenses of a hybrid microgrid by selecting the optimum size and number of diesel generators, and the optimum castor oil-diesel blend to reduce the fuel consumption and pollutant emissions of the system. The selection of diesel generators depends on the predetermined electricity demand profile and the preferred type of hybrid system configuration. The predetermined settings for solving the optimisation problem consider three Tanzanian electricity demand profiles (high, medium, and low) and eight hybrid configurations (SC1-SC8). For each electricity demand profile, the PV system can be sized to supply 40%, 60% or 100% of the daylight hours average load (assuming a high, regular or low PV performance), whereas the battery system can be sized to achieve 40%, 60% or 100% night demand peak shaving with three types of battery (Lead-acid, Li-ion, and repurposed). The predetermined settings also allow for the selection of the greenhouse gas emission source (i.e., tailpipe emissions or combined tailpipe and fuel production process emissions) to compare the environmental impact of each configuration, excluding the embedded CO₂ of the installed equipment (PV, genset and batteries).

Note that this work was focused on improving the performance of diesel generators operating within hybrid microgrids, by assessing the impact of castor oil-diesel blends on their performance and their interaction with different PV share and different battery capacity systems. Therefore, the optimisation target of this work differs from other optimisation models where the target is to minimise the system's life cycle cost (LCC) or its levelized cost of energy (LCOE). However, with the optimised yearly cash flow expenses of each configuration, an economic assessment was carried out to determine the system with the best LCC and LCOE.

The following subsections present the mathematical expressions of the cost optimisation model. The model was developed as a Linear Mixed Integer Problem (LMIP) implemented in Python with the Gurobi optimisation solver [140], the description of the indices, sets, parameters, and variables was included in the Nomenclature section. On the other hand, a detailed explanation of the model is included below and the Model Inputs section (see section 5.1.3) presents the details of the input parameters and the data required for solving the model.

5.1.1 Objective Function

The objective function of the proposed model is to minimise the total cost of investment (equipment purchase and installation), operation, maintenance, and replacement, for a specific standalone hybrid MG. The mathematical representation is:

$$\min C^{cap} + C^{op} + C^r + C^{mnt} \quad \text{Equation 5-1}$$

where C^{cap} is the capital cost, C^{op} the operating cost, C^r the replacement cost, and C^{mnt} the maintenance cost. Each term is explained below:

a) C^{cap} : this term corresponds to the initial investment, given by

$$C^{cap} = \sum_{g \in G} C_g^{gen} + C^{PV} + C^{inver} + C^{batt} \quad \text{Equation 5-2}$$

$$C_g^{gen} = g_g^{upc} \cdot P_g^{genmax} \cdot \max(s_{g,t}) \quad \forall g \quad \text{Equation 5-3}$$

$$C^{PV} = cost^{PV} \cdot inst^{PV} \quad \text{Equation 5-4}$$

$$C^{inver} = cost^{inver} \cdot inst^{PV} \quad \text{Equation 5-5}$$

$$C^{batt} = cost^{batt} \cdot Cap^{batt} \quad \text{Equation 5-6}$$

where C_g^{gen} , C^{PV} , C^{inver} , and C^{batt} are the initial investment costs in £ of the selected diesel generators, PV system, inverter, and battery system respectively. The upfront cost per genset in £/kW is represented by g_g^{upc} , and P_g^{genmax} is the genset's maximum power indicated for continuous operation in kW. The upfront cost considers the cost of the generator and the housing (~12% of the upfront cost) [204]. The binary decision variable $s_{g,t} \in \{0,1\}$ indicates if a diesel generator is selected or not. The costs of the PV and the inverter in £/kW are represented by $cost^{PV}$ and $cost^{inver}$. The battery cost is indicated in £/kWh by $cost^{batt}$. The installed PV in kW is $inst^{PV}$, similarly Cap^{batt} is the installed battery system capacity in kWh calculated using the

power storage capacity sizing equation (Equation 5-7¹) adapted from the Handbook on Battery Energy Storage System [205], given by

$$BESS\ Capacity\ [kWh] = \frac{Power\ required[kW] \cdot duration\ required\ [h]}{depth\ of\ discharge\ [\%] \cdot battery\ efficiency[\%]} \quad \text{Equation 5-7}$$

- b) C^{op} : this term corresponds to the total operational costs derived from the fuel consumption and emissions of the diesel generators for one year of operation ($pdays \sim 365$), given by

$$C^{op} = pdays \left(\sum_{t \in T} \sum_{g \in G} \sum_{bld \in B} C_{bld,g,t}^{fuel} + \sum_{t \in T} \sum_{g \in G} \sum_{bld \in B} C_{bld,g,t}^{CO_2e} + \sum_{t \in T} \sum_{g \in G} \sum_{bld \in B} C_{bld,g,t}^{NO_x} + \sum_{t \in T} \sum_{g \in G} \sum_{bld \in B} C_{bld,g,t}^{PM_{2.5}} \right) \quad \text{Equation 5-8}$$

where, for each operating hour, generator, and blend, $C_{bld,g,t}^{fuel}$, $C_{bld,g,t}^{CO_2e}$ carbon dioxide equivalent (CO₂e) emission cost, and $C_{bld,g,t}^{NO_x}$ and $C_{bld,g,t}^{PM_{2.5}}$ are the emission costs for nitrogen oxides (NO_x) and particulate matter (PM_{2.5}), respectively. Equation 5-9 to Equation 5-16 show the extended terms in the operational cost.

$$C_{bld,g,t}^{fuel} = bp_{bld} \cdot Fu_{bld,g,t} \quad \forall bld, g, t \quad \text{Equation 5-9}$$

$$bp_{bld} = diesel\ price \cdot \left(\frac{bld}{100} \right) + castor\ oil\ price \cdot \left(1 - \frac{bld}{100} \right) \quad \text{Equation 5-10}$$

$$bld \in \{100, 80, 60, 50\}$$

$$Fu_{bld,g,t} = \left(\frac{a_{bld} \cdot P_{g,t}^{gen} + b_{bld}}{\rho_{bld}} \right) \cdot k_{g,t,bld} \quad \forall bld, g, t \quad \text{Equation 5-11}$$

where bp_{bld} is the purchase price of blends in £/litre calculated using Equation 5-10. Note that bld was defined to take the values from 100 to 50 as it denotes the amount of diesel in the blend, which in turn is correlated to the blend name (e.g., $bld = 100$ denotes 100% diesel fuel which corresponds to COD0, where COD0 represents 0% castor oil in the blend or 100% diesel). Defining bld in that specific order, allows the model to select the correct blend according to the developed algorithm. $Fu_{bld,g,t}$ is the total fuel consumed per genset in l/h obtained using Equation 5-11 where a_{bld} and b_{bld} are the coefficients found for

¹ The equation is used for sizing the power storage capacity when renewable integration, peak shaving or MGs applications are considered.

each fuel blend and ρ_{bld} is the density of each blend in kg/l. The decision variables $P_{g,t}^{gen}$ and $k_{g,t,bld} \in \{0,1\}$ determine the genset output power and the fuel selection in every operating period, respectively. In Equation 5-11 the coefficients a_{bld} and b_{bld} correspond to the slope and the Y-intercept of the linear regression that appears in Figure 5-2, respectively. These coefficients were found after comparing the specifications from 83 diesel generators available from 5 different suppliers/manufacturers within a 6 kVA to 100 kVA range. Some manufacturers present the fuel consumption in g/kWh but the volumetric representation in l/h is commonly used. The reported values vary from full prime rating to 25% genset's prime rating. Most manufacturers only report the fuel flow at prime and 75% or 70% prime rating. Therefore, only the models having more than one fuel consumption specification in l/h were selected. The selection includes engines of different sizes from Perkins, Deutz, Iveco, and Yanmar. The data obtained was converted into its mass-based form (kg/h) using the typical density value for diesel at 15°C [180]. The diesel density at 15°C was chosen as manufacturers report the fuel consumption complying with the fuel specification standard BS2869 [206]. The density from each castor oil-diesel blend (COD) was used to adapt the original data to the corresponding fuel blend. Then a linear regression was done to find the fuel consumption equations for each fuel type. Figure 5-2 shows the mass-based fuel consumption data obtained with the density values from Table 5-1.

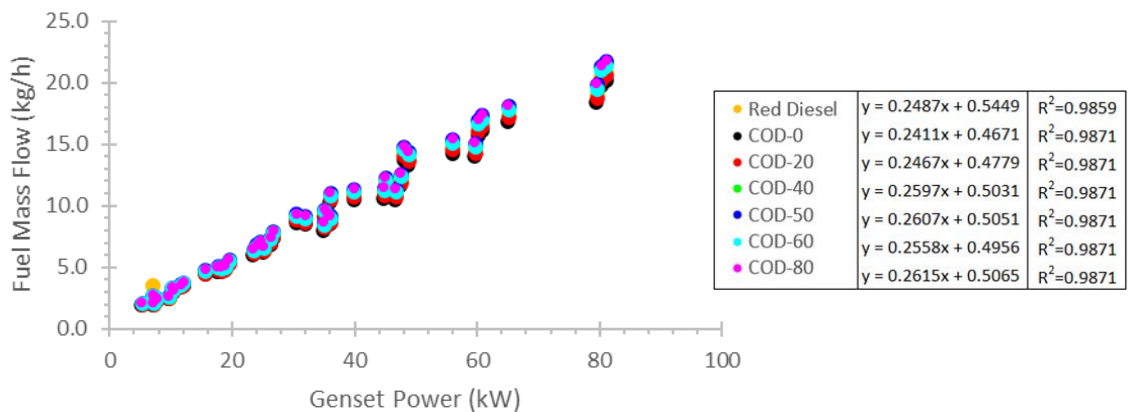


Figure 5-2 Mass-based fuel consumption for selected diesel generators.

Table 5-1 Diesel and Castor oil-diesel blends density values at different temperatures.

Fuel	Density [kg/l]	Fuel Temperature [°C]
Red Diesel ²	0.86	15
COD0	0.830	30
COD20	0.849	30
COD40	0.894	30
COD50	0.897	30
COD60	0.880	60
COD80	0.900	70

$$C_{bld,g,t}^{CO_2e} = tax^{carbon} \cdot bEF_{bld} \cdot Fu_{bld,g,t} \quad \forall bld, g, t \quad \text{Equation 5-12}$$

$$bEF_{bld} = EF^{diesel} \cdot \left(\frac{bld}{100}\right) + EF^{biofuel} \cdot \left(1 - \frac{bld}{100}\right) \quad \text{Equation 5-13}$$

$bld \in \{100,80,60,50\}$

where tax^{carbon} is the cost in £/kgCO₂e for CO₂e emissions and bEF_{bld} is the fuel blend emission factor in kgCO₂e/litre for specific fuel blends as calculated in Equation 5-13. EF^{diesel} and $EF^{biofuel}$ are the diesel and biofuel corresponding emission factors, also in kgCO₂e/litre.

$$C_{bld,g,t}^{NOx} = ecost^{NOx} \cdot e_{bld,g,t}^{NOx} \quad \forall bld, g, t \quad \text{Equation 5-14}$$

$$e_{bld,g,t}^{NOx} = size_g^{eng} \cdot glfa_g \cdot BEF_g^{NOx} \cdot EFA_{bld}^{NOx} \cdot k_{g,t,bld} \quad \forall bld, g, t \quad \text{Equation 5-15}$$

where $ecost^{NOx}$ is the NOx emissions cost in £/gNO_x. $e_{bld,g,t}^{NOx}$ represents the NOx emissions per hour per genset, $size_g^{eng}$ is the genset's engine prime power in kW, while $glfa_g$ and BEF_g^{NOx} are the load factor adjustment and the NOx baseline emission factor in g/kWh, respectively, according to the methodology for estimating pollutant emissions for non-road machinery [207].

² From manufacturer's specifications. The density of the red diesel (0.86 kg/l) is higher than the density value reported for COD0 (0.83 kg/l) due to the different fuel temperatures at which their densities were tested.

The NOx emission factor adjustment EFA_{bld}^{NOx} is the coefficient found from experimental work³ for each biofuel blend.

$$C_{bld,g,t}^{PM_{2.5}} = ecost^{PM_{2.5}} \cdot e_{bld,g,t}^{PM_{2.5}} \quad \forall bld, g, t \quad \text{Equation 5-16}$$

$$e_{bld,g,t}^{PM_{2.5}} = size_g^{eng} \cdot glfa_g \cdot BEF_g^{PM_{2.5}} \cdot EFA_{bld}^{PM_{2.5}} \cdot k_{g,t,bld} \quad \forall bld, g, t \quad \text{Equation 5-17}$$

where $ecost^{PM_{2.5}}$ is the PM_{2.5} emissions cost in £/gPM_{2.5}. $e_{bld,g,t}^{PM_{2.5}}$ represents the PM_{2.5} emissions per hour per genset, $BEF_g^{PM_{2.5}}$ is the PM_{2.5} baseline emission taken from [207], and $EFA_{bld}^{PM_{2.5}}$ is the emission factor adjustment coefficient calculated from experimental work³ for each biofuel blend.

c) C^r : this term refers to the cost of replacing the diesel generators and is given by

$$C^r = \sum_{g \in G} (0.88C_g^{gen}/2) \cdot \sum_{m \in M} replace_{g,m}^{engine} + \sum_{g \in G} (0.88C_g^{gen}/2) \cdot \sum_{m \in M} replace_{g,m}^{alternator} \quad \text{Equation 5-18}$$

$$replace_{g,m}^{engine} = \begin{cases} 1 & \text{if } Hgcm_{g,m} \geq glf_g \quad \forall g, m \\ 0 & \text{otherwise} \end{cases} \quad \text{Equation 5-19}$$

$$replace_{g,m}^{alternator} = \begin{cases} 1 & \text{if } Hgcm_{g,m} \geq 20000 \quad \forall g, m \\ 0 & \text{otherwise} \end{cases} \quad \text{Equation 5-20}$$

where $replace_{g,m}^{engine}$ and $replace_{g,m}^{alternator}$ indicate the decision of replacing the engine or the alternator of genset g in month m , respectively, and glf_g represents the lifetime of each engine. Note that the 0.88 constant multiplying the initial investment cost of the generators (C_g^{gen}) was required to only account for the cost of the generator without the housing cost, which is about 12% of the upfront cost as mentioned above, when the upfront cost was defined (see Equation 5-3).

d) C^{mnt} : this term represents the maintenance required for the gensets, which is divided into two terms, the first one refers to the cost of the fuel

³ See section 5.1.4.1 An Extended Explanation of Emission Factor Adjustment Coefficient Calculation.

used during the service time and the second refers to the labour service cost.

$$C^{mnt} = bp_{bld=100} \left(\sum_{g \in G} mntdays_g \left(\frac{(a_{bld=100} P_g^{genmax} + b_{bld=100}) \cdot \max(s_{g,t})}{\rho_{bld=100}} \right) \cdot K_{p=1,bld} \right) + servc \left(\sum_{g \in G} P_g^{genmax} \cdot \max(s_{g,t}) \cdot K_{p=1,bld} \right) \quad \text{Equation 5-21}$$

$$mntdays_g = \begin{cases} 12 \cdot (t/4) & \text{if } k_{p=1,bld=100} \\ 365 \cdot (t/4) & \text{otherwise} \end{cases} \quad \forall g \quad \text{Equation 5-22}$$

where $bp_{bld=100}$ is the diesel price in £/l, $mntdays_g$ represents the estimated maintenance days, depending on the type of fuel used during the operating periods. P_g^{genmax} is the prime power of the selected gensets in kW, as indicated by $s_{g,t}$, and $K_{p=1,bld}$ represents the blend selected during the analysis period. The annual service cost is represented by $servc$ in £/kW, based on the operation and maintenance cost from the MG REopt LCOE Results Explorer [208].

5.1.2 Model Constraints

The constraints below were needed to account for the operational limitations of the energy sources (i.e., diesel generators, PV, and BESS).

The system power balance to meet the load demand at each hour of the day d_t , considering the PV system output power P_t^{RE} and the power supplied ($P_t^{battdischar}$) or consumed ($P_t^{battchar}$) by the batteries, both in kW is given by

$$\sum_{g \in G} P_{g,t}^{gen} + P_t^{RE} + P_t^{battdischar} - P_t^{battchar} = d_t \quad \forall t \quad \text{Equation 5-23}$$

A load demand security margin D_t is considered, where the maximum power from the selected gensets P_g^{genmax} and the maximum battery discharging power $P_t^{battmaxdischar}$ can be used according to Equation 5-24.

$$\sum_{g \in G} (P_g^{genmax} \cdot w_{g,t}) + P_t^{RE} + P_t^{battmaxdischar} \geq D_t \quad \forall g, t \quad \text{Equation 5-24}$$

The constraints related to the selection of the diesel generators are given by

$$\sum_{g \in G} s_{g,t} \leq U \quad \text{Equation 5-25}$$

$$P_{g,t}^{gen} \geq P_g^{genmin} \cdot w_{g,t} - genslack_{g,t} \quad \forall g, t \quad \text{Equation 5-26}$$

$$P_{g,t}^{gen} \leq P_g^{genmax} \cdot w_{g,t} \quad \forall g, t \quad \text{Equation 5-27}$$

$$s_{g,t} \geq w_{g,t} - w_{g,t-1} \quad \forall t > 0, g \quad \text{Equation 5-28}$$

$$s_{g,t} - w_{g,t} \geq 0 \quad \forall g, t \quad \text{Equation 5-29}$$

where the binary decision variable $s_{g,t} \in \{0,1\}$ determines which genset is selected without exceeding the maximum number represented by U . P_g^{genmin} refers to the lowest acceptable genset output power in kW and the slack variable $genslack_{g,t}$ may allow operating a genset below the predetermined load factor limit. This limit was investigated because sometimes in optimisation the limit is set to 30% of the genset's prime power [82]. However, according to [209] the optimum genset operating range goes from 70-89% of its rated power and [210] mentions that the highest efficiency of the diesel engine occurs above 60% load. The model considers the operating limits determined by the specific fuel consumption (SFC) and the brake thermal efficiency (BTE) results from experimental work using a 6kVA diesel generator. The optimal operating limits are represented by the region where the lowest SFC values and the highest BTE occur, above 60% of the genset's prime power, as shown in Figure 5-3.

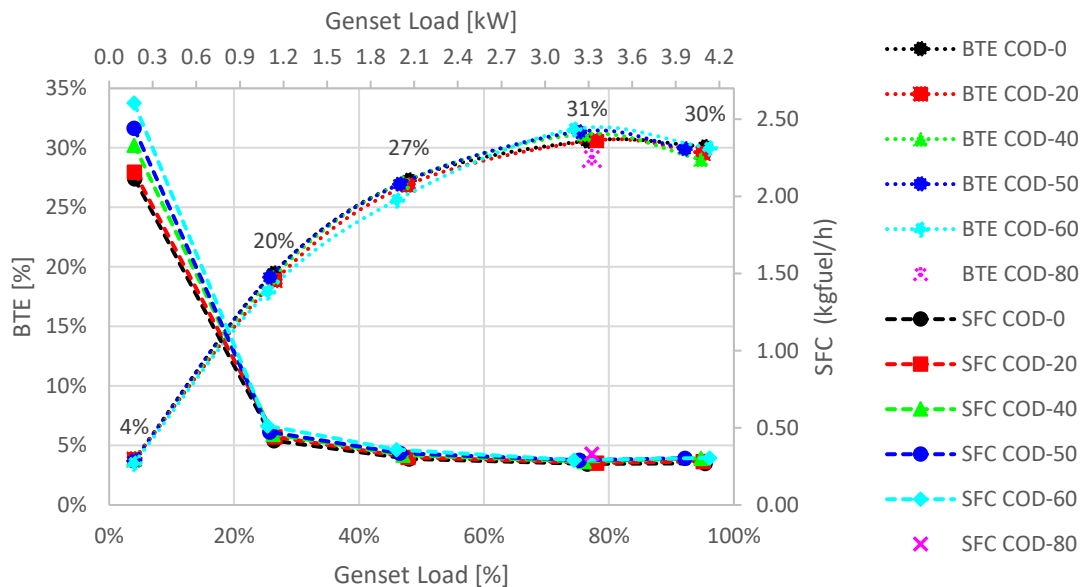


Figure 5-3 BTE and SFC curves from a diesel generator running with castor oil-diesel (COD) blends.

The constraints related to the selection of the fuel blend are given by

$$\sum_{bld \in B} k_{g,t,bld} \leq 1 \quad \forall g, t \quad \text{Equation 5-30}$$

$$w_{g,t} = \max(k_{g,t,bld}) \quad \forall g, t \quad \text{Equation 5-31}$$

where Equation 5-30 and Equation 5-31 ensure that the gensets only operate with one type of fuel blend.

The constraints related to the battery are given by

$$E_t^{batt} = E_{t-1}^{batt} + \left(\eta^{batt} \cdot P_t^{battchar} - \frac{P_t^{battdischar}}{\eta^{batt}} \right) \quad \forall t \quad \text{Equation 5-32}$$

$$E_t^{batt} \leq SoC^{max} \cdot Cap^{batt} \quad \forall t \quad \text{Equation 5-33}$$

$$E_t^{batt} \geq SoC^{min} \cdot Cap^{batt} \quad \forall t \quad \text{Equation 5-34}$$

$$E_0^{batt} = SoC^{max} \cdot 0.8Cap^{batt} \quad \text{Equation 5-35}$$

$$E_{23}^{batt} = E_0^{batt} \quad \text{Equation 5-36}$$

$$P_t^{battchar} \geq 0 \cdot char_t \quad \forall t \quad \text{Equation 5-37}$$

$$P_t^{battchar} \leq P^{battmax} \cdot char_t \quad \forall t \quad \text{Equation 5-38}$$

$$P_t^{battdischar} \geq 0 \cdot dischar_t \quad \forall t \quad \text{Equation 5-39}$$

$$P_t^{battdischar} \leq P^{battmax} \cdot dischar_t \quad \forall t \quad \text{Equation 5-40}$$

$$P^{battmax} = Cap^{batt} / 5 \quad \text{Equation 5-41}$$

$$char_t + dischar_t \leq 1 \quad \forall t \quad \text{Equation 5-42}$$

where E_t^{batt} is the energy available from the batteries at a specific operating period. The battery efficiency is represented by η^{batt} , SoC^{max} and SoC^{min} are the battery's maximum and minimum state of charge. The charging and discharging battery periods are determined by the binary decision variables $char_t \in \{0,1\}$, and $dischar_t \in \{0,1\}$.

Finally, the constraints on the replacement of the diesel generators are given by

$$Hgcm_{g,m} \geq Hgm_g \cdot (1 - replace_{g,m}^{engine}) \quad \forall g, m \quad \text{Equation 5-43}$$

$$Hgcm_{g,m} \leq glf_g \cdot (1 - replace_{g,m}^{engine}) \quad \forall g, m \quad \text{Equation 5-44}$$

$$Hgcm_{g,m} \geq Hgm_g \cdot (1 - replace_{g,m}^{alternator}) \quad \forall g, m \quad \text{Equation 5-45}$$

$$Hgcm_{g,m} \leq 20000 \cdot (1 - replace_{g,m}^{alternator}) \quad \forall g, m \quad \text{Equation 5-46}$$

$$Hgd_g = \sum_{t \in T} w_{g,t} \quad \forall g \quad \text{Equation 5-47}$$

$$Hgm_g = 30 \cdot Hgd_g \quad \forall g \quad \text{Equation 5-48}$$

$$Hgcm_{g,m} = m \cdot Hgm_g \quad \forall g, m \quad \text{Equation 5-49}$$

$$Hga_g = Hgcm_{g,m=12} \quad \forall g \quad \text{Equation 5-50}$$

where $Hgcm_{g,m}$, Hgm_g , Hgd_g , and Hga_g are the monthly cumulative, monthly, daily, and annual operating hours of the gensets, respectively. The binary decision variable $w_{g,t}$ indicates if a genset is operating or not during the daily or monthly operating periods.

5.1.3 Model Inputs

The model parameters for finding the optimisation results are shown in Table 5-2, note that the fuel and emission costs depend on the operating periods of the diesel generators and are used to find the incurred cost per year. The calculated cost per year should be repeated every year within the lifetime assessment of the system. In contrast, the costs of the physical equipment (genset, PV, inverters, and batteries) depend on the required installed capacity of each component and occur during the initial investment (year zero). These costs should be repeated at specific years, over the lifetime assessment, according to the corresponding lifespan or maintenance period of each component (see section 5.1.4). It is worth mentioning that for calculating the emission costs, the South African Carbon Tax was used as no tax or carbon price is yet available in Tanzania. Also, the pollutant costs for the PM_{2.5} and NO_x emissions were taken from the estimated external costs reported by IRENA related to the use of fossil fuels for electricity generation and other activities in European countries as no data was found for African countries. Seven diesel generators (G1-G7) of different sizes (6.88, 9.76, 14.96, 22.56, 33.76, 44.0, and 143.12 kW) were included for the genset selection, where the smallest power corresponds to G1. Finally, it should be mentioned that the price for the repurposed battery (66.95 £/kWh) was assumed to be 50% of the original Li-ion price according to the second life of batteries scenario presented in the Li-ion batteries for mobility and stationary storage applications report [211].

Table 5-2 Input parameters for the optimisation model.

Model Input		Source
Diesel price (£/litre) *	0.88	Tanzania Diesel prices [212].
Castor oil price (£/litre) *	0.44	Tanzania Castor Oil Prices [213].
Carbon tax (£/kgCO ₂ e) *	0.0075	Carbon Pricing Dashboard [214].
Diesel: average biofuel blend emission factor (kg CO ₂ e/litre)	2.51233	UK Government Conversion Factors for greenhouse gas reporting [215].
Biofuel emission factor (kg CO ₂ e/litre)	0.02529	Experimental data from Castor oil-diesel blends engine tests. ⁴
PM _{2.5} emission cost (£/g) *	0.0527	The true cost of fossil fuels: Externality cost assessment methodology [216].
NOx emission cost (£/g) *	0.0089	
Genset upfront cost (£/kW) *	614.72 (genset size < 100kW) 388.00 (genset size > 100kW)	Detailed Cost Models and Benchmarks [204].
Genset maintenance cost (£/kW) *	19.02	Microgrid Load and LCOE Modelling Results [208].
PV cost (£/kWp) *	1,673.74	Tariff Considerations for Micro-Grids in Sub-Saharan Africa [217].
Inverter cost (£/kW) *	912.95	
Lead-acid battery cost (£/kWh) *	60.86	State of the global Mini-Grid Market Report 2020 [5].
Li-ion battery cost (£/kWh) *	133.90	
Repurposed battery cost (£/kWh)	66.95	Calculated from Li-ion price.
Curve slope values (a_{bld}) used in Equation 5-11	$a_0=0.2411$	Linear regression (see Figure 5-2).
	$a_1=0.2467$	
	$a_2=0.2597$	
	$a_3=0.2607$	
"Y" intercept values (b_{bld}) used in Equation 5-11	$b_0=0.4671$	
	$b_1=0.4779$	
	$b_2=0.5031$	

⁴ See section 5.2.5 Greenhouse Gas Emission Source

	$b_3=0.5051$	
Maximum number of gensets (U) used in Equation 5-25	4	
Battery maximum state of charge (SoC^{max})	Lead-acid=1 Li-ion=1 repurposed= 0.8	Comparative Study of Techno-economics of Li-ion and Lead-acid batteries in micro-grids in SSA [218] and Circular Economy Perspectives for the Management of Batteries used in Electric Vehicles [219]
Battery minimum state of charge (SoC^{min})	Lead-acid=0.4 Li-ion=0.2 repurposed=0.2	
Load demand security margin (D_t)	This variable considers the possibility of having a 10% higher load demand (i.e., $1.1 \cdot d_t$).	
Lowest genset output power ($P_g^{gen_min}$)	For every genset $P_g^{gen_min}$ was calculated as 60% of their corresponding prime power.	
Slack variable ($genslack_{g,t}$)	The slack variable was included to prevent a system blackout caused by overgeneration during periods when no batteries can supply the demand. Including the slack variable may allow the gensets to operate below the recommended limit of 60% prime power, for matching the very low demand to the power generated by the gensets. Operating the generators below the recommended limit adds a penalty cost of $10000 \cdot genslack_{g,t}$ where the $genslack_{g,t}$ variable accounts for the low load operating periods of the gensets. The penalty cost and slack variable utilisation is a common practice in linear programming optimisation problems [220].	

* Prices converted to £ from their original values in USD, considering the average exchange rate history of 1 USD=0.76079 GBP (Dec-May 2022) [221]. The diesel price corresponds to the average value reported from 14 Feb 2022 to 23 May 2022. The castor oil price corresponds to the value reported in May 2022. The carbon tax (US\$9.84/tCO₂e) corresponds to the last updated available data from April 2022.

5.1.3.1 An Extended Explanation of Emission Factor Adjustment Coefficient Calculation

In Chapter 3 the specific emissions (SE) of CO, HC, and NO_x, measured with the MEXA analyser, were reported for each engine test condition for the different biofuel blends (COD0 to COD60). The PM_{2.5} SE were also reported for the same conditions and biofuel blends. However, from these pollutants, only NO_x and PM_{2.5} were included in the optimisation model, as those pollutants are considered by IRENA to have an external cost [216]. To account for the cost of such pollutants, equations Equation 5-15 and Equation 5-17 were used in agreement with the pollutant emission methodology for non-road machinery [207]. For adopting this methodology to the biofuel blends used in this work, it was necessary to find the Emission Factor Adjustment (EFA) coefficient for each blend of both pollutants. The EFA was calculated with Equation 5-51 and Equation 5-52, using the test points and weighting factors established in the Test Cycles of ISO 8178 [222], the international standard for exhaust emission measurement.

$$EFA_{bld}^{NOx} = \frac{TWSE_{bld}^{NOx}}{TWSE_{bld=100}^{NOx}} \quad \text{Equation 5-51}$$

$$EFA_{bld}^{PM_{2.5}} = \frac{TWSE_{bld}^{PM_{2.5}}}{TWSE_{bld=100}^{PM_{2.5}}} \quad \text{Equation 5-52}$$

where $TWSE_{bld}^{NOx}$ and $TWSE_{bld}^{PM_{2.5}}$ are the total weighted SE in g/kWh of each castor oil-diesel blend from their NO_x and PM_{2.5} emissions, whereas $TWSE_{bld=100}^{NOx}$ and $TWSE_{bld=100}^{PM_{2.5}}$ are the total weighted SE of diesel (COD0=100% diesel, 0% castor oil) from the NO_x and PM_{2.5} emissions.

The test points and weighting factors required for a constant speed (type D2) engine are summarised in Table 5-3. The Type D2 engine refers to generating sets with intermittent load [207].

Table 5-3 Test Points and weighting factors from ISO 8178 Test Cycles for type D2 engines.

ISO 8178-Type D2 Emission Test Cycles					
Torque Test Point	100%	75%	50%	25%	10%
Test Point Weighting Factors	0.05	0.25	0.3	0.3	0.1

For each engine test carried out during the engine lab work, the engine torque in Nm was calculated from the engine power in kW (P^{eng}) and the engine speed in rpm (N) using Equation 5-53.

$$T = \frac{P^{eng} \cdot 30 \cdot 1000}{\pi \cdot N} \quad \text{Equation 5-53}$$

Then the load factor by torque was calculated as a percentage of the maximum achievable torque (18.14 Nm), considering the engine's continuous rated output power (5.7 kW). Table 5-4 summarises the results for each blend at five engine test conditions.

Table 5-4 Torque and load factor by torque for COD blends at five engine conditions from lab work engine tests.

Engine Test	COD0		COD20		COD40		COD50		COD60	
	Torque [Nm]	Load Factor by Torque								
	1	16.72	92%	16.70	92%	16.75	92%	16.45	91%	17.13
2	13.73	76%	13.93	77%	13.72	76%	13.65	75%	13.57	75%
3	9.04	50%	9.01	50%	8.92	49%	8.87	49%	8.81	49%
4	5.13	28%	5.15	28%	5.11	28%	5.04	28%	5.00	28%
5	0.80	4%	0.79	4%	0.79	4%	0.79	4%	0.79	4%

As the engine torque during the engine tests was not a perfect match of the test points of the ISO 8178, it was needed to estimate the corresponding specific emissions that would be generated if the engine was running at the exact torque test points (i.e., 100%, 75%, 50%, 25%, and 10% torque). To do that, the SE found from the engine tests were plotted against their real test torque to generate the pollutant vs. torque curves with their corresponding equations from the polynomial regression as shown in Figure 5-4 and Figure 5-5.

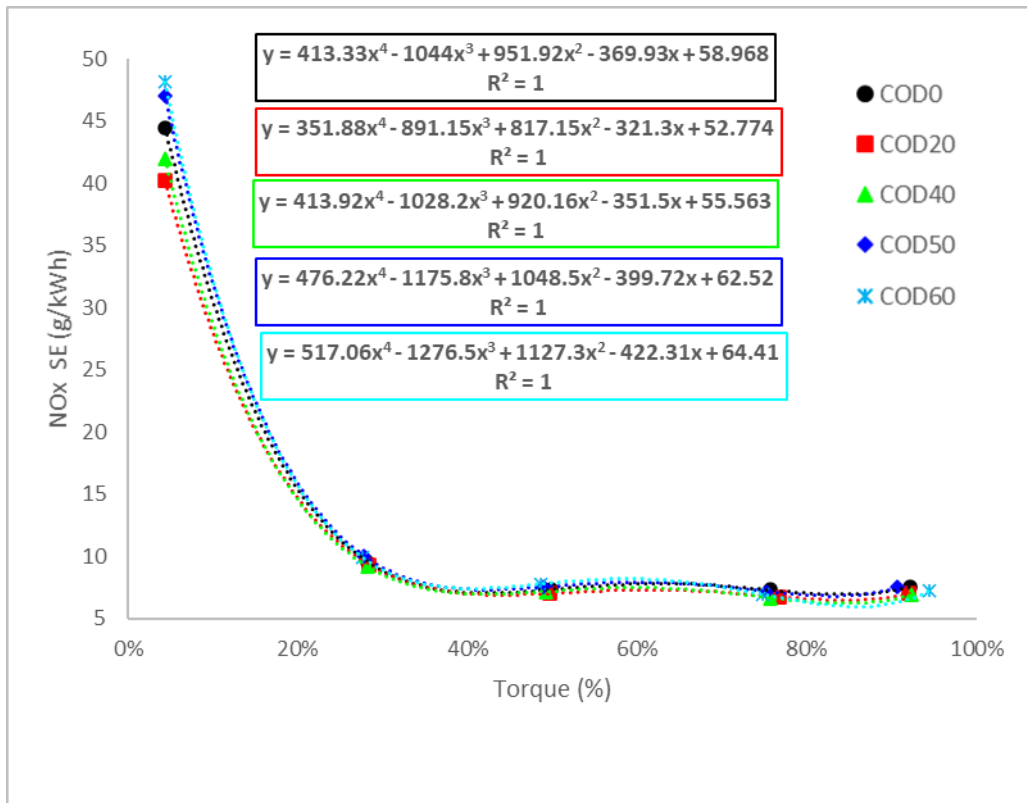


Figure 5-4 NOx specific emissions against engine torque for 5 COD blends.

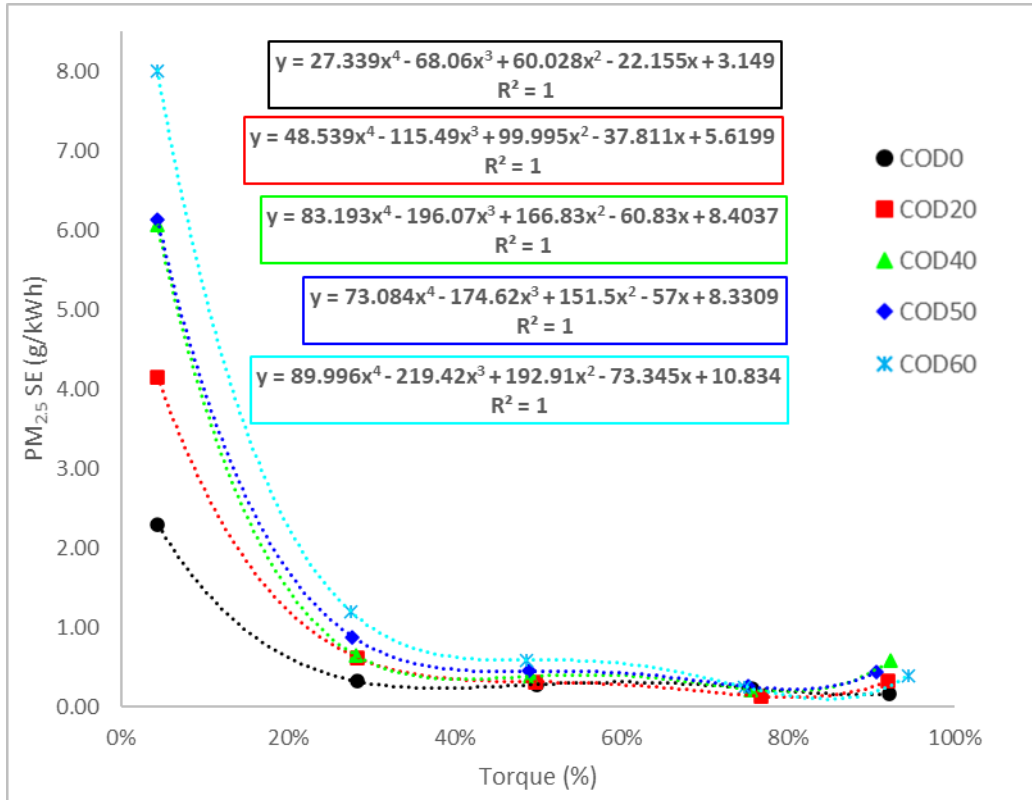


Figure 5-5 PM_{2.5} specific emissions against engine torque for 5 COD blends.

The equations found with the polynomial regression were then used to estimate the SE at the ISO8178 test torques. The new-found SE values were then multiplied by the corresponding ISO8178 weighting factor to obtain the weighted specific emissions (WSE), the total weighted specific emissions (TWSE) and the emission factor adjustment (EFA) coefficients, using Equation 5-51 and Equation 5-52. The findings are summarised in Table 5-5.

Table 5-5 NO_x and PM_{2.5} total weighted specific emissions and emission factor adjustment coefficients for 5 COD blends.

ISO 8178 Test Point Torque	COD0		COD20		COD40		COD50		COD60	
	NO _x	PM _{2.5}								
	WSE [g/kWh]	WSE [g/kWh]								
100%	0.51	0.02	0.47	0.04	0.50	0.08	0.59	0.06	0.50	0.02
75%	1.83	0.06	1.71	0.04	1.68	0.06	1.79	0.06	1.72	0.00
50%	2.20	0.08	2.10	0.09	2.16	0.12	2.27	0.13	2.35	0.14
25%	3.39	0.12	3.29	0.24	3.22	0.27	3.48	0.33	3.41	0.43
10%	3.05	0.15	2.80	0.27	2.86	0.38	3.19	0.40	3.22	0.52
Total Weighted SE [g/kWh]	10.98	0.43	10.37	0.69	10.42	0.90	11.32	0.99	11.20	1.11
Emission Factor Adjustment	1.00	1.00	0.94	1.61	0.95	2.10	1.03	2.33	1.02	2.61

5.1.4 Economic Assessment

This section includes the equations for the economic assessment of the optimisation results, based on the Life Cycle Cost (LCC) and Levelized Cost of Energy (LCOE), using the discounting method. The discounting method was selected, as according to Lai and McCulloch [223] is an appropriate methodology for calculating LCOE when renewable sources are included.

The LCC, also known as Net Present Cost (NPC) for the system within the analysis period P is given by

$$LCC^{system} = LCC^{gen} + LCC^{PV} + LCC^{batt}$$

Equation 5-54

where LCC^{gen} , LCC^{PV} , LCC^{batt} , are the costs associated with the diesel generators, the PV system, and the battery respectively. The three terms of the LCC^{system} are defined as follows:

- a) LCC^{gen} : this term includes the costs of the energy generated by the gensets given by

$$LCC^{gen} = LCC^{gen_{load}} + LCC^{gen_{batt}} \quad \text{Equation 5-55}$$

$$LCC^{gen_{load}} = \sum_{p \in P} \left(YCF_p^{gen} \cdot df_p \cdot \frac{E_p^{gen_{load}}}{E_p^{gen}} \right) \quad \text{Equation 5-56}$$

$$LCC^{gen_{batt}} = \sum_{p \in P} \left(YCF_p^{gen} \cdot df_p \cdot \left(1 - \frac{E_p^{gen_{load}}}{E_p^{gen}} \right) \right) \quad \text{Equation 5-57}$$

$$df = \frac{1}{(1+r)^p} \quad \text{Equation 5-58}$$

$$YCF_p^{gen} = \sum_{g \in G} \sum_{bld \in B} \left(C_{g,p=0}^{gen} + C_{bld,g,p}^{fuel} + C_{bld,g,p}^{CO_2e} + C_{bld,g,p}^{NO_x} + C_{bld,g,p}^{PM_{2.5}} + C_{g,p=estglf,estalt}^r + C_{g,p}^{mnt} \right) \quad \text{Equation 5-59}$$

$$estglf = \left(\frac{glf_g}{Hga_g} \right) \cdot i \quad \text{if } \frac{P}{\left(\frac{glf_g}{Hga_g} \right)} \leq i \leq 1 \quad \text{Equation 5-60}$$

$$estalt = \left(\frac{20000}{Hga_g} \right) \cdot i \quad \text{if } \frac{P}{\left(\frac{20000}{Hga_g} \right)} \leq i \leq 1 \quad \text{Equation 5-61}$$

where $LCC^{gen_{load}}$ and $LCC^{gen_{batt}}$ are the associated costs of the energy generated by the gensets to supply the load and/or charge the battery. YCF_p^{gen} represents the genset's yearly cash flow, df is the discount factor that considers the real discount rate r (10%). $E_p^{gen_{load}}$ is the electricity delivered by the gensets to the load and E_p^{gen} is the total electricity delivered by the gensets, both in kWh/year. The initial and replacement cost of the gensets are represented by $C_{g,p=0}^{gen}$ and $C_{g,p=estglf}^r$. The estimated genset replacement period ($estglf$) and the estimated alternator replacement period ($estalt$) depend on the lifetime of each engine ($glf_g \in \{3000, 7500\}$) or alternator (20000 hours), and their operating hours during the first year of the project (Hga_g) as represented in Equation 5-60 and Equation 5-61. $C_{bld,g,p}^{fuel}$ is the fuel consumption cost, the pollutant emission costs for CO_{2e}, NO_x and PM_{2.5} are represented by $C_{bld,g,p}^{CO_2e}$, $C_{bld,g,p}^{NO_x}$, and $C_{bld,g,p}^{PM_{2.5}}$. C^{mnt} is the maintenance cost from Equation 5-21.

- b) LCC^{PV} : this term includes the costs of the energy generated by the PV system given by

$$LCC^{PV} = LCC^{PVload} + LCC^{PVbatt} \quad \text{Equation 5-62}$$

$$LCC^{PVload} = \sum_{p \in P} \left(YCF_p^{PV} \cdot df_p \cdot \frac{E_p^{PVload}}{E_p^{PV}} \right) \quad \text{Equation 5-63}$$

$$LCC^{PVbatt} = \sum_{p \in P} \left(YCF_p^{PV} \cdot df_p \cdot \left(1 - \frac{E_p^{PVload}}{E_p^{PV}} \right) \right) \quad \text{Equation 5-64}$$

$$YCF_p^{PV} = C_{p=0}^{PV} + C_{p=0}^{inver} + C_{p=20}^{PVrpl} + C_{p=10,20}^{inverpl} \quad \text{Equation 5-65}$$

where LCC^{PVload} and LCC^{PVbatt} are the associated costs of the energy generated by the PV to supply the load or charge the battery. YCF_p^{PV} represents the PV's yearly cash flow, E_p^{PVload} is the electricity delivered by the PV to the load and E_p^{PV} is the total electricity delivered by the PV, both in kWh/year. $C_{p=0}^{PV}$ and $C_{p=0}^{inver}$ are the initial costs of the PV and the corresponding inverters. $C_{p=20}^{PVrpl}$ and $C_{p=10,20}^{inverpl}$ represent the replacement costs of the PV and the inverters, where $p = 10, 20$ indicates that the inverters should be replaced in year 10 and year 20, whereas the PV should be replaced in year 20, according to their respective lifespan.

- c) LCC^{batt} : this term includes the costs of the energy supplied by the batteries given by

$$LCC^{batt} = \sum_{p \in P} YCF_p^{batt} \cdot df_p \quad \text{Equation 5-66}$$

$$YCF_p^{batt} = C_{p=0}^{batt} + C_{p=battlf}^{battrpl} \quad \text{Equation 5-67}$$

where YCF_p^{batt} is the battery system's yearly cash flow, $C_{p=0}^{batt}$ is the battery's initial cost and $C_{p=battlf}^{battrpl}$ is its replacement cost, which depends on the lifetime of a specific battery type, which gives different battery replacement periods ($battlf$), in years. For a Lead-acid battery, $battlf \in \{6, 12, 18, 23\}$, for a Li-ion battery, $battlf \in \{10, 20\}$, and for a repurposed battery, $battlf \in \{5, 10, 15, 20\}$.

Finally, the LCOE of the system is given by

$$LCOE^{system} = \frac{LCC^{system}}{\sum_{p \in P} (E_p^{system} \cdot df_p)} \quad \text{Equation 5-68}$$

$$E_p^{system} = E_p^{load} + E_p^{batt} \quad \text{Equation 5-69}$$

$$E_p^{load} = E_p^{genload} (1 - dr^{gen})^p + E_p^{PVload} (1 - dr^{PV})^p \quad \text{Equation 5-70}$$

$$E_p^{batt} = \eta \cdot (E_p^{genbatt} (1 - dr^{gen})^p + E_p^{PVbatt} (1 - dr^{PV})^p) \quad \text{Equation 5-71}$$

$$E_p^{gen_{batt}} = E_p^{gen} - E_p^{gen_{load}}$$

Equation 5-72

$$E_p^{PV_{batt}} = E_p^{PV} - E_p^{PV_{load}}$$

Equation 5-73

where E_p^{system} is the total electricity delivered by the system, E_p^{load} is the electricity delivered by the genset and the PV to the load, and E_p^{batt} is the electricity delivered by the battery to the load, all of them in kWh/year. η is the roundtrip efficiency of the battery and dr is the degradation rate [223] considered for each element in the system. Figure 5-6 exemplifies the importance of computing E_p^{system} according to Equation 5-69, to prevent double counting the electricity delivered from the battery to the load as the battery is not a generating source itself.

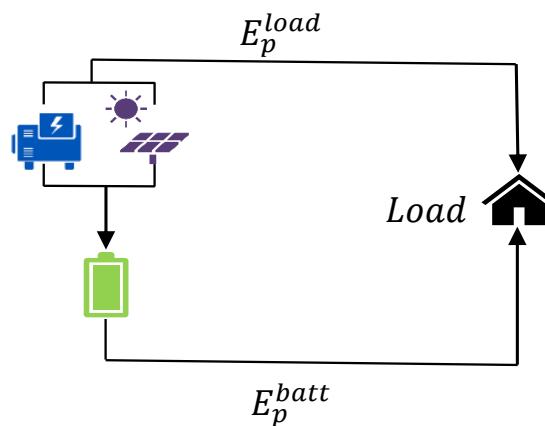


Figure 5-6 Electricity flow diagram for a genset/PV/battery hybrid system.

5.2 Scenarios for Cost Optimisation

To test the applicability of the model, several scenarios were created to present how a different electricity demand profile and the different installed capacity of PV systems, with and without a BESS affect the genset selection for installing a microgrid in a rural ward (Mpigamiti), located within the Lindi Region of Tanzania. This region is of particular interest as it belongs to one of the top five countries without electricity access in sub-Saharan Africa. Figure 5-7 shows the Lindi Region and the mini-grid locations within Tanzania. The assumptions and considerations for creating the scenarios are explained in the following subsections.

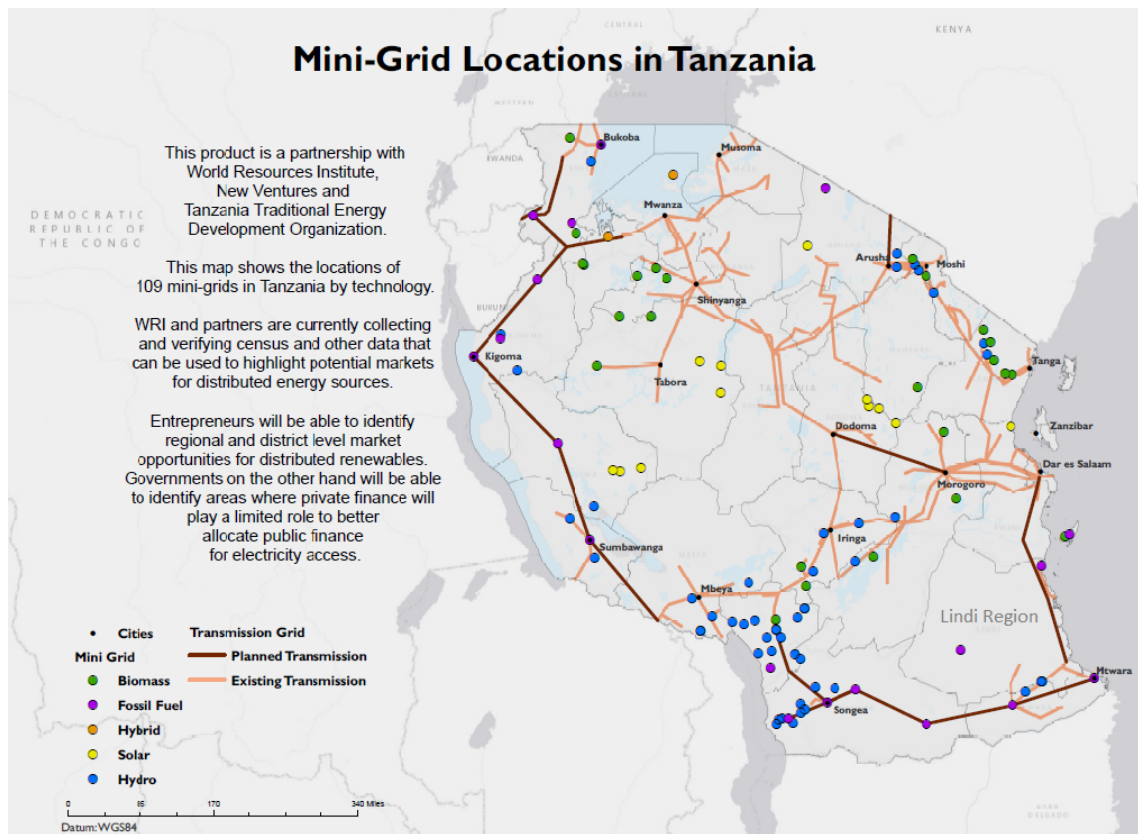


Figure 5-7 PDF version of the energy access interactive map showing the Lindi Region and the mini-grid locations in Tanzania [224].

5.2.1 Electricity Demand Profiles

Three electricity demand scenarios (HED: high electricity demand, MED: medium electricity demand, and LED: low electricity demand) were defined for testing the optimisation model. Each scenario was created using the Rural African Load Profile Tool developed by the National Renewable Energy Laboratory (NREL) [208]. The load profile tool provides hourly electrical load profiles for different household configurations and commercial facilities (schools, clinics, etc.) as specified by the user inputs. This work considered 350 households with an average household size of 6 people [27] for the 2096 inhabitants in Mpigamiti [225]. The electrical load from the commercial facilities was unchanged across the scenarios but a different percentage of low, medium and high-income households was considered for comparison purposes. For the household load, the tool considers low and high-wattage appliances. The low-wattage appliances are lights, mobile phones and chargers and radios; the high-wattage appliances are televisions, DVD players, irons, and refrigerators. The ownership of the different appliances varies according to the type of household income. The tool assumes that high-income households have a higher percentage of appliance ownership compared to medium and low-income households (e. g. television ownership is 82%,45% or 16% of the total

households per income level). The other assumption in this tool is that high-income households have 3 lights, whereas, medium and low-income households have 2 and 1 light, respectively [208]. The household configuration and commercial inputs for each scenario are summarised in Table 5-6.

Table 5-6 Specifications for the high, medium, and low electricity demand scenarios (HED, MED, and LED).

		High Electricity Demand (86,537.78 kWh/y)	Medium Electricity Demand (60,647.32 kWh/y)	Low Electricity Demand (40,512.52 kWh/y)
Household Configuration	Number of Households	350	350	350
	% of High-income Households	70%	20%	10%
	% of Medium-income Households	20%	70%	20%
	% of Low-income Households	10%	10%	70%
Commercial Facilities	Number of Water Pumping Operations	1	1	1
	Number of Milling Operations	1	1	1
	Number of Small Shops	1	1	1
	Number of Schools	1	1	1
	Number of Clinics	1	1	1
	Number of Street Lights	23	23	23

Figure 5-8 shows the load profiles that represent the three electricity demand scenarios created.

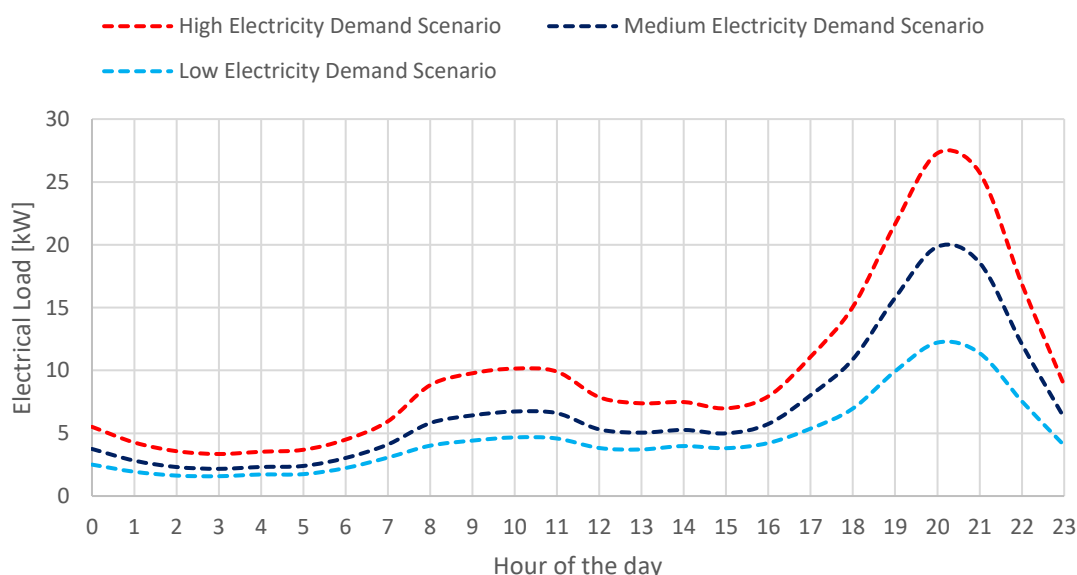


Figure 5-8 Electricity demand scenarios created for Mpigamiti, Tanzania.

5.2.2 PV System Installed Capacity

For the electricity demand scenarios presented above, the average electrical loads during daylight hours, from 7 am to 6 pm, were calculated for selecting the PV system required, able to supply 40%, 60%, or 100% of the average load. The numbers gave three PV scenarios corresponding to a low (40%), medium (60%), or high (100%) PV installed capacity as summarised in Table 5-7.

Table 5-7 Relevant data for PV array selection (low, medium, and high installed capacity).

Electricity Demand Scenario	Average	Peak	Min	Low PV	Medium PV	High PV
	electrical load during daylight (kW)	electrical load (kW)	electrical load (kW)	installed capacity required (kW)	installed capacity required (kW)	installed capacity required (kW)
High	9	27	3.35	5	7	12
Medium	6	20	2.17	3	5	8
Low	4	12	1.58	2	3	6

5.2.3 PV System Performance

For every PV scenario, the hourly output power was calculated using the Photovoltaic Geographical Information System (PVGIS) interactive tool from the European Commission website, with the solar radiation data from 2016 to 2020 [226]. Once the hourly output power was calculated, the clustering K-Means algorithm was applied, to obtain the representative operating day from each PV system. The representative operating day gives a good estimate of the possible PV system power generation considering the solar radiation fluctuation for the whole year. As the clusters classify the PV system output power according to the available solar radiation, then, for each PV system three scenarios can be considered: high PV performance, regular PV performance (most likely performance), and low PV performance, Figure 5-9 shows the clustering for a 2 kW PV system to illustrate the procedure done for all of them. The blurred lines correspond to the daily hourly power output during the 5 years and the dashed lines show the three clusters created after grouping the data according to their hourly output values.

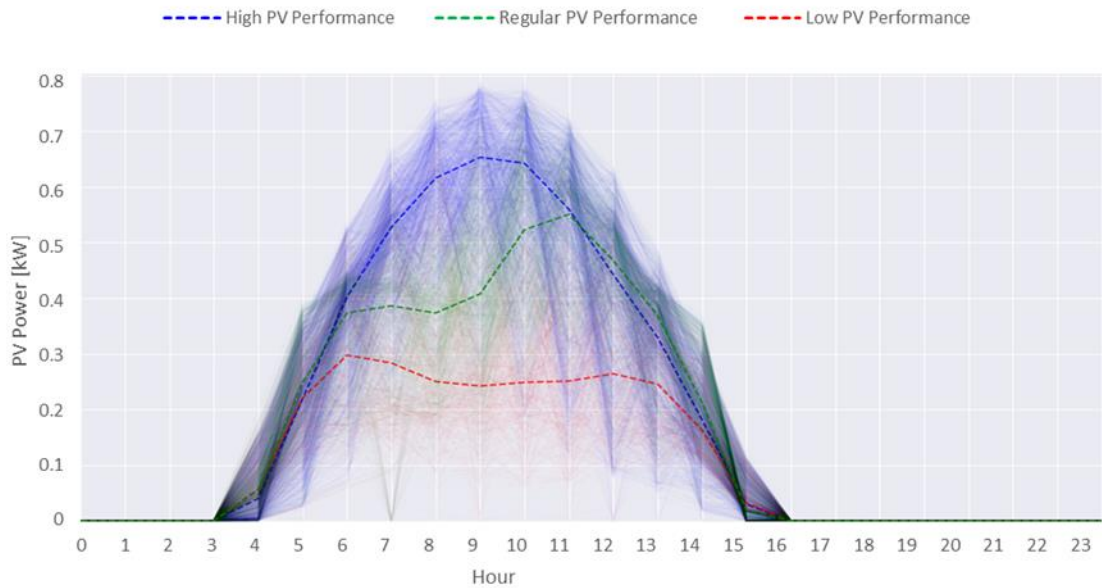


Figure 5-9 Output power and representative operating day clusters for a 2kW PV system over five years.

5.2.4 Battery System Type and Installed Capacity

The model considers three types of battery (Lead-acid, Li-ion, and repurposed) to address the current and the expected battery selection for microgrid systems deployment. According to [218] Lead-acid batteries are the major type of batteries used in microgrids around the world, however, their performance is challenged by climate and applications in SSA. Therefore, the use of Li-ion batteries has been considered due to their higher efficiency compared to the Lead-acid type and other characteristics that make Li-ion batteries competitive for rural electrification systems [227]. Moreover, the growing demand for electric vehicles offers the opportunity of reusing Lithium-ion batteries (repurposed batteries) in stationary storage applications. The most promising opportunity identified by the National Renewable Energy Laboratory is the utility-scale peak-shaving application [228].

The model determines the battery capacity according to Equation 5-7, the capacity depends on the percentage of the night demand (between 6 pm and 11 pm) that should be supplied by the battery (peak shaving), as well as on the battery characteristics shown in Table 5-8. There are three possible scenarios for the battery capacity selection (high, medium, and low), which represent the battery power required to supply 100%, 60% or 40% of the night demand, respectively.

Table 5-8 Round-trip efficiency and DOD for Lead-acid, Li-ion, and repurposed batteries

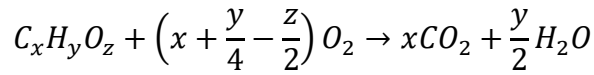
	Lead-acid	Li-ion	Repurposed (Li-ion) ⁵
Depth of Discharge (DOD)	60.0%	80.0%	80.0%
Round-trip Efficiency [218]	86.8%	97.5%	95.0%

5.2.5 Greenhouse Gas Emission Source

The Greenhouse Gas Emissions (GHG) depend on the amount and type of fuel burned during the operating hours of the diesel generators. However, the fuel production process could also be accounted for the GHG emissions generation. With this regard, the model considers two GHG emission scenarios. The first scenario only considers the direct GHG emissions coming from the tailpipe of the engine after the combustion process, this scenario is known as the tank-to-wheels (TTW) scenario. The second scenario considers the GHG emissions generated during the production process of the fuel (i.e., well-to-tank emissions or WTT) and the GHG emissions from the engine tailpipe (TTW). Therefore, the second scenario is known as the well-to-wheels (WTW) scenario. In other words, the WTW adds up the WTT and the TTW GHG emissions, which is a representation of the complete life cycle of the GHG emissions. For assessing the GHG emissions in either of the two GHG scenarios, the value of the blend emission factor (bEF_{blid}) should be modified accordingly in Equation 5-13, by selecting the right fuel emission factor in kgCO₂e/litre for diesel (EF^{diesel}) and castor oil ($EF^{biofuel}$). For the EF^{diesel} , the average biofuel blend TTW and WTW values, reported in the UK Government Conversion Factors for greenhouse gas reporting [215], were assumed (see Table 5-11). On the other hand, the $EF^{biofuel}$ (for castor oil) were calculated following the methodology for biofuels included in the Methodology Paper for conversion factors from the UK government [229], using data from the engine and analytical lab work. The biofuels methodology states that for biofuels, the TTW emissions should only consider the methane (CH₄) and the nitrous oxides (N₂O) emissions generated by the combustion process. The CO₂ emissions should not be included because the biofuels are considered “carbon neutral”, where any CO₂ generated by burning the fuel is cancelled out by the CO₂ absorption that occurs during the biofuel feedstock growth. In contrast, the WTT emissions should consider the CO₂, CH₄ and N₂O emissions of the biofuel production process.

The CO₂ emissions for castor oil were calculated using the general combustion equation assuming complete combustion:

⁵ The round-trip efficiency for the repurposed battery was calculated as multiplicative from the Li-ion battery efficiency (i.e., 97.5%*97.5%=95%).



Equation 5-74

where $x = 6.161$, $y = 10.09$, and $z = 0.9825$, the kmol per 100kgfuel values, were obtained from the CHONS analysis reported in Chapter 4. It was found that castor oil emits 271.084kgCO₂/100kg (2.71084kgCO₂/kg).

For calculating the CH₄ and N₂O emissions (in gCH₄/kg and gN₂O/kg), a similar procedure, as that for finding the NO_x and PM_{2.5} total weighted specific emissions, was needed. For these calculations, the torque data presented in Table 5-4, the ISO 8178 test cycle conditions from Table 5-3, and the CH₄ and N₂O emission index (EI) values reported in Chapter 4 were used. The total weighted emission index (TWEI) for CH₄ and N₂O were found using the corresponding equations that appear in the polynomial regressions shown in Figure 5-10 and Figure 5-11.

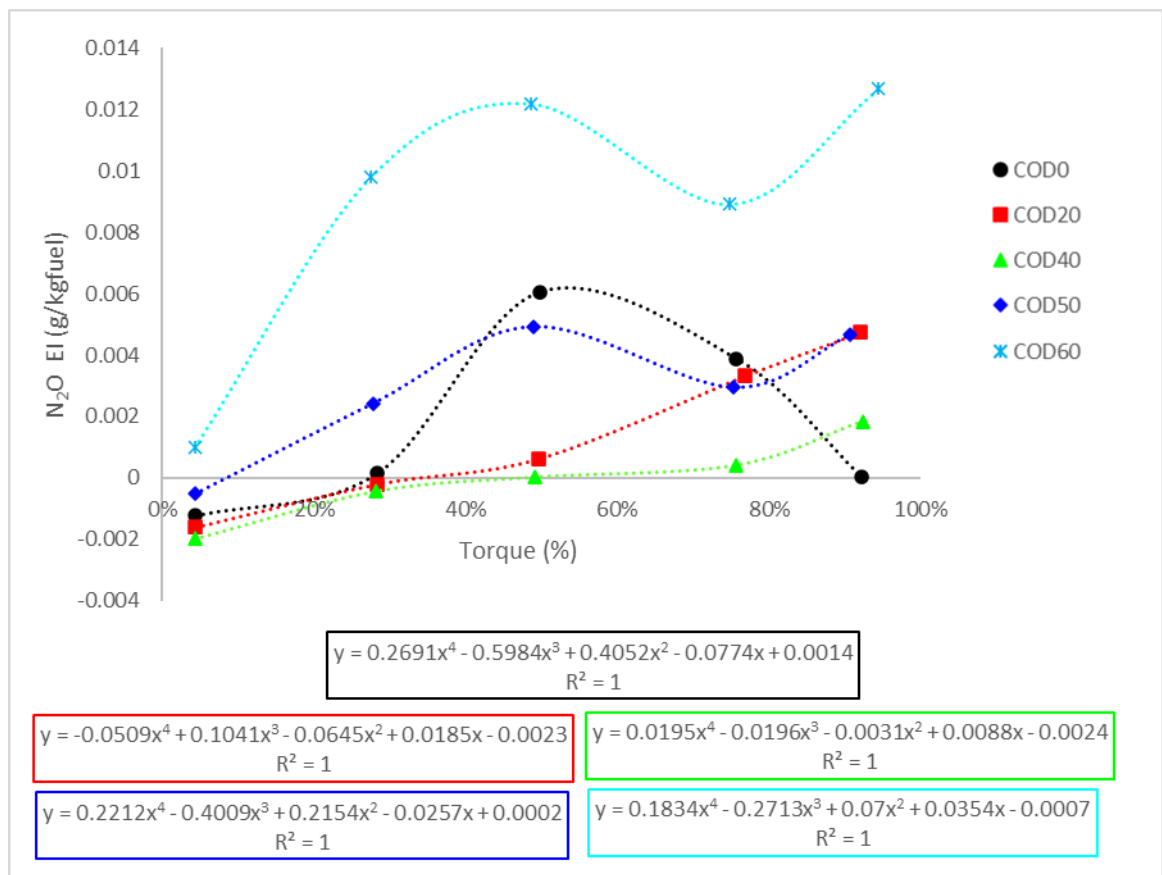


Figure 5-10 N₂O emission index against engine torque for 5 COD blends.

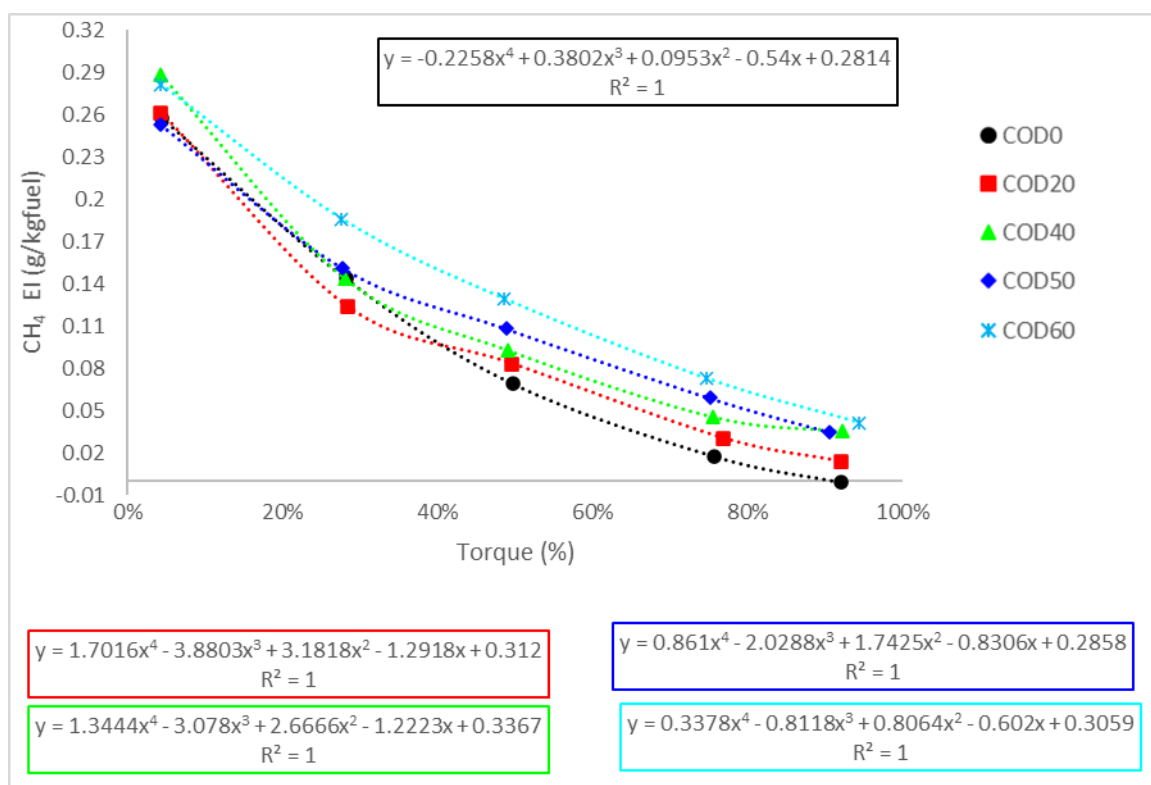


Figure 5-11 CH₄ emission index against engine torque for 5 COD blends.

The CH₄ TWEI findings are summarised in Table 5-9, the N₂O TWEI results were omitted as they were all found to be zero.

Table 5-9 CH₄ total weighted emission index for 5 COD blends.

ISO 8178 Test	CH ₄ Weight Emission Index [g/kgfuel]				
Point Torque	COD0	COD20	COD40	COD50	COD60
100%	0.00	0.00	0.00	0.00	0.00
75%	0.00	0.01	0.01	0.01	0.02
50%	0.02	0.02	0.03	0.03	0.04
25%	0.05	0.04	0.05	0.05	0.06
10%	0.02	0.02	0.02	0.02	0.03
Total Weighted EI [g/kgfuel]	0.09	0.10	0.11	0.12	0.14

The CH₄TWEI for 100% castor oil had to be estimated from the TWEI above by generating the curve shown in Figure 5-12, as no engine test was done with pure castor oil. Using this fitted curve implies certain limitations on data accuracy derived from extrapolation for estimated emissions beyond 60% castor oil. Therefore, more experimental data would be needed to support the data presented for the GHG scenarios as mentioned in Section 8.6.

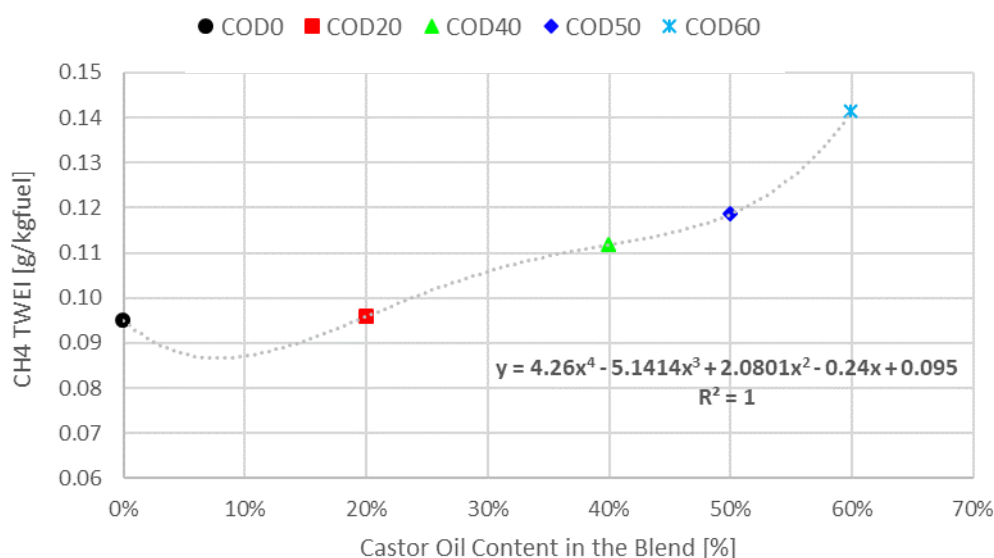


Figure 5-12 CH₄ total weighted emission index against castor oil content in the fuel blend

The CH₄TWEI value found for 100% castor oil fuel was 1.0537g/kgfuel (1.0537kg/tonnefuel).

To find the CO₂e emitted from castor oil, the CO₂ and CH₄ values found, were multiplied by their respective Global Warming Potential (GWP) as reported in [229] and divided by the castor oil specific volume (1041.66 l/tonne), based on the COD100 (100% castor oil-0% diesel) density at 20°C (960 kg/m³) reported in Chapter 4. The results are summarised in Table 5-10.

Table 5-10 CO₂e emissions calculated from the CO₂ and CH₄ emissions generated by the combustion of castor oil.

GHG	Castor Oil direct		CO ₂ e [kg/tonnefuel]	CO ₂ e [kg/litrefuel]
	Emissions [kg/tonnefuel]	GWP		
CO ₂	2710.84	1	2710.84	2.60241
CH ₄	1.0537	25	26.3425	0.02529

It is important to remember that the CO₂ emissions from castor oil should be ignored in the direct emission analysis, therefore the CO₂e from that GHG is only indicative in this work. The summary of the CO₂e emission factors (EF^{diesel} and $EF^{biofuel}$) that should be used to compute the bEF_{blid} to carry on the TTW or the WTW analysis is included in Table 5-11. Note that the WTT CO₂e emission factor for castor oil was considered as the average from the WTT values (in kgCO₂e/ kg) reported by [230], as no castor oil WTT value was found for Tanzania. The average was then converted to kgCO₂e/litre using the castor oil-specific volume discussed above. Table 5-11 shows a high WTT

value for castor oil which can be attributed to the emissions generated by the fertilization process. This process emits about 74 to 89% of the total emissions as reported by [230]. The high WTT value for castor oil was found to be about twice the value reported as the global median of 3.81 kgCO₂e per kg of oil [231]. Given that no value was found for the castor oil WTT emissions in Africa, it was prioritised to present the optimisation baseline results considering the TTW emissions instead, to compare the environmental impact of the fuel blends, rather than the fuel production process. Note that for the scenario analysis, the WTT emissions were considered to show the importance of including the emissions generated by the fuel production process, but a local value would be needed to give a better estimate of the emissions that could be accounted for in SSA.

Table 5-11 CO₂e emission factors for tank-to-wheel and well-to-wheel GHG emission scenarios.

Fuel Type	Emission Factor ID	CO ₂ e Emission Factors for TTW Analysis [kg/litrefuel]	CO ₂ e Emission Factors for WTT Analysis [kg/litrefuel]	CO ₂ e Emission Factors for WTW [kg/litrefuel]
Diesel	EF^{diesel}	2.51233	0.60986	3.1222
Castor oil	$EF^{biofuel}$	0.02529	8.2608	8.2861

5.2.6 Scenario Summary

The previous sections presented the details of the scenarios that can be simulated with the cost optimisation model. For better visualisation of the scenarios, Figure 5-13 shows the selection possibilities for the optimisation scenarios.

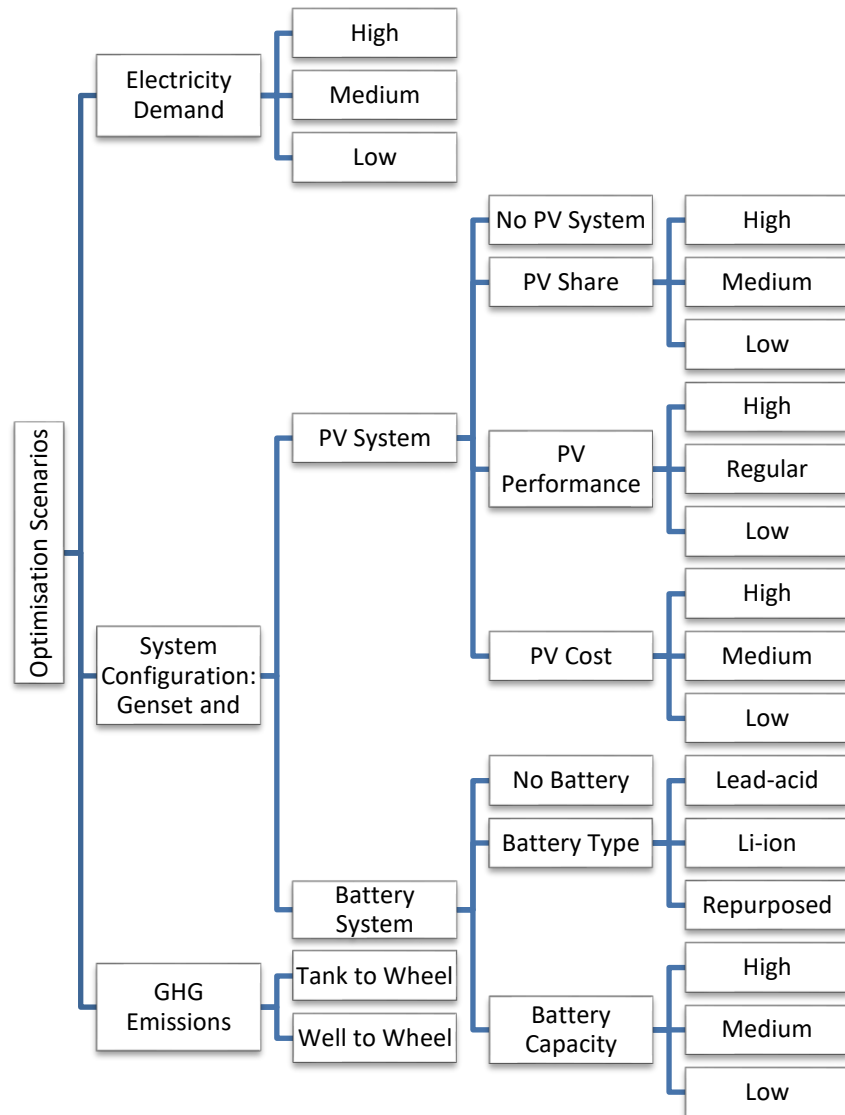


Figure 5-13 Possible optimisation scenario selection.

5.3 Optimisation Model Graphical User Interface

For an easier interaction between the user and the optimisation model, a graphical user interface (GUI) was created within the cost optimisation algorithm. The GUI enables the optimisation scenario selection, data visualisation and sensitivity analysis computation. Figure 5-14 shows the main interface for initialising the optimisation model.

Load Profile, PV System and Batteries

Select the system parameters:

Load Profile	PV Share	PV Performance	PV Install Cost
High Load	No PV		

Include Battery?

Yes		
-----	--	--

Battery Type

--	--

Installed Battery System

--

How would you like to consider the emissions?

From Tank to Wheel
From Tank to Wheel
From Well to Wheel

Close Window

Figure 5-14 GUI's main screen for running the cost optimisation model.

The dropdown menus from the main interface allow the user to select a scenario and enable the optimisation process, according to the process block diagram that appears in Figure 5-15.

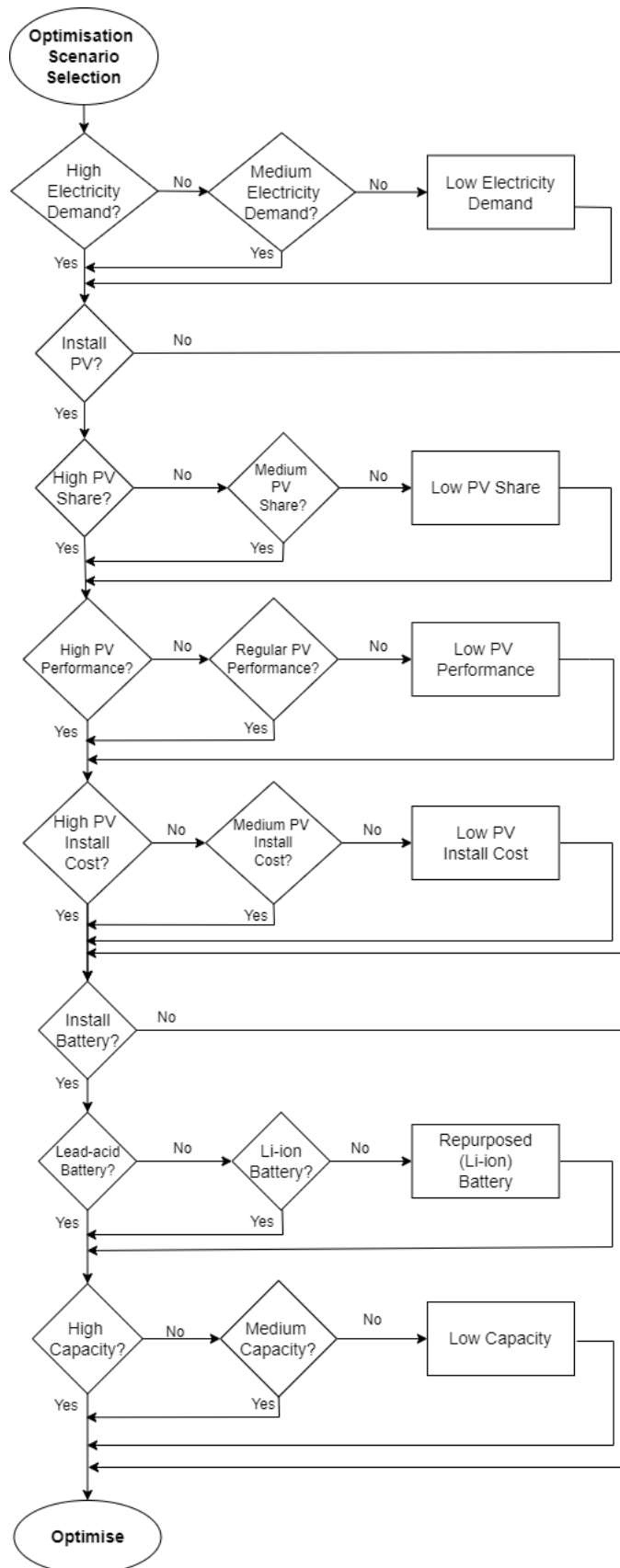


Figure 5-15 Process block diagram representation of the scenario selection algorithm implemented in the graphical user interface for initialising the cost optimisation model.

Once the optimisation is completed, the “Results” window, like the one shown in Figure 5-16, facilitates the visualisation of the system’s power generation curves and enables the sensitivity analysis options. Each sensitivity analysis option runs the initialised optimisation scenario but with the indicated modified variable. For example, the Zero Emission Cost sensitivity analysis sets the CO_{2e}, PM_{2.5}, and NO_x pollutant costs to zero and recalculates the optimisation results for the previously selected scenario.



Figure 5-16 GUI’s window for optimisation results visualisation and sensitivity analysis selection.

After running the sensitivity analyses, the results can be displayed using the “Select a file” window (see Figure 5-17A) to compare the new values with the original optimisation results that appear in the “Second window” (see Figure 5-17B).

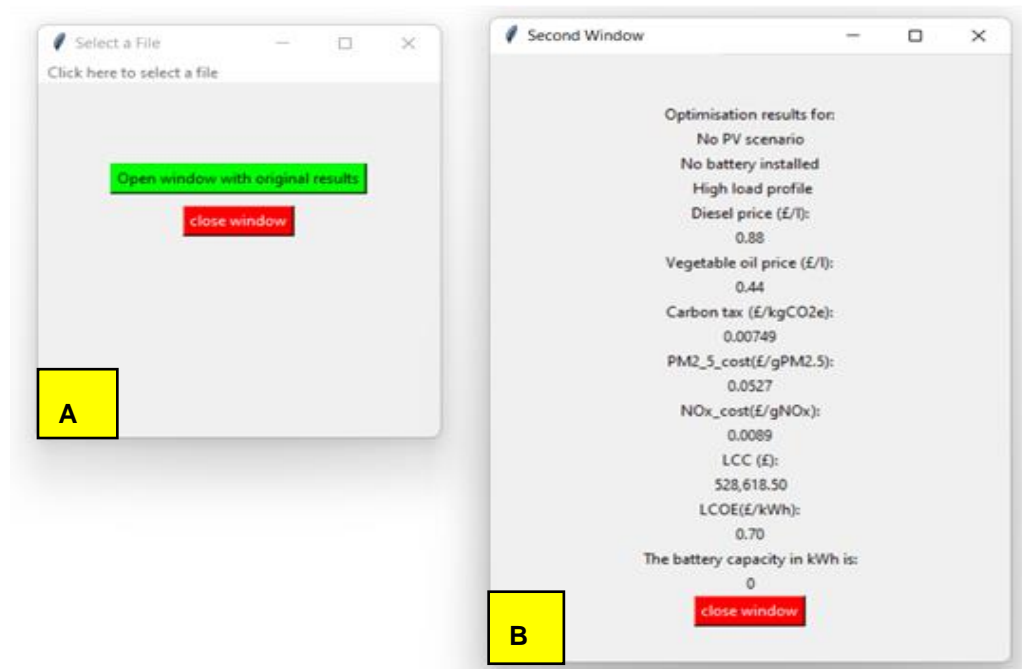


Figure 5-17 GUI's windows for sensitivity analysis results selection and original optimised results comparison.

The model presented in this chapter brings a new perspective to microgrid design by addressing one of the major drawbacks found in the literature related to diesel generator sizing. The formulation of this model allows for the inclusion of more fuel choices for assessing cost-effective solutions for microgrids and encourages better design practices, that may benefit the ongoing electrification challenge in remote areas. In the coming chapter, the results from the baseline optimisation scenario are presented, followed by their economic assessment.

Chapter 6

Cost Optimisation Model Implementation: Baseline Optimisation Scenario

The cost optimisation model presented in Chapter 5 is a useful tool for selecting the optimum number and size of diesel generators to work in different hybrid microgrid system configurations (diesel/PV/battery), considering the effect of biofuel blends, the PV share, and the battery energy storage system (BESS) type on the engine performance. The model allows comparing the microgrid configurations under different scenarios to assess the financial and environmental benefits (or drawbacks) of each configuration. This chapter presents the optimisation results found for 8 system configurations using the baseline scenario assumptions as detailed in section 6.1. The findings compare the fuel consumption, pollutant emissions (CO_{2e}, PM_{2.5}, and NO_x), Life Cycle Cost (LCC), and the Levelized Cost of Energy (LCOE) from the 8 system configurations (SC) for the three Tanzanian estimated electricity demand profiles presented in Chapter 5.

The chapter is divided into four sections. The first one presents the assumptions and specifications considered for the baseline optimisation scenario, the second one includes the findings of the baseline optimisation scenario for 8 system configurations, the third section is dedicated to the economic assessment of the 8 optimised systems, and the last section summarises the main findings presented in this chapter.

6.1 Baseline Optimisation Scenario Specifications and Assumptions

To carry on with the optimisation process, the three electricity demand profiles (HED: high electricity demand, MED: medium electricity demand, and LED: low electricity demand) described in Chapter 5 were used. For comparison purposes the 8 different system configurations (SC1 to SC8) that appear in Table 6-1 were considered, assuming the baseline optimisation scenario (BOS) input conditions, included in the same table. The BOS input conditions are related to the PV and Battery systems (i.e., PV share, PV performance, PV cost, and Battery capacity) as well as the emission assessment mode (tank-to-wheel or well-to-tank). The baseline optimisation scenario represents as much as possible the existing fuel prices and the estimated costs for the PV and battery technologies. The BOS reflects the need for as high as possible renewable energy share inclusion in hybrid systems. It also considers the

interest of assessing the impact of using biofuel blends in all cases, therefore no system configurations comprising only battery and PV arrays were considered in the optimisation.

Table 6-1 Baseline optimisation scenario input conditions.

System Configuration	PV Share	PV Performance	PV Cost	Battery Capacity	Diesel Emission Mode	Castor Oil Emission Mode
SC1-Genset						
SC2-Genset and PV						
SC3-Genset and Battery (Lead-acid)						
SC4-Genset and Battery (Li-ion)						
SC5-Genset and Battery (repurposed)	High	Regular	High	High*	TTW**	TTW**
SC6-Genset, PV, and Battery (Lead-acid)						
SC7-Genset, PV, and Battery (Li-ion)						
SC8-Genset, PV, and Battery (repurposed)						

* The battery capacity depends on the electricity demand profile, see Table 6-2 for more details.

**TTW= tank-to-wheel or tailpipe emissions.

6.2 Baseline Optimisation Scenario Findings for 8 System Configurations.

Table 6-2 shows the optimised diesel generator selection for the 8 system configurations in each electricity demand profile. The optimisation results for the baseline scenario at the high electricity demand showed that three diesel generators (G1, G2, and G3) should be installed in the scenarios without a battery (SC1 and SC2) to allow the optimum performance of the diesel generators preventing excessive fuel consumption and higher pollutant emissions. On the other hand, when the battery system was included, only one diesel generator was required for the rest of the hybrid configurations with the exception found in the HED scenario when using a repurposed battery. The generator size selection across the scenarios varied from G1 to G4 (as the selection depends on the electricity demand, the BESS installed capacity and its charging-discharging periods).

Table 6-2 Optimised genset selection for high, medium, and low electricity demand profiles.

Load Profile	System Configuration	Optimised Genset Selection	BESS Capacity [kWh]
High Electricity Demand (HED)	SC1-Genset***	G1, G2, G3	-
	SC2-Genset and PV	G1, G2, G3	-
	SC3-Genset and Battery (Lead-acid)	G3	191
	SC4-Genset and Battery (Li-ion)	G3	136
	SC5-Genset and Battery (repurposed)	G4	137
	SC6-Genset, PV, and Battery (Lead-acid)	G3	191
	SC7-Genset, PV, and Battery (Li-ion)	G3	136
	SC8-Genset, PV, and Battery (repurposed)	G1, G2	137
Medium Electricity Demand (MED)	SC1-Genset***	G1, G2, G3	-
	SC2-Genset and PV	G1, G2, G3	-
	SC3-Genset and Battery (Lead-acid)	G2	138
	SC4-Genset and Battery (Li-ion)	G3	98
	SC5-Genset and Battery (repurposed)	G3	99
	SC6-Genset, PV, and Battery (Lead-acid)	G2	138
	SC7-Genset, PV, and Battery (Li-ion)	G3	98
	SC8-Genset, PV, and Battery (repurposed)	G3	99
Low Electricity Demand (LED)	SC1-Genset***	G1, G2, G3	-
	SC2-Genset and PV	G1, G2, G3	-
	SC3-Genset and Battery (Lead-acid)	G1	86
	SC4-Genset and Battery (Li-ion)	G1	61
	SC5-Genset and Battery (repurposed)	G2	62
	SC6-Genset, PV, and Battery (Lead-acid)	G1	86
	SC7-Genset, PV, and Battery (Li-ion)	G1	61
	SC8-Genset, PV, and Battery (repurposed)	G2	62

***G1: 6.88 kW, G2: 9.76 kW, G3: 14.96 kW, G4:22.56

The fuel selected by the model was COD0 (diesel) in the three electricity demand profiles for all the SCs regardless of the low castor oil price (0.44 £/litre), which is 50% lower than that of diesel (0.88 £/litre). This fuel selection can be attributed to the pollutant emission costs (CO_{2e} and PM_{2.5}) calculated in Equation 5-12 and Equation 5-16, where the fuel blend emission factor (bEF_{blnd}) in kgCO_{2e}/litre and the PM_{2.5} emission factor adjustment coefficient ($EFA_{blnd}^{PM_{2.5}}$) are included. Recall from Chapter 5 that according to Table 5-11, the emission factor considered for diesel was 2.51233, whereas for biofuels the emission factor was 0.02529. It should also be noted that the experimental work indicated

that the PM_{2.5} emissions increase as the castor oil content increases in the fuel blend. Therefore, as the fuel selection is based on the fuel price, the emission factors and the emission costs, the model would always select the fuel having the lowest overall cost, in this case, COD0. The results suggest then that the PM_{2.5} emission cost of biofuels should be considered in hybrid microgrids optimisation processes as it affects the fuel selection.

It was observed that the BESS capacity was only affected by the electricity demand and the characteristics of each battery type but not by the PV inclusion. The latter suggests that as the PV power contribution does not impact the night peak demand when battery peak shaving occurs, then, the available PV power is not a determining factor for sizing the batteries or the diesel generators. However, the PV system may reduce the power required from the diesel generators during the daylight peak or even contribute to charging the batteries in the same period, which in turn contributes to reduced fuel consumption.

6.2.1 Diesel Generators Selection and Performance

This section presents the load demand and power generation curves found for every SC in each electricity demand profile. For every case, the genset performance below the recommended operating limit (or the lowest value found), at the corresponding operating period (low performance operating period) is presented next to or below the load and power generation curves. The genset performance is represented by the genset operating power at a given period as a percentage of the genset's prime power and it is referred to hereafter as the genset load factor. For all the systems a graph showing the total power generation matching the total load demand is presented and for the systems including more than one electricity generation source (i.e., genset and battery, genset and PV, and genset, PV, and battery) a second graph is included, which shows the power generation by source. The curves legend with a brief description is summarised in Table 6-3.

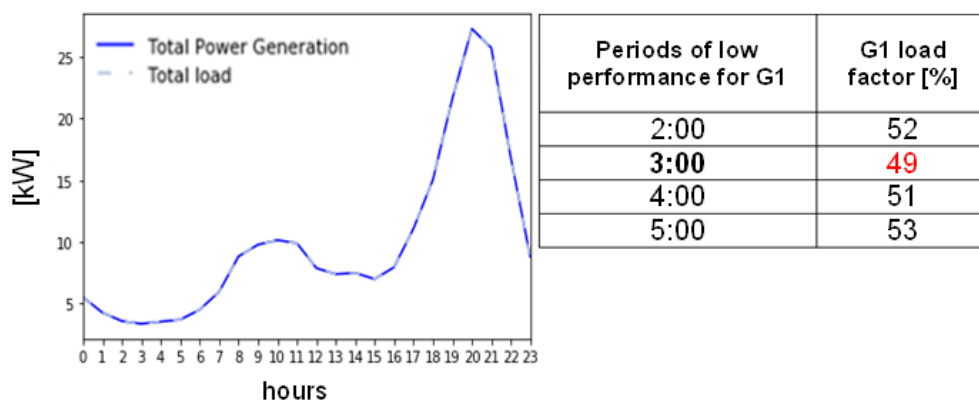
Table 6-3 Legend description for the total power and power generation by source curves.

Graph type	Legend description	
Total power generation curve	 Total Power Generation	the sum of the power generated by all the sources in the system.
	 Total load	the sum of the load demand, which considers the electricity demand plus the battery charging power or only the electricity demand for the non-battery systems.
Power generation by source curve	 Load Profile	electricity demand.
	 Genset Power	power generated by the genset or all the gensets combined in the system.
	 PV Power	power generated by the PV system.
	 Battery discharging power	power supplied by the batteries to the system.
	 Battery charging power	power consumed by the batteries from the system.

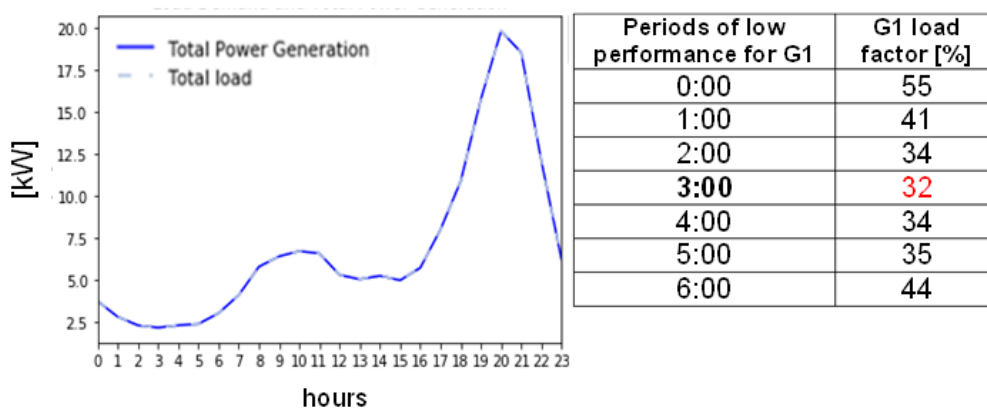
6.2.1.1 Non-Battery Systems

Although the optimised genset selection aims to avoid operating the diesel generators below 60% of their prime power (as explained in the previous chapter), it was found that in the system configurations without battery (SC1 and SC2), even the smallest genset would be operating below the threshold. The low engine load operation in those cases was required to match the specific demand (very low demand) while preventing any power overgeneration, to avoid potential blackouts by overcharging the system. The amount by which the recommended operating limit was breached, was highly dependent on the electricity demand profile. In the SC1 the smallest genset selected (G1) was operating at 49%, 32%, and 23% of its prime power in the HED, MED, and LED profiles, respectively. Figure 6-1 summarises the findings from the SC1-Genset configuration. In the figure, the total power generation and the total load curves are shown as well as the operating hours at which the smallest genset worked below the recommended limit. The curves appear completely overlapped, which reflects that the optimisation process was properly done and the electricity demand was matched at all times.

A. High Electricity Demand



B. Medium Electricity Demand



C. Low Electricity Demand

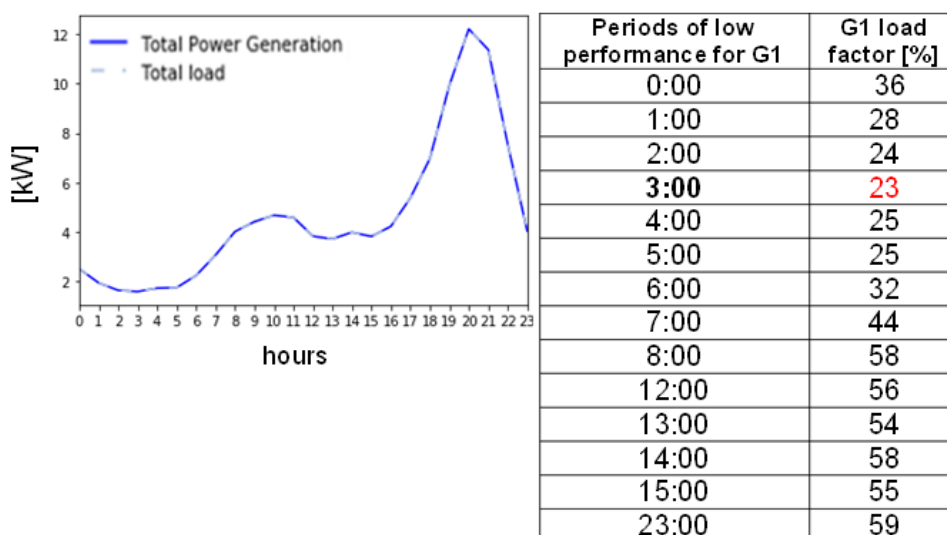
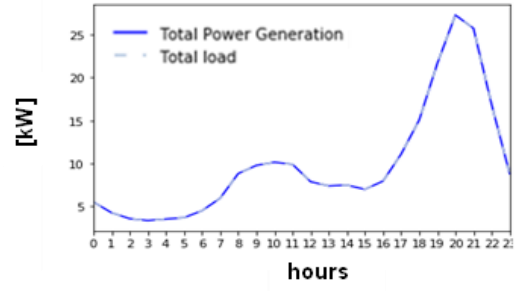
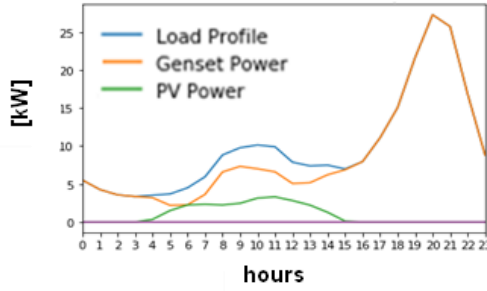


Figure 6-1 Load and power generation curves and the identified low genset performance (below 60%) operating periods in the SC1-Genset for three electricity demand profiles.

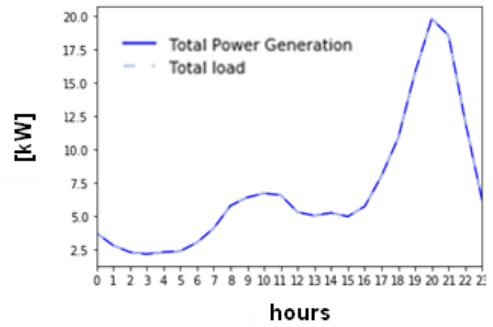
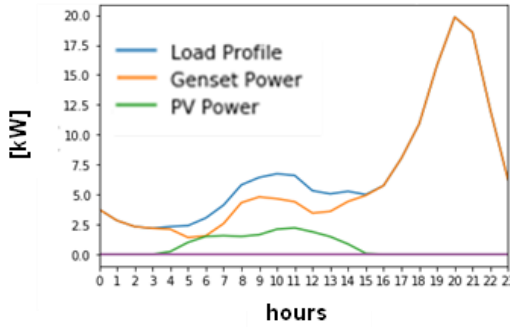
In the SC2-Genset and PV configuration, it was also found that the smallest generator (G1) worked below 60% of its prime power in the three electricity demand profiles. The lowest genset power factor was found in the LED profile (15%) at 5 am, whereas for MED and HED, it was 20% and 32%, respectively at the same operating hour (see Figure 6-2). During that operating period, the lowest power factor was caused by combining two factors: the low electricity demand and the PV system power generation, which on its own is not capable of fully supplying the demand. In Figure 6-2, besides the total power generation and the total load matching curves that appear on the right-hand side, the power generation by source curves are also included (left-hand side), to appreciate each power source's contribution to the total power generation and the electricity demand profile (load profile).

A. High Electricity Demand



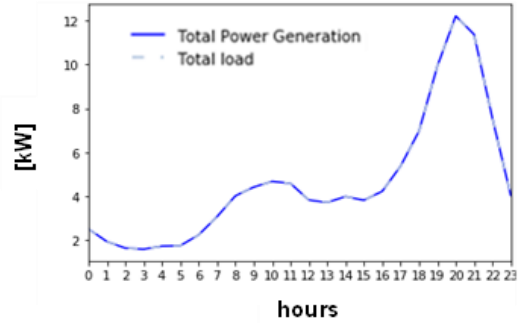
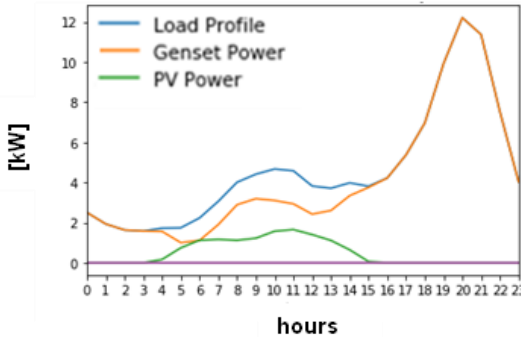
Periods of low performance	2:00	3:00	4:00	5:00	6:00	7:00
G1 load factor [%]	52	49	46	32	33	53

B. Medium Electricity Demand



Periods of low performance	0:00	1:00	2:00	3:00	4:00	5:00	6:00	7:00	12:00	13:00
G1 load factor [%]	55	41	34	32	30	20	22	37	50	52

C. Low Electricity Demand



Periods of low performance	0:00	1:00	2:00	3:00	4:00	5:00	6:00	7:00	8:00	9:00	10:00	11:00	12:00	13:00	14:00	15:00
G1 load factor [%]	36	28	24	23	23	15	16	28	42	46	45	43	35	38	49	55

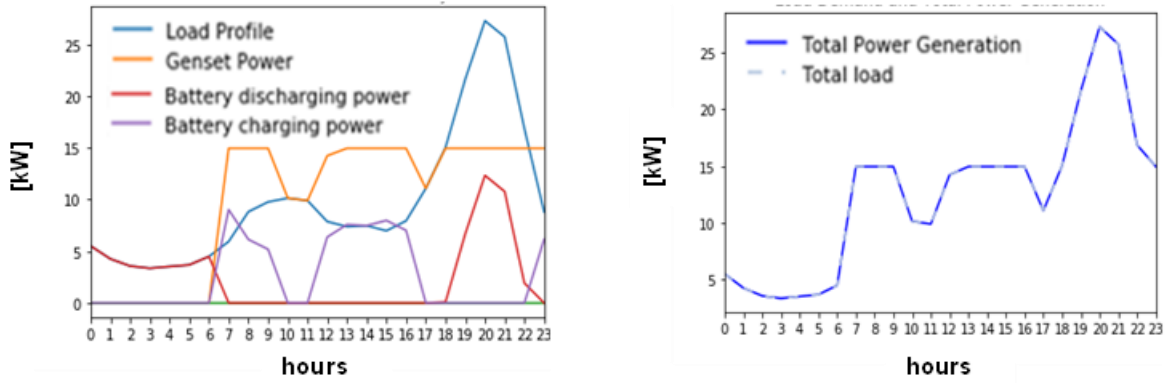
Figure 6-2 Load and power generation curves and the identified low genset performance (below 60%) operating periods in the SC2-Genset and PV for three electricity demand profiles.

6.2.1.2 Battery Systems

The findings for the system configurations that include diesel generators and BESS (SC3, SC4, and SC5) are presented for each electricity demand profile respectively, to appreciate the effect of each battery type (Lead-acid, Li-ion, and repurposed) under a specific electricity demand profile.

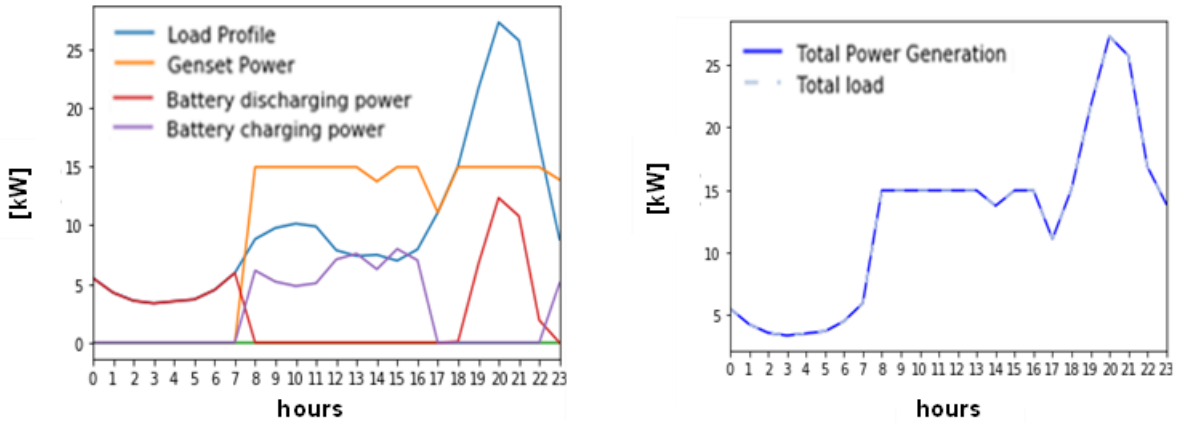
Figure 6-3 shows the results for the high electricity demand profile. It was found that the selected diesel generators operate at or above the recommended operating limit at all times for the three BESS included. However, it was found that when a repurposed battery was included, a bigger genset (G4) was required to supply the electricity demand, compared to the Lead-acid and Li-ion configurations where G3 was selected. The need for a bigger genset when using a repurposed battery could be attributed to its lower efficiency compared to the Li-ion battery and its deeper DOD compared to the Lead-acid battery. Those two characteristics of the repurposed battery combined with its lower power contribution at night, relative to the other two batteries, might difficult for G3 to match the total high load demand at all times, therefore G4 was selected instead. The lowest load factors found in this electricity profile were 66%, 74%, and 60% for the Lead-acid, Li-ion, and repurposed battery systems, respectively. In the figure (left diagram), the power supplied to the system by the gensets and the batteries (battery discharging power) can be appreciated, as well as the electricity demand and the power consumed from the system by the batteries (battery charging power). As in the previous case, the diagram on the right-hand side of the figure shows the power generation and the total load curves completely overlapped, which represents a successful optimisation process.

A. HED: SC3-Genset and Battery (Lead-acid)



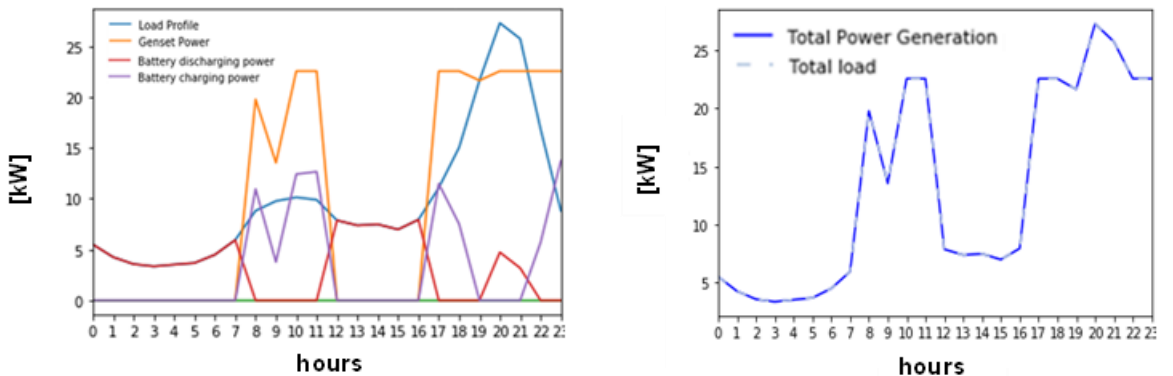
Period of low performance	11:00
G3 load factor [%]	66

B. HED: SC4-Genset and Battery (Li-ion)



Period of low performance	17:00
G3 load factor [%]	74

C. HED: SC5-Genset and Battery (repurposed)

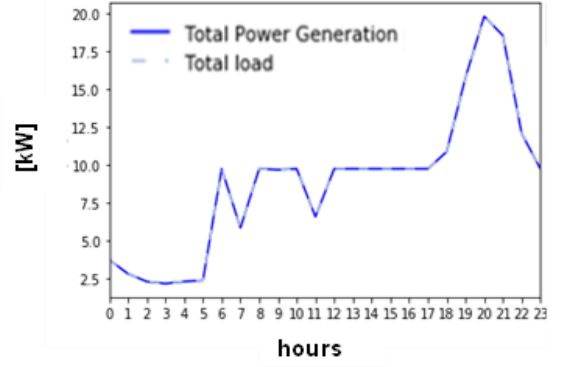
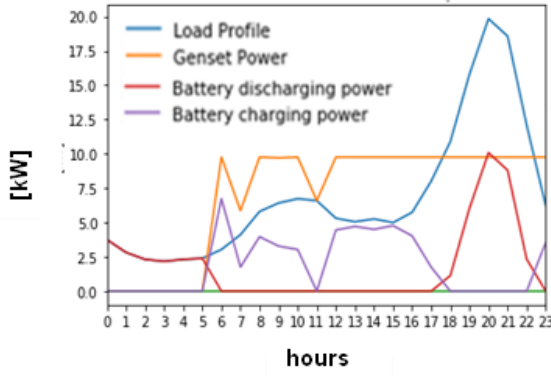


Period of low performance	09:00
G4 load factor [%]	60

Figure 6-3 Load and power generation curves and the identified low genset performance operating periods in the SC3, SC4, and SC5 for the high electricity demand profile.

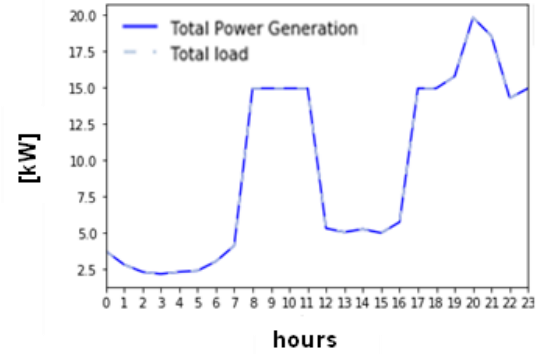
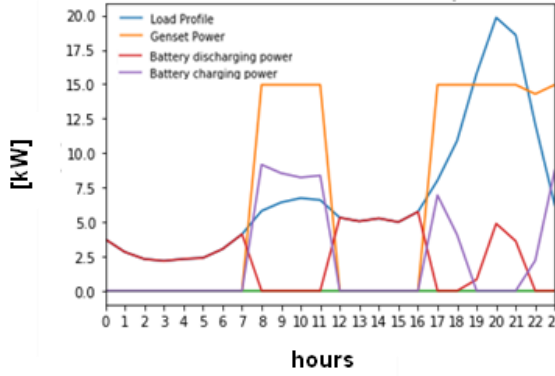
Similarly to the HED profile, it was found that for the medium electricity demand profile, the gensets operate at or above the recommended load factor with the three battery types. It should be noted that using a Lead-acid battery required a smaller genset (G2) compared to the Li-ion or the repurposed battery configurations that required G3 instead. The need for a smaller genset when using the Lead-acid battery can be explained by the battery's high power contribution at night, which reduced the power to be supplied by the genset. The latter was not the case with the other two battery types, hence a bigger genset was needed to supply the night peak for matching the load demand at all times. In the MED profile, the genset had the lowest load factor at 60% with the Lead-acid and repurposed batteries, whereas for the Li-ion battery, it was 96%, as shown in Figure 6-4. The high load factor reported for the Li-ion battery can be explained by the periods where the genset was supplying the electrical load and charging the battery, especially after 16:00 hrs, when high electricity demand was required. The successful optimisation process in this electricity demand profile was supported by the well-matching curves from the right-hand side diagram that appears in the figure.

A. MED: SC3-Genset and Battery (Lead-acid)



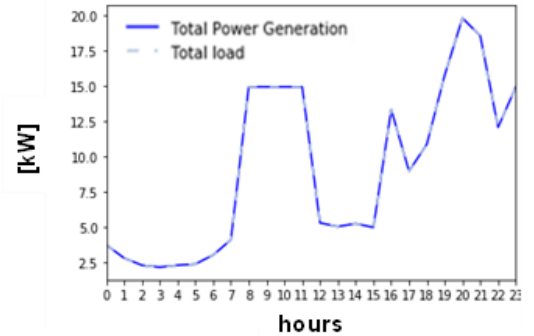
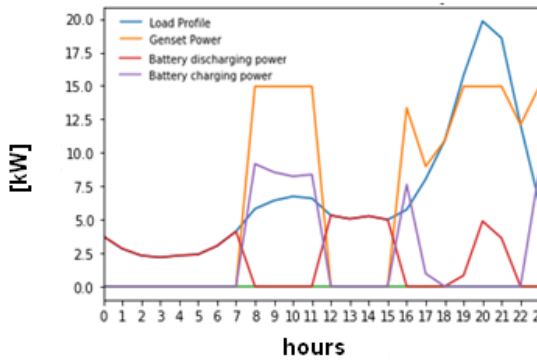
Period of low performance	07:00
G2 load factor [%]	60

B. MED: SC4-Genset and Battery (Li-ion)



Period of low performance	22:00
G3 load factor [%]	96

C. MED: SC5-Genset and Battery (repurposed)

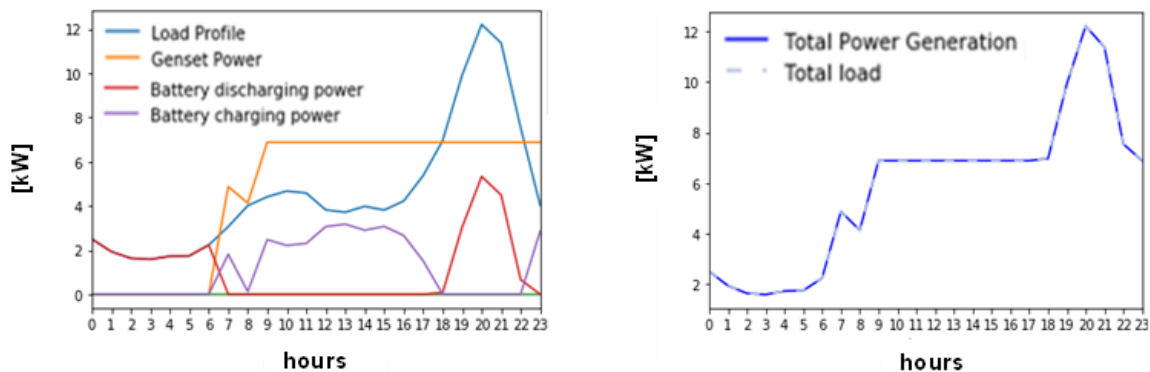


Period of low performance	17:00
G3 load factor [%]	60

Figure 6-4 Load and power generation curves and the identified low genset performance operating periods in the SC3, SC4, and SC5 for the medium electricity demand profile.

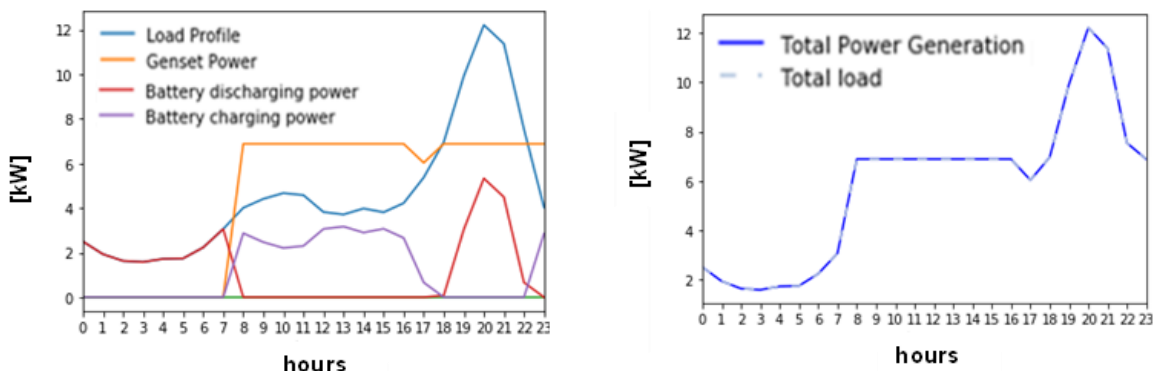
Finally, Figure 6-5 shows the results for SC3, SC4, and SC5 found in the low electricity demand profile. As in the MED profile, the Li-ion battery system had better performance (88%), compared to the Lead-acid (60%) and the repurposed (60%) battery systems during the lowest load operating period. In this profile, the high performance of the Li-ion SC can be attributed to the battery charging periods, which occurred during the high electricity demand hours before the night peak. It was observed that a bigger genset (G2) was needed with the repurposed battery system, whereas with the other two batteries, G1 was selected. The need for a bigger genset when using the repurposed battery can be explained by the battery's low power contribution during the night peak, which required more power from the genset to match the demand. The selection of the bigger genset can also be attributed to the amount of power required for charging the battery during the high electricity demand periods before the night peak.

A. LED: SC3-Genset and Battery (Lead-acid)



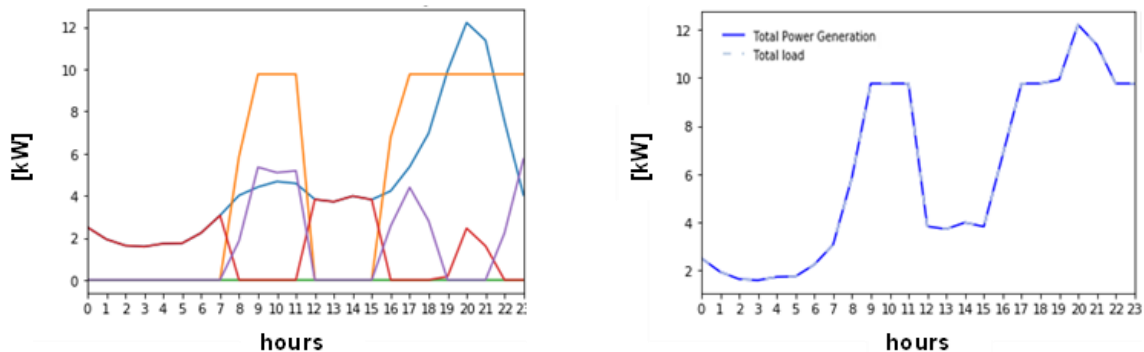
Period of low performance	08:00
G1 load factor [%]	60

B. LED: SC4-Genset and Battery (Li-ion)



Period of low performance	17:00
G1 load factor [%]	88

C. LED: SC5-Genset and Battery (repurposed)



Period of low performance	08:00
G2 load factor [%]	60

Figure 6-5 Load and power generation curves and the identified low genset performance operating periods in the SC3, SC4, and SC5 for the low electricity demand profile.

6.2.1.3 Diesel/PV/BESS Hybrid Systems

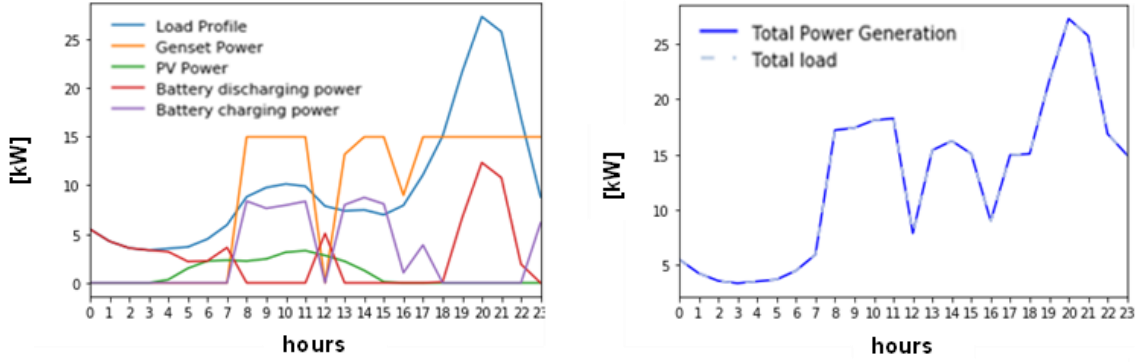
This section presents the findings of the three hybrid system configurations (diesel/PV/BESS) SC6, SC7, and SC8 for each electricity demand profile. For all the cases, the optimisation process was confirmed by their matching total power generation and total load curves.

Figure 6-6 shows the results found for the high electricity demand profile. For this electricity demand, it was found that using a Lead-acid or a Li-ion BESS, only one genset was required (G3) whereas when using the repurposed BESS two gensets were needed (G1 and G2). It was observed that with the Lead-acid battery, the lowest genset performance was 60% (see Figure 6-6 A.) but with the Li-ion the genset worked at 100% during its operating periods (see Figure 6-6 B.). On the other hand, by inspecting the results with the repurposed battery (see Figure 6-6 C), it was found that G1 worked at 100% during its operating periods, whereas G2 had a performance of 85% at 18:00. The 85% performance at that operating period can be attributed to the combined power generation as G1 was also working at full load and the battery system was supplying energy as well. Table 6-4 shows the power generated by each genset in the SC8 for a better understanding of Figure 6-6 C.

Table 6-4 Power generation of G1 and G2 per operating period for the HED profile with SC8-Genset, PV, and Battery (repurposed).

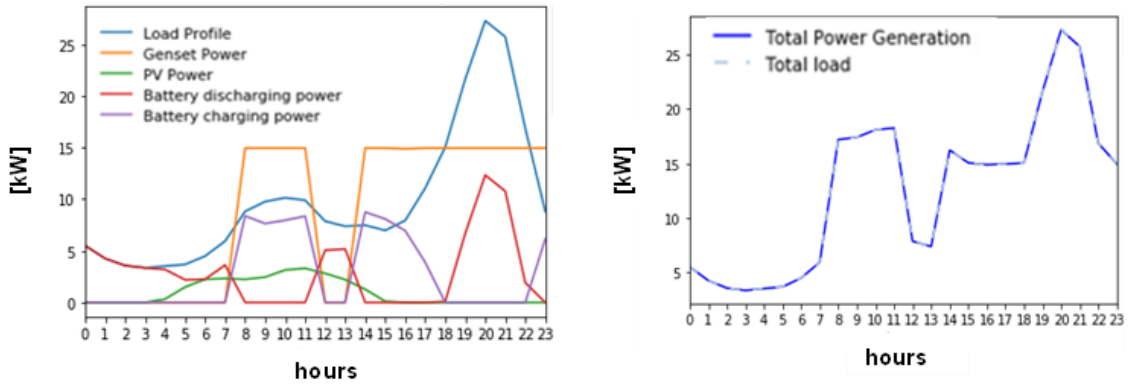
Operating Period	Power of Genset 1 [kW]	Power of Genset 2 [kW]
1	-	9.76
7	6.88	-
8	-	9.76
9	-	9.76
10	-	9.76
11	-	9.76
12	-	9.76
13	-	9.76
14	6.88	-
15	-	9.76
16	-	9.76
17	-	9.76
18	6.88	8.34
19	6.88	9.76
20	6.88	9.76
21	6.88	9.76
22	6.88	9.76
23	6.88	9.76

A. HED: SC6-Genset, PV, and Battery (Lead-acid)



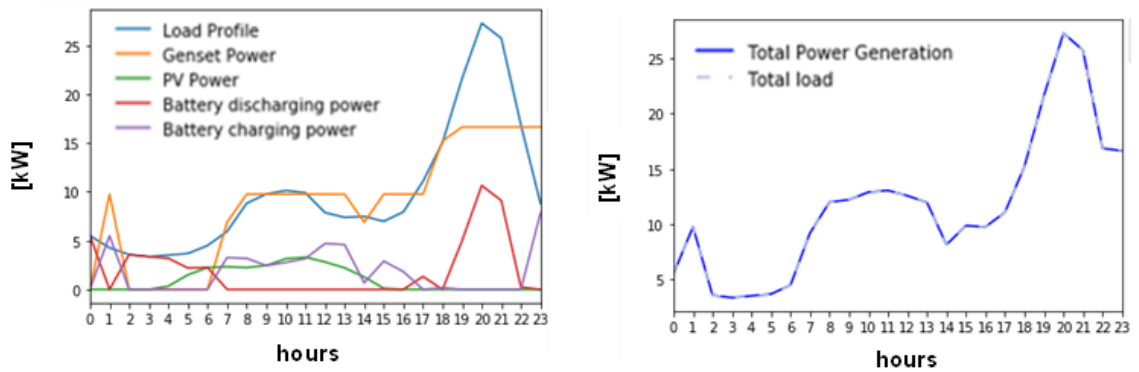
Period of low performance	16:00
G3 load factor [%]	60

B. HED: SC7-Genset, PV, and Battery (Li-ion)



Period of low performance	none
G3 load factor [%]	100

C. HED: SC8-Genset, PV, and Battery (repurposed)

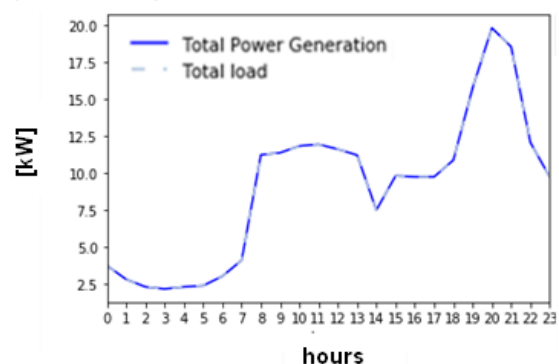
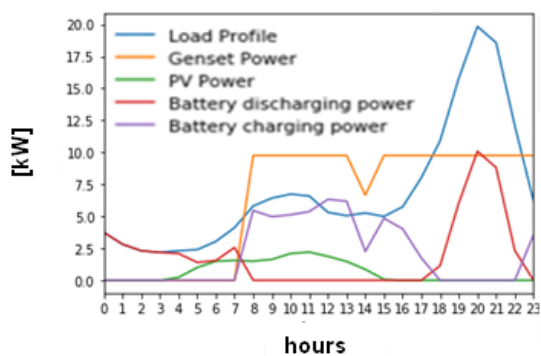


Period of low performance	18:00
G2 load factor [%]	85

Figure 6-6 Load and power generation curves and the identified low genset performance operating periods in the SC6, SC7, and SC8 for the high electricity demand profile.

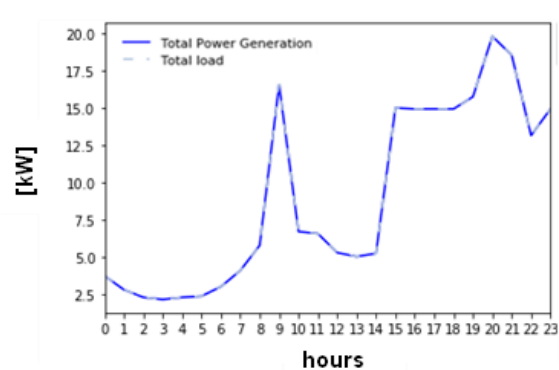
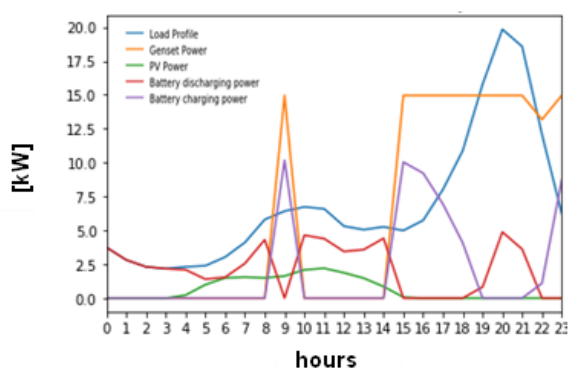
The results found for the medium electricity demand profile are shown in Figure 6-7. In this profile, the Lead-acid BESS required G2, which had its lowest operating load (68%) at 14:00. On the other hand, G3 was required for the configurations with Li-ion and repurposed batteries. The lowest operating load using G3 was 88% and 96% at 22:00 hrs and 17:00 hrs with the Li-ion and the repurposed batteries, respectively. As in previous cases, the selection of a smaller genset (G2 for the Lead-acid battery) can be attributed to the battery power contribution during the night peak, which reduced the power demand to be supplied by the genset.

A. MED: SC6-Genset, PV, and Battery (Lead-acid)



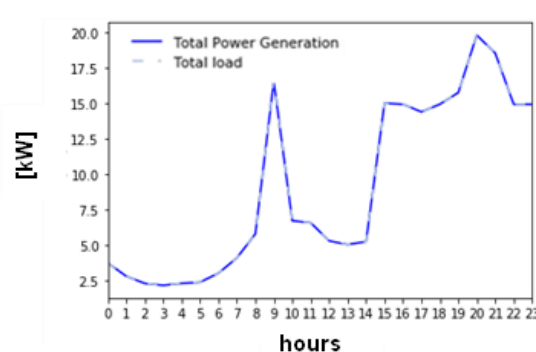
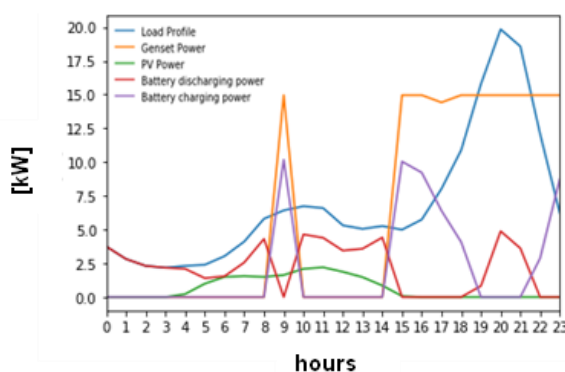
Period of low performance	14:00
G2 load factor [%]	68

B. MED: SC7-Genset, PV, and Battery (Li-ion)



Period of low performance	22:00
G3 load factor [%]	88

C. MED: SC8-Genset, PV, and Battery (repurposed)

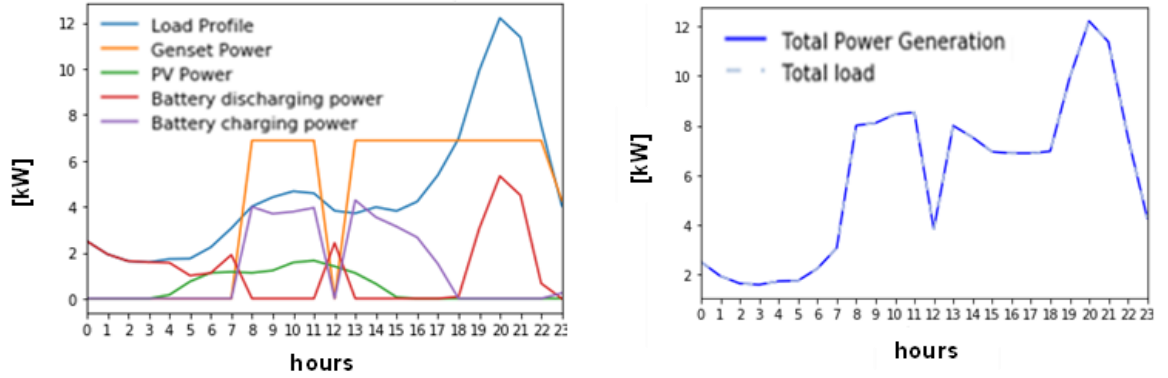


Period of low performance	17:00
G3 load factor [%]	96

Figure 6-7 Load and power generation curves and the identified low genset performance operating periods in the SC6, SC7, and SC8 for the medium electricity demand profile.

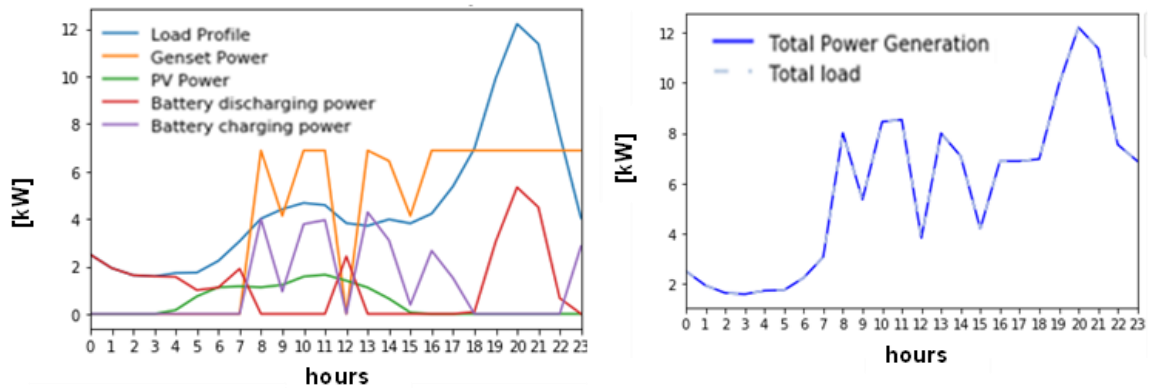
Finally, in the low electricity demand profile, it was found that G1 was required if the Lead-acid or the Li-ion batteries were used. In contrast, when the repurposed battery was included in the system, G2 was required. In the Lead-acid configuration, the lowest genset operating load was 62% at 23:00 hrs, whereas for the Li-ion and repurposed batteries, the lowest genset operating load was 60% but at different operating periods (Li-ion: 09:00 and 15:00 hrs., repurposed: 09:00 and 14:00 hrs.), as shown in Figure 6-8. From the results, it can be appreciated that the low performance of G1 in the Lead-acid configuration was attributed to the battery power contribution, whereas for the other two configurations, the low genset performance could be attributed to the PV power contribution during the battery charging periods.

A. LED: SC6-Genset, PV, and Battery (Lead-acid)



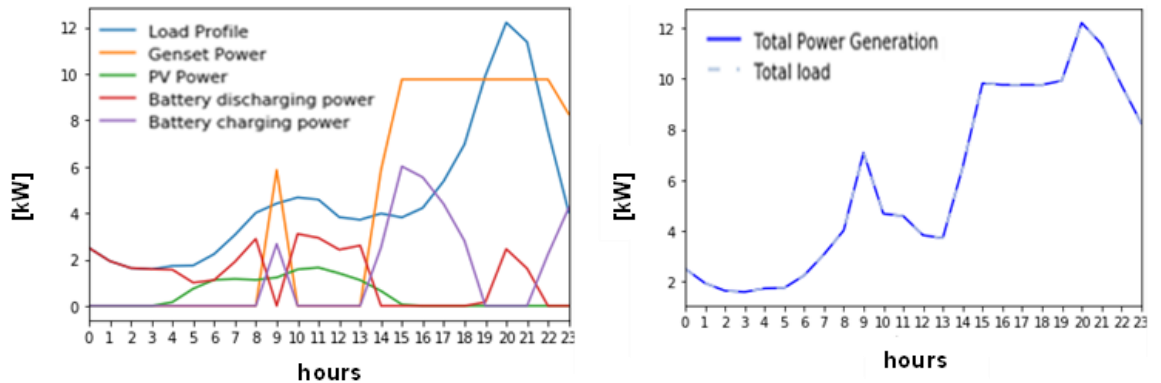
Period of low performance	23:00
G1 load factor [%]	62

B. LED: SC7-Genset, PV, and Battery (Li-ion)



Period of low performance	09:00 and 15:00
G1 load factor [%]	60

C. LED: SC8-Genset, PV, and Battery (repurposed)



Period of low performance	09:00 and 14:00
G2 load factor [%]	60

Figure 6-8 Load and power generation curves and the identified low genset performance operating periods in the SC6, SC7, and SC8 for the low electricity demand profile.

6.2.2 Fuel Consumption and Pollutant Emissions

After looking at the genset selection and specific performance of the different system configurations, it was of interest to compare the fuel consumption and the pollutant emissions of each system.

Figure 6-9 (a) shows the fuel consumption and Figure 6-9 (b) shows the CO_{2e} emissions of the 8 system configurations for the three electricity demand profiles. The highest yearly fuel consumption in all the electricity demand scenarios was found in the SC1-Genset (HED: 31,504.40 l/y, MED: 23,166.60 l/y, and LED: 16,698.80 l/y). As expected, using hybrid configurations (Genset/PV/battery) reduces the fuel consumption for the three scenarios as less power is required from the diesel generators. It was found that fuel consumption can be reduced by up to 20% in the HED scenario using the SC7-Genset, PV, and Battery (Li-ion). In the MED scenario, the fuel consumption could be reduced by up to 23.5% using the SC7-Genset, PV, and Battery (Li-ion) and up to 24% in the LED scenario using the SC8-Genset, PV, and Battery (repurposed). Similar fuel savings were reported in [232], where the total diesel consumption was reduced by about 21% by replacing a standalone diesel generating system with a hybrid PV/Diesel/Battery system. Also, Atmaja et al. [233] reported potential fuel savings between 30% to 40% by replacing a 60kVA diesel generator with a smaller one (42kVA) supported by a PV and battery system.

Correspondingly to the fuel consumption, the highest CO_{2e} emissions (HED: 79,149.40 kg/y, MED: 58,202.00 kg/y, and LED: 41,952.80 kg/y) were also found in the SC1-Genset. The emissions can be reduced by 20%, 23.5%, and 24% in the HED, MED and LED scenarios respectively using the hybrid systems mentioned above for the fuel consumption reduction (SC7 and SC8). These emissions reduction findings are comparable to the carbon dioxide emissions reduction of about 21% reported by Lau et al. [232] after implementing a hybrid PV/Diesel /Battery system.

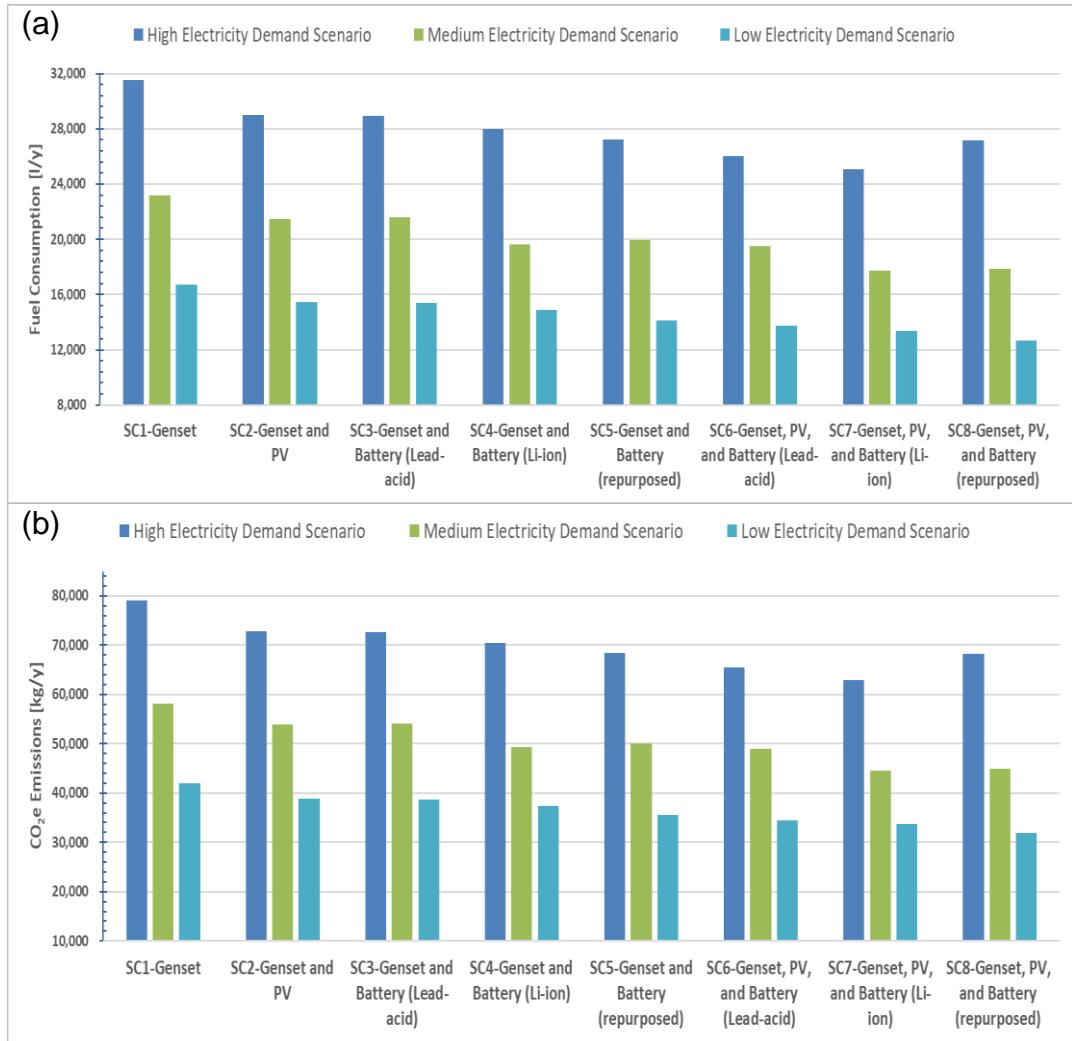


Figure 6-9 Fuel consumption and CO₂e emissions per year for different microgrid configurations with different electricity demand profiles.

Similarly, the highest pollutant emission values for PM_{2.5} (HED:214.71 kg/y, MED: 164.83 kg/y, LED: 135.32 kg/y) and NO_x (HED: 1,502.95 kg/y, MED: 1,153.82 kg/y, LED: 947.21 kg/y) were found in the SC1-Genset. Figure 6-10 (a) shows the PM_{2.5} and Figure 6-10 (b) shows the NO_x emission values found for the different configurations. The figures indicate that both pollutants can be reduced up to 47% in the LED scenario with the SC6-Genset, PV, and Battery (Lead-acid) or the SC7-Genset (Li-ion). A 37% reduction is possible in the MED scenario using the SC7-Genset, PV, and Battery (Li-ion) or the SC8-Genset, PV, and Battery (repurposed). In the HED scenario, these pollutant emissions can be reduced by 32% with the SC7-Genset, PV, and Battery (Li-ion).

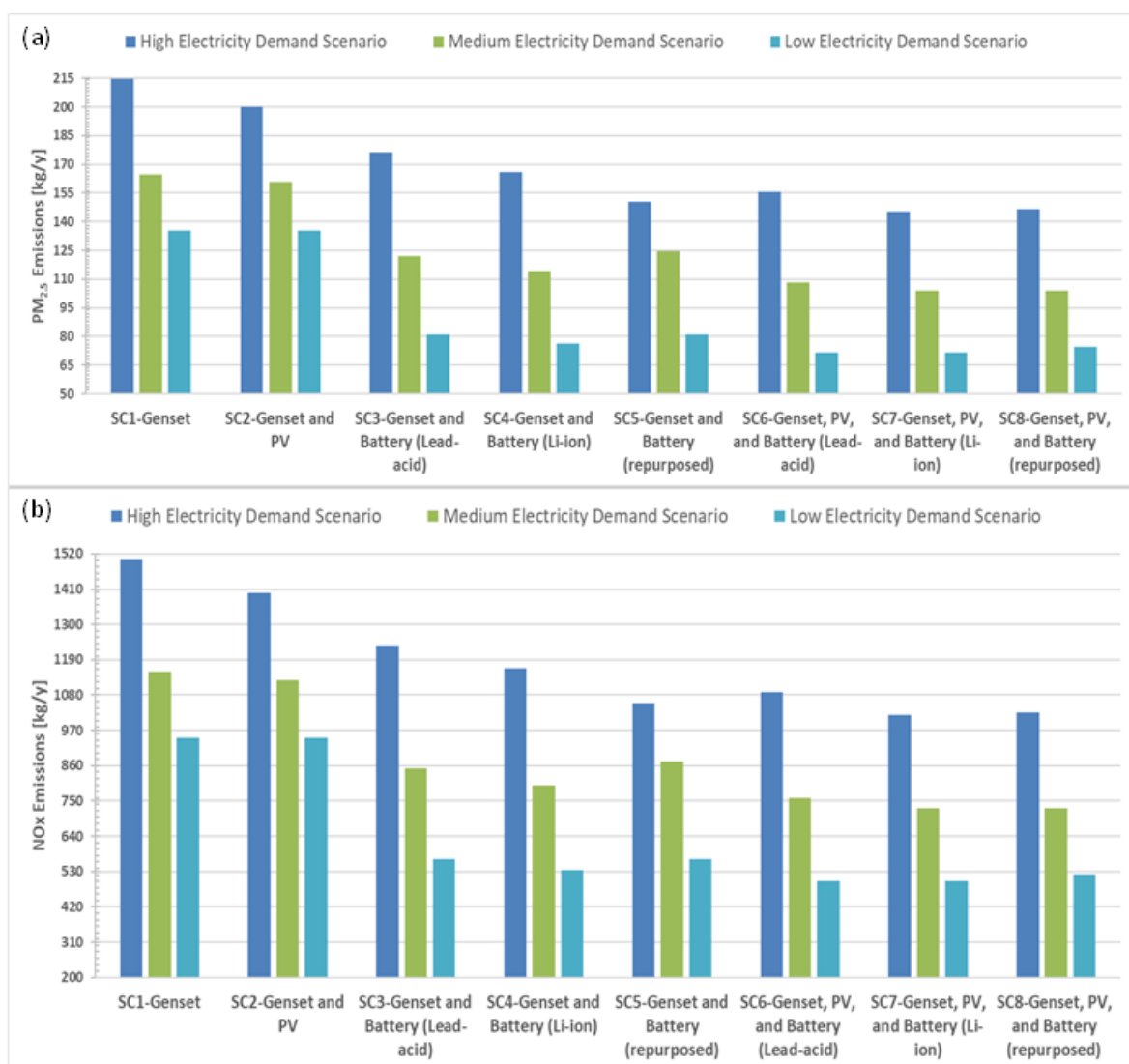


Figure 6-10 PM_{2.5} and NO_x emissions per year for different microgrid configurations with different load profiles.

It should be noted that the higher reduction in pollutant emissions for PM_{2.5} and NO_x compared to the CO_{2e} reduction is attributed to the size of the diesel generators that play an important role in Equation 5-15 and Equation 5-17 included in Chapter 5 for the emission calculations. This means that the size of any generator considered within the hybrid systems (G1, G2, G3 or G1+G2) will give lower PM_{2.5} and NO_x emissions than those from the SC1-Genset with a higher installed capacity (G1+G2+G3). The size effect is not reflected in the CO_{2e} emissions as they are calculated from the fuel consumption computed in Equation 5-12 from Chapter 5, in terms of the genset's operating power rather than on the actual generator's size.

An important remark from this section is that overall, with hybrid systems (diesel/PV/Battery), fuel consumption and emissions can be reduced. However with SC8 in the HED profile, higher fuel consumption and emissions were reported, relative to the other hybrid systems. The higher fuel consumption and

emissions can be attributed to the combined power of generators G1 and G2 during the high-demand periods (after 18:00 hrs) as both generators were working at full load. This combined power (16.64 kW) is greater than the power generated by G3 at full load (9.76 kW), therefore more fuel was consumed and higher CO_{2e} emissions were generated. Also, the higher NO_x and PM_{2.5} emissions can be attributed to the combined size (combined prime power) of the two generators which would lead to higher emissions according to Equation 5-15 and Equation 5-17 presented in Chapter 5.

6.3 Economic Assessment for 8 System Configurations

Considering the different characteristics of the 8 optimised microgrid configurations presented above, an economic assessment was done to determine which configuration would have more benefits from a financial and environmental perspective. The Life Cycle Cost and the Levelized Cost of Energy of each configuration were computed with the equations presented in section 5.1.5 from Chapter 5, the findings are as follows.

6.3.1 Life Cycle Cost and Levelized Cost of Energy

For the LCC (with a 10% discount rate) and the LCOE computations, a 25-year horizon was selected as it is a common project lifetime considered for microgrids analysis reported in the literature [234-236]. In the LCC comparison from Figure 6-11, the numbers indicate that the highest LCC corresponds to the SC2: Genset and PV, in all the electricity demand profiles (HED: £549,457.78, MED: £427,943.46, and LED: £323,644.75). These high costs are attributed to the *per se* high fuel consumption costs plus the initial investment in PV arrays that do not help to reduce the diesel generators operating hours during the night peak. Therefore, according to the data presented, it is recommended to include energy storage systems when using hybrid configurations to reduce the LCC values. The lowest LCC were found in the SC8: Genset, PV, and Battery (repurposed), for the three profiles (HED: £ 457,929.81, MED: £328,786.48, and LED: 230,541.23). Those values corresponded to 16.7%, 23%, and 28.8% reductions in LCC, respectively, compared to the reference configuration (SC2-Genset and PV).

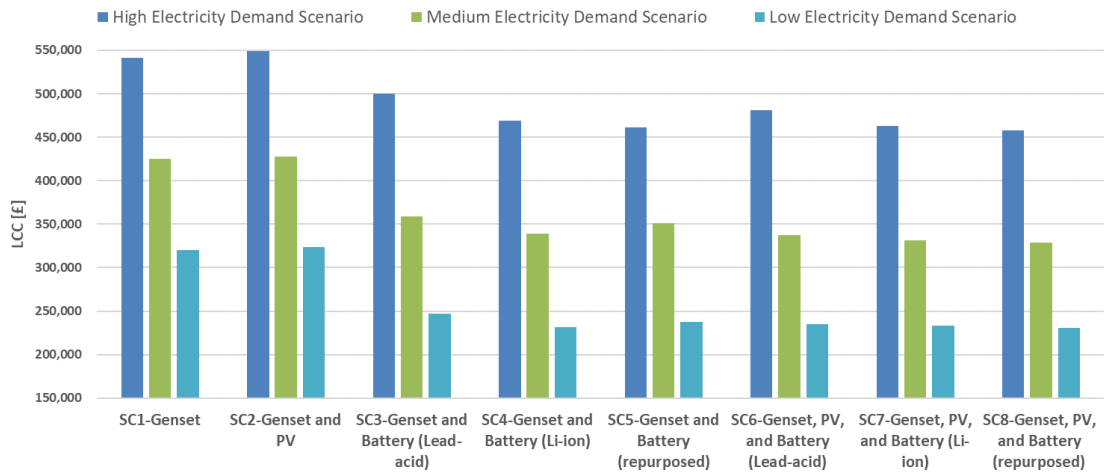


Figure 6-11 Life Cycle Cost over 25 years for different microgrid configurations with different load profiles.

The LCC determined the cheapest configuration over the useful life of different system configurations but still, a fair comparison in terms of per unit of electricity generation for the diverse technologies was required. Therefore, a second comparison, over the same 25-year horizon, based on the overall cost and the total electricity produced by each SC was done using the Levelized Cost of Energy. Figure 6-12 shows the LCOE of each SC for the three electricity demand profiles. The best value for the HED profile was found in the SC5-Genset and the Battery (repurposed) (0.47 £/kWh). The MED scenario showed the best value (0.48 £/kWh) in two configurations, the SC4 and the SC8. For the LED scenario, the best value (0.52 £/kWh) appeared in the two configurations with the repurposed battery system (SC5 and SC8).

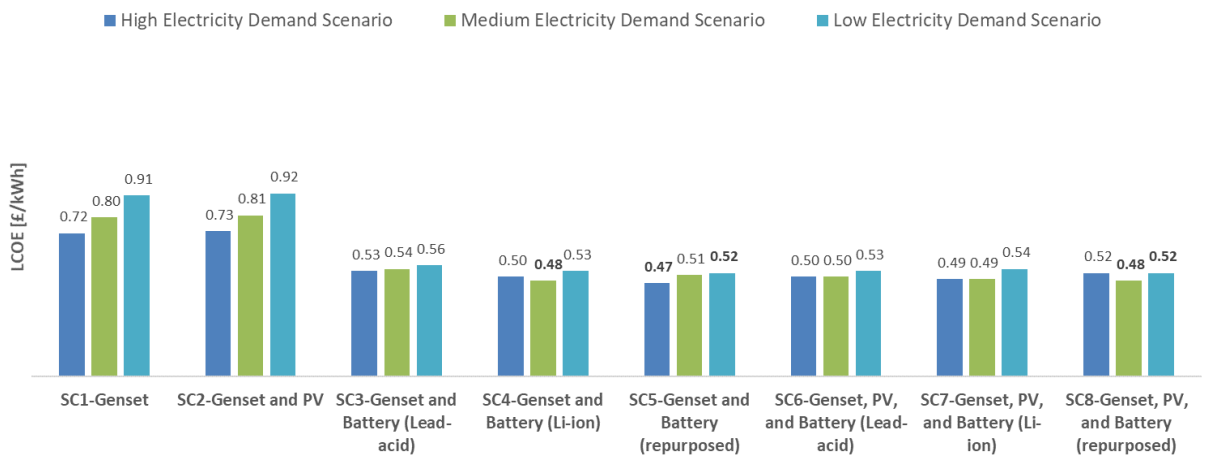


Figure 6-12 Levelized Cost of Energy over 25 years for different microgrid configurations with different electricity demand profiles.

These LCOE results showed a similar trend as that reported for an off-grid mobile base station in Tanzania [237] where a hybrid Genset/PV/battery configuration gives the lowest LCOE of 0.433 USD/kWh (0.33 £/kWh) when compared against a Genset only configuration with LCOE of 0.945 USD/kWh (0.72 £/kWh). Similarly, the results from a case study in three rural villages in Ethiopia [238] showed that the LCOE of 1.673 USD/kWh (1.27 £/kWh) from a Genset configuration is less favourable than the 0.84, 0.90, and 1.00 USD/kWh (0.64, 0.68, 0.76 £/kWh) LCOE values reported for the hybrid systems considered in that study. Also, the best LCOE values reported for a diesel/PV/battery system in the techno-economic analysis done by Amupolo et al. [239] were about 0.32 £/kWh (0.386 USD/kWh and 0.388 USD/kWh). Despite the similarity found in the LCOE trend from this work and the studies cited above, it cannot be ignored that the LCOE values in this work are slightly different. The difference in the results can be attributed to the pollutant emissions costs considered in this optimisation, which are neglected in the other studies. The difference is also attributed to the lower electricity load demand considered by the other authors, which is only about half of the load profile considered for the LED scenario presented in this work. However, according to [240] the current cost for solar hybrid mini-grids is 0.55 USD/kWh, therefore the findings of this work are close to the LCOE range for hybrid microgrids. Moreover, according to [241] the estimated cost for electricity generation with diesel gensets in Tanzania ranges between 0.40 to 2 USD/kWh, which suggests that the LCOE found for the SC1-genset configuration is also within the correct LCOE range.

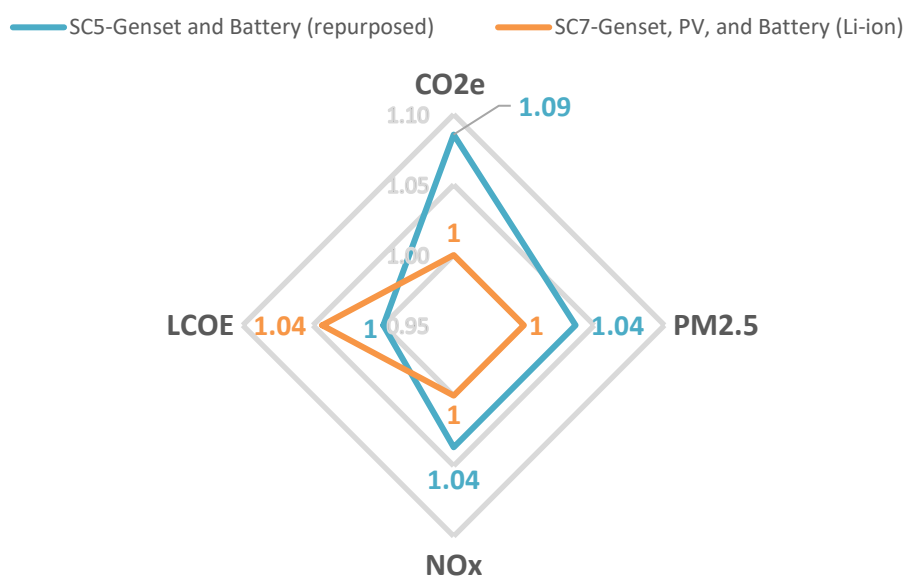
6.3.2 LCOE vs Emissions Analysis

With the LCOE results presented in section 6.3.1, it was possible to find the most profitable configurations, but no information was obtained regarding the environmental aspects of the systems. An LCOE vs. emissions analysis was done to a better understanding of what hybrid configuration might bring more benefits (financial and environmental). The LCOE vs. emissions analysis was done by comparing the system with the lowest CO_{2e}, NO_x, and PM_{2.5} emissions versus the systems with the lowest LCOE highlighted in Figure 6-12. The results are shown in Figure 6-13, Figure 6-14, and Figure 6-15 in the form of normalised values, i.e. normalised to the lowest value for each category (CO_{2e}, PM_{2.5}, NO_x, and LCOE), which was considered as the baseline. The baseline values for each category are summarised in Table 6-5.

Table 6-5 Baseline values for the LCOE vs emissions analysis.

Scenario	CO ₂ e Emissions Baseline (kg/y)	PM _{2.5} Emissions Baseline (kg/y)	NO _x Emissions Baseline (kg/y)	LCOE-25 years Baseline (£/kWh)
HED	62,994.90	145.25	1,016.73	0.47
MED	44,535.30	103.75	726.23	0.48
LED	31,794.30	71.57	500.98	0.52

The results for the HED scenario (see Figure 6-13) showed that by selecting SC7, which has the lowest pollutant emissions (CO₂e, NO_x, and PM_{2.5}), the LCOE would be 4% higher than the LCOE baseline (SC5). If, on the other hand, the SC5 with the lowest LCOE is selected, then the CO₂e, PM_{2.5}, and NO_x emissions would be 9% and 4% higher respectively, when compared to the system with the lowest pollutant emissions (SC7). Therefore, based on the possible increase of pollutant emissions and LCOE values, for the HED scenario, option SC7 might be a better choice if the environmental benefit is prioritised.

**Figure 6-13 Pollutant emissions and LCOE comparison for selected HED scenario hybrid system configurations.**

The results for the MED scenario (see Figure 6-14) showed that when the environmental benefit is prioritised, SC7 should be selected. The SC7 configuration only represents a 2% increase in the LCOE value compared to the lowest LCOE found in SC4 and SC8. However, even if the financial benefit is

prioritised, SC8 would be an acceptable choice as it only represents a 1% increase in CO_{2e} emissions whereas NO_x and PM_{2.5} remained unchanged from the best environmental option (SC7). It should be noted that SC4 would not be the recommended selection, regardless of its low LCOE (the same as SC8), as it represents an increase of 11% in CO_{2e} emissions and a 10% increase in NO_x and PM_{2.5} emissions.

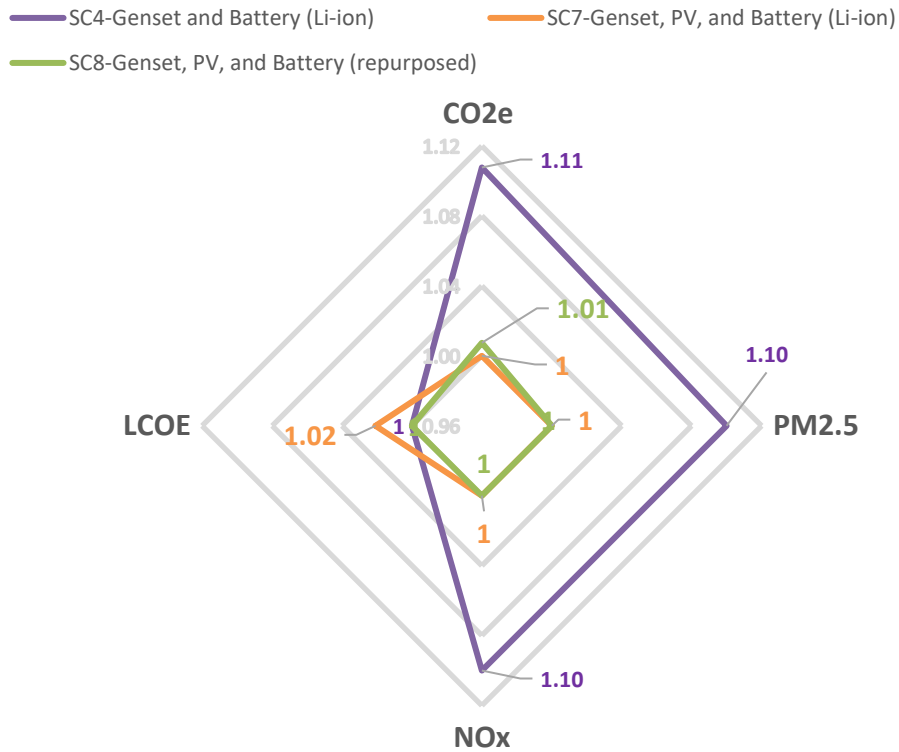


Figure 6-14 Pollutant emissions and LCOE comparison for selected MED scenario hybrid system configurations.

Finally, in the LED scenario, the results showed that four configurations should be considered in the LCOE vs emissions analysis (see Figure 6-15). The numbers suggest that if the financial benefit is prioritised, then SC5 or SC8 should be selected. At the same time, if the environmental benefit is prioritised (with the focus on CO_{2e} abatement), then SC8 is still the best option as it generates 6% and 12% less CO_{2e}, compared to SC7 and SC6, respectively. However, it should be noted that the PM_{2.5} and NO_x emissions from SC8 are 4% higher than their respective baseline emissions found in SC6 and SC7.

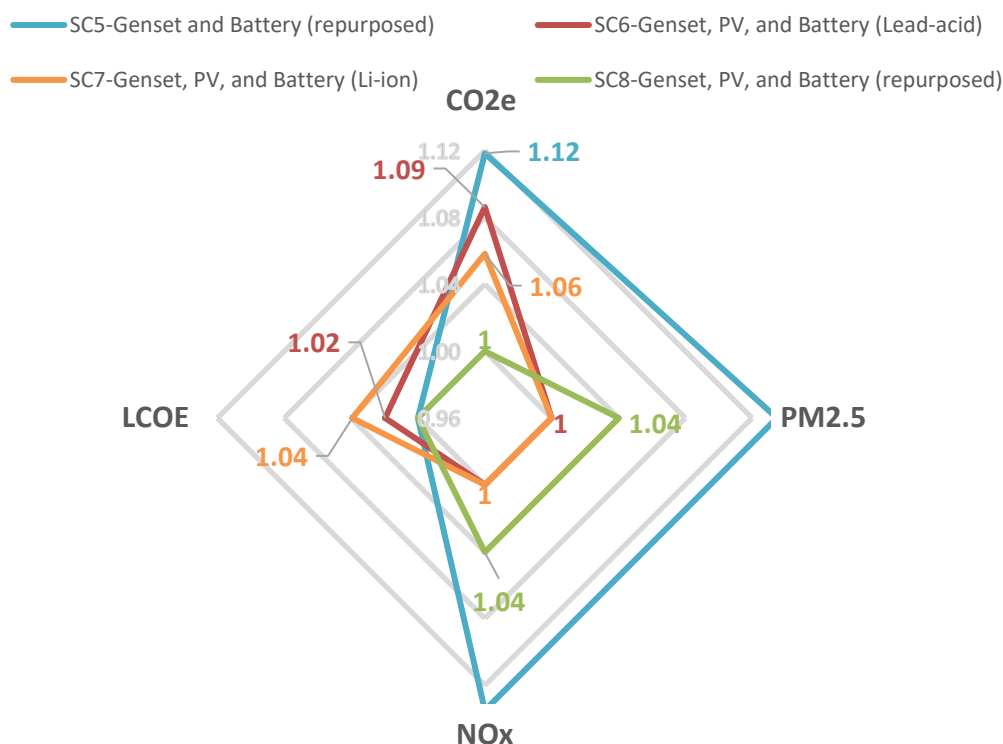


Figure 6-15 Pollutant emissions and LCOE comparison for selected LED scenario hybrid system configurations.

6.4 Summary

This Chapter presented the results of the cost optimisation model implementation for 8 system configurations with 3 electricity demand profiles. The optimisation was done for the baseline scenario, where a high PV share, a regular PV performance, a high PV Installation cost, a high BESS capacity, and a tank-to-wheel pollutant assessment were selected. For each system configuration, the optimum diesel generator was assessed in section 6.2.1, the main findings are listed below:

- More than one diesel generator was needed to prevent a low load operation of most of the selected gensets in the systems without BESS (SC1 and SC2) in the three electricity demand profiles. Also, more than one diesel generator was needed in the high electricity demand profile when using the SC8-Genset, PV, and Battery (repurposed). Using more than one diesel generator prevents excessive fuel consumption that might lead to higher pollutant emissions.
- From the genset selection in SC1 and SC2, the smallest genset (G1) had to operate below 60% of the engine's prime power, and the lowest operating loads detected (HED: 32%, MED: 20%, and LED: 15%) occurred at 5 am in SC2. In all the low load operating periods the low

operation was needed, despite breaching the recommended limit, to match the electricity demand at all times, as represented by the overlapped Total Power Generation and Total Load curves shown in Figure 6-1 and Figure 6-2. The overlapped curves reflect a proper optimisation process where no overgeneration occurs, thus preventing any electrical complication in the system, such as a blackout incident.

- For the system configurations with genset and BESS (SC3, SC4, and SC5) the lowest engine operating load detected was always at or above 60% of the engine's prime power. It was observed that the best performance was achieved using a Li-ion battery (SC4) for the three electricity demand profiles.
- In the hybrid systems (genset, PV, BESS) the engine load was also at or above 60% of the engine's prime power for the three electricity demand profiles. However, it was observed that the best performance was achieved with the Li-ion battery in the high electricity demand case, whereas for the medium and low electricity demand profiles, it was achieved with the repurposed and Lead-acid batteries, respectively.

The main findings from the fuel consumption and pollutant emissions comparison carried out for the 8 optimised system configurations presented in section 6.2.2 can be summarised as follows:

- The highest fuel consumption and CO_{2e} emissions were found in SC1 for the three electricity demand profiles. The latter was attributed to the fact that in SC1 the load is only supplied by the diesel generators, hence more fuel is required, which in turn produces more CO_{2e} emissions compared to the other 7 system configurations. In contrast, the lowest fuel consumption and CO_{2e} emissions were found in the SC7 for the HED and MED profiles, whereas for the LED profile, the best results were found with SC8.
- Similarly, the highest PM_{2.5} and NO_x emissions were found with SC1 in the three electricity demand profiles. The best values for these pollutants were found in SC7 for the HED profile, in SC7 and SC8 for the MED profile, and in SC6 and SC7 for the LED profile. The higher pollutant emissions produced by SC1 were attributed to the overall genset size (from the 3 selected gensets) and the total operating hours of the generators.
- For all the system configurations COD0 was the fuel selected, the selection was attributed to the PM_{2.5} emission costs given that the blends with higher castor oil content produce higher PM_{2.5} emissions, compared to COD0. It should be noted that the fuel consumption and the pollutant

emission calculations for the blends with a castor oil content above 40% may have been altered by the deposits found in the fuel injector. In Chapter 4 it was discussed that the deposit formation was suspected to start during the COD40 engine tests. Therefore, the presence of the deposits altered the combustion process, leading to increased fuel consumption and higher PM_{2.5} emissions. Also, it must be mentioned that for finding the castor oil emission factor ($EF^{biofuel}$) that was used to determine the blend emission factor (bEF_{bld}), as presented in Chapter 5, a fitted curved was used. Using the fitted curve for estimating $EF^{biofuel}$ may have led to uncertainty on the real castor oil emission factor. Therefore more experimental data would be needed for improving the accuracy of the emission factor.

The main findings from the economic assessment done of the 8 system configurations for a 25-year analysis period, included in section 6.3, are:

- The highest LCC values were found in SC2, the high values were attributed to the fuel consumption costs plus the PV initial investment. On the other hand, the lowest LCC values were found in SC8.
- The best LCOE value (0.47 £/kWh) for the high electricity demand appeared in SC5. For the medium electricity demand, the best LCOE value (0.48 £/kWh) was found in SC4 and SC8. And for the low electricity demand profile, the best LCOE (0.52 £/kWh) was found in SC5 and SC8. It was found that the LCOE values reported for the hybrid systems in this work are close to the LCOE value reported by [240] (0.55 USD/kWh). It was also found that the LCOE value determined for SC1 is within the LCOE range (0.40 to 2 USD/kWh) reported for diesel mini-grids in Tanzania [241].

Finally, the LCOE vs emissions analysis that was done on the systems of each electricity demand profile suggested that:

- With a high electricity demand, if the financial benefit is prioritised, SC5 should be selected; but if the environmental benefit is prioritised, then SC7 is the best option.
- With a medium electricity demand, SC8 should be selected when the financial benefit is prioritised, and SC7 is the best option when the environmental benefit is prioritised.
- With a low electricity demand, SC8 is the best option as it gives the best values for the economic and environmental benefits.

In the coming chapter, a further analysis (scenario and sensitivity analyses) of the selected configurations with the major environmental benefit (HED: SC7, MED: SC7, and LED: SC8), according to the LCOE vs emissions analysis included in this chapter will be presented.

Chapter 7

Scenario and Sensitivity Analyses for Selected Microgrid Systems.

In the cost optimisation model implementation results presented in Chapter 6, eight microgrid system configurations were compared to determine the convenient system, when considering financial and environmental aspects. The comparison was done assuming baseline optimisation scenario input conditions for three Tanzanian electricity demand profiles and one system configuration was chosen as the best option per electricity demand profile (HED: SC7, MED: SC7, LED: SC8).

In this chapter, further analysis of each selected configuration is included. The focus of the chapter is to analyse the impact that varying some of the baseline optimisation input conditions and certain economic parameters have on the genset and fuel type selection, the genset performance, and the LCOE. For this purpose, the chapter presents the results of the scenario and sensitivity analyses done on the three configurations previously selected per electricity demand profile. The sensitivity analysis results were compared against the conventional system configuration (SC1, diesel only) to highlight the potential benefits of including renewable energy and battery energy storage systems (BESS) in the microgrid configuration.

7.1 Baseline Optimisation Scenario Review

In Chapter 6 it was explained that the baseline optimisation scenario was done considering a high PV share, a regular PV performance, a high PV cost, a high battery capacity, and the tank-to-wheel pollutant emissions assessment. Table 7-1 summarises the findings from the baseline optimisation scenario for SC1 and the configurations with the major financial and environmental benefits per electricity load profile. Note that in the LED profile, SC8 represents both, the major financial and environmental benefits. Although the conventional system configuration (SC1) presents the highest pollutant emissions in the three electricity demand profiles, it was included for comparison purposes. The findings from SC1 are also useful to exemplify the importance of using more than one diesel generator to avoid oversized generators that might operate at very low loads, depending on the electricity demand.

Table 7-1 Summary of the baseline optimisation scenario findings for three electricity demand profiles.

	High Electricity Demand			Medium Electricity Demand			Low Electricity Demand	
	SC1-Genset ¹	SC5-Genset and Battery (repurposed) ²	SC7-Genset, PV, and Battery (Li-ion) ³	SC1-Genset ¹	SC8-Genset, PV, and Battery (repurposed) ²	SC7-Genset, PV, and Battery (Li-ion) ³	SC1-Genset ¹	SC8-Genset, PV, and Battery (repurposed) ⁴
Genset Selection	G1, G2, G3	G4	G3	G1, G2, G3	G3	G3	G1, G2, G3	G2
Fuel Blend Selection	COD0	COD0	COD0	COD0	COD0	COD0	COD0	COD0
Lowest Genset Power Factor [% of prime power]	49	60	100	32	96	88	23	60
BESS Capacity [kWh]	-	137	136	-	99	98	-	62
Fuel Consumption [l/y]	31504.4	27221.5	25074.3	23166.6	17858.7	17726.7	16698.8	12655.3
CO_{2e} Emissions [kg/y]	79149.4	68389.4	62994.9	58202	44867	44535.3	41952.8	31794.3
PM_{2.5} Emissions [kg/y]	214.708	150.587	145.247	164.831	103.748	103.748	135.316	74.4542
NO_x Emissions [kg/y]	1502.95	1054.11	1016.73	1153.82	726.233	726.233	947.21	521.179
LCC [£]	541715.26	461186.82	462870.17	425044.64	328786.48	331368.08	319772.94	230541.23
LCOE [£/kWh]	0.72	0.47	0.49	0.8	0.48	0.49	0.91	0.52

¹ Conventional SC, ² Financial Benefit SC, ³ Environmental Benefit SC, ⁴ Financial and Environmental Benefit SC.

7.2 Scenario Analysis

To investigate the impacts of varying the optimisation input conditions on the baseline optimisation scenario results, found for the system configurations with the major environmental benefit of each electricity demand profile (HED: SC7, MED: SC7, LED: SC8), the inputs of the cost optimisation model highlighted were modified as shown in blue font in Table 7-2. The model inputs correspond to the values specified in the scenario description given in Chapter 5, where TTW stands for tank-to-wheel and WTW stands for well-to-wheel pollutant emission assessment. For each scenario, only one variable was modified at a time to assess the individual impact compared to the baseline optimisation conditions. The findings for each electricity demand profile are included in the coming subsections.

Table 7-2 Cost optimisation model inputs required for the scenario analysis.

Optimisation Scenario	Cost Optimisation Model Inputs				Pollutant Emissions Assessment
	PV Share	PV Performance	PV Cost	Battery Energy Storage System Capacity	
Baseline	High	Regular	High	High	TTW
Moderate PV Share	Medium	Regular	High	High	TTW
Low PV Share	Low	Regular	High	High	TTW
Optimistic PV Performance	High	High	High	High	TTW
Pessimistic PV Performance	High	Low	High	High	TTW
Moderate PV Cost	High	Regular	Medium	High	TTW
Low PV Cost	High	Regular	Low	High	TTW
Moderate BESS Capacity	High	Regular	High	Medium	TTW
Low BESS Capacity	High	Regular	High	Low	TTW
Well to Wheels	High	Regular	High	High	WTW

7.2.1 High Electricity Demand Profile with SC7-Genset, PV, and Battery (Li-ion).

In the high electricity demand profile with SC7-Genset, PV, and Battery (Li-ion), it was found that the genset selection was not affected by the PV attributes (share, performance, or cost), but by changing the high BESS capacity to a medium or low capacity, a bigger genset (G4) was needed instead of G3. However, the fuel selection was not affected, and diesel was still the preferred option (see Table 7-3).

Regarding the genset's performance or genset load factor, as defined in Chapter 6, it was important to compare how the variation of the optimisation inputs altered the genset's power profile. Figure 7-1 shows the load demand and power generation by source diagrams of the baseline scenario and each scenario where the genset's power generation was modified, relative to the baseline scenario. It was observed that with a moderate PV share, the genset performance decreased by 27% at 14:00 hrs (see Figure 7-1b), whereas, with a low PV share,

the performance only decreased by 7% at 9:00 (see Figure 7-1c). The smaller reduction in the performance of the diesel generator with a low PV share, compared to the moderate PV share can be attributed to the operating period at which the genset reduced its power generation. From Figure 7-1b and Figure 7-1c it can be appreciated that with the moderate PV share the reduced power occurred at a low demand period, whereas with the low PV share, the low performance was detected during the daylight peak demand. During the daylight peak demand, the genset still provides most of the power, especially considering the small PV contribution. On the other hand, when an optimistic PV performance was assumed, the diesel generator's performance decreased by 20% at 9:00 hrs (see Figure 7-1d), but with a pessimistic PV performance, the generator's power factor dropped by 40% at 8:00 hrs (see Figure 7-1e). The observed reduction in performance might be attributed to the power delivered by the BESS, which contributes to reducing the energy generation from the diesel generator. However, when the BESS capacity was reduced (moderate and low BESS), and a bigger generator was required, the performance decreased by 40% in both cases. For the moderate BESS the decreased performance occurred at 9:00 hrs (see Figure 7-1f) and for the low BESS the low performance occurred at 17:00 hrs (see Figure 7-1g). In these two scenarios, the low performance of the diesel generator might be attributed to the reduced power required to charge the BESS in combination with having a bigger genset.

Table 7-3 summarises the high electricity demand profile scenario findings as a percentage variation from the baseline scenario, "No change" was reported for all the cases where no variation was observed. The numbers from the table suggest that more fuel was consumed when the moderate and low PV share were considered, whereas the opposite trend was observed for the reduced BESS configurations. Finally, it should be noted that the LCOE could increase up to 4% with a pessimistic PV performance, but it can be reduced up to 6% with a low PV cost or a moderate BESS. In Table 7-4 the specific findings from each scenario were included for completeness of data visualisation.

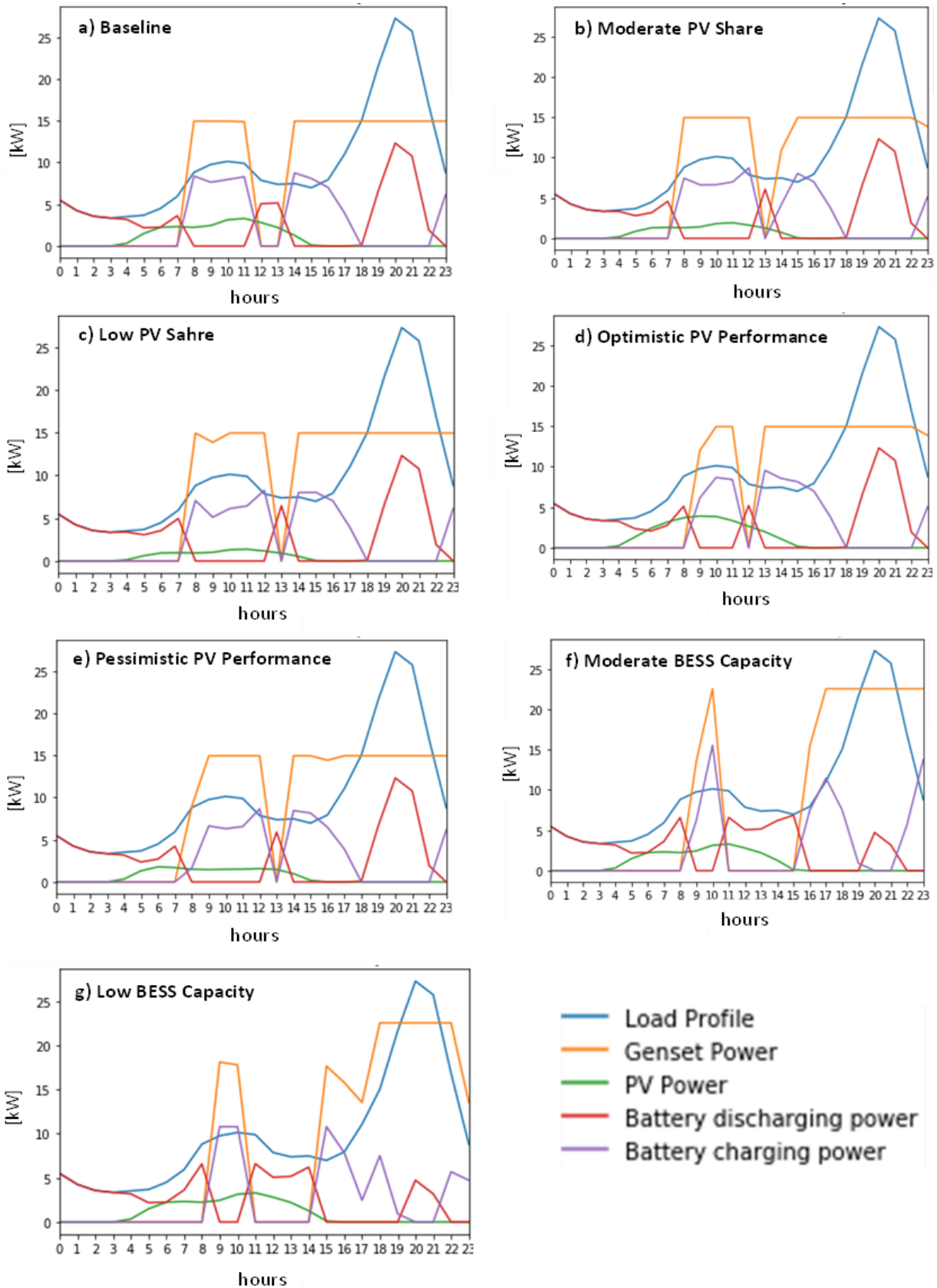


Figure 7-1 Load demand and power generation by source diagrams of selected scenarios (a) Baseline, b) Moderate PV Share, c) Low PV Share, d) Optimistic PV performance, e) Pessimistic PV Performance, f) Moderate BESS Capacity, and g) Low BESS Capacity) from the scenario analysis of the high electricity demand profile with SC7-GensetPV, and Battery (Li-ion).

Table 7-3. Summary of the high electricity demand profile scenario analysis reported as percentage variation from the baseline scenario.

Optimisation Variables	Baseline Scenario	Moderate PV Share	Low PV Share	Optimistic PV Performance	Pessimistic PV Performance	Moderate PV Cost	Low PV Cost	Moderate BESS Capacity	Low BESS Capacity	Well to Wheels	
Genset Selection	G3	No change						G4	G4	No change	
Fuel Blend Selection	COD0	No change									
Lowest Genset Performance [% of prime power]	100	↓ 27%	↓ 7%	↓ 20%	↓ 40%	No change		↓ 40%	↓ 40%	No change	
BESS Capacity [kWh]	136	No change						81	54	No change	
Fuel Consumption [l/y]	25074	↑ 5%	↑ 7%	↓ 2%	↑ 4%	No change		↓ 3%	↓ 3%	No change	
CO ₂ e Emissions [kg/y]	62995	↑ 5%	↑ 7%	↓ 2%	↑ 4%			↓ 3%	↓ 3%	↑ 24%	
PM _{2.5} Emissions [kg/y]	145	↑ 7%	↑ 7%	No change				↑ 7%	↓ 6%	↑ 4%	No change
NO _x Emissions [kg/y]	1017	↑ 7%	↑ 7%	No change				↑ 7%	↓ 6%	↑ 4%	
LCC [£]	462,870.17	↑ 2%	↑ 2%	↓ 1%	↑ 5%	↓ 1%	↓ 4%	↓ 1%	↓ 1%	No change	
LCOE [£/kWh]	0.49	↑ 2%	No change	↓ 2%	↑ 4%	↓ 2%	↓ 6%	↓ 6%	No change	No change	

Table 7-4 Summary of the high electricity demand profile scenario analysis findings.

Optimisation Variable	SC7-Genset, PV, and Battery (Li-ion)									
	Baseline Scenario	Moderate PV Share	Low PV Share	Optimistic PV Performance	Pessimistic PV Performance	Moderate PV Cost	Low PV Cost	Moderate BESS Capacity	Low BESS Capacity	Well to Wheels
Genset Selection	G3	G3	G3	G3	G3	G3	G3	G4	G4	G3
Fuel Blend Selection	COD0	COD0	COD0	COD0	COD0	COD0	COD0	COD0	COD0	COD0
Lowest Genset Performance [% of prime power]	100	73	93	80	60	100	100	60	60	100
BESS Capacity [kWh]	136	136	136	136	136	136	136	81	54	136
Fuel Consumption [l/y]	25074	26332	26758	24654	26183	25074	25074	24259	24445	25074
CO₂e Emissions [kg/y]	62995	66154	67224	61938	65780	62995	62995	60948	61415	78287
PM_{2.5} Emissions [kg/y]	145	156	156	145	156	145	145	137	151	145
NOx Emissions [kg/y]	1017	1089	1089	1017	1089	1017	1017	958	1054	1017
LCC [£]	462,870.17	473,383.13	471,685.83	459,438.34	485,103.30	456,312.00	449,753.95	444,837.14	458,601.52	463,909.95
LCOE [£/kWh]	0.49	0.50	0.49	0.48	0.51	0.48	0.47	0.46	0.49	0.49

7.2.2 Medium Electricity Demand Profile with SC7-Genset, PV, and Battery (Li-ion).

In the medium electricity demand profile with SC7-Genset, PV, and Battery (Li-ion), it was found that the genset and fuel selection remained unchanged in all the scenarios, compared to the baseline scenario. However, it was observed that most of the scenarios lead to an increase in fuel consumption, pollutant emissions and LCOE (up to 6%), compared to the baseline scenario. The increase in these three parameters could be attributed to the low battery power contribution during the night peak demand (see Figure 7-2), which required more power from the genset to match the electricity demand. It was noticed that in this profile the genset performance had less reduction, compared to the HED profile, as it was found that the genset performance was only reduced up to 20% relative to the baseline value (see Table 7-5). The latter can be attributed to the fact that no bigger generator was needed, even when the BESS system was reduced, and because the baseline genset performance was 88% instead of 100% as reported for the HED profile baseline scenario. Figure 7-2 shows the power demand and power generation by source diagrams of the baseline scenario and each scenario where the genset's power generation was modified, relative to the baseline scenario. In Figure 7-2a it can be observed that in the baseline scenario, the genset operated at its lowest performance (88%) at 22:00 hrs when the night peak was decreasing although the battery was being charged. In contrast, with the Moderate PV Share, the lowest performance (73%) occurred at 18:00 hrs (see Figure 7-2b), when the battery started to supply energy for peak shaving and less power was needed from the diesel generator. Similar behaviour was observed at 11:00 hrs when the power contribution of the PV system and the battery reduced the genset performance to 74%. In the Low PV Share scenario, the genset had its lowest performance (74%) at 23:00 hrs (see Figure 7-2c), when the night electricity demand decreased, similar to the baseline scenario. With the Optimistic PV Performance, it was found that the generator had its lowest performance (70%) at 15:00 hrs (see Figure 7-2d) during the low demand period between the day and night peak. It was noted that with the combined power from the PV system and the battery, the diesel generator was not required for supplying the peak demand during daylight hours, which reduced the genset's fuel consumption as reported in Table 7-5. In contrast, with the Pessimistic PV Performance the diesel generator had its lowest performance (60%) at 9:00 hrs (see Figure 7-2e) just before charging the battery and supplying the daylight hours peak demand that was not supplied by the PV system. In the Low BESS Capacity scenario, the lowest genset performance (61%) was found at 10:00 hrs (see Figure 7-2f) as a result of the combined power supplied by the PV system and the battery.

Table 7-5 summarises the medium electricity demand profile scenario findings as a percentage variation from the baseline scenario, "No change" was reported for all the cases where no variation was observed. The table shows that the LCOE can be reduced up to 4%

with the low PV cost or the moderate BESS scenarios. The detailed findings of each scenario are included in Table 7-6 for completeness of data visualisation.

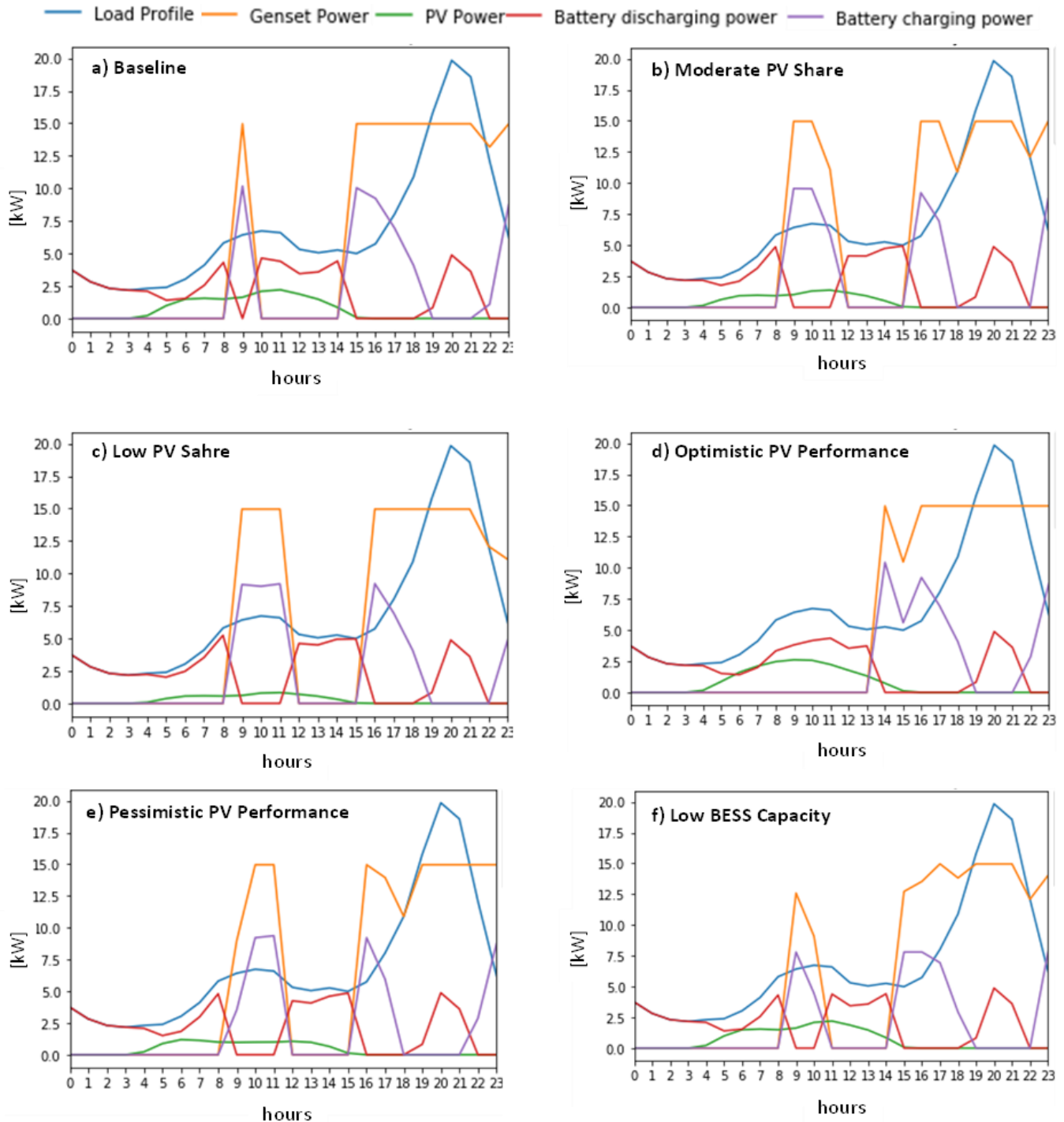


Figure 7-2 Load demand and power generation by source diagrams of selected scenarios (a) Baseline, b) Moderate PV Share, c) Low PV Share, d) Optimistic PV performance, e) Pessimistic PV Performance, and f) Low BESS Capacity) from the scenario analysis of the medium electricity demand profile with SC7-GensetPV, and Battery (Li-ion).

Table 7-5 Summary of the medium electricity demand profile scenario analysis, reported as percentage variation from the baseline scenario.

Optimisation Variables	Baseline Scenario	Moderate PV Share	Low PV Share	Optimistic PV Performance	Pessimistic PV Performance	Moderate PV Cost	Low PV Cost	Moderate BESS Capacity	Low BESS Capacity	Well to Wheels
Genset Selection	G3	No change								
Fuel Blend Selection	COD0	No change								
Lowest Genset Performance [% of prime power]	88	↓ 5%	↓ 4%	↓ 9%	↓ 20%	No change			↓ 19%	No change
BESS Capacity [kWh]	98	No change						59	39	
Fuel Consumption [l/y]	17727	↑ 5%	↑ 7%	↓ 2%	↑ 5%	No change			↑ 1%	↑ 24%
CO _{2e} Emissions [kg/y]	44535	↑ 5%	↑ 7%	↓ 2%	↑ 5%				↑ 1%	
PM _{2.5} Emissions [kg/y]	104	↑ 10%	↑ 10%	No change	↑ 10%				↑ 10%	
NO _x Emissions [kg/y]	726	↑ 10%	↑ 10%		↑ 10%					
LCC [£]	331368.08	↑ 4%	↑ 3%	↓ 1%	↑ 6%	↓ 1%	↓ 3%	↓ 2%	↑ 1%	No change
LCOE [£/kWh]	0.49	↑ 4%	↑ 2%	No change	↑ 6%	↓ 2%	↓ 4%	↓ 4%	↑ 2%	

Table 7-6 Summary of the medium electricity demand profile scenario analysis findings.

Optimisation Variable	SC7-Genset, PV, and Battery (Li-ion)									
	Baseline Scenario	Moderate PV Share	Low PV Share	Optimistic PV Performance	Pessimistic PV Performance	Moderate PV Cost	Low PV Cost	Moderate BESS Capacity	Low BESS Capacity	Well to Wheels
Genset Selection	G3	G3	G3	G3	G3	G3	G3	G3	G3	G3
Fuel Blend Selection	COD0	COD0	COD0	COD0	COD0	COD0	COD0	COD0	COD0	COD0
Lowest Genset Performance [% of prime power]	88	73	74	70	60	88	88	88	61	88
BESS Capacity [kWh]	98	98	98	98	98	98	98	59	39	98
Fuel Consumption [l/y]	17727	18562	18992	17438	18534	17727	17727	17727	17919	17727
CO_{2e} Emissions [kg/y]	44535	46634	47714	43810	46563	44535	44535	44535	45019	55346
PM_{2.5} Emissions [kg/y]	104	114	114	104	114	104	104	104	114	104
NO_x Emissions [kg/y]	726	799	799	726	799	726	726	726	799	726
LCC [£]	331368.08	343577.79	341913.69	329012.96	351107.46	326940.15	322512.3	323352.15	333965.72	332103.14
LCOE [£/kWh]	0.49	0.51	0.5	0.49	0.52	0.48	0.47	0.47	0.5	0.49

7.2.3 Low Electricity Demand Profile with SC8-Genset, PV, and Battery (repurposed)

In the low electricity demand profile with SC8-Genset, PV, and Battery (repurposed), the fuel type and the genset selection remained unchanged compared to the baseline scenario (see Table 7-7). Differently from the previous two electricity demand profiles, in the LED profile, it was found an improvement in the diesel generator's performance in some of the scenarios, relative to the lowest performance (60%) reported for the baseline scenario. Figure 7-3 shows the power demand and power generation by source diagrams of the baseline scenario and each scenario where an improvement of the genset's power generation was found. In the baseline scenario, the lowest performance occurred at two operating periods (9:00 and 14:00 hrs) as shown in Figure 7-3 a. In the first period, the low performance could be attributed to the PV system power contribution, which reduced the power required from the genset. On the other hand, at 14:00 hrs the low performance of the diesel generator can be mostly attributed to the reduced electricity demand and a lesser extent to the PV system power contribution. From the scenarios that showed a better genset performance, it was found that they occurred at different operating periods. Figure 7-3b shows that the lowest performance (68%) in the Moderate PV Share scenario occurred at 10:00 hrs as a result of the PV system and battery power contribution during the daylight peak demand. However, the genset performance during that period was about 14% higher than the baseline scenario because a smaller PV system was considered and more power was required from the genset to match the demand. Similarly, with the Low PV Share scenario, the lowest genset performance (89%) occurred during the daylight peak at 9:00 hrs (see Figure 7-3c). The genset performance at that operating hour was 49% higher than the baseline performance. The 49% increase shows a logical upward trend as there was less contribution from the PV system, therefore more power was needed from the diesel generator to supply the load demand. In contrast, with the Optimistic PV Performance scenario (see Figure 7-3d), no power from the diesel generator was required during the daylight peak and the lowest genset performance (85%) occurred at 16:00 hrs when less power was required to charge the battery. Finally, in the Low BESS Capacity scenario, it was found that the lowest genset performance (76%) occurred at 17:00 hrs (see Figure 7-3e) when the genset started to charge the battery just before the night peak.

Table 7-7 summarises the low electricity demand profile scenario findings as a percentage variation from the baseline scenario, "No change" was reported for all the cases where no variation was observed. The table shows that the scenario with the highest diesel generator performance improvement (49%) was the Low PV Share scenario, as discussed above, which increased the fuel consumption by 7%. The table also shows that for most of the scenarios, the LCOE decreased and the best LCOE (0.49 £/kWh) was found in the Optimistic PV

Performance scenario, which was 6% lower than the LCOE reported for the baseline scenario (0.52 £/kWh).

The detailed findings of each scenario are included in Table 7-8 for completeness of data visualisation.

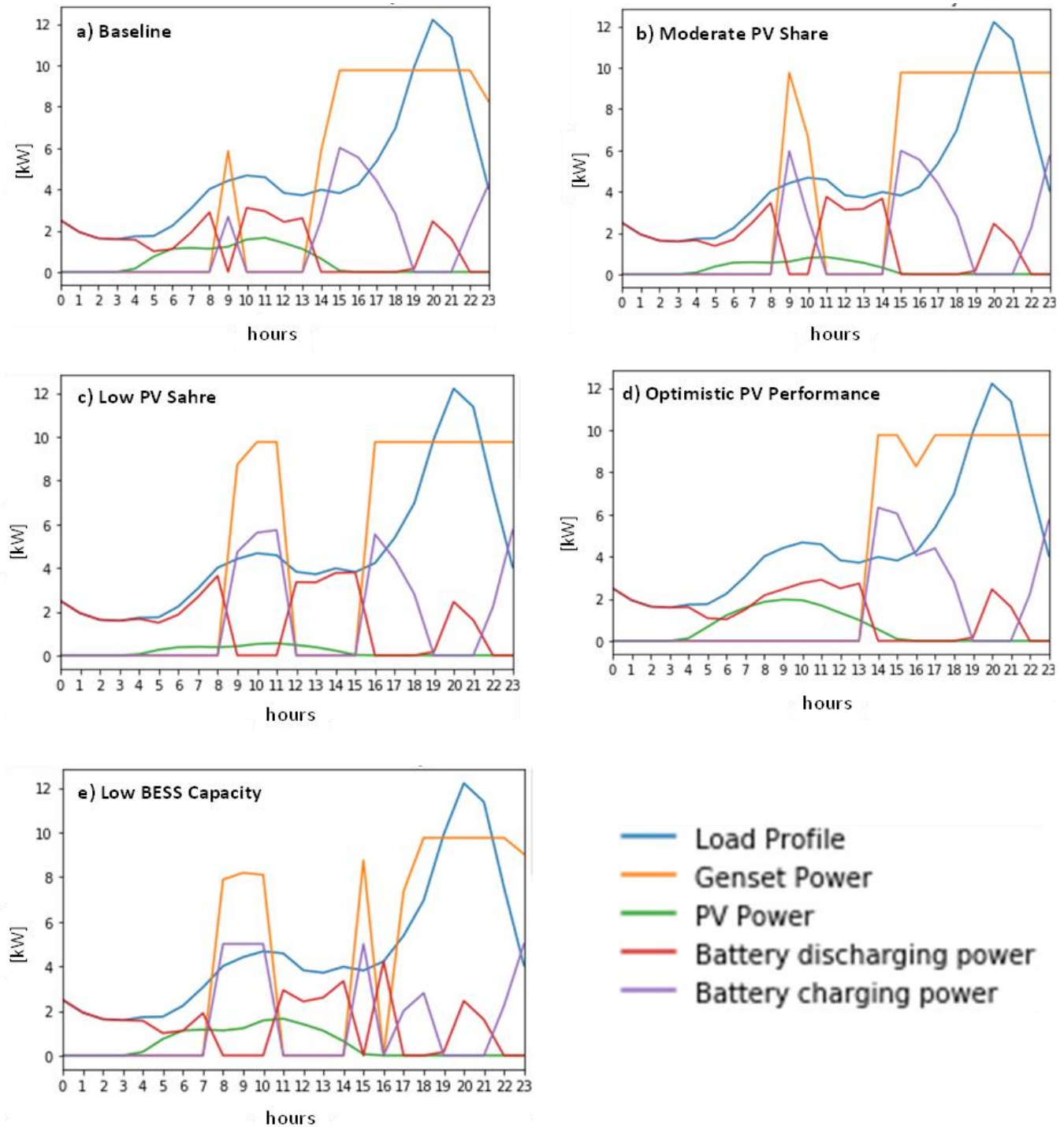


Figure 7-3 Load demand and power generation by source diagrams of selected scenarios (a) Baseline, b) Moderate PV Share, c) Low PV Share, d) Optimistic PV performance, e) Pessimistic PV Performance, and f) Low BESS Capacity) from the scenario analysis of the low electricity demand profile with SC8-Genset, PV, and Battery (repurposed).

Table 7-7 Summary of the low electricity demand profile scenario analysis, reported as percentage variation from the baseline scenario.

Optimisation Variables	Baseline Scenario	Moderate PV Share	Low PV Share	Optimistic PV Performance	Pessimistic PV Performance	Moderate PV Cost	Low PV Cost	Moderate BESS Capacity	Low BESS Capacity	Well to Wheels
Genset Selection	G2	No change								
Fuel Blend Selection	COD0	No change								
Lowest Genset Performance [% of prime power]	60	↑ 14%	↑ 49%	↑ 41%	No change				↑ 26%	No change
BESS Capacity [kWh]	62	No change						37	25	
Fuel Consumption [l/y]	12655	↑ 5%	↑ 7%	↓ 3%	↑ 4%	No Change				↑ 24%
CO _{2e} Emissions [kg/y]	31794	↑ 5%	↑ 7%	↓ 3%	↑ 4%					
PM _{2.5} Emissions [kg/y]	74	No change		↓ 9%	No change					
NO _x Emissions [kg/y]	521			↓ 9%						
LCC [£]	230,541.23			↓ 5%	↑ 2%	↓ 1%	↓ 2%	↓ 2%	↓ 3%	No change
LCOE [£/kWh]	0.52			↓ 4%	↓ 4%	↓ 6%	No change	↓ 2%	↓ 2%	

Table 7-8 Summary of the low electricity demand profile scenario analysis findings.

Optimisation Variable	SC8-Genset, PV, and Battery (repurposed)									
	Baseline Scenario	Moderate PV Share	Low PV Share	Optimistic PV Performance	Pessimistic PV Performance	Moderate PV Cost	Low PV Cost	Moderate BESS Capacity	Low BESS Capacity	Well to Wheels
Genset Selection	G2	G2	G2	G2	G2	G2	G2	G2	G2	G2
Fuel Blend Selection	COD0	COD0	COD0	COD0	COD0	COD0	COD0	COD0	COD0	COD0
Lowest Genset Performance [% of prime power]	60	68	89	85	60	60	60	60	76	60
BESS Capacity [kWh]	62	62	62	62	62	62	62	37	25	62
Fuel Consumption [l/y]	12655	13315	13534	12245	13126	12655	12655	12657	12664	12655
CO₂e Emissions [kg/y]	31794	33451	34001	30764	32977	31794	31794	31798	31816	39512
PM_{2.5} Emissions [kg/y]	74	74	74	68	74	74	74	74	74	74
NOx Emissions [kg/y]	521	521	521	474	521	521	521	521	521	521
LCC [£]	230,541.23	230,747.92	229,948.87	218,612.21	234,383.21	227,710.98	224,880.78	226,389.43	224,451.06	231,066.01
LCOE [£/kWh]	0.52	0.50	0.50	0.49	0.52	0.51	0.51	0.51	0.50	0.52

Finally, for ease of scenarios comparison, Figure 7-4, Figure 7-5, and Figure 7-6 show six optimisation variables (fuel consumption, CO_{2e}, PM_{2.5}, NO_x, LCC, and LCOE), in the form of normalised values, normalised to the corresponding baseline scenario values, for eight of the nine scenarios presented above. The scenarios were ranked from low to high fuel consumption, to identify the scenario with the lowest environmental impact. In the figures, the Well to Wheels scenario was not included as it was shown in previous tables (see Table 7-3, Table 7-5, and Table 7-7) that no change was reported in most of the optimisation variables. However, it is worth noting that, as expected, the highest CO_{2e} pollutant emissions were found in that scenario, for the three electricity demand profiles. The findings show that the emissions increased by 24% compared to the baseline scenario due to the higher fuel emission factor considered, as explained in Chapter 5.

Figure 7-4 shows the scenario ranking for the HED profile. In this profile, the Moderate BESS Capacity scenario had the lowest fuel consumption, whereas the Low PV Share scenario had the highest. The results show that reducing the high battery installed capacity to a moderate capacity reduces the environmental impact generated by fuel consumption, even though a bigger genset (G4) was selected compared to the baseline case (G3). In this case, as the bigger generator was kept operating above the recommended conditions and only operated during higher electricity demand periods, the fuel consumption was optimised, bringing environmental benefits and reducing the overall cost of the system. In contrast, reducing the PV performance and PV share increases the environmental impact as more power was required from the diesel generator, which should operate over longer periods. The latter also impacted the LCOE, especially when the PV show a pessimistic performance. The findings of the HED profile show that the battery system has the highest positive impact on the optimisation variables.

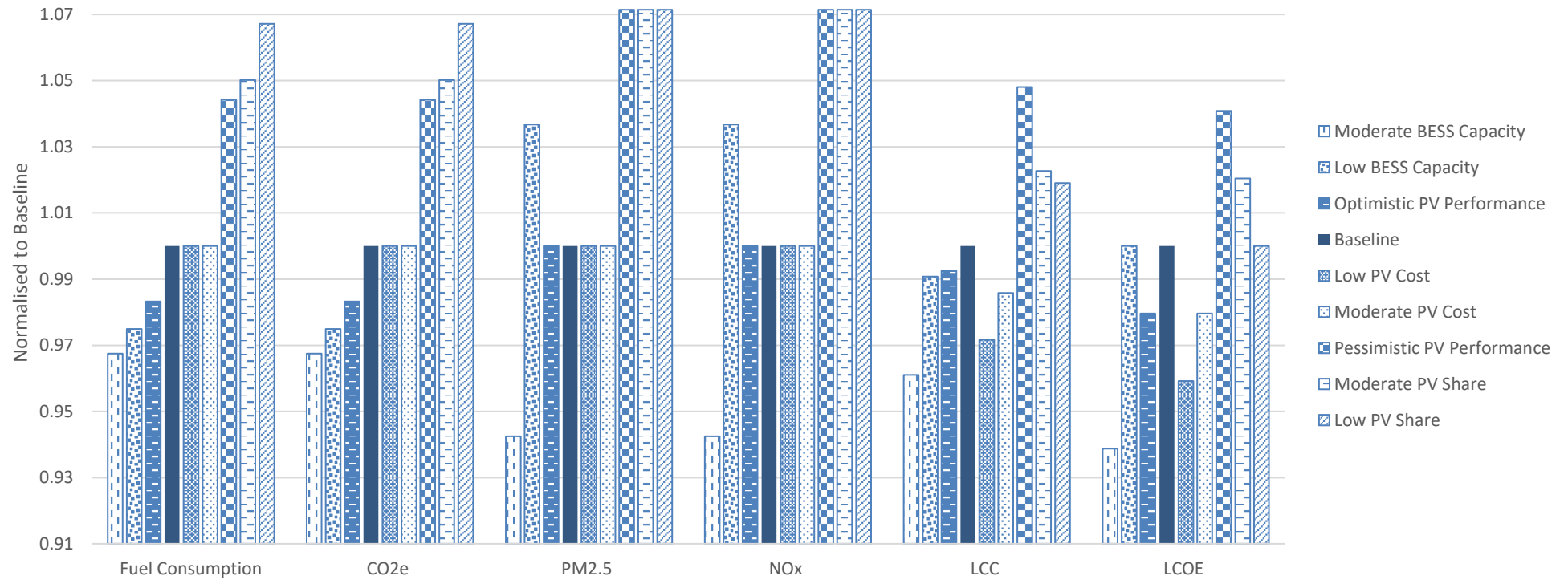


Figure 7-4 Scenario ranking for the high electricity demand profile considering six optimisation variables.

In the MED profile, the lowest fuel consumption was found with the Optimistic PV Performance scenario and the highest corresponded to the Low PV Share scenario as shown in Figure 7-5. It should be mentioned that regardless of the environmental benefit caused by reducing fuel consumption, with the optimistic PV performance, the other pollutant emission remained unchanged. The latter can be attributed to the fact that the same diesel generator was selected in all the scenarios (G3), therefore the size of the genset didn't vary the pollutant emissions. It was noted that the Moderate BESS Capacity scenario reduced the LCOE just as it was reduced with the Low PV Cost scenario. Therefore, in this electricity demand profile, the battery size and the PV have the highest positive impact on the cost of the system but it is the pessimistic PV performance the scenario with the major negative impact on most of the optimisation variables.

Figure 7-6 shows the scenario ranking for the LED profile. In this profile, the lowest and highest fuel consumption was found for the same scenarios as in the previous profile (i.e., lowest: Optimistic PV Performance, highest: Low PV Share scenario). However, with the low electricity demand, although the diesel generator selection remained unchanged across the scenarios (G2), the PM_{2.5} and NO_x emissions were reduced. The reduction in the emission of those pollutants can be attributed to the reduced operating periods of the diesel generator. Therefore, the combined effect of fuel and emissions reductions resulted in lower LCOE and it was concluded that the PV performance (optimistic) had the greatest positive impact on the optimisation variables.

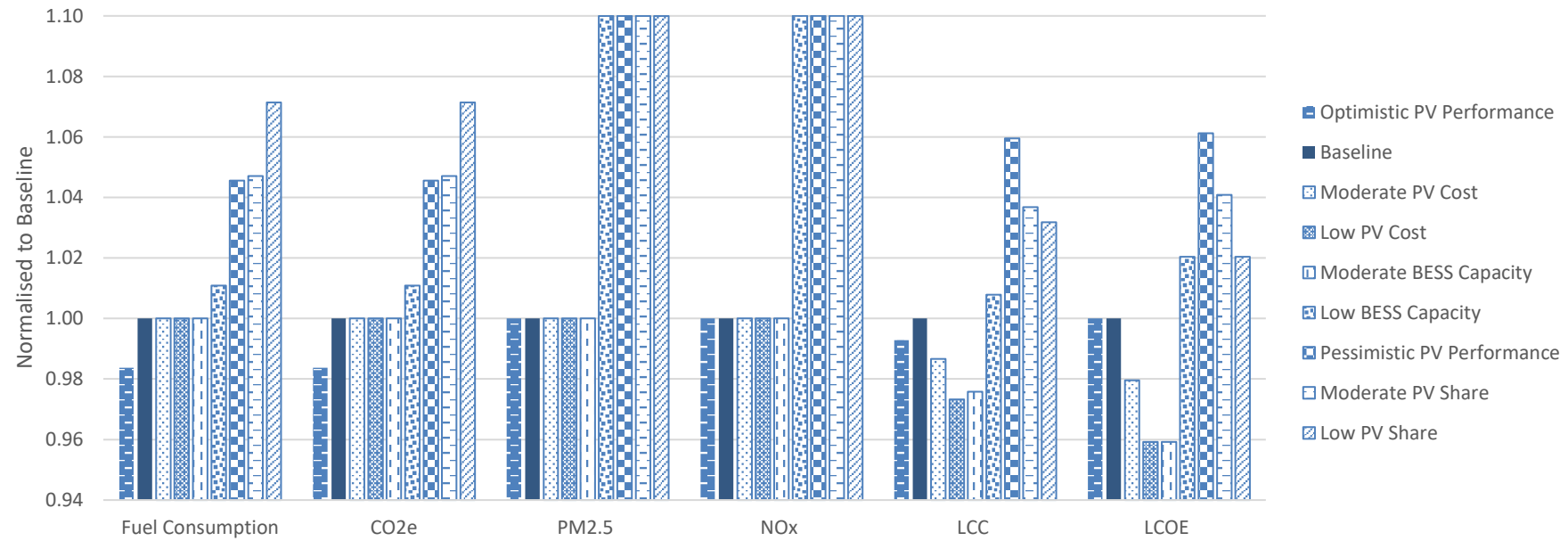


Figure 7-5 Scenario ranking for the medium electricity demand profile considering six optimisation variables.

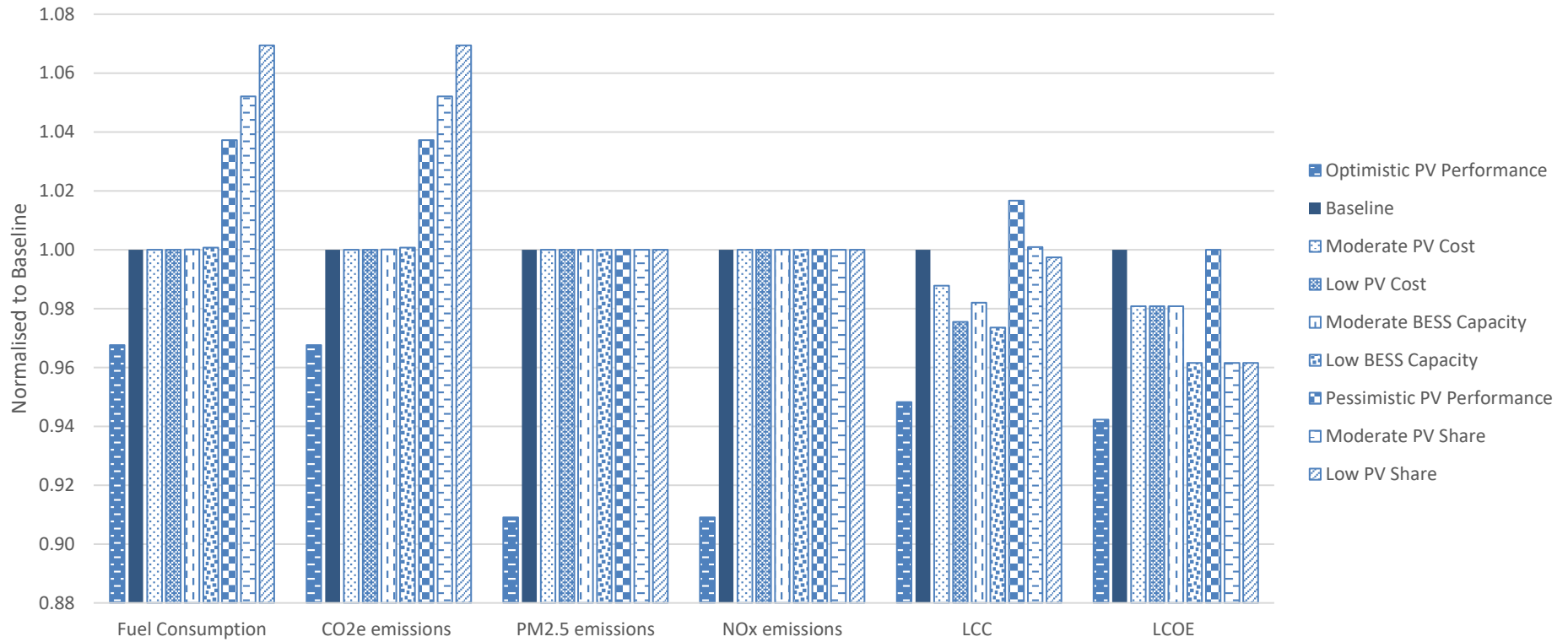


Figure 7-6 Scenario ranking for the low electricity demand profile considering six optimisation variables.

7.3 Sensitivity Analysis

A sensitivity analysis was carried out with the optimisation model using modified diesel prices and pollutant emission costs (carbon tax, PM_{2.5}, and NO_x). The castor oil price was kept constant as it was inferred from the optimisation results that increasing its price would lead to the same fuel selection (COD0), as presented in the optimisation baseline scenario findings. Table 7-9 shows the low and high values used in the sensitivity analysis.

Table 7-9 Sensitivity analysis input values with a brief description.

Modified Parameter	Low Cost	High Cost	
Diesel Price (£/l) *	0.441	1.765	It was considered a 50% reduction (low cost) and a 2 times increase (high cost) from the diesel price reported for Tanzania (.88 £/l) in Chapter 5 (see Table 5-2).
Carbon Tax (£/kgCO _{2e}) *	0	0.1497	It was considered a zero-carbon tax (low cost) and a 20 times increase (high cost) in the current South African carbon tax (9.84 US/tCO _{2e}) which equals the highest existing carbon tax in the world (Uruguay:137.30 US/tCO _{2e}) [214]. The baseline cost was 0.0075 £/kgCO _{2e} as reported in Table 5-2 (see Chapter 5 section 5.1.4).
PM _{2.5} Emissions (£/gPM _{2.5}) *	0	0.1519	It was considered a zero PM _{2.5} emission cost (low cost) and the high cost of 199,630 USD/tonne [216]. The baseline cost was 0.0527 £/g as reported in Table 5-2 (see Chapter 5 section 5.1.4).
NOx Emissions (£/gNOx) *	0	0.0243	It was considered a zero NOx emission cost (low cost) and the high cost of 31,941 USD/tonne [216]. The baseline cost was 0.0089 £/g as reported in Table 5-2 (see Chapter 5 section 5.1.4).

* Prices converted to £ from their original values in USD, considering the average exchange rate history of 1 USD=0.76079 GBP (Dec-May 2022) [221].

The sensitivity analysis was done for the hybrid configurations with the lowest CO_{2e} emissions (HED: SC7, MED: SC7, and LED: SC8) and the corresponding SC1-Genset configuration (conventional diesel genset only) per electricity demand scenario. The selected configurations for the sensitivity analysis are the most representative systems within each scenario that allow a straightforward LCOE comparison between the conventional and the hybrid MG systems optimised in this work.

7.3.1 High Electricity Demand Profile

Figure 7-7 and Figure 7-8 show the sensitivity analysis results for the HED scenario. In the SC1 analysis (see Figure 7-7), it was found that when only one parameter was modified at a time (diesel price, carbon tax, PM_{2.5} emission cost or NO_x emission cost) the scenario with zero-PM_{2.5} cost produced a low LCOE at 0.51 £/kWh. The lower LCOE value with zero-PM_{2.5} emission cost, compared to the LCOE produced by varying the other parameters, can be explained by looking into the operational costs computed in Equation 5-8 presented in Chapter 5. In the equation, by reducing the most expensive emission cost (PM_{2.5}), the operational costs would be reduced, contributing to reducing the overall LCOE. In contrast, the scenario with high NO_x cost gave a higher value of 0.99 £/kWh, regardless of its lower cost compared to the PM_{2.5} cost. The higher LCOE produced with the high NO_x cost can be attributed to the higher emission factor reported in [207], which is about 6 times higher than the PM_{2.5} emission factor. When these two pollutant emission parameters were set to zero (PM_{2.5} and NO_x emission costs) the lowest LCOE (0.32 £/kWh) was found, and this value remained unchanged when the three pollutants' costs were set to zero. The lowest LCOE was produced because no PM_{2.5} or NO_x costs adding up effect was reflected in the operational cost. However, given that the baseline carbon tax (0.0075 £/kgCO_{2e}) is already very low, setting it to zero made no difference to the overall LCOE. It should be noted that even when only the carbon tax was set to zero, almost no variation was observed in the LCOE. As expected, when the pollutant emission costs were set to their highest value, the worst LCOE was found (1.37 £/kWh).

In the SC7 analysis (see Figure 7-8.) a similar trend was found but the best LCOE was 0.27 £/kWh and the highest was 0.86 £/kWh. In both SC, diesel was the preferred fuel selected by the model. It was found that only for the high diesel price and for all the cases where the PM_{2.5} emission cost was set to zero, the fuel blend with 50% castor oil (COD50) was selected. The selection of COD50 for these assumptions can be also explained by looking into the

operational cost (see Equation 5-8) mentioned above. Having a high diesel price or including the $PM_{2.5}$ emission costs would give a high operational cost, but by cutting the diesel by 50%, the operational costs could then be minimised. It was also found that only with the high carbon tax cost, the fuel with 40% castor oil was selected (COD40). For this scenario, when comparing the best LCOE values from SC1 and SC7, installing the hybrid system represents an LCOE reduction of about 16%. But also, when comparing the worst LCOE values from both configurations, the LCOE from the hybrid systems is 37% lower than the LCOE from the conventional system.

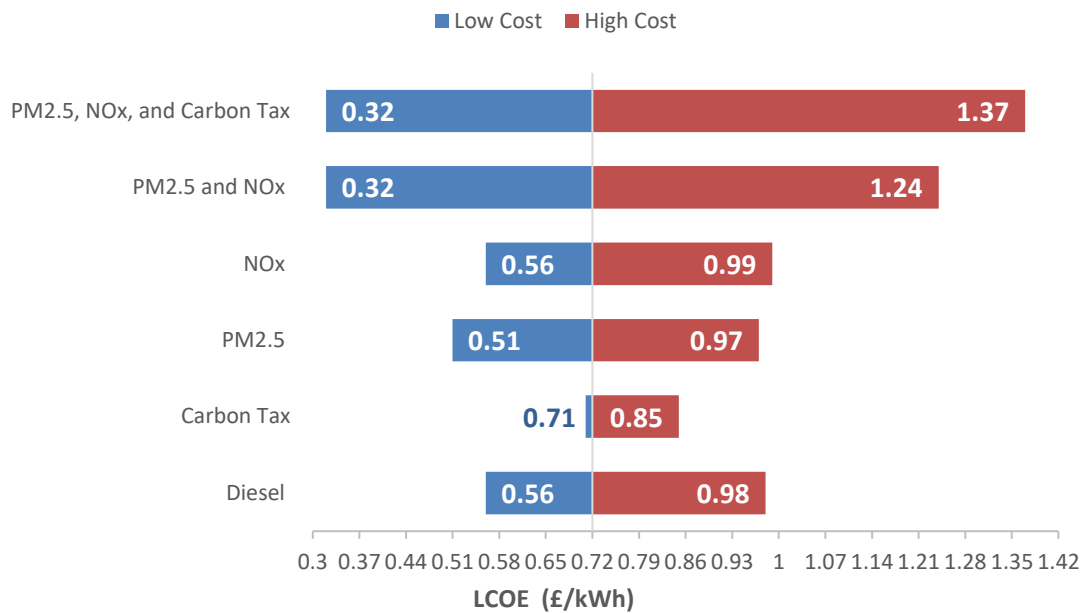


Figure 7-7 Sensitivity analysis for the HED profile with SC1-Genset.

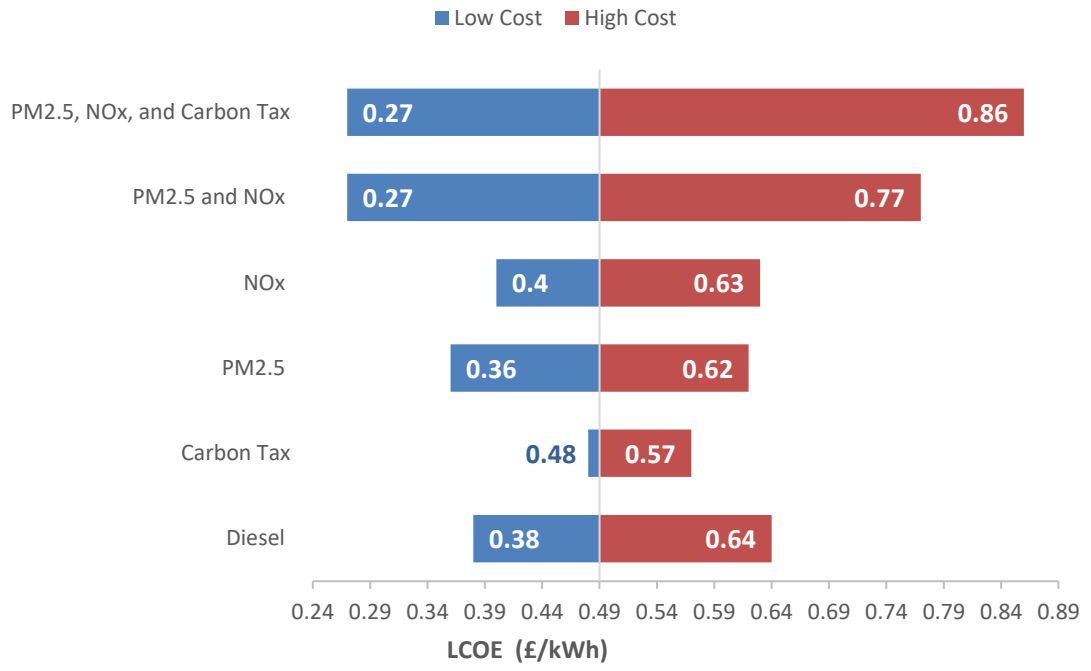


Figure 7-8 Sensitivity analysis for the HED profile with SC7-Genset, PV, and Battery (Li-ion).

7.3.2 Medium Electricity Demand Profile

Figure 7-9 and Figure 7-10 show the sensitivity analysis results for the MED scenario. In the SC1 analysis (see Figure 7-9) a favourable LCOE of 0.57 £/kWh appeared with the zero- PM_{2.5} emission cost and a less favourable LCOE of 1.11 £/kWh appeared with the high NO_x cost when only one parameter was varied at a time. The best LCOE (0.38 £/kWh) and the worst LCOE (1.53 £/kWh) were found when the three pollutants were set to zero and their highest values, respectively. The results for SC7 (see Figure 7-10) show that the best LCOE went down to 0.27 £/kWh whereas the highest LCOE was 0.86 £/kWh. Similarly, to the HED scenario analysis, it was found that COD50 was selected for all the cases with zero cost of PM_{2.5} emissions and high diesel price options; and COD40 was selected when the high carbon tax cost was assessed. For this scenario, when comparing the best LCOE values from SC1 and SC7, installing the hybrid system represents a reduction of about 29%. But also, when comparing the worst LCOE values from both configurations, the LCOE from the hybrid systems is 44% lower than the LCOE from the conventional system.

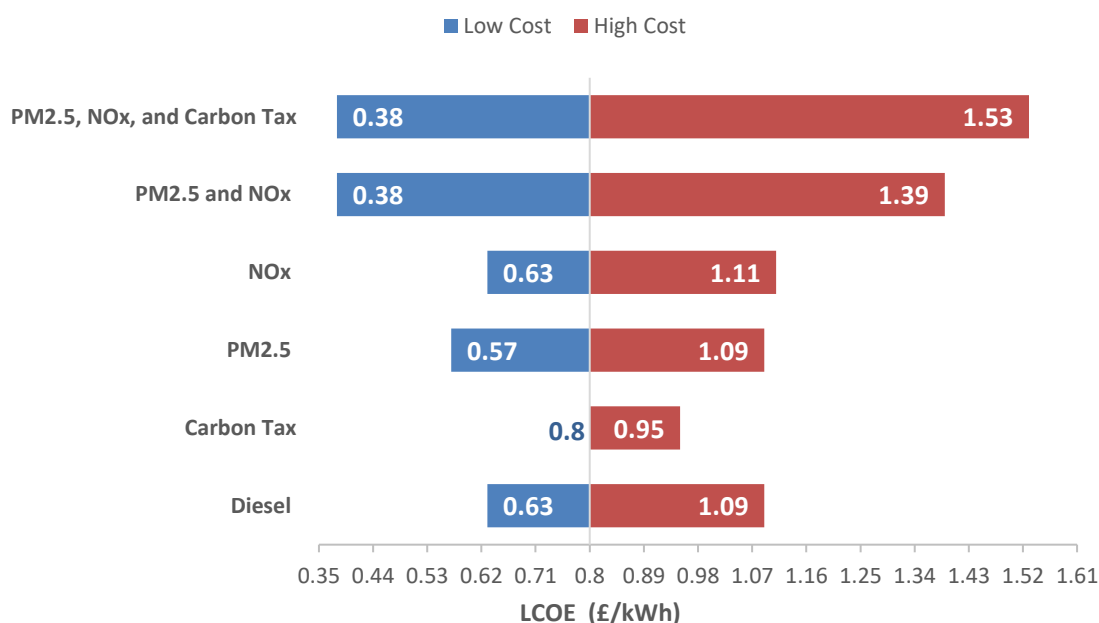


Figure 7-9 Sensitivity analysis for the MED profile with SC1-Genset.

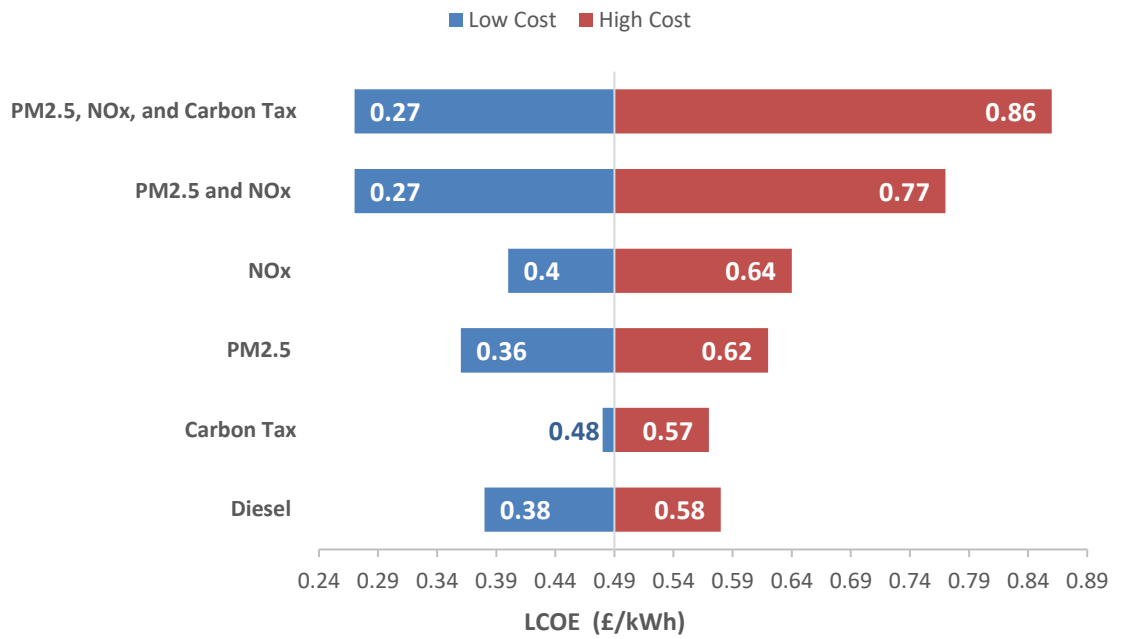


Figure 7-10 Sensitivity analysis for the MED profile with SC7-Genset, PV, and Battery (Li-ion).

7.3.3 Low Electricity Demand Profile

The sensitivity analysis results for the LED scenario are shown in Figure 7-11 and Figure 7-12. In the SC1 results (see Figure 7-11), a favourable LCOE of 0.65 £/kWh appeared with the zero PM_{2.5} emission cost and a less favourable LCOE (1.26 £/kWh) appeared with the high NO_x cost when only one parameter was varied at a time. The best LCOE (0.43 £/kWh) and the worst LCOE (1.74 £/kWh) were found when the three pollutants were set to zero and their highest value, respectively. It should be noted that again, only a small variation was observed in the LCOE when the carbon tax was set to zero. The results for the SC8 (see Figure 7-12) show that the best LCOE was 0.28 £/kWh and the worst LCOE was 0.92 £/kWh. Finally, as in the previous scenarios it was found that COD50 was selected by the model for all the cases where the PM_{2.5} cost was set to zero, and also for the option with the high diesel price. As expected, COD40 was selected with the high carbon tax cost. For this scenario, when comparing the best LCOE values from SC1 and SC8, installing the hybrid system represents a reduction of about 35%. But also, when comparing the worst LCOE values from both configurations, the LCOE from the hybrid systems is 47% lower than the LCOE from the conventional system.

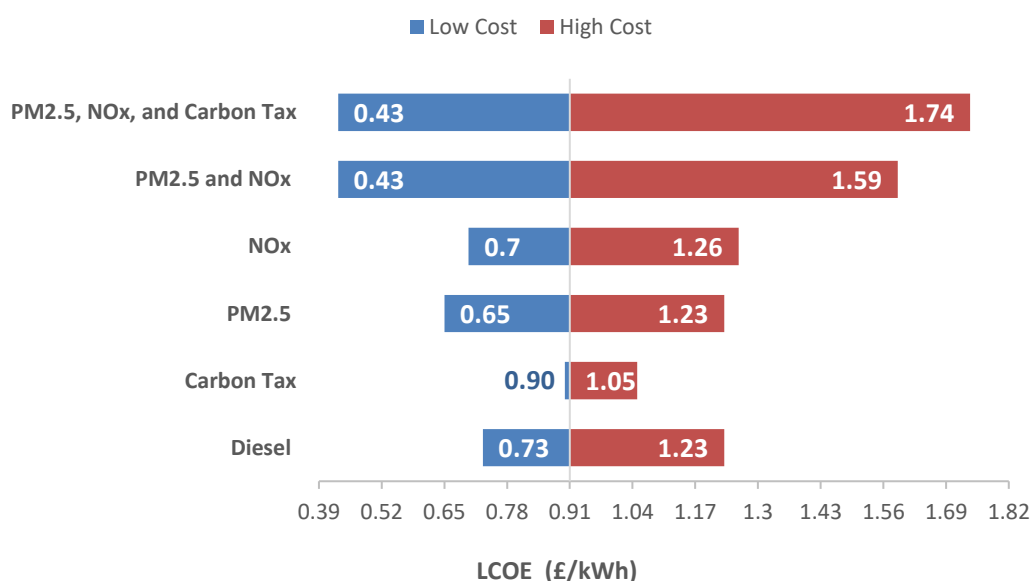


Figure 7-11 Sensitivity analysis for the LED profile with SC1-Genset.

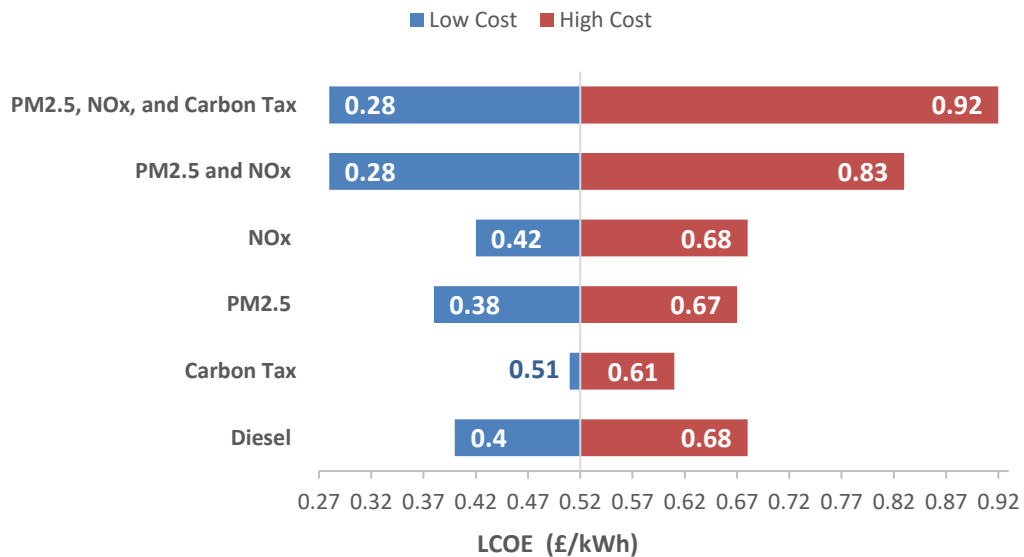


Figure 7-12 Sensitivity analysis for the LED profile with SC8-Genset, PV, and Battery (repurposed).

7.4 Summary

This Chapter presented the scenario and sensitivity analyses findings for the two optimised hybrid microgrid system configurations (SC7 and SC8) compared to the pure diesel genset configuration SC1. SC7 and SC8 are the two hybrid configurations that had the lowest pollutant emissions, therefore were considered as the configurations with the major environmental benefit, according to the analysis presented in Chapter 6, for three electricity demand profiles.

The scenario analysis results were compared against the optimisation baseline scenario results to determine how the variation in the system's PV share, PV cost, PV performance, BESS capacity, and the type of pollutant assessment would affect the genset selection and performance, hence the fuel consumption, the pollutant emissions, and the LCOE per electricity demand profile. The main findings are listed below:

- In the high electricity demand profile, the scenario analysis revealed that when the capacity of the BESS was reduced, a bigger Genset was required to supply the demand. It was observed that when the PV share and performance were decreased, the genset performance (genset load factor) also decreased during daylight hours with low electricity demand or when the PV power contributed to charging the batteries due to less

power being required from the diesel generator. The best values for the pollutant emissions, the fuel consumption and the LCOE were found in the Moderate BESS Capacity scenario, although in that scenario, the genset performance decreased by 40%.

- For the medium electricity demand profile, a bigger genset was not required but it was observed that in 5 out of the 9 scenarios, the genset load factor dropped between 5% and 20% compared to the baseline scenario at specific operating periods. It was noted that the fuel consumption and the CO_{2e} emissions only decreased with the Optimistic PV Performance scenario. In that scenario, no power was required from the diesel generator during the day peak as the electricity demand was supplied by the PV system and the batteries. The best LCOE values were found in two scenarios, the Low PV Cost and the Moderate BESS Capacity.
- A different trend appeared in the low electricity demand profile where the diesel generator's performance increased when the PV share and PV performance were reduced, as well as with the Low BESS Capacity scenario. In this profile, the best values for fuel consumption, pollutant emissions and LCOE were found in the Optimistic PV Performance scenario.

The sensitivity analysis was done for the SC7 and SC8 but also for the SC1 to compare the potential economic benefits of installing hybrid microgrids to replace the conventional systems (diesel generator systems). The sensitivity analysis was also carried out to identify the major factors that determine the fuel type selection and alter the LCOE. To assess the fuel selection and the LCOE variation, the diesel price and the pollutant emission costs (carbon tax, PM_{2.5}, and NO_x) were modified. The main findings across the three electricity demand profiles are as follows.

The fuel selection was affected by the PM_{2.5} cost, for all the cases where the PM_{2.5} emission cost was set to zero, the fuel blend with 50% castor oil was selected. The same fuel was selected when the high diesel price was assumed. However, it was found that with a high carbon tax, the fuel blend with 40% castor oil was selected. Selecting the 40% castor oil fuel instead of the 50% fuel blend can be attributed to the fact that fuel blends with higher castor oil content emit more PM_{2.5} than diesel. Therefore, although selecting COD50 would reduce the carbon emission total cost, the PM_{2.5} total cost would increase, creating an add-up effect in the operational cost, which in turn would produce higher LCOE. The analysis revealed that installing hybrid systems (SC7 for the

HED and the MED profile or the SC8 for the LED profile) gives better LCOE values compared to the corresponding baseline values per electricity profile. In the HED profile, the best LCOE (0.32 £/kWh) found for the SC1 can be reduced by 16% and the worst LCOE (1.37 £/kWh) can be reduced by 37% if the hybrid system is considered. Similarly, in the MED profile, the best LCOE (0.38 £/kWh) found with SC1 could be reduced by 29%, whereas the worst LCOE (1.53 £/kWh) can be reduced by 44% when using a hybrid system. Finally, in the LED profile, the best LCOE(0.43 £/kWh) found for the conventional system could be reduced by up to 35% when using the hybrid system, whereas the worst LCOE (1.74 £/kWh) could be reduced up to 47%.

Chapter 8

Conclusions and Future Work

This research work was dedicated to developing a cost optimisation model to incorporate the effect of biofuels and other factors affecting the performance of diesel generators, to reduce their operating cost and environmental impact when operating in hybrid microgrids, to contribute to the SDG7 in sub-Saharan African rural areas. Special attention was given to assessing the interaction of two major factors that influence the performance of diesel generators, the fuel and the operating load. Improving the interaction between those factors could be translated to better genset sizing for better microgrid planning. The research was divided into three stages, each stage with its corresponding main findings is included after the contribution to knowledge section, followed by the concluding remarks and the recommendations for future work.

8.1 Contribution to knowledge

The contribution of this work relies on the cost optimisation model developed for a diesel-solar-battery hybrid microgrid, which highlights the importance of considering diesel generators as key elements for improving hybrid microgrid planning. The model aimed to minimise the identified consequences of operating oversized diesel generators running at low loads, to reduce their pollutant emissions and operating costs. Moreover, the model included new equations for estimating the fuel consumption of diesel generators considering the effect of castor oil-diesel blends on their performance. The inclusion of those equations enabled the assessment of locally produced vegetable oils that can be used in sub-Saharan Africa hybrid microgrids to reduce diesel consumption and expand rural electrification.

8.2 Stage 1: Fuel Selection and Characterisation.

In the first stage, the selection and characterisation of a biofuel blend were carried out for assessing its physicochemical characteristics and its suitability for diesel substitution and for powering a diesel generator. Castor oil was selected as it is second-generation vegetable oil (from a not food crop), which is locally available in SSA. Castor oil-diesel blends (COD blends) were prepared by blending red diesel with different proportions of castor oil (0%, 20%, 40%, 60%,80%, and 100%) and it was found that:

- The volatility and the net calorific value (NCV) of the fuel decrease as the castor oil increases in the blend. The lower volatility leads to higher onset temperatures of volatilisation (T_{onset}) according to the thermogravimetric (TGA) results presented in Chapter 4. The T_{onset} for COD20 is only 4°C higher than the COD0 T_{onset} (131°C), whereas for COD100 a difference of 231°C was found. The NCV of COD100 (36 MJ/kg) is 18.5% lower than the NCV of COD0 (44.19 MJ/kg).
- The density and kinematic viscosity of the fuel increase as castor oil content increases in the blend. Both properties are temperature-dependent and decrease as temperature increases. The highest density and kinematic viscosity values found for the fuel blends that were used without preheating (COD0, COD20, COD40, and COD50) during the engine tests, corresponded to COD50 and were 8% and 11.75 times higher than the COD0 values. On the other hand, for the only blend with more than 50% castor oil that was used during the engine tests (COD60), the density and viscosity values were 6% and 4.10 times higher than the COD0 values at room temperature. Those values were reported as COD 60 was preheated at 60°C.

8.3 Stage 2: Engine Tests and Pollutant Emissions

During stage 2 several engine tests were carried out to evaluate the impact of the fuel blends on the performance of a 6 kVA diesel generator. Red diesel was first used to determine the baseline parameters and further tests were done with 20%, 40%, 50% and 60% castor oil-diesel blends.

Regarding the performance of the diesel generator, it was determined that:

- The genset output power was slightly lower for the blends with higher castor oil content compared to the output power produced by COD0. The output power reduction was ~1% with COD40 whereas, for COD50 and COD60, the reduction was ~2% and 3%, respectively. No reduction was observed with COD20.
- The mass-based fuel consumption increased with higher castor oil content in the blend. The highest fuel consumption of 1.63 kg/h (with COD60) at 92% engine load was ~14% higher than the fuel consumption with COD0 (1.43 kg/h) at the same load. Operating the engine at 77% load only increased the fuel consumption up to 7% for the blend with the highest castor oil content (COD60). In contrast, at 4% load, using COD60 increased the fuel consumption by 20%, relative to the COD0 values. The higher increase in fuel consumption at 4% engine load, compared to

the increase in fuel consumption at 77% found for COD60, relative to COD0 could be attributed to the lower in-cylinder pressure and temperature that causes incomplete combustion of the fuel, requiring more fuel to be injected.

- The volumetric fuel consumption showed a similar trend to that of the mass-based fuel consumption results. However, it showed an apparent lower percentage fuel consumption increase compared to COD0 at all loads. Using the volumetric fuel consumption may mislead the interpretation of the real fuel consumption if the wrong density values are used, therefore the mass-based fuel consumption was preferred.
- The blends with higher castor oil content had higher specific fuel consumption (SFC) and higher brake specific energy consumption (BSEC), especially at low load engine operating conditions. Therefore, the highest SFC (2.61 kgfuel/kWh) and BSEC (102.33 MJ/kWh) values were found for COD60 at 4% engine load. Those values were 23% and 10% higher than the values found for COD0, respectively. The best SFC and BSEC values for all blends were found at 77% and 92% engine load, where the engine operating conditions allow for better fuel consumption and energy utilisation.
- The maximum brake thermal efficiency (BTE) for all blends occurred at 77% engine load, as shown in the BTE vs load curve presented in Chapter 4. The BTE vs load curve is a second-order polynomial (parabolic curve) whose values show that the maximum BTE for COD0 to COD50 was 31% whereas for COD60 it was 32%.

In terms of pollutant emissions, it was found that:

- The THC emissions increased as the castor oil increased in the blends. With COD0, the THC emissions decreased when the load increased. A similar trend was found for the other blends at 4%, 29%, 50% and 77% engine load. However, at 92% engine load the THC emissions produced by COD20, COD40, COD50, and COD60 were higher than the emissions produced at lower loads. The high emissions at 92% engine load were attributed to the fuel injector's deposits that altered the fuel flow.
- The NO_x emissions produced by COD0 were higher than the emissions produced by the rest of the COD blends at all loads. The highest emissions were found at 92% engine load, where the NO_x emissions produced by COD0 were between 1% and 9% higher than the emissions produced by the other COD blends.
- The PM_{2.5} emissions increased as the engine load increased and with higher castor oil content in the blend. At 92% engine load, the emissions

of the blends with higher castor oil content were between 1.4 and 2.5 times higher than the COD0 emissions. However, it was noted that regardless of the increasing trend in emissions at higher loads, if the engine worked below 50% load, the emissions produced by the blends with higher castor oil can be up to 3.5 times higher (with COD60) than the COD0 emissions.

- From the total particle number comparison done across the fuel blends, two different trends were observed. For COD0 and COD20 it was noticed that the particle number increased when the engine load decreased. Therefore, the highest particle number for these blends was found at 4% engine load, which was 65% and 96% higher than the particle number found at 92% engine load, respectively. On the other hand, for COD40, COD50, and COD60, the particle number decreased when the engine load decreased. Therefore, the lowest particle number for these blends was found at 4% engine load, which was 32%, 72%, and 54% lower than the values found at 92% engine load. Also, it was found that the total particle number increased as the castor oil content increased in the fuel blend. The findings showed that using COD60 increased the particle number by 3 and 10 times compared to diesel at 4% and 92% engine load, respectively.
- The FTIR analyser results revealed the presence of the following unregulated volatile organic compounds: ethylene, methane, acetylene, benzene, ethane, hexane, ethanol, and formaldehyde.
- The use of castor oil-diesel blends during the engine tests leads to the formation of deposits in the fuel injector. The deposits covered one of the five nozzle's holes and it was suspected that their formation started after using COD40. Therefore, it is recommended to preheat castor-oil blends when the blend has more than 20% castor oil fraction, for further viscosity reduction of the fuel blend.

8.4 Stage 3: Cost Optimisation Model Development and Implementation

In this stage, the main objective of this research was addressed by developing a cost optimisation model for improving the performance of diesel generators, operating within hybrid microgrids, considering the effect of biofuel blends. The model was defined as a Mix Integer Linear Problem written in Python and solved using the Gurobi Optimizer, to minimise the cost of investment, operation, maintenance, and part replacement, for a standalone hybrid microgrid. The model was implemented for three electricity demand profiles

(high, medium, and low) for the 8 microgrid system configurations shown in Table 8-1.

Table 8-1 Microgrid configurations considered in the cost optimisation model.

SC1-Genset
SC2-Genset and PV
SC3-Genset and Battery (Lead-acid)
SC4-Genset and Battery (Li-ion)
SC5-Genset and Battery (repurposed)
SC6-Genset, PV, and Battery (Lead-acid)
SC7-Genset, PV, and Battery (Li-ion)
SC8-Genset, PV, and Battery (repurposed)

The relevant aspects of the model development are listed below.

- Diesel generators should operate above 60% engine load or load factor of 0.6 and above for maximum efficiency.
- New fuel consumption equations including various castor oil-diesel blends were generated for widening the fuel options in optimisation processes to assess the performance of diesel generators.
- Although Tanzania has no current carbon tax or pollutant emission cost for PM_{2.5} and NO_x emissions, the three emission factors were included in the optimisation model for accounting for the environmental impact of fuel blends and diesel consumption. For calculating the emission costs, the South African carbon tax and the external costs estimated by IRENA for PM_{2.5} and NO_x emissions were considered, as reported in Table 5-2.
- LCOE was used for the economic assessment of the optimisation findings of the 8 microgrid configurations with three different electricity load profiles (high, medium, and low).
- An LCOE vs emissions analysis was done to determine the configuration with major financial and environmental benefits.
- A graphical user interface was included in the code for ease of optimisation findings visualisation and further data analysis (sensitivity and scenario analyses).

The main optimisation findings for each system configuration with the corresponding electricity demand profile are presented below.

8.4.1 Baseline Optimisation Scenario Findings

The model implementation with the baseline optimisation scenario was done assuming a high PV share, a regular PV performance, a high PV installation

cost, a high BESS capacity, and the tank-to-wheel pollutant emission was considered for the three electricity demand profiles. It was noted that despite the low castor oil price (0.44 £/litre), which is 50% lower than that of diesel (0.88 £/litre), the fuel selected by the model was diesel (COD0) for all the system configurations in the three electricity demand profiles. It was concluded that a very important factor that determined the fuel type selection was the pollutant emission cost. The main findings of each system configuration (SC) are included in the coming subsections.

8.4.1.1 Microgrid without Battery System: SC1-Genset and SC2- Genset and PV

It was found that more than one diesel generator was required to prevent a low load operation of most of the selected gensets in the systems without BESS in the three electricity demand profiles. However, in both systems SC1 and SC2, the smallest genset selected (G1) had to operate below 60% of the engine's prime power. The lowest operating loads were found in the SC2 at 5 am (HED: 32%, MED: 20%, and LED: 15%), followed by the lowest values found in SC1 at 3 am (HED:49%, MED:32%, and LED:23%). The specific low load operation periods were needed for avoiding any overgeneration and preventing a potential blackout incident.

8.4.1.2 Microgrid with Battery Energy Storage System: SC3-Genset and Battey (Lead-acid), SC4-Genset and Battery (Li-ion), and SC5-Genset and Battery (repurposed)

The findings of the three systems with genset and BESS were very dependent on the electricity demand profile.

In the high electricity demand profile, the lowest engine operating load detected was always at or above 60% of the engine's prime power. It was found that using a repurposed battery requires a bigger genset (G4) compared to the genset required (G3) for the systems with Lead-acid or Li-ion batteries. The selection of G4 was attributed to the lower efficiency of the repurposed battery, compared to the Li-ion battery but also its deeper depth of discharge, compared to the Lead-acid battery. Those characteristics of the repurposed battery resulted in less power contribution during the night peak, hence a bigger genset was required. The lowest power factors were 66%, 74%, and 60% for the Lead-acid, the Li-ion, and the repurposed batteries, respectively.

In the medium electricity demand profile, the selected gensets operated above the recommended load factor. The lowest genset performance observed in the system with the Li-ion battery was 96%, whereas, in the other two systems, the

lowest genset performance was 60%. In this electricity demand profile, using a Lead-acid battery required a smaller genset (G2) compared to the other two batteries that required G3 instead.

In a similar trend, when the low electricity demand profile was assumed, the system with the Li-ion battery showed a higher performance (88%) compared to the other two systems (60%) during the periods of low demand. It was found that a bigger genset (G2) was required for the repurposed battery system, whereas with the other batteries, G1 was selected.

8.4.1.3 Hybrid Microgrid (genset, PV, and BESS): SC6-Genset, PV and Battery (Lead-acid), SC7-Genset, PV and Battery (Li-ion), and SC8-Genset, PV and Battery (repurposed)

The findings of the hybrid systems were also dependent on the electricity demand profile.

In the HED profile, it was found that only one genset was required (G3) if a Lead-acid or a Li-ion battery were selected. However, when the repurposed battery was selected, two gensets were needed (G1 and G2) for having a good power-demand matching profile. According to the type of battery selected, the diesel generator had a different performance. With the Lead-acid battery, the genset operated always above the recommended limit, its minimum performance (60%) was found at 16:00 hrs. On the other hand, with the Li-ion battery, the genset operated at 100% during each operating period. It was found that, when the repurposed battery was used, G1 worked at 100% during its operating periods whereas G2 had a performance of 85% at 18:00 hrs. The 85% performance was attributed to the combined power generation as G1 was working at full load.

With the medium electricity demand, it was found that the Lead-acid battery required G2, which had its lowest performance (68%) at 14:00hrs. On the other hand, G3 was selected for the Li-ion and the repurposed batteries. With the Li-ion battery, the lowest genset performance (88%) was observed at 22:00 hrs, whereas with the repurposed system, the lowest value (96%) was found at 17:00 hrs.

Finally, with the low electricity demand profile, it was found that the lowest genset performance was around 60% but at different operating periods (Lead-acid: 23:00 hrs, Li-ion: 09:00 and 15:00 hrs, and repurposed: 09:00 and 14:00 hrs). A similar genset performance was observed regardless of the genset selected for each battery, G2 was selected for the repurposed battery and G1 for the Lead-acid and the Li-ion systems.

8.4.1.4 Microgrid Fuel Consumption and Pollutant Emissions

For the 8 optimised microgrid systems, the fuel consumption and pollutant emissions were compared. It was found that the highest yearly fuel consumption in all the electricity demand profiles corresponded to the SC1 (HED: 31,504.40 l/y, MED: 23,166.60 l/y, and LED: 16,698.80 l/y). In contrast, when the hybrid systems were selected, the fuel consumption was reduced by up to 20% in the HED profile with SC7 (Li-ion battery). Similarly, in the MED profile, the fuel consumption was reduced by up to 23.5% with the SC7, whereas in the LED profile, the reduction was up to 24% when the SC8 was implemented. Correspondingly, due to the fuel consumption, the highest CO_{2e} emissions (HED: 79,149.40 kg/y, MED: 58,202.00 kg/y, and LED: 41,952.80 kg/y) were found in the SC1. Those emissions were reduced by 20%, 23.5%, and 24% in the HED, MED and LED scenarios respectively using the hybrid systems mentioned above for the fuel consumption reduction (SC7 and SC8).

In terms of the other two pollutant emissions (PM_{2.5} and NO_x) the highest values were found in SC1: PM_{2.5} (HED: 214.71 kg/y, MED: 164.83 kg/y, LED: 135.32 kg/y) and NO_x (HED: 1,502.95 kg/y, MED: 1,153.82 kg/y, LED: 947.21 kg/y). However, both pollutants were reduced when the hybrid systems were implemented. In the LED profile, the emissions were reduced by up to 47% with the SC6 or the SC7. In the MED profile, the emissions were reduced by up to 37% with the SC7 or the SC8. Finally, in the HED profile, it was found that the emissions could be reduced by 32% with the SC7.

8.4.1.5 Economic Assessment of 8 Optimised Microgrid Configurations

The economic assessment of the 8 microgrids considered in the cost optimisation model was done using the Life Cycle Cost (LCC) and the Levelized Cost of Energy (LCOE) over a 25-year horizon.

The highest LCC values were found with the SC2 in all the electricity demand profiles (HED: £549,457.78, MED: £427,943.46, and LED: £323,644.75). The high LCC was attributed to the high fuel consumption costs plus the initial investment in PV arrays that do not reduce the diesel generators' operating hours during the night peak. In contrast, the lowest LCC were found in the SC8 for the three profiles (HED: £ 457,929.81, MED: £328,786.48, and LED: 230,541.23). Those values corresponded to 16.7%, 23%, and 28.8% reductions in LCC, respectively, compared to the reference configuration.

The LCOE comparison revealed that in the HED profile, the best LCOE (0.47 £/kWh) was found with the SC5. In the MED profile, the best LCOE (0.48 £/kWh) was found in two configurations, the SC4 and the SC8. Finally, in the

LED scenario, the best value (0.52 £/kWh) appeared in the two configurations with the repurposed battery system (SC5 and SC8).

8.4.1.6 LCOE vs Emissions Analysis of 8 Optimised Microgrid Configurations.

An LCOE vs emissions analysis was done to determine what microgrid configuration represents higher benefits (financial and environmental). The analysis was done by comparing the lowest pollution system in terms of CO_{2e}, NO_x, and PM_{2.5} emissions versus the systems with the lowest LCOE values per electricity demand profile.

For the HED profile it was determined that implementing SC7 might be a convenient choice if the environmental benefit is prioritised as it has the lowest pollutant emissions in kg/y (CO_{2e}: 62,994.90, NO_x: 1,016.73, and PM_{2.5}: 145.25), relative to SC5, which has the lowest LCOE(0.47 £/kWh). Therefore, selecting SC7 represents a 4% increase in LCOE, but selecting SC5 represents an increase in pollutant emissions (CO_{2e}:9%, PM_{2.5}:4%, and NO_x:4%).

For the MED profile, it was determined that if the environmental benefit is prioritised SC7 should be selected, as it has the lowest pollutant emissions in kg/y (CO_{2e}: 44,535.30, NO_x: 726.23, and PM_{2.5}: 103.75). The SC7 configuration only represents a 2% increase in the LCOE value, relative to the lowest LCOE (0.48 £/kWh) found in SC4 and SC8. However, even if the financial benefit is prioritised, SC8 would be an acceptable choice as it only represents a 1% increase in CO_{2e} emissions whereas NO_x and PM_{2.5} remained unchanged compared to SC7.

Finally, for the LED profile, it was determined that SC8 is a convenient choice as it has the lowest CO_{2e} emissions (31,794.30 kg/y) and the lowest LCOE value (0.52 £/kWh), relative to the other systems considered in the analysis (SC5, SC6, and SC7). However, it was noted that the PM_{2.5} and NO_x emissions from SC8 are 4% higher than the lowest values (PM_{2.5}: 71.57 kg/y and NO_x: 500.98 kg/y) found in SC6 and SC7.

8.4.2 Scenario and Sensitivity Analyses Findings for Selected Microgrid Configurations

With the LCOE vs emissions analysis presented earlier, the convenient configurations per electricity demand profile were determined for the baseline optimisation case. It was found that for the HED and MED profiles, SC7 was the configuration with major environmental benefits, whereas, for the LED profile, it was SC8; which also had major financial benefits. For those configurations,

further analysis was done to assess the impact on the genset and fuel type selection, the genset performance, and the LCOE after varying some of the baseline optimisation input conditions and certain economic parameters. The findings on both, the sensitivity and the scenario analyses are shown below.

8.4.2.1 Scenario Analysis for Selected Microgrid Configurations

The variation in the baseline optimisation results was assessed by modifying 5 parameters of the cost optimisation inputs as shown by the scenarios from Table 8-2. In each scenario, only the parameter highlighted in blue was modified.

Table 8-2 Cost optimisation model inputs required for the scenario analysis.

Optimisation Scenario	Cost Optimisation Model Inputs				
	PV Share	PV Performance	PV Cost	Battery Energy Storage System Capacity	Pollutant Emissions Assessment
Baseline	High	Regular	High	High	TTW
Moderate PV Share	Medium	Regular	High	High	TTW
Low PV Share	Low	Regular	High	High	TTW
Optimistic PV Performance	High	High	High	High	TTW
Pessimistic PV Performance	High	Low	High	High	TTW
Moderate PV Cost	High	Regular	Medium	High	TTW
Low PV Cost	High	Regular	Low	High	TTW
Moderate BESS Capacity	High	Regular	High	Medium	TTW
Low BESS Capacity	High	Regular	High	Low	TTW
Well to Wheels	High	Regular	High	High	WTW

For every electricity demand profile, the nine scenarios were evaluated using the selected microgrid configuration (HED: SC7, MED: SC7, and LED: SC8) and the optimisation results were compared against the baseline findings. During the scenario analysis, the optimisation variables listed below were assessed:

- Genset Selection
- Fuel Blend Selection
- Lowest Genset Power Factor [% of prime power]
- BESS Capacity [kWh]
- Fuel Consumption [l/y]
- CO_{2e} Emissions [kg/y]
- PM_{2.5} Emissions [kg/y]

- NO_x Emissions [kg/y]
- LCC [£]
- LCOE [£/kWh]

In the HED profile it was found that for the two scenarios with reduced BESS (medium and low BESS capacity), a bigger genset (G4) was required instead of G3. It was noticed that in all the scenarios, diesel was the preferred fuel option. Regarding the PV share, it was found that with a moderate PV share, the genset performance decreased by 27%, whereas with a low PV share, the performance only decreased by 7%. Similarly, when the Optimistic PV Performance scenario was selected, the performance of the diesel generator decreased by 20% and it dropped by 40% with the Pessimistic PV Performance scenario. It was noted that the LCOE may increase up to 4% with a Pessimistic PV Performance, but it can be reduced up to 6% with a Low PV Cost or a Moderate BESS Capacity. It should be added that the best values regarding the pollutant emissions and the fuel consumption were found in the Moderate BESS Capacity scenario, however, the genset performance was reduced by 40%, relative to the baseline scenario.

In the MED profile, the genset selection (G3) was unchanged throughout the 9 scenarios, however, the genset performance decreased between 4% (Low PV Share scenario) and 20% (Pessimistic PV Performance scenario). It was observed that the fuel consumption and CO_{2e} emissions only decreased by 2% when the Optimistic PV Performance scenario was selected. The best LCOE value (0.47 £/kWh) was found in the Low PV Cost and the Moderate BESS Capacity scenarios, which represent a 4% decrease compared to the baseline scenario LCOE (0.49 £/kWh).

A different trend was found in the LED profile, it was observed that the performance of the diesel generator increased when the PV share and the PV performance were reduced, and also with a low installed battery capacity. The highest value was found when the Low PV Share scenario was selected, the performance was 49% higher relative to the baseline case. Also, in this electricity profile, it was noticed that the LCOE decreased in 7 out of the 9 scenarios, whereas in the other two, it remained unchanged. The best LCOE was found in the Optimistic PV Performance scenario, which was 6% lower compared to the baseline scenario. Finally, it should be added that the best values for fuel consumption and pollutant emissions were also found in the Optimistic PV Performance scenario. The fuel consumption and the CO_{2e} emissions decreased by 3%, whereas the NO_x and the PM_{2.5} emissions dropped by 9%, compared to the baseline values.

8.4.2.2 Sensitivity Analysis for Selected Microgrid Configurations

A sensitivity analysis was done for the configurations with major environmental benefits per electricity demand profile (SC7 and SC8). The analysis was also done on SC1 for comparison purposes and to explore the potential economic benefits of installing hybrid microgrids to replace conventional systems (only diesel generator systems). The sensitivity analysis helped to assess the variation in the fuel selection and the LCOE after modifying the original diesel price and the pollutant emission costs (carbon tax, PM_{2.5}, and NO_x) that were used in the baseline optimisation process. Across the three-electricity demand profile, it was found that:

The model selected the fuel blend with 50% castor oil (COD50) instead of diesel (COD0) in all the cases where the PM_{2.5} cost was set to zero. COD50 was also selected when a high diesel price (£/l 1.765) was assumed. It was observed that the fuel with 40% castor oil (COD40) was selected when the high carbon tax was used in the optimisation process.

In the HED profile, it was found that installing SC7 reduces the LCOE by 16% assuming the zero-emission costs (best case) or by 37% assuming the high emission costs (worst case) compared to the corresponding SC1 values. On the other hand, the LCOE could be reduced by 29% and 44% in the best and the worst cases, respectively, within the MED profile. Finally, in the LED profile, the LCOE could be reduced up to 35% in the best case and up to 47% in the worst case.

8.5 Concluding Remarks

This section summarises the concluding remarks from the three stages of this work.

From Stage 1 it was concluded that castor oil could be considered a viable option for powering diesel generators and increasing electricity access in SSA as it is one of the two non-food crops widely available in the region. Jatropha oil is the other non-food crop available in SSA and although it has a higher oil yield per hectare, compared to castor oil (see Table 3-2) literature already has plenty of studies on this oil. Therefore, for exploring another alternative to diesel substitution from which few studies can be found in the literature, castor oil was selected. The fuel characterisation done to the castor oil-diesel blends (COD0, COD20, COD40, COD50, COD60, COD80 and COD100) confirmed that the higher kinematic viscosity and density of castor oil could be a major drawback to use COD blend in diesel engines. However, using the blends at temperatures

ranging from 40°C to 100°C gives similar viscosity and density values to that of diesel for most of the blends, except for COD80 and COD100. The different composition of castor oil, compared to diesel, especially the higher oxygen content found in castor oil (15.72%) according to the elemental analysis results (see Table 4-3) suggested that higher castor oil content in the blend would impact the combustion process of diesel generators and their pollutant emissions, which were further investigated in Stage 2.

From the results presented in Stage 2 it was concluded that although castor oil would be a viable option to power diesel generators, if blended with diesel, the following aspects should be considered before using COD blends. It was found that COD0, COD20, COD40, and COD50 can be used at room temperature (~30°C) to power the diesel generator producing similar output power as that produced with COD0 at all the engine loads tested, with the exception found at 92% engine load with COD50. At that load, the power produced with COD50 was 4% lower compared to the power produced by COD0. The reduced power suggested that the engine was not receiving the required fuel to maintain the same load as with the other blends. The power reduction was first attributed to the higher viscosity of COD50 compared to COD0, which altered the fuel injection, however, it was later attributed to the deposits found in the fuel injector. Nevertheless, it should be noted that the viscosity might have had a major impact on the reduced power because it was found that with COD60 at the same load, the output power was consistent with the COD0 values. The latter was possible because COD60 was preheated at 60°C, which reduced the blend viscosity to 16.17mm²/s (a lower value than that of COD50 at room temperature). Therefore, even with the existing deposits, when using a blend with lower viscosity, the engine was able to maintain the output power as that produced with diesel. The power output findings were in line with the fuel consumption results that showed that more fuel was used by the engine as the castor oil increased in the blend. The higher fuel consumption was derived from the higher density of castor oil, which led to having more fuel injected, which in turn led to incomplete combustion of the fuel, requiring then more fuel to be injected. As expected, lower fuel consumption was detected with COD50 at 92% due to the lower output power produced, compared to the output power produced by the other fuel blends. A significant finding regarding the output power and the fuel consumption was revealed by the specific fuel consumption (SFC) in gfuel/kWh included in Figure 4-12 and the brake thermal efficiency (BTE) curve (see Figure 4-14). The SFC figure showed that running the engine at low load (4% engine load) would increase the fuel consumption by 8 times compared to the fuel consumption reported at 92% engine load for the

corresponding fuel blend, whereas operating the engine at 77% load would give the best SFC and BTE values for all blends. The higher SFC values agree with the values reported by [118], where the high SFC was attributed to the higher viscosity of vegetable oils compared to the viscosity of diesel. It was concluded then, that according to the SFC and BTE values found, the diesel generator should be operated above 60% engine load.

In this section, it was pointed out that the oxygen content of castor oil plays an important role in the fuel combustion process, which may lead to shorter combustion duration (premixed combustion) and higher combustion temperatures [81], which may impact the pollutant emissions of the diesel generator. The combustion performance results confirmed a shorter ignition delay (ID) for all the blends with castor oil, compared to the ID reported for diesel (COD0). With diesel, the combustion started at 5.5 ± 0.5 CAD, whereas for the other blends the combustion started at 5 ± 0.5 CAD instead. The shorter ID values found for the COD blends agree with the values reported by [179] for fuels with oxygen content between 3% and 9%, but also with the findings reported by [181], where the shorter ID values were attributed to the fatty acid composition of vegetable oils. The effect of the shorter ID was reflected in the heat release rate (HRR) observed for the fuel blends. The HRR findings showed that as less fuel was burned during the premixed combustion when castor oil was included in the blend, a lower peak heat release rate (PHRR) was reported for COD20, COD40, COD50, and COD60, compared to the PHRR found for COD0. The lower PHRR values of the COD blends agree with the findings reported by [188].

One of the major objectives of this work was to improve the performance of diesel generators to reduce their environmental impact, therefore, the pollutant emissions produced by the COD blends were assessed. Three regulated pollutant emissions (CO, HC, and NO_x) were measured with a MEXA Analyser and a single-stage filtration unit was used to measure the other regulated pollutant emission, the particulate matter (PM_{2.5} emissions). The findings showed that higher CO, HC and PM_{2.5} emissions were produced when castor oil was included in the blend. Higher CO and HC emissions were also reported by [242] when using used vegetable oil, maize oil, cotton oil, and their blends with different diesel percentages. The review made by [114] also showed higher CO, HC and PM emissions for some of the vegetable oils and their blends included in their work. Agarwal et al. [129] reported higher CO and HC emissions when using jatropha oil and its blends with diesel. However, the emissions of preheated jatropha oil (at temperatures between 80 °C to 90°C) were close to the emissions produced by diesel due to the similar viscosity

values of the preheated jatropha oil and diesel. Therefore, it may be concluded that although castor oil-diesel blends (COD20, COD40, and COD50) can be used at room temperature to power the diesel generator, preheating each blend (including COD60) to the right temperature to make their viscosity close enough to diesel viscosity, would be beneficial for reducing these pollutant emissions. On the other hand, the NO_x emissions produced by the castor oil-diesel blends were lower than the NO_x emissions produced by diesel at all engine loads, similar results were reported by [114] for some of the vegetable oils included in that review. It should be noted that despite the different trends observed for the 4 pollutants (CO, HC, NO_x, and PM_{2.5}), their specific emission (EI) in g/kWh found for each blend was reduced when the engine operated at or above 50% engine load. The latter supports the previous recommendation of operating the diesel generator above 60% engine load for having the best engine performance and fewer pollutant emissions.

Another important conclusion of this stage was that the VOCs emitted by the castor oil-diesel blends could be attributed to the high viscosity and oxygen content of the blends as it was observed that the VOCs emissions increased as the castor oil content increased in the fuel blend. Those findings agree with the trends shown by other authors [197-199] that studied the effect of using vegetable oils and biodiesel derived from vegetable oils to fuel diesel engines.

Finally, from the findings presented in stage 2, it was concluded that preheating the castor-oil diesel blends would also be required for preventing the fuel injector deposits. Although the deposits were suspected to appear after using the fuel blend with 40% castor oil, it cannot be ignored that castor oil is highly viscous. Literature shows that castor oil is about 7 times more viscous than jatropha oil but about 74 times more viscous than diesel at 40°C (see Table 3-3), therefore, the deposits might as well have started after running the COD20 engine tests. Regardless of the specific moment at which the deposits may have started, the conclusion is that preheating the blends would bring benefits if vegetable oil-diesel blends are to be used in diesel engines. Moreover, it would be required to adopt a maintenance schedule to control carbon deposits as suggested by [129]. Adopting such a maintenance schedule may reduce the practicality of using vegetable oils but more engine tests should be done to determine if the maintenance would be required during long-term usage of preheated castor oil-diesel blends.

From stage 3 it was concluded that the performance of diesel generators should be considered in cost optimisation models for better estimation of fuel consumption and pollutant emissions, especially if liquid biofuels such as vegetable oils-diesel blends are to be used to power diesel generators in hybrid

microgrids. Assessing the performance of diesel generators could be translated into reduced operating costs and less environmental impact of hybrid systems.

This section highlighted that although literature provides various studies related to optimisation models for sizing hybrid microgrids, the studies rely on fuel estimation equations for diesel fuel and their focus is on renewable energy technologies in terms of better sizing for minimising the overall cost of the system. The section also considered that not many authors have investigated the benefits of replacing oversized diesel generators with smaller units that may improve the performance of the diesel generators to reduce their fuel consumption and pollutant emissions. Moreover, this section considered the fact that even with the very robust and most utilised hybrid microgrid sizing tool (HOMER), the assessment of diesel generators powered with castor oil-diesel blends (or other vegetable oil blends) is not yet explored. The latter limits the possibility of assessing the effect of locally produced biofuels that might be of interest to hybrid systems in rural and remote areas. Therefore, the model presented in this section was focused on assessing how the performance of diesel generators is affected by the interaction with PV and battery systems for 8 microgrid configurations listed in Table 8-1 (SC1-SC8), assuming three different electricity demand profiles (high, medium, and low), while considering the costs and pollutant emissions (CO_2e , NO_x , and $\text{PM}_{2.5}$) of 4 different fuels (diesel and 3 castor oil-diesel blends). For that matter, the cost optimisation model included a new set of equations for better fuel consumption estimation of each fuel blend and incorporated the recommended operating limit of 60% engine load to avoid low load operation of the diesel generators.

By looking at the optimised results from the 8 microgrid configurations it was concluded that three diesel generators (G1, G2, and G3) were required in the systems without batteries (SC1 and SC2) for achieving the best genset performance, regardless of the assumed electricity demand profile. However, the results showed that the smallest genset selected per profile (G1) operated below the recommended limit during the very low load demand periods. It was noted that the worst performance of the generators was produced in SC2 during the lowest electricity demand period (at 5 am). At that period, the genset and the PV system were supplying power at the same time as the PV power was not enough to meet the demand. In those cases, operating the generators below the recommended limit was required to prevent a blackout due to the overgeneration that would have been produced at 60% engine load of the selected gensets. Nevertheless, it was determined that for the rest of the microgrid configurations (SC3 to SC8), the selected gensets operated at or

above the recommended limit, which contributed to reducing their pollutant emissions.

It was concluded that the selection of the diesel generators relies on the type of battery installed although it is mainly determined by the electricity demand profile. However, the selection is always done for installing the smallest genset applicable to each case. Selecting the smallest genset prevents the low load operation of the generators, especially if PV systems are included. It should be highlighted how with the high electricity demand profile, the G4 that was selected for the SC5-Genset, Battery (repurposed) was then substituted with two smaller gensets (G1 and G2) in SC8-Genset, PV, Battery (repurposed) to avoid underloading the genset during the operating hours with PV power contribution. This case exemplifies the importance of setting the right operating limit for the generators during the optimisation process to improve their performance while interacting with other power sources in hybrid microgrids.

Another relevant finding from this section was that diesel (COD0) was the fuel selected by the model for all the microgrid configurations despite the low price of castor oil compared to diesel. The conclusion regarding the fuel selection was that as castor oil generates higher PM_{2.5} emissions than diesel, selecting the castor oil-diesel blends would have increased the overall cost, hence diesel was preferred. Although currently there are no pollutant emission costs for microgrids in Tanzania, these costs were included in the optimisation model (considering the values given in Table 5-2) for a better economic and environmental assessment of the 8 microgrid configurations and the castor oil-diesel blends used in this work. Overall, it was concluded that installing hybrid systems (HED: SC5 or SC7, MED: SC7 or SC8, and LED: SC8) represents a better option compared to the only diesel (SC1) or diesel and PV (SC2) configurations. The diesel configuration produced higher pollutant emissions than the rest of the configurations whereas the diesel-PV systems had the highest LCOE, relative to all the configurations. The high pollutant emissions reported for SC1 were derived from the continuous operation of the diesel generators without any other power source for supplying the demand. The high cost of the SC2 was attributed to the PV cost and to the fuel consumption cost as the PV system did not contribute to reducing the night peak demand. Specifically, from the LCOE vs emissions analysis carried out in this stage, it was concluded that for the high and medium electricity demand profiles it was SC7 the system with the major environmental benefit, whereas, for the low electricity demand profile, it was SC8.

At the end of Stage 3, a scenario analysis was done by modifying five optimisation input parameters (PV share, PV performance, PV cost, Battery

Energy Storage System Capacity and Pollutant Emissions Assessment) as shown in Table 7-2, to investigate the impact on the baseline optimisation results for the microgrid configuration with the major environmental benefit per electricity demand profile. The relevant conclusions of the scenario analysis regarding the genset selection were that only for the high electricity demand profile a bigger genset was required when the BESS was reduced to a medium capacity, but the fuel consumption was not increased, relative to the baseline values, as the genset only operated during the periods where neither the battery nor the PV systems were able to meet the demand. Note that it was with the medium BESS capacity that the lowest fuel consumption was found in the HED profile, but for the MED and LED profiles, it was with the optimistic PV performance instead. On the other hand, when the PV share or the PV performance was reduced then the environmental impact increased in all the electricity demand profiles as more power was required from the diesel generator to meet the demand. Regarding the fuel selection, it was observed that diesel was the preferred option for all cases, which confirmed that it is the pollutant emission cost the key factor for the fuel selection.

To determine the cases where other fuel, different than diesel, would be selected by the model a sensitivity analysis was done by replacing the baseline diesel price and the pollutant emission costs with the low and high values listed in Table 7-9. The analysis confirmed that for all the cases where the PM_{2.5} emission cost was set to zero, regardless of the electricity demand profile, the fuel blend with 50% castor oil (COD50) was selected. It was found that also when the high diesel price was used, COD50 was selected. Nevertheless, it was still concluded that the PM_{2.5} emission cost is the key driver for fuel type selection because unless the baseline diesel price was doubled, diesel would remain the preferred option. In contrast, it was concluded that the NO_x emission cost has no impact on the fuel selection as the fuel blends have similar NO_x emission factors and the emission cost is not as high as the PM_{2.5} emission cost. It was noted that a high carbon tax would change the fuel selection for fuel with 40% castor oil (COD40). COD40 was preferred over COD50 due to the carbon tax and PM_{2.5} add-up effect that impacted the operational cost. Overall, the sensitivity analysis showed that without the pollutant emission costs, the microgrid LCOE would range between 0.27 £/kWh and 0.28£/kWh (0.34 USD/kWh and 0.35 USD/kWh) for hybrid systems and between 0.32£/kWh and 0.43£/kWh (0.40 USD/kWh and 0.54 USD/kWh) for diesel systems. These values are not that far from the estimated values for sub-Saharan Africa hybrid systems and Tanzanian diesel systems, 0.55 USD/kWh [240] and 0.40 to 2 USD/kWh [241], respectively.

8.6 Limitations and Future Work

This work presented a cost optimisation model developed for comparing the environmental and economic parameters of different microgrid configurations, giving special attention to improving the performance of diesel generators and assessing 4 possible castor oil-diesel blends to power diesel generators in Tanzania. Although the optimisation findings agreed with comparable data reported for hybrid microgrids in Tanzania and SSA, the model development was impacted by the reduced experimental work period derived from the COVID-19 restrictions in place during the research work. The reduced experimental work limited the assessment of preheated castor oil-diesel blends as well as the assessment of other vegetable oils to power the diesel generator. Therefore, the following recommendations should be considered for future work and further model improvements:

1. More engine tests are required using preheated (above 70°C) castor oil-diesel blends to investigate if the reduced viscosity of the blends prevents the early formation of fuel injector deposits.
2. The temperature at which pure castor oil should be preheated to power the diesel generator needs to be determined by experimental work for running engine tests with the preheated oil. The engine tests with pure castor oil are required to assess the pollutant emissions generated and compute the specific emission (SE), emission index (EI) and total weighted emission index (TWEI) directly from the experimental data rather than from the fitted curved that was presented in Figure 5-12. Using the experimental data from the castor oil engine tests will reduce the uncertainty of using fitted values and will give more accurate inputs for the optimisation model.
3. For widening the fuel options in the model, the characterisation of other vegetable oils (not food crops) is needed. Although this work was focused on one of the suitable vegetable oils (castor oil) for SSA microgrids, it would be beneficial to include other fuels that might be used to power diesel generators in hybrid microgrids in remote areas around the world. Even the characterisation of jatropha oil-diesel blends is recommended for having a complete data set of the physicochemical and TGA characteristics of this potential biofuel.
4. Expanding the vegetable oil-diesel blend options in the optimisation model requires more engine tests to determine their pollutant emission factors and their corresponding fuel consumption equations. The findings

of the engine tests could then be included as a database in the optimisation model for assessing microgrids with a wider variety of biofuel options according to different locations' availability.

5. Besides widening the fuel options in the optimisation model, it would be beneficial to expand the scope of the greenhouse gas emission source scenario to incorporate the embedded CO₂ in physical equipment (i.e., genset, PV and battery systems). Expanding the scope of this scenario would lead to a more complete assessment of the environmental impact of the different microgrid configurations.
6. A final recommendation for future work would be to consider other renewable energies (e.g., wind) in the cost optimisation model to enable the assessment of diesel generators fuelled with biofuels interacting with other power generation sources where PV is not a feasible solution.

List of References

1. Nations, U., *Transforming our world: the 2030 Agenda for Sustainable Development*. 21 October 2015, United Nations.
2. *Ensure Access to Affordable, Reliable, Sustainable and Modern Energy for All*. [cited 2020; Available from: <https://sdgs.un.org/goals/goal7>].
3. Organization, W.H., *Tracking SDG 7*. 2020.
4. Electrification, A.f.R. *Off-Grid Electricity Systems*. Available from: <http://www.ruralelec.org/grid-electricity-systems>.
5. SEforALL, B., *State of the global Mini-Grid Market Report 2020*. Sustainable Energy For All, 2020.
6. Burrell, L. *What's so important about mini-grids?* 2021 [cited 2023; Available from: <https://www.unido.org/stories/whats-so-important-about-mini-grids>].
7. Daniel Schnitzer, et al., *Microgrids for Rural Electrification: A critical review of best practices based on seven case studies*. 2014, United Nations Foundation. p. 120.
8. Kimera, R., et al., *Considerations for a sustainable hybrid mini-grid system: A case for Wanale village, Uganda*. *Journal of Energy in Southern Africa*, 2014.
9. *Africa Energy Outlook*. 2014, IEA: Paris.
10. *Africa Energy Outlook 2022*. 2022.
11. *World Energy Outlook 2021*. 2021, International Energy Agency.
12. Nations, U. *United Nations Development Programme Human Development Reports*. February 2019]; Available from: <http://hdr.undp.org/en/content/developing-regions>.
13. Franz, M., et al., *Mini-grid Policy Toolkit Policy and Business Frameworks for Successful Mini-grid Roll-outs*. 2014.
14. Camblong, H., et al., *Micro-grids project, Part 1: Analysis of rural electrification with high content of renewable energy sources in Senegal*. *Renewable Energy*, 2009. **34**(10): p. 2141-2150.
15. Longe, O.M., F.I. Oluwajobi, and F. Omowole, *Electricity access in Sub-Saharan Africa - Case for renewable energy sources microgrid*. 2013: p. 253-257.
16. *Energy Access Outlook 2017: From Poverty to Prosperity*. 2017, IEA: Paris.

17. Ainah, P.K. and K.A. Folly, *Development of Micro-Grid in Sub-Saharan Africa: an Overview*. International Review of Electrical Engineering (IREE), 2015. **10**(5): p. 633.
18. Kempener, R., et al., *Off-grid Renewable Energy Systems: Status and Methodological Issues*. 2015, IRENA. p. 36.
19. Hirsch, A., Y. Parag, and J. Guerrero, *Microgrids: A review of technologies, key drivers, and outstanding issues*. Renewable and Sustainable Energy Reviews, 2018. **90**: p. 402-411.
20. Pedersen, M.B., *Deconstructing the concept of renewable energy-based mini-grids for rural electrification in East Africa*. Wiley Interdisciplinary Reviews: Energy and Environment, 2016. **5**(5): p. 570-587.
21. *Africa's Pulse (English)*. 2018, World Bank Group.
22. *Africa 2030: Roadmap for a Renewable Energy Future*. 2015, IRENA: Abu Dhabi.
23. Knuckles, J., *State of the Mini Grid Market Globally Mini Grids for Half a Billion People*. 2019, World Bank Group.
24. Hobson, E.L., *Mapping and assessment of existing clean mini-grid experiences in West Africa*. 2016.
25. *Opportunities and challenges in the mini-grid sector in Africa lessons learned from the EEP portfolio*. 2018, EEP Africa.
26. Castalia and Ecoligo, *Mini Grids in Kenya a Case Study of a Market at a Turning Point*. 2017, The World Bank.
27. *Kenya Market Assessment for Off-Grid Electrification*. 2015, Carbon Africa Limited.
28. Day, T. and M.-J. Kurdziel, *The role of renewable energy mini-grids in Kenya's electricity sector Evidence of a cost-competitive option for rural electrification and sustainable development*. 2019, New Climate Institute.
29. Odarno, L., et al., *Accelerating Minigrid Deployment in Sub-Saharan Africa Lessons from Tanzania*. 2017, World Resources Institute.
30. Akinyele, D., *Techno-economic design and performance analysis of nanogrid systems for households in energy-poor villages*. Sustainable Cities and Society, 2017. **34**: p. 335-357.
31. *PD IEC/TS 62257-4:2015: Recommendations for renewable energy and hybrid systems for rural electrification. System selection and design*. 2016, British Standards Institute.
32. Szabó, S., et al., *Energy solutions in rural Africa: mapping electrification costs of distributed solar and diesel generation versus grid extension*. Environmental Research Letters, 2011.
33. *Operating Guidelines Off-grid Component of Tanzania Energy Development and Access Project*. 2014, The United Republic

- of Tanzania Ministry of Energy and Minerals/ Rural Energy Agency. p. 54.
34. Lane, J., et al., *Mini-Grid Market Opportunity Assessment: Senegal*. 2019, African Development Bank Group.
 35. PERACOD, *The Rural Electrification Senegal (ERSEN) Project: Electricity for over 90,000 persons*.
 36. *Min-Grid Design Manual*. 2000, ENERGY SECTOR MANAGEMENT ASSISTANCE PROGRAMME: Washington, D.C., U.S.A. p. 284.
 37. Blechinger, P., et al., *What size shall it be? A guide to mini-grid sizing and demand forecasting*. 2016, Deutsche Gesellschaft für Internationale Zusammenarbeit (GIZ) GmbH.
 38. Fu, Q., et al., *Microgrid Generation Capacity Design With Renewables and Energy Storage Addressing Power Quality and Surety*. IEEE Transactions on Smart Grid, 2012.
 39. *Considerations for a sustainable hybrid mini-grid system_Wanale Village, Uganda*.
 40. Díaz, P., et al., *Far from the grid: A rural electrification field study*. Renewable Energy, 2010.
 41. Mamaghani, A.H., et al., *Techno-economic feasibility of photovoltaic, wind, diesel and hybrid electrification systems for off-grid rural electrification in Colombia*. Renewable Energy, 2016.
 42. Azoumah, Y., et al., *Sustainable electricity generation for rural and peri-urban populations of sub-Saharan Africa: The "flexy-energy" concept*. ENERGY POLICY, 2011. **39**(1): p. 131-141.
 43. Zhao, B., et al., *Optimal sizing, operating strategy and operational experience of a stand-alone microgrid on Dongfushan Island*. Applied Energy, 2014.
 44. Yamegueu, D., et al., *Experimental study of electricity generation by Solar PV/diesel hybrid systems without battery storage for off-grid areas*. Renewable Energy, 2011.
 45. Mellit, A., et al., *Artificial intelligence techniques for sizing photovoltaic systems: A review*. Renewable and Sustainable Energy Reviews, 2009.
 46. Bernal-Agustín, J.L. and R. Dufo-López, *Simulation and optimization of stand-alone hybrid renewable energy systems*. Renewable and Sustainable Energy Reviews, 2009.
 47. *HOMER Software*. 2022; Available from: <https://www.homerenergy.com/index.html>.
 48. Connolly, D., et al., *A review of computer tools for analysing the integration of renewable energy into various energy systems*. Applied Energy, 2010.

49. Sinha, S. and S. Chandel, *Review of software tools for hybrid renewable energy systems*. Renewable and Sustainable Energy Reviews, 2014.
50. Suman, G.K., J.M. Guerrero, and O.P. Roy, *Optimisation of solar/wind/bio-generator/diesel/battery based microgrids for rural areas: A PSO-GWO approach*. Sustainable Cities and Society, 2021.
51. Fathima, A.H. and K. Palanisamy, *Optimization in microgrids with hybrid energy systems – A review*. Renewable and Sustainable Energy Reviews, 2015. **45**: p. 431-446.
52. Dimitriou, A., P. Kotsampopoulos, and N. Hatziaargyriou, *Best practices of rural electrification in developing countries: Technologies and case studies*. 2014.
53. Haghghat Mamaghani, A., et al., *Techno-economic feasibility of photovoltaic, wind, diesel and hybrid electrification systems for off-grid rural electrification in Colombia*. Renewable Energy, 2016.
54. Alzola, J.A., et al., *Microgrids project, Part 2: Design of an electrification kit with high content of renewable energy sources in Senegal*. Renewable Energy, 2009. **34**(10): p. 2151-2159.
55. Hamilton, J.M., et al., *Utilization and Optimization of Diesel Generation for Maximum Renewable Energy Integration*. 2017: p. 21-70.
56. Cooper, A.R., D.J. Morrow, and K.D.R. Chambers. *Performance modelling of generator sets during load acceptance*. IEEE.
57. Knudsen, J., et al., *Control-Oriented First Principles-Based Model of a Diesel Generator*. 2016 European Control Conference (Ecc), 2016: p. 321-327.
58. Colin R. Ferguson, A.T.K., *Internal Combustion Engines*. Second Edition ed. 2001: John Willey & Sons, Inc.
59. *Diesel Generators: Improving Efficiency and Emission Performance in India*. 2014, Shakti Sustainable Energy Foundation: New Delhi.
60. Sinn, M., *Cost recovery of isolated microgrids in sub-Saharan Africa: causalities and prerequisites*. 2014, Chalmers University of Technology: Göteborg, Sweden.
61. Schnitzer, D.A.K., *Microgrids and High - Quality Central Grid Alternatives: Challenges and Imperatives Elucidated by Case Studies and Simulation*, in *Engineering and Public Policy*. 2014, Carnegie Mellon University: Pittsburgh, PA.
62. Kusakana, K. and H.J. Vermaak, *Hybrid Diesel Generator - battery systems for offgrid rural applications*. 2013: p. 839-844.

63. Jabeck, B. *The Impact Of Generator Set Underloading*. [cited 2023; Available from: https://www.cat.com/en_US/by-industry/electric-power/Articles/White-papers/the-impact-of-generator-set-underloading.html].
64. Reiniger, K., T. Schott, and A. Zeidler. *Optimization of hybrid stand-alone systems*. in *European Wind Energy Association Conference and Exhibition*. 1986.
65. Skarstein, Ø. and K. Uhlen, *Design Considerations with Respect to Long-Term Diesel Saving in Wind/Diesel Plants*. *Wind Engineering*, 1989. **13**(2): p. 72-87.
66. Maleki, A. and A. Askarzadeh, *Optimal sizing of a PV/wind/diesel system with battery storage for electrification to an off-grid remote region: A case study of Rafsanjan, Iran*. *Sustainable Energy Technologies and Assessments*, 2014. **7**: p. 147-153.
67. Rangel, N., H. Li, and P. Aristidou, *An optimisation tool for minimising fuel consumption, costs and emissions from Diesel-PV-Battery hybrid microgrids*. *Applied Energy*, 2023. **335**: p. 120748.
68. Rohani, G. and M. Nour, *Techno-economical analysis of stand-alone hybrid renewable power system for Ras Musherib in United Arab Emirates*. *Energy*, 2014. **64**: p. 828-841.
69. Lilienthal, P. *Generator Fuel Curve Intercept Coefficient*. 2009; Available from: https://www.homerenergy.com/products/pro/docs/3.10/generator_fuel_curve_intercept_coefficient.html.
70. Lambert, T., P. Gilman, and P. Lilienthal, *Micropower system modeling with HOMER*. *Integration of alternative sources of energy*, 2006. **1**(1): p. 379-385.
71. *Generator Fuel Curve Intercept Coefficient*. HOMER Pro 3.14:[Available from: https://www.homerenergy.com/products/pro/docs/latest/generator_fuel_curve_intercept_coefficient.html].
72. Ashok, S., *Optimised model for community-based hybrid energy system*. *Renewable Energy*, 2007.
73. Agarwal, N. and A. Kumar, *Optimization of grid independent hybrid PV–diesel–battery system for power generation in remote villages of Uttar Pradesh, India*. *Energy for Sustainable Development*, 2013.
74. Pelland, S., et al., *Nemiah valley photovoltaic-diesel mini-grid: System performance and fuel saving based on one year of monitored data*. *IEEE Transactions on Sustainable Energy*, 2011. **3**(1): p. 167-175.

75. Gan, L.K., J.K.H. Shek, and M.A. Mueller, *Hybrid wind–photovoltaic–diesel–battery system sizing tool development using empirical approach, life-cycle cost and performance analysis: A case study in Scotland*. Energy Conversion and Management, 2015. **106**: p. 479-494.
76. Soto, D., *Modeling and measurement of specific fuel consumption in diesel microgrids in Papua, Indonesia*. Energy for Sustainable Development, 2018.
77. Díaz, P., et al., *Field analysis of solar PV-based collective systems for rural electrification*. Energy, 2011.
78. Booth, S., et al., *Productive use of energy in African micro-grids: Technical and business considerations*. 2018.
79. Edwards, R.E., J. New, and L.E. Parker, *Predicting future hourly residential electrical consumption: A machine learning case study*. Energy and Buildings, 2012. **49**: p. 591-603.
80. Bjornstad, E. *Diesel Engine Troubleshooting: Black Smoke*. Available from: <https://www.bellperformance.com/bell-performs-blog/diesel-engine-troubleshooting-black-smoke#:~:text=Black%20diesel%20smoke%20means%20something,coming%20out%20of%20the%20stack>.
81. Tree, D.R. and K.I. Svensson, *Soot processes in compression ignition engines*. Progress in energy and combustion science, 2007. **33**(3): p. 272-309.
82. Alramlawi, M., et al. *Optimal operation of pv-diesel microgrid with multiple diesel generators under grid blackouts*. in *2018 IEEE International Conference on Environment and Electrical Engineering and 2018 IEEE Industrial and Commercial Power Systems Europe (EEEIC/I&CPS Europe)*. 2018. IEEE.
83. Kusakana, K. *Optimal operation of parallel-connected diesel generators for remote electrification through energy management approach*. in *2017 IEEE PES PowerAfrica*. 2017. IEEE.
84. Knudsen, J., et al. *Fuel optimization in multiple diesel driven generator power plants*. in *2017 IEEE Conference on Control Technology and Applications (CCTA)*. 2017. IEEE.
85. Belyaev, M.E., et al., *Design of Diesel Engine Mathematical Model Oriented to Speed Control*. Journal of Computer and Systems Sciences International, 2018. **57**(4): p. 626-639.
86. Yu, M., et al., *Diesel engine modeling based on recurrent neural networks for a hardware-in-the-loop simulation system of diesel generator sets*. Neurocomputing, 2018. **283**: p. 9-19.
87. Tibola, J.R., et al., *Modeling and speed control design of an ethanol engine for variable speed gensets*. Control Engineering Practice, 2015. **35**: p. 54-66.

88. Singh, B. and R. Niwas, *Fuel-efficient Induction Generator Based Diesel Generator Set for Stand-alone Supply Systems*. *Electric Power Components and Systems*, 2015. **43**(18): p. 2019-2028.
89. Ailing, C., *Speed Regulator of Diesel-Generator Based on Model Free Adaptive Control*. 2010: p. 193-196.
90. Wei, H., R. Min, and T. Yingqi. *A Fuzzy Control System of Diesel Generator Speed*. IEEE.
91. Benhamed, S., et al., *Dynamic Modeling of Diesel Generator Based on Electrical and Mechanical Aspects*. 2016 IEEE Electrical Power and Energy Conference (Epec), 2016.
92. J. Salazar, F. Tadeo, and C. Prada, *Modelling of Diesel Generator Sets That Assist Off-Grid Renewable Energy Micro-grids*. *Renewable Energy and Sustainable Development*, 2015.
93. Iwanski, G. and W. Koczara, *Power Management in an Autonomous Adjustable Speed Large Power Diesel Gensets*. 2008 13th International Power Electronics and Motion Control Conference, Vols 1-5, 2008: p. 2164-2169.
94. Di Noia, L.P., D. Lauria, and R. Rizzo, *A Control Strategy of a Stand Alone Induction Generator coupled with a Diesel Engine for Distributed Generation with Renewable Sources*. 2015 International Conference on Clean Electrical Power (Iccep), 2015: p. 448-453.
95. Koczara, W. and N. Al Khayat. *Variable speed integrated generator VSIG as a modern controlled and decoupled generation system of electrical power*. IEEE.
96. Koczara, W., et al. *Variable speed integrated generating set an emerging technology for distributed power generation*. IEEE.
97. Hamilton, J., M. Negnevitsky, and X.L. Wang, *Economics of Renewable Energy Integration and Energy Storage via Low Load Diesel Application*. *Energies*, 2018. **11**(5).
98. Hamilton, J., M. Negnevitsky, and X. Wang, *Low load diesel perceptions and practices within remote area power systems*. 2015: p. 121-126.
99. Britannica, E. *four-stroke diesel engine*. 16 de febrero de 2022]; Available from: <https://www.britannica.com/technology/diesel-engine#/media/1/162716/19423>.
100. Hwang, J., et al., *Investigations on air-fuel mixing and flame characteristics of biodiesel fuels for diesel engine application*. *Applied Energy*, 2017. **206**: p. 1203-1213.
101. Salave, H., *Combustion Stages in S.I and C.I Engine*. 2022.

102. Yusop, A.F., et al., *Analysis of particulate matter (PM) emissions in diesel engines using palm oil biodiesel blended with diesel fuel*. *Energies*, 2018. **11**(5): p. 1039.
103. Reşitoğlu, İ.A., K. Altinişik, and A. Keskin, *The pollutant emissions from diesel-engine vehicles and exhaust aftertreatment systems*. *Clean Technologies and Environmental Policy*, 2015. **17**(1): p. 15-27.
104. Lam, N., et al., *The dirty footprint of the broken grid: the impacts of fossil fuel back-up generators in developing countries*. 2019.
105. Allan, J., R. Harrison, and R. Maggs, *Measurement Uncertainty for PM_{2.5} in the Context of the UK National Network*. Department for Environment Food & Rural Affairs.
106. *What is PM_{2.5} and PM₁₀? Info about particulate matter (particle pollution)*. Available from: <https://airly.org/en/what-is-pm10-and-what-is-pm2-5/>.
107. Biofuel.org.uk. *Biofuels The fuel of the future*. 2010 [cited 2019; Available from: <http://biofuel.org.uk/>].
108. Sajjadi, B., A.A.A. Raman, and H. Arandiyan, *A comprehensive review on properties of edible and non-edible vegetable oil-based biodiesel: Composition, specifications and prediction models*. *Renewable and Sustainable Energy Reviews*, 2016. **63**: p. 62-92.
109. Mahmudul, H.M., et al., *Production, characterization and performance of biodiesel as an alternative fuel in diesel engines – A review*. *Renewable and Sustainable Energy Reviews*, 2017. **72**: p. 497-509.
110. Sakthivel, R., et al., *A review on the properties, performance and emission aspects of the third generation biodiesels*. *Renewable and Sustainable Energy Reviews*, 2018. **82**: p. 2970-2992.
111. Ramadhas, A.S., S. Jayaraj, and C. Muraleedharan, *Use of vegetable oils as I.C. engine fuels—A review*. *Renewable Energy*, 2004. **29**(5): p. 727-742.
112. Dhamodaran, G., et al., *A comparative study of combustion, emission, and performance characteristics of rice-bran-, neem-, and cottonseed-oil biodiesels with varying degree of unsaturation*. *Fuel*, 2017. **187**: p. 296-305.
113. Altın, R., S. Çetinkaya, and H.S. Yücesu, *The potential of using vegetable oil fuels as fuel for diesel engines*. *Energy Conversion and Management*, 2001. **42**(5): p. 529-538.
114. Che Mat, S., et al., *Performance and emissions of straight vegetable oils and its blends as a fuel in diesel engine: A*

- review*. Renewable and Sustainable Energy Reviews, 2018. **82**: p. 808-823.
115. Atabani, A.E., et al., *Non-edible vegetable oils: A critical evaluation of oil extraction, fatty acid compositions, biodiesel production, characteristics, engine performance and emissions production*. Renewable and Sustainable Energy Reviews, 2013. **18**: p. 211-245.
 116. No, S.-Y., *Inedible vegetable oils and their derivatives for alternative diesel fuels in CI engines: A review*. Renewable and Sustainable Energy Reviews, 2011. **15**(1): p. 131-149.
 117. de Almeida, S.C.A., et al., *Performance of a diesel generator fuelled with palm oil*. Fuel, 2002. **81**(16): p. 2097-2102.
 118. Hossain, A.K. and P.A. Davies, *Plant oils as fuels for compression ignition engines: A technical review and life-cycle analysis*. Renewable Energy, 2010. **35**(1): p. 1-13.
 119. Agarwal, D., A.K. Agarwal, and L. Kumar, *Performance evaluation of a vegetable oil fuelled compression ignition engine*. Renewable Energy, 2008. **33**(6): p. 1147-1156.
 120. Patel, P.D., et al., *Bio fuels for compression ignition engine: A review on engine performance, emission and life cycle analysis*. Renewable and Sustainable Energy Reviews, 2016. **65**: p. 24-43.
 121. Nazzal, I.T., *Experimental Study Of Vegetable Oil-Diesel Blends On The performance Of Compression Ignition Engine*. Anbar Journal for Engineering Sciences, 2011. **4**(2): p. 33-44.
 122. Agarwal, A.K. and K. Rajamanoharan, *Experimental investigations of performance and emissions of Karanja oil and its blends in a single cylinder agricultural diesel engine*. Applied Energy, 2009. **86**(1): p. 106-112.
 123. Haldar, S.K., B.B. Ghosh, and A. Nag, *Utilization of unattended Putranjiva roxburghii non-edible oil as fuel in diesel engine*. Renewable Energy, 2009. **34**(1): p. 343-347.
 124. Karthikeyan, R. and N. Mahalakshmi, *Performance and emission characteristics of a turpentine–diesel dual fuel engine*. Energy, 2007. **32**(7): p. 1202-1209.
 125. Ruban, M., L. Karikalán, and S.K. Chakraborty, *Performances and emissions characteristics of diesel engine by using Jatropha oil*. Materials Today: Proceedings, 2021. **37**: p. 631-633.
 126. Piloto-Rodríguez, R., I. Tobío-Pérez, and J. Suárez-Hernández, *Diesel engine fuelled with blends of Jatropha curcas oil and diesel fuel*. Revista Cubana de Ingeniería, 2020. **11**(2): p. 12-19.

127. Forson, F.K., E.K. Oduro, and E. Hammond-Donkoh, *Performance of jatropha oil blends in a diesel engine*. Renewable Energy, 2004. **29**(7): p. 1135-1145.
128. Pramanik, K., *Properties and use of jatropha curcas oil and diesel fuel blends in compression ignition engine*. Renewable Energy, 2003. **28**(2): p. 239-248.
129. Agarwal, D. and A.K. Agarwal, *Performance and emissions characteristics of Jatropha oil (preheated and blends) in a direct injection compression ignition engine*. Applied Thermal Engineering, 2007. **27**(13): p. 2314-2323.
130. Prasad, C.S.N., et al. *Performance and emission characteristics of a diesel engine with castor oil*. 2009.
131. Nand Agrawal, B., et al., *Effects of blends of castor oil with pure diesel on performance parameters of direct injection compression ignition engine*. Materials Today: Proceedings, 2019.
132. Uddin, S.A., et al., *Performance Study of DI diesel engine by using pure mustard oil as alternative fuel for diesel engine at various load condition*. Technology (BUET), 2014. **1877**: p. 7058.
133. *Diesel Fuels Technical Review*. 2007, Chevron Corporation. p. 116.
134. Blin, J., et al., *Characteristics of vegetable oils for use as fuel in stationary diesel engines—Towards specifications for a standard in West Africa*. Renewable and Sustainable Energy Reviews, 2013. **22**: p. 580-597.
135. DieselNet. *Emission Standards*. 2019 [January 2019]; Available from: <https://www.dieselnet.com/standards/eu/nonroad.php#s5>.
136. Chauhan, A. and R.P. Saini, *A review on Integrated Renewable Energy System based power generation for stand-alone applications: Configurations, storage options, sizing methodologies and control*. Renewable and Sustainable Energy Reviews, 2014. **38**: p. 99-120.
137. Koopialipoor, M. and A. Noorbakhsh, *Applications of Artificial Intelligence Techniques in Optimizing Drilling*. 2020.
138. Gupta, A., R.P. Saini, and M.P. Sharma, *Steady-state modelling of hybrid energy system for off grid electrification of cluster of villages*. Renewable Energy, 2010. **35**(2): p. 520-535.
139. Mehdi, M., *PARALLEL HYBRID OPTIMIZATION METHODS FOR PERMUTATION BASED PROBLEMS*. 2011.

140. *The Gurobi Python Modeling and Development Environment*. Available from: <https://www.gurobi.com/resource/modeling-in-python/>.
141. Technology, N.U.o.S.a., *MILP algorithms: branch-and-bound and branch-and-cut*.
142. *Urban and rural development: Access to electricity, rural (% of rural population)*. Available from: <http://datatopics.worldbank.org/world-development-indicators/themes/environment.html>.
143. Sekoai, P. and K. Yoro, *Biofuel Development Initiatives in Sub-Saharan Africa: Opportunities and Challenges*. Climate, 2016. 4(2): p. 33.
144. Ltd, C.O. *Red Diesel (Gas Oil) delivered across the UK*. 2019; Available from: <https://www.crownoiluk.com/downloads/>.
145. Sayyed, S., K. Renuka, and D. Swapnil, *Effects of Thermal, Physical, and Chemical Properties of Biodiesel and Diesel Blends*. Vol. 2. 2016. 24-31.
146. Satyanarayana, M. and C. Muraleedharan, *Comparative Studies of Biodiesel Production from Rubber Seed Oil, Coconut Oil, and Palm Oil Including Thermogravimetric Analysis*. Energy Sources, Part A: Recovery, Utilization, and Environmental Effects, 2011. 33(10): p. 925-937.
147. *Organic Elemental Analysis Flash 2000 Elemental Analyzer Operating Manual*. 2008, Thermo Fisher Scientific: Cambridge, United Kingdom.
148. Thompson, M., *AMC technical briefs: CHNS elemental analysers*. Analytical Methods Committee: AMCTB, 2008(29).
149. Hillstone. *AC Load Banks*. Available from: <https://hillstone.co.uk/>.
150. NI. *National Instruments Solutions: Lab View -DAQ Products*. Available from: <https://www.ni.com/en-gb.html>.
151. Hillstone. *ACLoadView*. Available from: <https://hillstone.co.uk/software-ac.php>.
152. Ohashi, H., *Motor Exhaust Gas Analyzer MEXA-7000 Series 1*. Product Concept, Readout, 1995(11).
153. Takeda, K. and H. Koike, *Motor Exhaust Gas Analyzer MEXA-7000 Series 2*. Downsizing and Modular Configuration of Analyzers, Readout, 1995(11).
154. Cambustion. *Fast FID Principles*. Available from: <https://www.cambustion.com/products/knowledgebase/fast-fid-principles>.
155. Martyr, A.J. and M.A. Plint, *Chapter 16 - Engine Exhaust Emissions*, in *Engine Testing (Fourth Edition)*, A.J. Martyr and

- M.A. Plint, Editors. 2012, Butterworth-Heinemann: Oxford. p. 407-450.
156. Gaset. *Portable Gas Analyzers*. Available from: <https://www.gasmet.com/products/category/portable-gas-analyzers/>.
 157. Gaset, *Instruction and Operating Manual for the Gaset DX4000 and Gaset DX4015 models*. 2015.
 158. Cambustion, *DMS500 Fast Particulate Analyzer: User Manual*.
 159. Cambustion. *Application Note: DMS500 Installation Guide for Engine Sampling (Direct Sampling of Engine Exhaust with the DMS500)*. Available from: <https://www.cambustion.com/products/application-notes/dms-particle-size-mass-and-number>.
 160. Cambustion. *DMS500 Brochure: The Rapid Response Engine Particulate Analyzer*. Available from: <https://www.cambustion.com/products/engine-exhaust-emissions/dms500-particulate-analyzer>.
 161. Lindsley, W.G., et al., *Sampling and characterization of bioaerosols*. National Institute for Occupational Safety and Health, 2017.
 162. Instruments, N. *Components in a SEM*. [cited 2022; Available from: <https://www.nanoscience.com/techniques/scanning-electron-microscopy/components/#bsd>].
 163. Leonardo, R., J. Dweck, and M. Murta Valle, *Evaluation of the volatility characteristics of diesel/biodiesel blends using thermal analysis techniques*. Blucher Eng Proceed, 2019. **2019**(6): p. 98-113.
 164. *Thermal Stability*. Available from: <https://analyzing-testing.netzsch.com/es/training-know-how/glosario/thermal-stability>.
 165. *TGA-50 Series -Specs*. Available from: <https://www.shimadzu.com/an/products/thermal-analysis/thermogravimetric-analysis/tga-50-series/spec.html>.
 166. *The Chemistry & Chemical Modifications of Castor Oil*. 2022; Available from: <https://www.ambujasolvex.com/blog/the-chemistry-chemical-modifications-of-castor-oil/>.
 167. Tong, K., et al., *Fuel volatility effects on mixture preparation and performance in a GDI engine during cold start*. SAE Transactions, 2001: p. 2301-2318.
 168. Ristić, I., et al., *Thermal stability of polyurethane materials based on castor oil as polyol component*. Journal of Thermal Analysis and Calorimetry, 2013. **111**: p. 1083-1091.

169. Ruhul, A., et al., *State of the art of biodiesel production processes: a review of the heterogeneous catalyst*. RSC Advances, 2015. **5**(122): p. 101023-101044.
170. Yeboah, A., et al., *Castor oil (Ricinus communis): a review on the chemical composition and physicochemical properties*. Food Science and Technology, 2020.
171. Demirbas, A., *Relationships derived from physical properties of vegetable oil and biodiesel fuels*. Fuel, 2008. **87**(8): p. 1743-1748.
172. SVM 3000 Stabinger Viscometer. 2015, Anton Paar GmbH.
173. Jargon Buster Explaining key terms for specifiers and end users. 2022; Available from: <https://www.amps.org.uk/jargon-buster>.
174. Load Bank Basics. 2022; Available from: <https://www.ascopower.com/uk/en/resources/articles/load-bank-basics.jsp>.
175. Sp-E1 catalogue. Available from: <https://www.linzelectric.com/index.cfm/en/download/#3>.
176. Tüccar, G., E. Tosun, and E. Uludamar, *Investigations of effects of density and viscosity of diesel and biodiesel fuels on NOx and other emission formations*. Academic Platform-Journal of Engineering and Science, 2018. **6**(2): p. 81-85.
177. N/A, Table 219. *Heat Capacity - Miscellaneous Liquids*.
178. N/A, Table 11.1. *The Properties of Methanol, Gasoline and Diesel*.
179. Song, H., et al., *Effects of oxygen content of fuels on combustion and emissions of diesel engines*. Energies, 2016. **9**(1): p. 28.
180. Class A2 Gas Oil Specifications. Available from: <https://www.crownoil.co.uk/fuel-specifications/bs-2869/a2-gas-oil/>.
181. Hellier, P., N. Ladommatos, and T. Yusaf, *The influence of straight vegetable oil fatty acid composition on compression ignition combustion and emissions*. Fuel, 2015. **143**: p. 131-143.
182. Harrington, K.J., *Chemical and physical properties of vegetable oil esters and their effect on diesel fuel performance*. Biomass, 1986. **9**(1): p. 1-17.
183. Shahidi, F., *Bailey's Industrial Oil and Fat Products, Volumes 1-6 (6th Edition)*. John Wiley & Sons.
184. Mubofu, E.B., *Castor oil as a potential renewable resource for the production of functional materials*. Sustainable Chemical Processes, 2016. **4**(1): p. 11.

185. Olanrewaju, F.O., et al., *Improved model for the analysis of the Heat Release Rate (HRR) in Compression Ignition (CI) engines*. Journal of the Energy Institute, 2020. **93**(5): p. 1901-1913.
186. *Pub Chem -Neoloid (Castor Oil)*. Available from: <https://pubchem.ncbi.nlm.nih.gov/compound/Neoloid>.
187. Parrilla, J. and C. Cortés. *Modelling of droplet burning for rapeseed oil as liquid fuel*. in *Proceedings of International Conference on Renewable Energies and Power Quality ICREPQ*. 2007.
188. Li, H., et al., *Assessing combustion and emission performance of direct use of SVO in a diesel engine by oxygen enrichment of intake air method*. Biomass and Bioenergy, 2013. **51**: p. 43–52.
189. Ganesan, V., *Internal Combustion Engines*. 1994: McGraw-Hill.
190. Silvis M, W., *The Algorithm Structure of the Air/Fuel Ratio Calculation (There is really only one A/F ratio equation)*. 1997, Horiba Instruments Inc.
191. Sisi, M.J., M.R. Ahmed, and D. Rohindra, *Performance and emission characteristics of a diesel engine employing straight vegetable oils from Vanuatu as fuels*. Advances in Mechanical Engineering, 2020. **12**(9): p. 1687814020962351.
192. Andrews, G., et al., *Influence of Ambient Temperature on Cold-start Emissions for a Euro 1 SI Car Using In-vehicle Emissions Measurement in an Urban Traffic Jam Test Cycle*. 2005.
193. Betha, R. and R. Balasubramanian, *Particulate Emissions from a Stationary Engine Fueled with Ultra-Low-Sulfur Diesel and Waste-Cooking-Oil-Derived Biodiesel*. Journal of the Air & Waste Management Association, 2011. **61**(10): p. 1063-1069.
194. Wang, Y., H. Liu, and C.-F.F. Lee, *Particulate matter emission characteristics of diesel engines with biodiesel or biodiesel blending: A review*. Renewable and Sustainable Energy Reviews, 2016. **64**: p. 569-581.
195. Andrews, G., H. Li, and S. Wright, *Particulate Mass Emissions From Aircraft: A First Order Approximation Method Based on Experience From Diesel Particulate Mass Emissions Measurement*. Vol. 2. 2009.
196. Chung, A., A.A. Lall, and S.E. Paulson, *Particulate emissions by a small non-road diesel engine: Biodiesel and diesel characterization and mass measurements using the extended idealized aggregates theory*. Atmospheric Environment, 2008. **42**(9): p. 2129-2140.

197. Lea-Langton, A., H. Li, and G.E. Andrews, *Investigation of aldehyde and VOC emissions during cold start and hot engine operations using 100% biofuels for a DI engine*. 2009, SAE Technical Paper.
198. Kim, H.Y. and N.J. Choi, *Study on volatile organic compounds from diesel engine fueled with palm oil biodiesel blends at low idle speed*. Applied Sciences, 2020. **10**(14): p. 4969.
199. Ge, J.C., et al., *Reducing volatile organic compound emissions from diesel engines using canola oil biodiesel fuel and blends*. Fuel, 2018. **218**: p. 266-274.
200. Barsic, N.J. and A.L. Humke, *Performance and Emissions Characteristics of a Naturally Aspirated Diesel Engine with Vegetable Oil Fuels*. SAE Transactions, 1981. **90**: p. 1173-1187.
201. Hoang, A.T., et al., *An investigation of deposit formation in the injector, spray characteristics, and performance of a diesel engine fueled with preheated vegetable oil and diesel fuel*. Energy Sources, Part A: Recovery, Utilization, and Environmental Effects, 2019. **41**(23): p. 2882-2894.
202. Barker, J., et al., *Diesel Injector Deposits – An Issue That Has Evolved with Engine Technology*. SAE Technical Papers, 2011.
203. KOZAK, M., *A comparison of thermogravimetric characteristics of fresh and used engine oils*. Combustion Engines, 2019. **178**(3): p. 289-292.
204. Economies, E. *Electrifying Economies : Detailed Cost Models and Benchmarks.*; Available from: <https://www.electrifyingeconomies.org/>.
205. Zhongming, Z., et al., *Handbook on Battery Energy Storage System*. 2018.
206. *British Standards Institution: BS2869:2017+A1:2022-Fuel oils for agricultural, domestic and industrial engines and boilers*. London: BSI; 2022.
207. *1.A.4 Non road mobile machinery 2019*. European Environment Agency.
208. Li, X., J. Salasovich, and T. Reber. *Microgrid Load and LCOE Modelling Results*. 2018 01/04/2018 [cited 2021 25/10]; Available from: <https://data.nrel.gov/submissions/79>.
209. El-Hefnawi, S.H., *Photovoltaic diesel-generator hybrid power system sizing*. Renewable Energy, 1998. **13**(1): p. 33-40.
210. Coleman, C. *Hybrid power system operational test results: wind/PV/diesel system documentation*. in *Conference Proceedings., Eleventh International Telecommunications Energy Conference*. 1989. IEEE.

211. Lebedeva, N., *Li-ion batteries for mobility and stationary storage applications*. Publications Office of the European Union, 2018.
212. *Tanzania Diesel prices*. 10/21 [cited 2021 25/10/21]; Available from:
https://www.globalpetrolprices.com/Tanzania/diesel_prices/.
213. Wamucii, S. *Tanzania Castor Oil Prices*. 2021 [cited 2021 25/10]; Available from:
<https://www.selinawamucii.com/insights/prices/tanzania/castor-oil/>.
214. Group, T.W.B. *Carbon Pricing Dashboard*. [cited 2020 28/07]; Available from:
https://carbonpricingdashboard.worldbank.org/map_data.
215. *Government conversion factors for company reporting of greenhouse gas emissions*. 2021 24/01/2022; Available from:
<https://www.gov.uk/government/collections/government-conversion-factors-for-company-reporting#full-publication-update-history>.
216. *The true cost of fossil fuels: Externality cost assessment methodology 2016*, IRENA.
217. Reber, T.J., et al., *Tariff Considerations for Micro-Grids in Sub-Saharan Africa*. 2018, National Renewable Energy Lab.(NREL), Golden, CO (United States).
218. Lockhart, E., et al., *Comparative Study of techno-economics of lithium-ion and lead-acid batteries in micro-grids in Sub-Saharan Africa*. 2019, National Renewable Energy Lab.(NREL), Golden, CO (United States).
219. Hill, N., et al., *Circular economy perspectives for the management of batteries used in electric vehicles*. Final Project Report by Ricardo Energy & Environment for the JRC, Publications Office of the European Union, Luxemburg, 2019.
220. Winston, W.L., *Operations research : applications and algorithms*. Second edition. ed. 1991, Boston: PWS-Kent Pub. Co.
221. *US Dollar (USD) to British Pound (GBP) exchange rate history*. Available from:
<https://www.exchangerates.org.uk/USD-GBP-exchange-rate-history.html>.
222. DieselNet. *Emission Test Cycles ISO8178*. [cited 2022; Available from:
<https://dieselnet.com/standards/cycles/iso8178.php>.
223. Lai, C.S. and M.D. McCulloch, *Levelized cost of energy for PV and grid scale energy storage systems*. arXiv preprint arXiv:1609.06000, 2016.

224. Group, W.B. *Energy Data.Info Mini-grids Locations in Tanzania*. [cited 2020 28/07]; Available from: <https://energydata.info/dataset/mini-grid-locations-in-tanzania/resource/754fe23c-d8de-43d5-8a52-42c6fca4fab7>.
225. Brinkhoff, T. *Liwale District in Coastal Tanzania*. [cited 2020 28/07]; Available from: https://www.citypopulation.de/en/tanzania/coastal/admin/0804_liwale/.
226. Commission, E. *Photovoltaic Geographical Information System*. [cited 2020 28/07]; Available from: https://re.jrc.ec.europa.eu/pvg_tools/en/tools.html#HR.
227. Merz, K., et al., *Battery energy storage for rural electrification systems*. EUROBAT-Association of European Automotive and Industrial Battery Manufacturers, 2013.
228. Hall, D. and N. Lutsey, *Effects of battery manufacturing on electric vehicle life-cycle greenhouse gas emissions*. 2018.
229. Hill, N., et al., *2021 Government greenhouse gas conversion factors for company reporting: Methodology paper for conversion factors final report*. 2021, Department for Business Energy & Industrial Strategy (BEIS).
230. Pari, L., et al., *Environmental and economic assessment of castor oil supply chain: a case study*. Sustainability, 2020. **12**(16): p. 6339.
231. Alcock, T.D., et al., *More sustainable vegetable oil: Balancing productivity with carbon storage opportunities*. Science of The Total Environment, 2022. **829**: p. 154539.
232. Lau, K.Y., et al., *Performance analysis of hybrid photovoltaic/diesel energy system under Malaysian conditions*. Energy, 2010. **35**(8): p. 3245-3255.
233. Atmaja, T.D., et al. *Fuel saving on diesel genset using PV/battery spike cutting in remote area microgrid*. in *MATEC Web of Conferences*. 2018. EDP Sciences.
234. Bohra, S.S., et al., *Multi-criteria planning of microgrids for rural electrification*. Journal of Smart Environments and Green Computing, 2021. **1**(2): p. 120-134.
235. Kowsar, A., et al. *Techno-economic evaluation of a 29-kW micro-grid hybrid photovoltaic system for a healthcare center in Bangladesh*. in *AIP Conference Proceedings*. 2022. AIP Publishing LLC.
236. Anderson, K.H., et al., *Resilient renewable energy microgrids*. 2017, National Renewable Energy Lab.(NREL), Golden, CO (United States).

237. Kitindi, E.J., *Techno-economic and environmental analysis for off-grid mobile base stations electrification with hybrid power system in Tanzania*. 2021.
238. Abraha, A.H., M.B. Kahsay, and C.Z. Kimambo, *Hybrid solar-wind-diesel systems for rural application in North Ethiopia: case study for three rural villages using HOMER simulation*. Momona Ethiopian Journal of Science, 2013. **5**(2): p. 62-80.
239. Amupolo, A., et al., *Techno-Economic Feasibility of Off-Grid Renewable Energy Electrification Schemes: A Case Study of an Informal Settlement in Namibia*. Energies, 2022. **15**(12): p. 4235.
240. Groh, S., et al., *Electricity Access, Decarbonization, and Integration of Renewables: Insights and Lessons from the Energy Transformation in Bangladesh, South Asia, and Sub-Saharan Africa*. 2023: Springer Nature.
241. Moner-Girona, M., et al., *Adaptation of Feed-in Tariff for remote mini-grids: Tanzania as an illustrative case*. Renewable and Sustainable Energy Reviews, 2016. **53**: p. 306-318.
242. Charalampos, A., *Emissions of Diesel - Vegetable Oils Mixtures*, in *Environmental Impact of Biofuels*, B. Marco Aurélio dos Santos, Editor. 2011, IntechOpen: Rijeka. p. Ch. 4.

Appendix A

Table A1 Electricity Access for the rural and total population in African countries from the World Development Indicators.

Country	Access to electricity, rural (% of rural population)		Access to electricity (% of population)	
	2012	2016	2012	2016
Angola	16.28	15.98	35.82	40.52
Burundi	1.20	1.65	6.50	7.59
Benin	14.50	17.97	38.40	41.40
Burkina Faso	1.63	0.77	16.40	19.16
Botswana	31.59	37.49	52.06	60.69
Central African Republic	0.36	0.36	11.60	13.99
Cote d'Ivoire	29.00	38.10	55.80	64.30
Cameroon	18.83	21.27	55.25	60.07
Congo, Dem. Rep.	1.00	-	15.40	17.15
Congo, Rep.	11.70	22.63	41.60	56.57
Comoros	61.40	72.19	69.30	77.84
Cabo Verde	71.41	91.83	83.15	92.61
Eritrea	33.15	39.27	42.03	46.68
Ethiopia	15.52	26.50	28.36	42.90
Gabon	44.90	54.96	89.30	91.40
Ghana	50.26	66.60	69.29	79.30
Guinea	2.90	6.90	26.20	33.50
Gambia, The	13.27	15.53	42.69	47.76
Guinea-Bissau	-	-	12.06	14.66
Equatorial Guinea	49.46	52.57	66.24	67.89
Kenya	18.39	39.30	30.27	56.00
Liberia	2.57	1.30	8.60	19.80
Lesotho	11.94	15.75	22.51	29.73
Madagascar	-	17.30	17.73	22.90
Mali	11.90	1.77	25.60	35.07
Mozambique	3.84	4.95	19.54	24.20
Mauritania	-	-	35.62	41.65
Mauritius	100.00	100.00	98.63	98.78
Malawi	2.30	4.00	7.40	11.00
Namibia	25.78	28.72	47.48	51.78
Niger	5.20	4.68	14.40	16.22
Nigeria	29.61	41.10	54.27	59.30
Rwanda	1.26	17.76	16.07	29.37

Sudan	20.21	22.20	36.46	38.53
Senegal	36.73	38.30	57.16	64.50
Sierra Leone	-	2.50	15.17	20.30
Somalia	8.33	11.63	23.51	29.89
South Sudan	2.59	5.87	4.91	8.95
Sao Tome and Principe	43.30	51.09	57.90	65.44
Eswatini	49.15	61.18	54.62	65.79
Seychelles	96.68	100.00	98.41	100.00
Chad	1.61	2.23	7.07	8.83
Togo	16.05	19.39	39.34	46.93
Tanzania	3.60	16.90	15.30	32.80
Uganda	9.98	18.00	16.21	26.70
South Africa	75.60	67.92	85.30	84.20
Zambia	3.38	2.66	24.89	27.22
Zimbabwe	12.98	15.58	36.73	38.15

*Red numbers indicate the bottom ten countries without electricity access. Green numbers correspond to the top ten countries with the highest electricity access.